PhD-FSTM-2021-049
The Faculty of Sciences, Technology and Medicine

DISSERTATION

Defence held on 15/07/2021 in Esch-sur-Alzette

to obtain the degree of

DOCTEUR DE L'UNIVERSITÉ DU LUXEMBOURG

EN CHIMIE

by

Dominique ABESSOLO ONDO
Born on 17 July 1992 in Assas (Oyem), Gabon

PLASMA INITIATED CHEMICAL VAPOUR DEPOSITION - FROM THE GROWTH MECHANISMS TO ULTRATHIN LOW-κ POLYMER INSULATING LAYERS

Dissertation defence committee

Dr Nicolas Boscher, dissertation supervisor
Doctor, Luxembourg Institute of Science and Technology

Dr Françoise Massines
Professor, PROMES-CNRS, Perpignan

Dr Phillip J. Dale, Chairman
Professor, Université du Luxembourg

Dr David Muñoz-Rojas
Doctor, Laboratoire des Matériaux et du Génie Physique, UMR 5628 CNRS – Grenoblte

Dr Mariadriana Creatore, Vice Chairman
Professor, Eindhoven University of Technology (TU/e)

Abstract

Plasma-assisted approaches are broadly used in thin-film deposition, surface preparation and top-down fabrication. Particularly, plasma processes, which can operate at atmospheric pressure, have ensured the simultaneous synthesis and deposition of numerous thin film compositions that have met multiple applications. Yet, the wide variety of reactive species composing plasmas induces a non-negligible amount of side reactions that result in a lack of regularity in polymeric materials compared to the ones formed by wet chemical polymerisation processes.

The combination of ultrashort nanosecond plasma discharge ($t_{ON} \approx 100$ ns) and long plasma OFF-time ($t_{OFF} = 0.1 – 100$ ms), for the initiation and propagation of the free-radical polymerisation reaction, was recently demonstrated to yield the formation of conventional polymer layers. Based on the current understanding of the process, i.e. significance of the plasma pulse frequency, this thesis aims at gaining a deeper insight in the influence of other important parameters. The nanosecond pulsed plasma deposition of low dielectric constant insulating thin films is studied. Providing additional dimensions to the characterisation, the dielectric layer's properties such as the leakage current and the dielectric constant, allow to discriminate mechanisms that would not have been identified from other techniques. Hence, ensuring the further development of the fundamental understanding of the nanosecond pulsed plasma approach.

From the nanosecond pulsed plasma deposition reaction of different tetra-organosiloxane compounds, the growth mechanisms driving the formation of insulating polymer layers are elucidated. For vinylic monomers, the plasma-induced polymerisation is demonstrated to be highly favour over plasma-state polymerisation at low plasma pulse frequency. This yields the excellent retention of the monomer structure and the prevalence of surface reactions, which are essential to obtain remarkable insulating properties.

In addition to the significance of the monomer structure, the saturation ratio, i.e. the monomer partial pressure over its saturated vapour pressure (P_M/P_{sat}), is demonstrated as a key parameter of the thin film's growth. While low P_M/P_{sat} values result in the prevalence of gas phase reactions, excessively high P_M/P_{sat} values lead to the formation of poorly reticulated and leaky polymer layers, when operating at low plasma pulse frequency. As such, three different regimes of growth are identified: the monomer deficient regime, the competition regime, and the energy deficient regime. Optimisation of saturation ratio ensures the formation of smooth and conformal low dielectric constant insulating thin films.

Taking advantage on the understanding gained on the nanosecond pulsed plasma deposition of insulating polymer layers, the dielectric constant is tuned from the careful selection of the starting monomer compound. Several vinylic cyclo-siloxane and -silazane compounds are notably studied. Dielectric constant values as low as 2.8 are obtained from the monomer possessing the lowest polarisable bonds and the larger ring size, i.e. the 1,3,5,7-tetramethyl-1,3,5,7-tetravinylcyclotrisiloxane, while retaining a low leakage current density in the range of 10^{-9} A/cm^2 at 20 V.

Table of Contents

CHAPTER I ─ Introduction

This chapter aims at providing a detailed review on the atmospheric pressure plasma-initiated chemical vapour deposition (AP-PiCVD) of polymer-like thin films elaborated using an ultrashort pulsed plasma-enhanced chemical vapour deposition (PECVD) process. The current understanding of the AP-PiCVD method is surveyed through the analysis of the relationships between the growth mechanisms, chemical structures and functional properties of the resulting thin films.

Contents

I-1 Motivations

In organic field-effect transistors (OFETs), the key component for modern flexible electronic circuitry, the dielectric layer is in direct contact with the active layer (i.e. semiconducting layer) irrespective of the OFETs configuration.[1-3] Charge transport occurs in the first few molecular layers near the surface of the gate dielectric under the application of an electric field. Consequently, the gate dielectric has a strong influence on the charge transport in OFET devices, and high capacitance densities from the dielectric are essential to lower the power operation of electronic devices. Although using high dielectric constant (high-k) thin films to achieve high capacitance densities is a theoretically suitable option, high-k materials suffer from rather high leakage current and dipole disordering that affects the carrier mobility of the underlying semiconductor layer. On the other hand, low-k materials can be used taking note that the capacitance of a dielectric layer is inversely proportional to the thickness. Thus, ultrathin low-k layers provide a good alternative as gate dielectric.[2-6] Apendix 1 provides the definitions and these physical relationships.

I-1.1 Organosilicon Thin Films as Low-k Dielectrics

Among the various low dielectric constant (low-k) materials suitable for the preparation of dielectric thin films, silicon-based polymeric dielectrics have attracted a continuous attention. Owing to their chemical stability, bio and chemical inertness, heat resistance, insulating and mechanical properties, organosilicon films are used in a wide range of applications, including (bio)passivation,[7,8] corrosion protection of metals,[9,10] scratch resistance on flexible substrate[11] and gas barrier films.[12] For their integration in microelectronics, carbon doped silicon oxides (SiOCH) based coating have been widely studied as an interlayer dielectric (ILD) during the effort of reducing the dielectric constant in the back-end-of-line (BEOL, the part of the integrated circuits manufacturing process where the interconnects are made) .[13-15]

The reduction of materials dielectric constant can be achieved by reducing the polarizability using low polar bonds (e.g. C─C, C─H, Si─CH_3, etc.) and/or by reducing the density of the material by introduction of porosity, according the Clausius–Mossotti equation (I-1-1):

$$\frac{\varepsilon_r - 1}{\varepsilon_r + 2} = \frac{N}{3\varepsilon_0}\alpha \qquad \text{(I-1-1)}$$

Where ε_0 is the vacuum permittivity (ε_0 = 8.854 x 10^{-12} $F.m^{-1}$), ε_r (ε_r = k) is the material dielectric constant, N is the number of molecules (dipoles) per unit volume (density) and α is the polarizability, which is the sum of the electronic, ionic and orientation (or dipolar) polarizations.[16] One should note that reducing the density is mandatory to reduce the film's dielectric constant close to unity, i.e. close to the k value of air that fill the porous structure.[15-17] Doping of silica (SiO_2) by carbon (C), mostly in the form of Si─CH_3, induces the reduction of the bonds polarizability in the SiCOH while also providing additional free volume. This additional free volume results in the formation of constitutive porous films allowing the further decrease of the material dielectric constant. Among the other strategies to provide a constitutive porosity to the films, one can cite the cyclic precursor approach consisting on the use of cyclic precursors, i.e. decamethylcyclopentasiloxane (D5).[18] To further increase the self-organised free-volume in the thin films, the cyclic precursor approach can be combined to the carbon-bridging approach using cyclic compounds bearing pendant vinyl groups such as 1,3,5-trimethyl-1,3,5-trivinylcyclotrisiloxane (V3D3) and 1,3,5,7-tetramethyl-1,3,5,7-tetravinylcyclotrisiloxane (V4D4).[19-21] Another route to obtain low-k dielectric materials is the subtractive porosity approach (Figure I-1-1), which aims at forming porosity using an adequate thermal treatment (e.g. UV, thermal[22] or plasma post-treatment[23]). In addition to the multiplication of the processing steps, subtractive porosity approaches are detrimental to the mechanical properties of the films.[16,17,24,25] Moreover, the thermal treatment can restraint the choice of substrates.

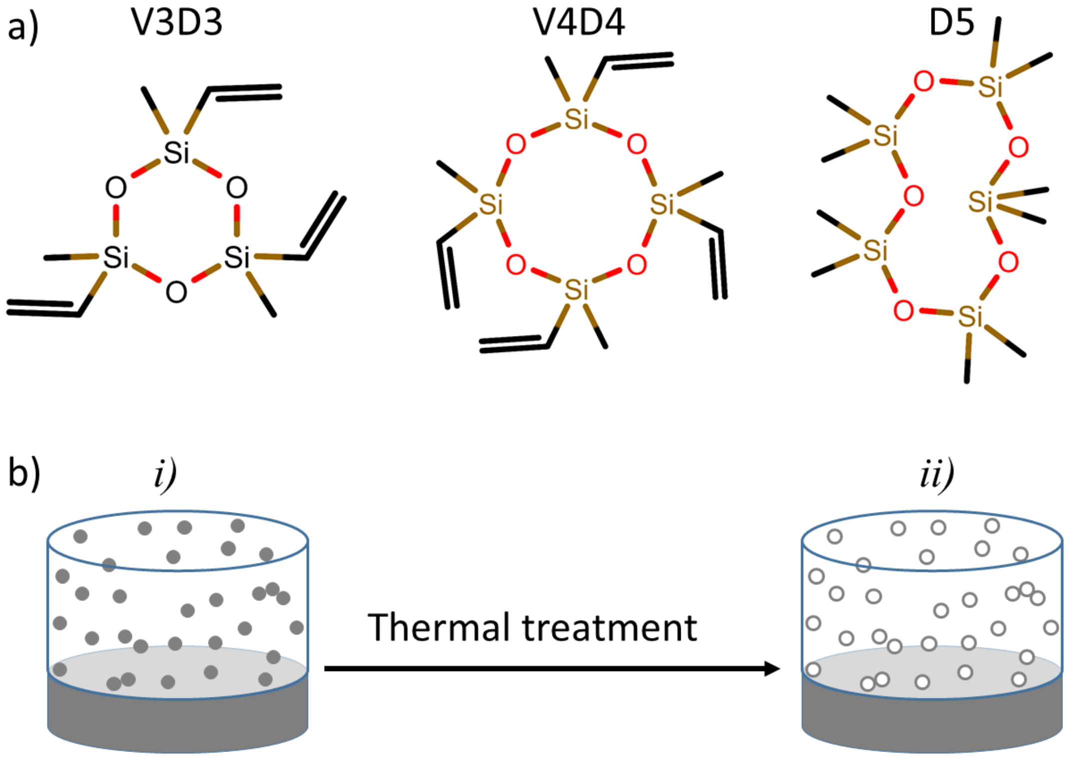

Figure I-1-1: a) Monomers used for the cyclic and the carbon-bridging approach. b) Schematisation of the substrative porosity process where (*i*) the matrix and the porogen (in gray) are co-deposited before (*ii*) being annealed to remove the porogen and creating pores.

To meet with the requirement of synthesizing ultrathin low-k layers and avoid any complication due to the de-wetting or post-thermal treatment, new vapour phase deposition methods have been developed for the production of ultrathin and pinhole free layers with good uniformity. Among the developed strategies, chemical vapour deposition (CVD) processes, including plasma-enhanced chemical vapor deposition (PECVD) processes, are widely used in the microelectronic sphere.

A huge variety of low or non-toxic organosilicon precursors are commercially available and affordable. A number of these organosilicon precursors are sufficiently volatile at room temperature and atmospheric pressure, making them appealing for CVD polymerisation.[26,27] Silicon oxycarbide films have notably been deposited from linear monomers such as methyldiethoxysilane,[23] 1,3,5-trivinyl-1,1,3,5,5-pentamethyltrisiloxane,[28] and cyclic ones such as octamethylcyclotetrasiloxane,[25] 1,3,5,7-tetramethyltetravinylcyclotrisiloxane,[19] 1,3,5-trimethyltrivinylcyclotrisiloxane[21] to obtain low-k materials. This short precursors' list is obviously non-exhaustive and several excellent reviews on the chemistry and the characterisation of organosilicon-based films are available in the literature.[13-16,26]

For films synthesized by CVD, the use of cyclic siloxane bearing polymerisable pendant groups (vinyl) promotes a better retention of the monomer's cyclic structure while ensuring the formation of highly cross-linked networks.[19,29] Notably, poly(1,3,5-trimethyltrivinylcyclotrisiloxane) has been demonstrated as good candidate for gate dielectric in organic field effect transistor (OFET) owing to their mechanical flexibility.[21]

I-1.2 Atmospheric-Pressure Plasma-Enhanced Chemical Vapour Deposition of Low-k Materials

PECVD approaches are drawing an ever-growing interest since they can be operated both under atmospheric-pressure (AP) and low-temperature conditions. Atmospheric-pressure plasmas are operated without using expensive vacuum-related equipment making them attractive cost-saving alternative to low-pressure plasmas.[30-32]

In addition, atmospheric plasmas can be generated using different configurations, e.g. plan-to-plan or torches. These features make AP-PECVD processes particularly suitable for the coating of large and unconventional substrate shapes and materials, including paper sheets or polymer fibres. Plan-to-plan dielectric barrier discharges (Figure I-1-2) are notably suitable for the roll-to-roll coating of various substrates, while micro plasma torches are suitable for the localized deposition, i.e. patterning, of functional thin films.[30]

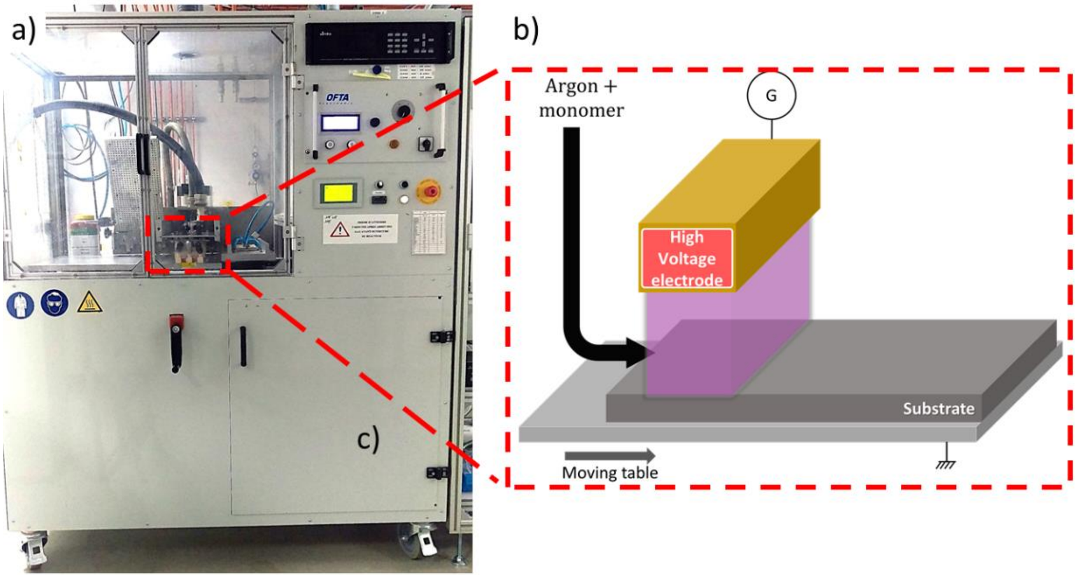

Figure I-1-2: a) Photograph and b) schematic representation of our plan-to-plan dielectric barrier discharges reactor setup.

Atmospheric-pressure plasmas are already implemented in the industry for several applications, e.g. adhesion primer coatings and barrier layers, and various commercial atmospheric-pressure plasma solutions are available, e.g. Molecular Plasma Group (www.molecularplasmagroup.com), Isytech Plasma (www.isytech-plasma.com), AcXys Technologies (www.acxys.com) and Plasmatreat (www.plasmatreat). In addition, research activities have extended the range of materials formed by AP-PECVD to a wide variety of transparent conductive thin films, crystalline transition metal oxide thin films, metallic thin films, organic and polymer thin films. As examples, works undertaken in parallel to this PhD thesis have yield the formation of highly conductive silver coatings inkjet printed on paper and highly transparent conductive polymer thin films on plastic foils.[33,34]

However, the numerous side reactions occurring in plasma-based processes obstruct the formation of regular polymer chains, leading to highly cross-linked materials called “plasma-polymers” presenting a chemical structure quite different from the starting organic monomer. To promote a better retention of the monomer functionality, pulsing the plasma discharge is a common approach which favours the occurrence of plasma-induced free-radical polymerisation that can persists over several tens of milliseconds during the plasma OFF-time (t_{OFF}) and afford a more chemically regular polymer layer. Yet, only few studies on the atmospheric plasma-enhanced chemical vapour deposition of low-k polymer thin films for gate dielectric applications have been reported to date, to the best of my knowledge.[2,35]

A recent approach called plasma-initiated chemical vapour deposition (PiCVD), combines ultrashort plasma pulses (t_{ON} < 100 ns) and plasma OFF-times in the range of the free-radical polymerisation lifetime (t_{OFF} from 1 to 100 ms), to yield the atmospheric-pressure synthesis and deposition of atomically smooth, conformal thin films with an unprecedented degree of polymerisation for plasma-enhanced and atmospheric-pressure CVD processes.[36] The approach, being relatively new, this thesis aims at gaining a deeper fundamental knowledge of the structure-property-processing relationships to enlarge the range of applications of the process by synthesising ultrathin low-k insulating layers.

I-2 Plasma-Enhanced Chemical Vapour Deposition

I-2.1 Plasmas

Plasma is an ionized gas which consists of electrons, photons, ions and neutrals in fundamental and excited states (Figure I-2-1).[32,37,38] The existence of charge carriers such as electrons and ions makes plasma electrically conductive. However, plasma is macroscopically electrically neutral due to the random directions taken by the generated free charged particles (electrons and ions).[32,38,39]

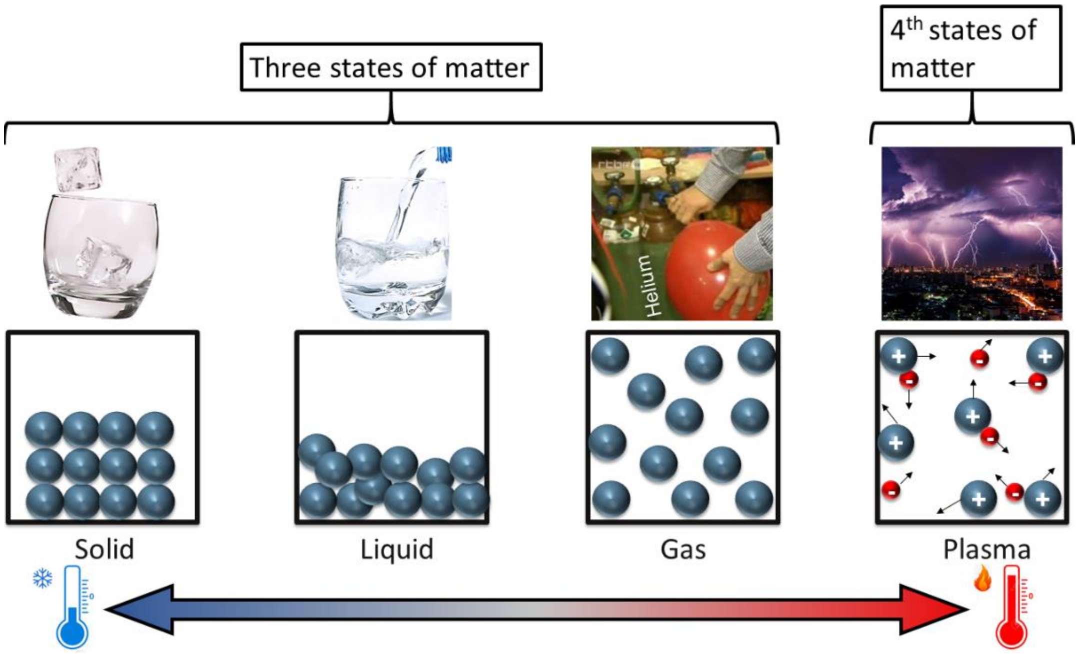

Figure I-2-1: Different states of matter.

Plasma, known as the fourth state of matter, can be generated by applying electromagnetic, thermal or electrical energy to gas. 99.9 % of the Universe is made up of plasma. The most common natural plasma observed on Earth are lightning and aurora borealis.[39] In laboratories, plasma is generally generated through application of electrical energy to a gas or a gas mixture that can contain precursor vapours or aerosol.

I-2.1.1 Classification of Plasmas

The different elements constituting plasma exhibit different densities and temperatures mainly depending on the configuration, pressure, type of energy supply and amounts of energy transferred to the plasma. Accordingly, plasmas are classified as thermal or non-thermal based on the temperatures of electrons, ions and neutrals.[32,39] Many books and reviews described the physics and the chemistry of thermal and non-thermal plasmas.[32,37-39] Hence, only a brief description of thermal and non-thermal plasma is introduced here.

In thermal plasma, also called hot plasma, electron and heavy particles, i.e. neutrals and ions, have almost the same temperature ($T_e \approx T_h \approx 10^4$ K) corresponding to a local thermodynamic equilibrium (LTE). Here, chemical reactions are governed by collisions and non-radiative processes.[32,39,40] In nature, thermal plasmas are found in the central part of lightning and the core of the sun.[39,41] In laboratories, systems like arc torches and electric arcs welding are used to generate hot plasmas which are suitable for pyrolytic processes and application in metallurgy for instance.[41]

On the other hand, non-thermal plasma, also called cold plasma, are weakly ionized plasmas where electron temperature ($T_e = 10^4$-10^5 K) far exceed that of heavy particles which are often close to room temperature (ca. $T_h \approx 200$-400 K).[32,38,39] This difference in temperature depends on the collision rates between plasma particles (i.e. electron-electron and electron-heavy particles). Only inelastic collisions from electrons to heavy particles allows the transfer of kinetic energy. Although resulting in excitation or ionization, these inelastic collisions do not raise the heavy particles temperature. Collision frequency of the plasma particles depends on the pressure (Figure I-2-2). As such, the non-equilibrium nature of cold plasmas are easily achieved at low-pressure (10^{-4} to 10^{-2} Torr), which are characterized by low atom densities yielding low collision rate among the particles.[32,38,41] Nevertheless, low-vapour pressure systems require expensive related vacuum equipment, directing a huge interest to non-equilibrium (cold) atmospheric pressure plasmas (APPs). However, it is challenging to generate non-equilibrium plasmas at atmospheric or higher pressures since collisions frequency among the plasma particles increase with the increase of pressure. This high collision rate favour the equilibration of temperatures between electron and heavy particles leading to arc formation and gas heating. [32,38,41]

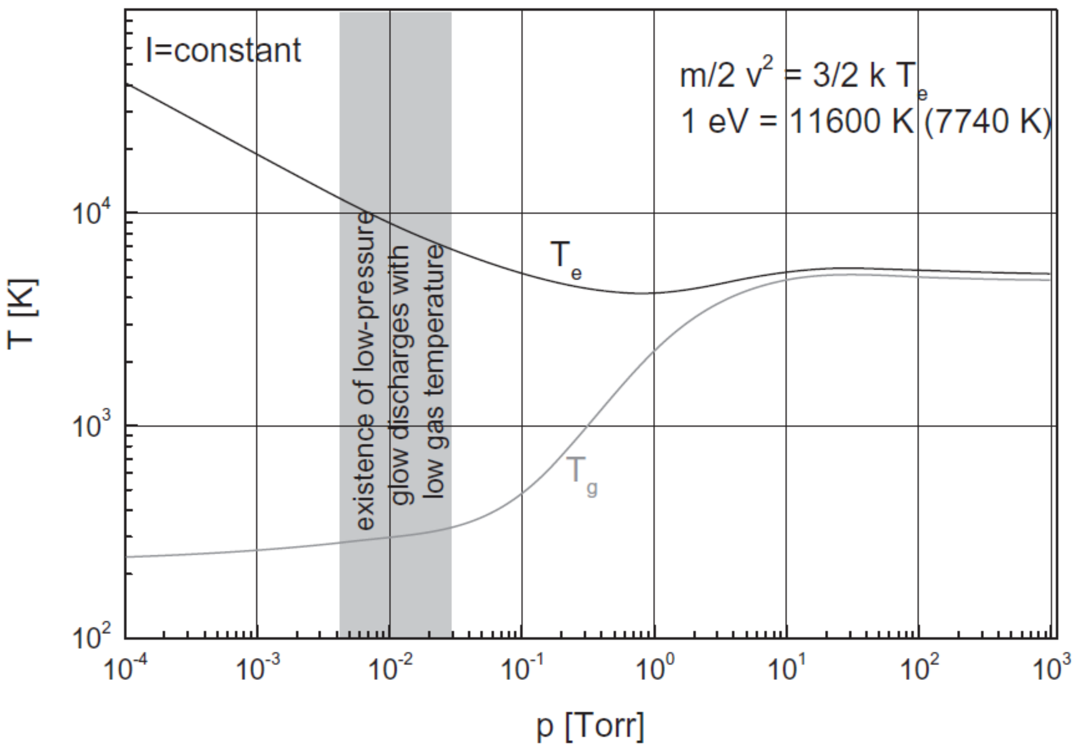

Figure I-2-2: General evolution of electrons and heavy particles temperature according to the pressure in glow discharges.[38] T_e and T_g are the electron and gas temperature (= heavy particle temperature) respectively. The higher the pressure, the shorter the difference between T_e and

T_h, due to the increase of of particles' collision frequency, resulting in plasma state close to the local thermodynamic equilibrium. Image taken from ref [38].

I-2.1.2 Generation of Cold Atmospheric Pressure Plasmas

The initiation of non-equilibrium plasmas is based on the development of electron avalanches.[31,42] In laboratories, plasma is ignited using high voltage sources to accelerate the existing charge carriers. The successive avalanche of free electrons to self-sustain the gas discharge is the main aspect of the Townsend-breakdown. This self-sustain or breakdown discharge occurs at a specific voltage, as studied by Paschen, corresponding to the gas used to produce the plasma.[31]

To maintain a non-equilibrium state at atmospheric pressure, special generation schemes are used to avoid gas heating and limit discharge current.[30,42] These generated schemes are adapted to the electrical excitation frequency used to produce non-thermal atmospheric pressure plasmas.[30,42]

For high frequency operations ($f > 1$ MHz), including radiofrequency (RF) and microwave (MW) discharges, the discharge is always virtually on. Hence, the current density should be lowered under 50 mA cm^{-2} to avoid the occurrence of gas heating.[42]

On the other hand, low frequency operation ($f < 1$ MHz) enables to limit the discharge duration and avoid gas heating by alternating the electrodes polarities (AC discharges) or by placing a dielectric material between the electrodes.[30,32,42,43] The latter approach is the most used for charge-limitation at atmospheric pressure plasmas leading to the production of stable glow discharge.[31] By adding the dielectric material (e.g. glass, quartz, ceramics, mica, Teflon) in series in the current path, the discharge is referred as dielectric barrier discharge (DBD). Several reviews reported the different existing electrodes arrangement.[30,31,41] In atmospheric pressure plasma DBDs, the discharge gap is usually in the range of 0.1-10 mm while the amplitude of the voltage necessary to sustain the discharge is in the range of 1-100 kV depending on the gas and the electrode gap dimension.[31]

The gas temperature in PECVD processes based on DBD can remain lower than 330 K opening the possibility to treat thermosensitive substrates. Moreover, the low electron density in atmospheric pressure glow DBD (~10^{11} cm^{-3}) combines to the ability of the electrons and ions to follow the oscillation of the electric field when operating at low plasma frequencies ($f < 1$ MHz) are responsible for the perfectly uniform discharge created over the electrodes. The lower energetic media of plasma when working at low-frequency compared to MW or RF plasma makes low-frequency plasmas more suitable for the formation of organic thin films where the retention of the chemistry is necessary.

In chemical vapour deposition (CVD), solid thin films are deposited on a substrate from the thermally activated chemical reaction undergone by a gaseous monomer in the gas phase. Plasma-enhanced chemical vapour deposition (PECVD) is a variant of CVD in which the plasma's reactive species (electron, ions, metastable, photons) are used to activate chemical reactions. The use of plasma enables the decrease of the deposition temperature in PECVD compared to thermal CVD methods, thus allowing the deposition on thermal sensitive substrates.[43-46] In addition, the reactive species in plasma can reach high energies (i.e. tens of eV), far above the bond dissociation energies of any organic or organometallic molecules. Hence, almost every molecule can react in PECVD and form a thin film. Thus, monomers in PECVD are not restricted to unsaturated compounds and the introduction of initiator species is not required.[30,42,43,46]

Similarly to CVD processes, chemical reactions in PECVD can occur both in the gas phase and at the substrate surface. Gas phase reactions leading to the formation of powdery depositions represent a crucial point to overcome when operating at atmospheric pressure PECVD (AP-PECVD). The amount of formed particle is higher in the case of filamentary discharge.[42] Hence, thin films obtained by surface reactions are often desired over thin films formed by gas phase reactions.

Surface reactions can occur either by the Langmuir-Hinshelwood or the Eley-Rideal mechanism where both involve the diffusion of reactant from the gas phase to the surface. In the former mechanism, (i) the reactants separately adsorbed on the surface before (ii) reacting while for the latter mechanism, a molecule from the gas phase (b-ii) collide and react with an adsorbed reactant (Figure I-2-3).[45]

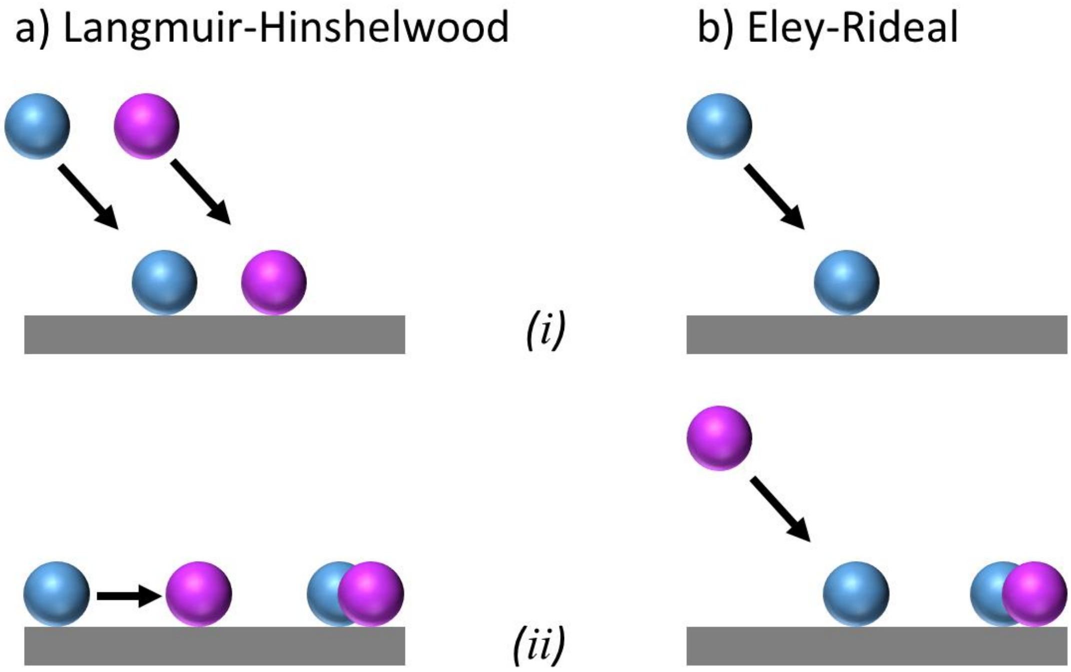

Figure I-2-3: (a) Langmuir-Hinshelwood and (b) Eley-Rideal mechanisms describing surface reactions between two reactants.

The uniform coverage of all the sides of a complex geometric substrate (e.g. trenched wafer) is termed as conformal coverage (Figure I-2-4). Conformal coatings are the result of a competition between vapour-phase reactants transport and surface reaction. Yet, conformality is best achieved when surface reaction rate is lower than gas phase diffusion rate.[45]

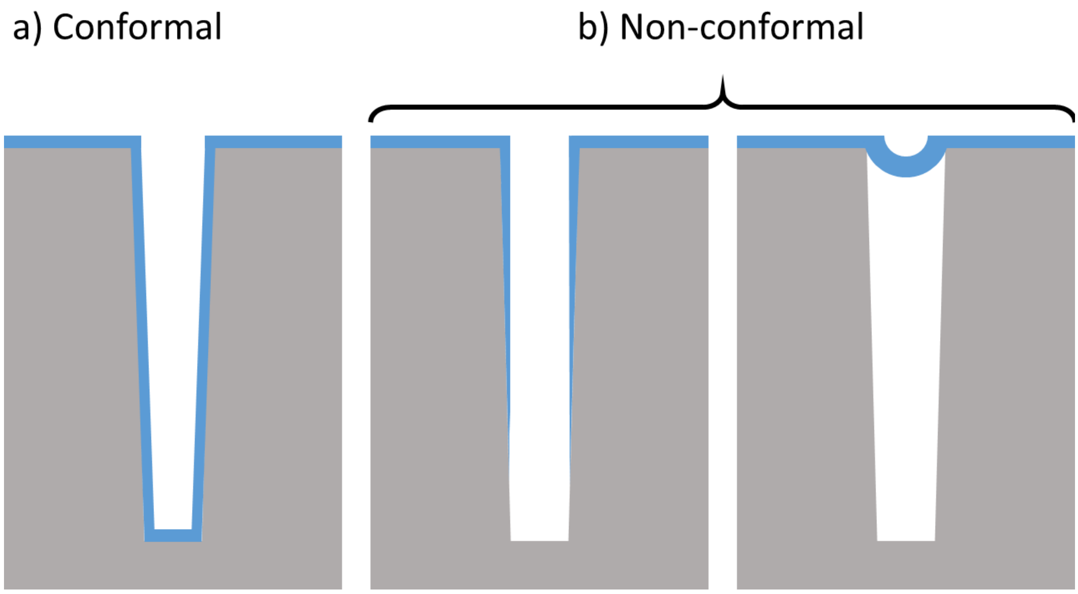

Figure I-2-4: Scheme of a)a conformal coating (blue) and b) non-conformal coating in a trenched wafer (gray).

I-2.2 Plasma Polymerisation

Plasma polymerisation can ensure the growth of thin films on various substrates from volatile organic monomers. However, plasma polymerisation significantly differs from conventional polymerisation. In particular, the numerous side reactions occurring during the plasma polymerisation of organic compounds obstruct the formation of regular polymer chains, leading to the formation of highly cross-linked thin films called "plasma-polymers".[14,44,47] These plasma-polymers exhibit an alteration of the chemical functionality required from the starting monomer. The extent of the monomer alteration during the plasma polymerisation depends on the PECVD conditions. Indeed, the retention of the monomer structure decrease with the increase of the energy input per molecule. This energy level is calculated using the Yasuda factor, that is, Y=W/FM, where W is the deposition power (discharge wattage in J/s), F is the monomer flow rate (mol/s) and M is the monomer molecular weight (g/mol). Based on the W/FM factor, Yasuda divided the materials formation in PECVD into two operating regimes,[44] which were later extended to three regimes,[48] that are: *(i)* the monomer-deficient regime, *(ii)* the competition regime and *(iii)* the energy-deficient regime (Figure I-2-5).

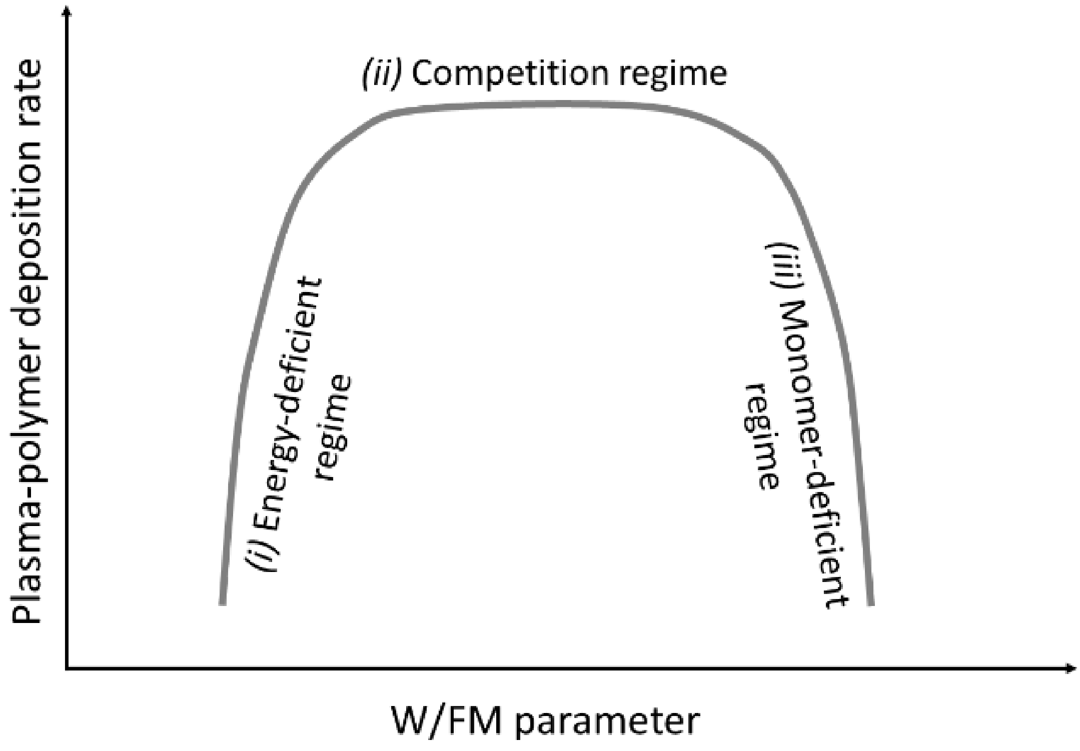

Figure I-2-5: The different regimes of plasma-polymer deposition. Adapted from Roualdes *et al.*[48]

The energy-deficient regime (also reported as the monomer-sufficient regime[48] or the monomer-rich regime[49]) is encountered in the case of low W/FM values where the power input is insufficient to create a sufficient amount of reactive species to ensure the reaction of a large proportion of the monomer molecules and their deposition in thin film form. In this region, the deposition rate increases with the increase of the W/FM (Figure I-2-5).

The competition regime corresponds to W/FM values for which the growth rate is maximum. In this region, the deposition rate is almost constant upon variation of W/FM.[48] The monomer-deficient regime (also reported as the power saturated domain[44] or the monomer-lean region[49]) is related to high W/FM. In this case, the deposition rate decrease with the increase of the W/FM due to the depletion of the monomer species.

Although the use of Yasuda parameter has been a subject of controversies when applied to atmospheric plasma polymerisation,[50-54] the deposition rates and the chemical compositions of atmospheric deposition plasma polymerisation reactions more than often comply with the Yasuda observations at low pressure.[55]

The ever growing interest to correlate the processing-property-structure relationships with the energy transferred to monomer’s molecules has mainly be involve in the evaluation of the W/FM value. This could enable comparison of data from different laboratories and particularly to have an insight on the mechanism undergone by a same monomer deposited at low pressure or at atmospheric pressure plasma using different reactor configurations.[49,55-57] If a thorough understanding and the accurate determination of the energy consumed per monomer molecules should enable to develop the knowledge on the growth mechanism of organic thin films elaborated in plasma polymerisation, better retention of the monomer functional group is systematically reported using unsaturated monomers.[44,49,58,59] In the presence of unsaturated bonds, the plasma polymerisation reaction is always attributed to the competition of two mechanisms: (i) plasma-state polymerisation and (ii) plasma-induced polymerisation.

I-2.2.1 Plasma-State Polymerisation

Plasma-state polymerisation is dominated by gas phase reaction (i.e. fragmentation, recombination) which occurs only under plasma conditions.[60-62] It is similar to atomic polymerisation and occurs predominantly for high W/FM values, hence encountered in the monomer-deficient regime. In plasma-state polymerisation, the monomer molecules are extensively fragmented into individual atoms and small fragments, which then recombine randomly into a highly cross-linked structure.[47,55,60,63]

I-2.2.2 Plasma-Induced Polymerisation

Plasma-induced or plasma-initiated polymerisation is assimilated to free-radical polymerisation where the polymerisation of polymerisable monomers (vinylic, triple bond, acrylic, cyclic monomers) is initiated by radicals produced under plasma exposure. Hence, conversely to plasma-state polymerisation, the chemical structure of the resulting thin film is expected to be more chemically regular.[38,47] Yet, the occurrence of plasma-state polymerisation as a side reaction cannot be neglected.

I-2.2.3 Fostering Plasma-Induced Polymerisation over Plasma-State Polymerisation

To overcome the limitations of plasma polymerisation of organic compounds and ensure a better control of the thin film chemistry, pulsed-plasma methods were developed to favour plasma-induced polymerisation over plasma-state polymerisation. Under pulsed conditions, reactive species are created periodically during the plasma ON time (t_{ON}). While the short lifetime reactive species rapidly disappear (i.e., ions, electrons and photons), the created polymerisation-initiating species can either recombine or initiate a free-radical polymerisation reaction during the following plasma OFF time (t_{OFF}). Hence, promoting a higher selectivity of the reaction and ensuring the growth of a more chemically regular plasma polymer.[38,62] Yet, the role of the penning ionisation should not be completely neglected at atmospheric pressure.[42,43] Penning ionisation is a process involving the reaction of neutral species with an excited metastable in the gas phase.

The composition of a plasma polymer elaborated under pulsed PECVD conditions depends on the ratio of plasma ON and OFF times, usually reported in term of the duty cycle (DC) which is defined as:

$$DC = \frac{t_{ON}}{t_{OFF} + t_{ON}} \qquad \text{I-2-1}$$

The duty cycle basically represents the percentage of time during which the plasma in on. The equivalent average power (<P>) delivered during plasma ON cycle is given by:

$$< P >= DC \times P_{peak} \qquad \text{I-2-2}$$

where P_{peak} is the peak power delivered during the plasma ON time. Consequently, decreasing the DC ultimately results on the decrease of the average power allowing a better retention of the monomer functional group during the deposition. Klages *et al.* have notably demonstrated the link between the retention of the monomer structure with the increase of the plasma-OFF time (with $0 \leq t_{OFF} \leq 180$ ms) while keeping the plasma ON-time constant to $t_{ON} = 1$ ms. Although the frequency at which they were working was not reported, this huge decrease of the duty cycle (through the increase of the t_{OFF}) resulted on 80% retention of the epoxy group of the used glycidyl methacrylate monomer for t_{OFF} longer than 9 ms.[64]

Beyond, several studies have shown that films produced at the same DC but employing different durations of t_{ON} and t_{OFF} yielding different pulse widths results in different thin film compositions and deposition rates.[62,65,66] Irrespective of the t_{OFF}, employing long plasma t_{ON} usually results in the formation of thin films showing similar characteristics to those achieved under continuous wave (CW) condition (Figure I-2-6). On the other end, employing excessively long t_{OFF} does not necessarily enhanced the retention of the monomer functional properties and rather have a negative impact on the morphology of the resulting film.[62,65,66] Consequently, the prevalence of the plasma-induced free-radical polymerisation mechanism over the plasma-state polymerisation, depends on the structure of the starting monomer and the conditions of the plasma discharge.

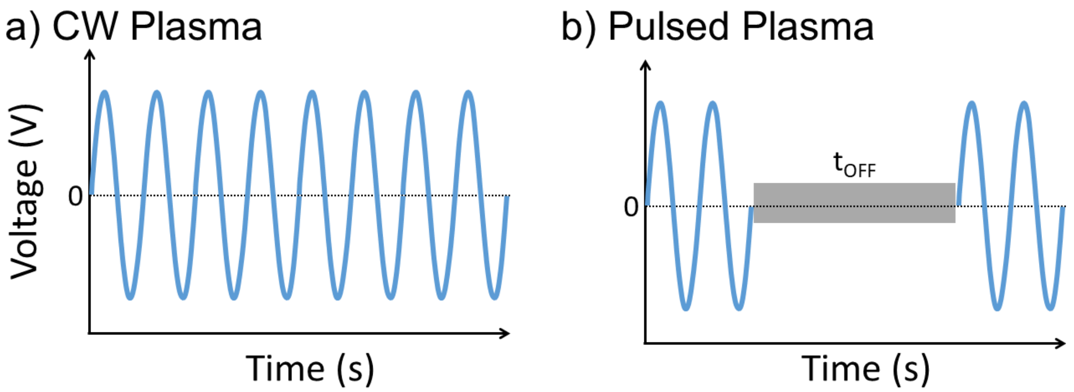

Figure I-2-6: Schematic representation of the applied voltage in continuous wave and pulsed low frequency dielectric barrier discharge processes.

Yasuda's early works highlighted the impact of the monomer structure on the deposition rate in plasma polymerisation. By measuring the hydrogen yield, hydrocarbon monomers were classified into three major groups allowing by extent to cover the behaviour of other organic compounds. Hence, the plasma polymerisation behaviour of organic compounds are categorised in four groups according to the structure of monomers: "group I" is comprised of compounds containing triple bond(s), aromatic or heteroaromatic structures; "group II" comprised of compounds containing double bond(s) and/or cyclic structures; "group III" comprised of saturated hydrocarbons and "group IV" which is comprised of the oxygen containing compounds such as carbonyl, ether, carboxylic acid.[44,60,61] The reactivity of the latter group has been extensively investigated through the use of methacrylate and allyl methacrylate monomers (family of esters compounds, Figure I-2-7). An increase of the growth rate (in nm•s^{-1}) of these methacrylate-based thin films and the better retention of the monomer structure during their AP-polymerisation was notably reported with the increase in the number of unsaturation of the starting monomer.[49,58,67]

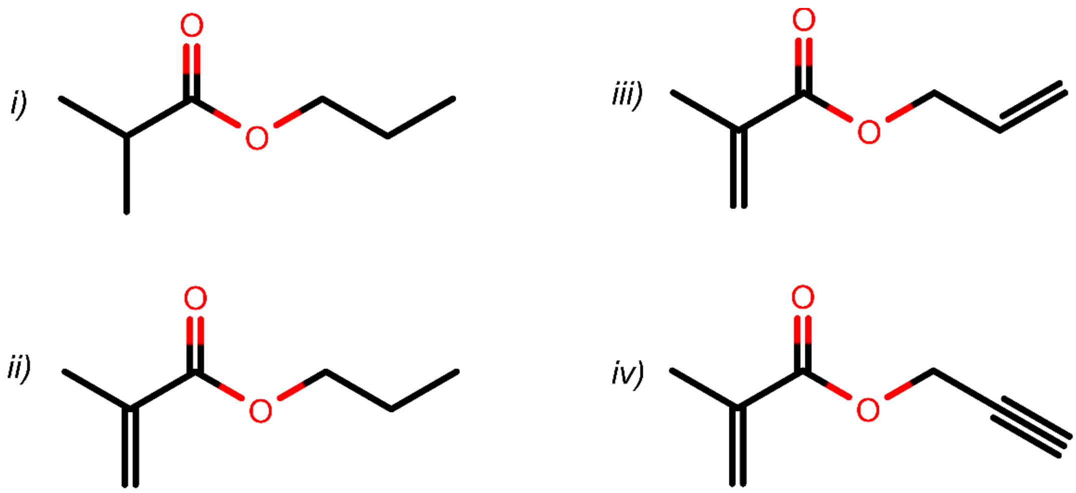

Figure I-2-7: Example of studied organic compounds from group IV. i) propyl isobutyrate, ii) n-propyl methacrylate, allyl methacrylate and iv) propargyl methacrylate.[56,58]

Nisol *et al.* notably investigated the influence of the monomer structure, through the use of five different esters (i.e. methyl methacrylate; propyl isobutyrate; n-propyl methacrylate; allyl methacrylate and propargyl methacrylate), on their respective reactivity in plasma using a low-frequency generator at a constant frequency of 20 kHz.[49] Owing to their developed method to measure the energy absorbed per molecule (E_m in eV), they reported the necessity of a higher E_m to obtain a total breakdown of the molecule bonds from unsaturated compounds, especially when the molecule presented a number of unsaturation higher than three such as for allyl methacrylate and propargyl methacrylate. In addition, by following the trend of the energy per molecule (E_m) with the increase of the monomer flows (F_d), they identified two regime of growths from their resulting thin films, i.e. the monomer lean and rich regions. Despite the reported better retention of the ester group with the increase of the number of unsaturation, no major changes in the chemical structure of the resulting thin films investigated by FTIR, was observed with the decrease of the monomer flow in the monomer rich region. However, they reported the formation of rough surface morphology indicating the rather preponderance of gas phase reaction when using their plasma conditions. Yet, the authors attributed this formation of powder to the high reactivity of allyl methacrylate.

Using a duty cycle (DC) of 45 % at a frequency f =7 kHz, Scheltjens *et al.* also reported a better retention of the monomer structure from the AP-polymerisation of allyl methacrylate compared to its saturated analogue propyl isobutyrate.[58] Unfortunately, the values of the plasma-OFF and ON time were not reported. Following the evolution of weight rate ($g \cdot m^{-2} \cdot s^{-1}$) with the increase of the plasma power, they also managed to identify the monomer-deficient and energy-deficient regimes. However, all their resulting thin films were reported to present a non-sticky oily morphology. This was assuredly due to the occurrence of an excess of termination mechanisms leading to the formation of short oligomers. The presence of these short oligomer chains was notably highlighted owing to the analysis of their thermal properties.[58]

In 2012, Coclite and Gleason investigated the benefit of free-radical forming species on the PECVD reaction of vinyl compounds. In particular, the method, called initiated PECVD (iPECVD), involves the use of an initiator with a weak peroxide bond (i.e. *tert*-butyl peroxide) to deposit to form more regular plasma-polymers from organosiloxane compound (i.e. 1,3,5-trivinyl-1,1,3,5,5-pentamethyltrisiloxane).[28] Although being a MW plasma, the plasma density delivered by the process was as low as 0.07 $W \cdot cm^{-2}$ owing to the large surface area of the electrodes used. Hence, the process takes advantage of this low plasma density to activate a low energy activated initiator, while promoting the retention of the monomer structure. A 10-fold increase of the deposition rate of the thin films deposited by iPECVD was reported compared to those deposited by the conventional initiator-free PECVD process using the same deposition conditions.[28] However, due to the short lifetime of the free-radical species under atmospheric pressure conditions, iPECVD is operated under vacuum conditions. Moreover, the continuous discharge used still presented a detrimental effect on the chemical structure of the resulting thin films.

I-3 Nanosecond Pulsed Plasma for the Atmospheric-Pressure Plasma-Initiated Chemical Vapour Deposition of Polymers

In 2015, Boscher *et al.* developed an atmospheric-pressure plasma deposition approach that combines ultra-short plasma pulses (t_{ON} < 100 ns) and long plasma OFF-times (t_{OFF}) for the initiation and propagation of the free-radical polymerisation reaction, respectively.[68] The approach, called atmospheric-pressure plasma-initiated chemical vapour deposition (AP-PiCVD) was implemented in an atmospheric pressure DBD reactor with high-voltage square-wave pulses that generate two distinct ultrashort current discharges (ca. 100 ns) at the voltage rising and falling edges (Figure I-3-1 a). The ultrashort plasma pulses repeated at a low frequency enable to reduce the undesired plasma side effect reactions. As a result, AP-PiCVD displays strong similarities with the initiated CVD (iCVD) process presented later in this thesis, by affording the formation of smooth and conformal thin films with an excellent retention of the functional group, highlighting the prevalence of free-radical mechanisms over plasma state polymerisation under these conditions (Figure I-3-1 a,b).[36-68] In particular, the significance of ultrashort plasma pulses (t_{ON} < 100 ns) over pulsed radio-frequency plasma discharges was demonstrated. Indeed, films produced at the same DC but employing different plasma pulses duration resulted in different growth rate (expressed in $nm \cdot s^{-1}$) and different film compositions. In a more informative way and to define the different mechanisms taking place during the plasma deposition process, the growth rates were plotted as thickness increment per discharge cycle ($t_{ON} + t_{OFF}$) for both nanosecond plasma pulses and pulsed radio-frequency plasma discharges (Figure I-3-1 c, d).[62,65,68] In contrast to pulsed radio-frequency plasma discharges, ultrashort plasma pulses allow the use of DC as low as 0.01 % (and even below in recent studies) while keeping t_{OFF} in the millisecond range. This results in both higher growth rates and better retention of the chemical functions for the films elaborated by AP-PiCVD.

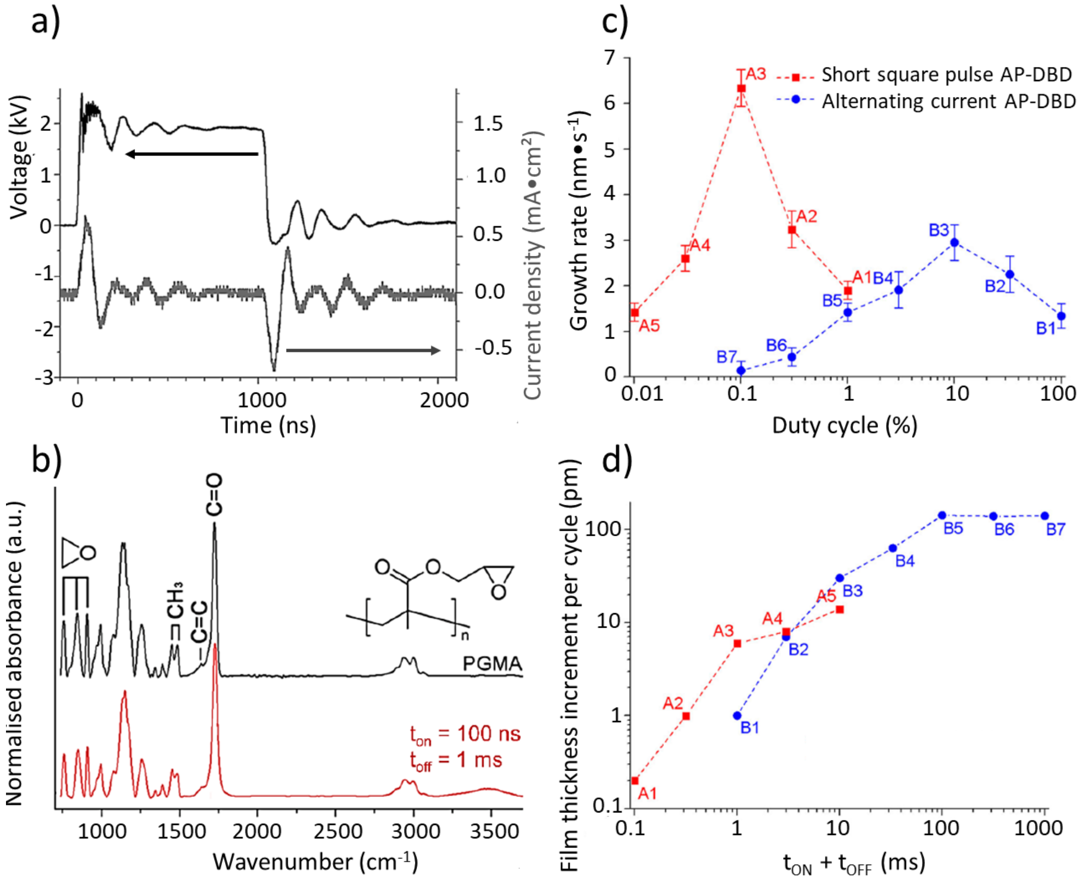

Figure I-3-1: (a) Traces of the high voltage pulse giving rise to ultrashort current discharges (ca. 100 ns). (b) FTIR spectra of a conventionally polymerised poly(glycidyl methacrylate) and a glycidyl methacrylate-based thin film formed using 100 ns plasma discharges (t_{ON}) and 1 ms OFF time (t_{OFF}). (c) Growth rate per second according to the duty cycle and (d) thickness increment per discharge cycle (t_{ON} + t_{OFF}) for the films prepared from GMA using nanosecond plasma discharges (red) and pulsed radio-frequency plasma discharges (blue). Data adapted from Boscher *et al*.[68]

I-3.1 Applications covered by AP-PiCVD

The potentiality of the AP-PiCVD process has been illustrated through the preparation of several functional coatings that are reported in the following sections.

I-3.1.1 Fire Retardant Polymer Thin Films

The AP-PiCVD reaction of the diethylallylphosphate (DEAP) monomer provided fire retardant properties to a sensitive bio-based cellulosic substrate (textile).[69] The fire retardant properties were attributed to the excellent retention of the monomer structure that was shown to undergo a conventional free-radical polymerisation pathway by mass spectrometry.[69] In particular, the P─O─C bonds of the resulting poly(DEAP) coating yield the formation of chars upon heating.

The AP-PiCVD principle, implemented in an atmospheric pressure dielectric barrier discharge (AP-DBD) configuration known to enable the treatment of large surfaces,[70] was applied to large cotton fabrics. Importantly, the efficient combination of ultrashort plasma ON-time and long OFF-time (in the range of free-radical polymerisation lifetime under these conditions), allow to circumvent the heating of the substrate and prevent any damage.

The effective fire protection conferred to the textile was also attributed to the conformality of the poly(DEAP) coating on the fabric fibres. Conformality was illustrated by the hollow shape of the chars formed after the burn test (Figure I-3-2).[69]

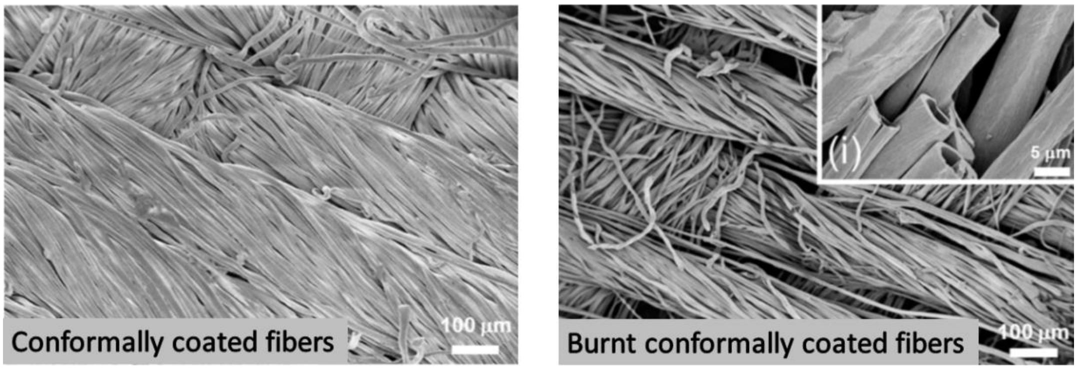

Figure I-3-2: SEM images of cotton fibres conformally coated by the AP-PiCVD poly(diethylallylphosphate) thin film (left) before and (right) after the burning test. The hollow shape of the chars formed upon heating illustrates the conformal nature of the poly(DEAP) coating. Data adapted from Hilt *et al*.[69]

I-3.1.2 Adhesion of Biomolecules

The epoxy-rich layers afforded by the AP-PiCVD reaction of GMA has been used for the immobilization of two different enzymes, i.e. laccase and *β*-lactamase, allowing the functionalisation of a bioactive surface layer, which ensured antibiotics degradation (Figure I-3-3).[71] In particular, the authors took advantage of the AP-PiCVD method to prepare poly(GMA) thin films with an optimal epoxy groups concentration, such as illustrated by FTIR (Figure I-3-1 b) to covalently bind enzymes to the surface. In agreement with previous studies,[72] the immobilised enzyme have shown a better enzymatic activity compared to their free form in solution. It is noteworthy that during the water erosion test performed over six days at a flow rate as high as 30 km•h^{-1}, no loss of antibiotics degradation activity was observed. This observation indicated that no delamination occurred due to the good adherence of the AP-PiCVD layer.[71]

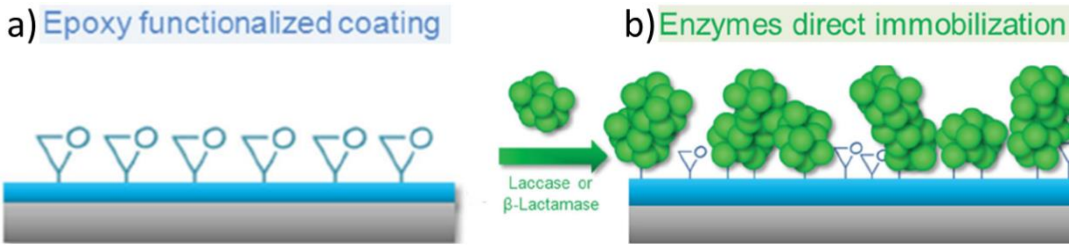

Figure I-3-3: Scheme of (a) the AP-PiCVD epoxy-rich coating and (b) the grafted enzymes, i.e. laccase and β-lactamase, through covalent bonding. Data adapted from Bonot *et al*.[71]

I-3.1.3 Thermoresponsive Polymer Thin Films

The AP-PiCVD reaction of N-vinyl caprolactam (NVCL) monomer enabled the formation of thermosresponsive thin films. The formation of true PNVCL homopolymer chains being essential to achieve thermoresponsive properties, the work reported by Loyer *et al*. provides the best demonstration of the capability of the PiCVD principle.[73] In accordance with the water-solubility of the PNVCL homopolymers synthesised from solution-based approaches, the PNVCL homopolymer thin film was soluble in water resulting in a completely transparent solution at room temperature. Interestingly, the PNVCL solution became cloudy (or turbid) upon heating, which is a typical behaviour of polymers obtain from NVCL,[74-75] due to the coiling of the polymer at high temperature (bottom and upper inset images of Figure I-3-4 a),[73] reducing the water solubility of the PNVCL chains. The temperature-responsive property afforded by the PNVCL homopolymer was attributed to the good retention of the monomer structure confirmed by mass spectrometry analysis, owing to the prevailing occurrence of free-radical polymerisation. SEC analysis of the films grown from NVCL at low plasma pulses shows an average molecular mass (M_w) of the PNVCL chains of 4,100 g·mol^{-1}.

The temperature at which the PNVCL homopolymer solution undergoes a phase transition is called a lower critical solution temperature (LCST).[76] In their study, the LCST was monitored by measuring the absorbance of the PNVCL solution using UV–Vis spectroscopy which allowed to observed a sharp transition around 40 °C in the range of values interesting for biomedical applications,[73] similar to their counterpart synthesized from wet chemistry methods.[74,77]

With the aim of synthesising water-stable PNVCL-based thin films, the potential of AP-PiCVD to form copolymer, through the successful copolymerisation of NVCL with EGDMA, was reported for the first time.[73] Ethylene glycol dimethacrylate (EGDMA) monomer was selected as a cross-linking agent due to its biocompatibility and potential to form water-stable thin films. The optimal ratio of the two monomers was determined to effectively combine the respective functionalities of NVCL and EGDMA. The as-deposited poly(NVCL-co-EGDMA) thin film elaborated with a low amount of EGDMA, i.e. 99.4 %:0.6 % equated to NVCL:EGDMA, exhibited excellent thermoresponsive properties but was demonstrated to be water-soluble after 30 minutes immersion in water. On the other hand, the use of high amount of EGDMA systematically resulted in water-stable thin films but with limited thermoresponsive properties. Interestingly, the as-deposited poly(NVCL-co-EGDMA) thin film composed of NVCL:EGDMA molar ratios of 98.5 %:1.5 % demonstrated both excellent thermoresponsive properties and an excellent chemical stability, including the retention of its smooth morphology even after soaking in water. Owing to the water stability of the AP-PiCVD poly(NVCL-co-EGDMA), their thermoresponsive properties were assessed by measuring their water contact angle from 7°C to 65°C. Unsurprisingly, their optimal poly(NVCL-co-EGDMA) composed of NVCL:EGDMA molar ratios of 98.5 %:1.5 % displayed a LCST of 27.6°C, several degrees lower than PNVCL homopolymer layers.[73] Indeed, the introduction of hydrophobic co-monomers is known to induce the decreases of LCST.[75] Notably, the presence of EGDMA within the thin film was evidenced by FTIR which displayed the peak related to ester C(O)O at ca. 1732 cm^{-1} and ether COC group at ca. 1169 cm^{-1} and 1040 cm^{-1}, well separated to the NVCL's characteristic functions that is the lactam group $(N{-}C{=}O)_{ring}$ located at ca.1620 cm^{-1}.[73] Subsequently, the thermoresponsive properties of the water-stable poly(NVCL-co-EGDMA) layers was demonstrated for anti-biofouling applications (*Figure I-3-4* b).[78]

Overall, these proof-of-concept studies illustrate the significance of combining the nanosecond plasma discharges and long plasma OFF-time (1-100 ms), on the resulting chemistry and properties of AP-PiCVD coatings. Notably, by simply using a co-monomer, thermoresponsive thin films LCST value was easily tune opening a new route toward chemical vapour deposition of other functional homo and copolymers. In addition, the conformal nature of the PiCVD process makes it appropriate for the coverage of 3-dimensional structures, which is highly desirable for the preparation of functional devices such as sensors and transistors.

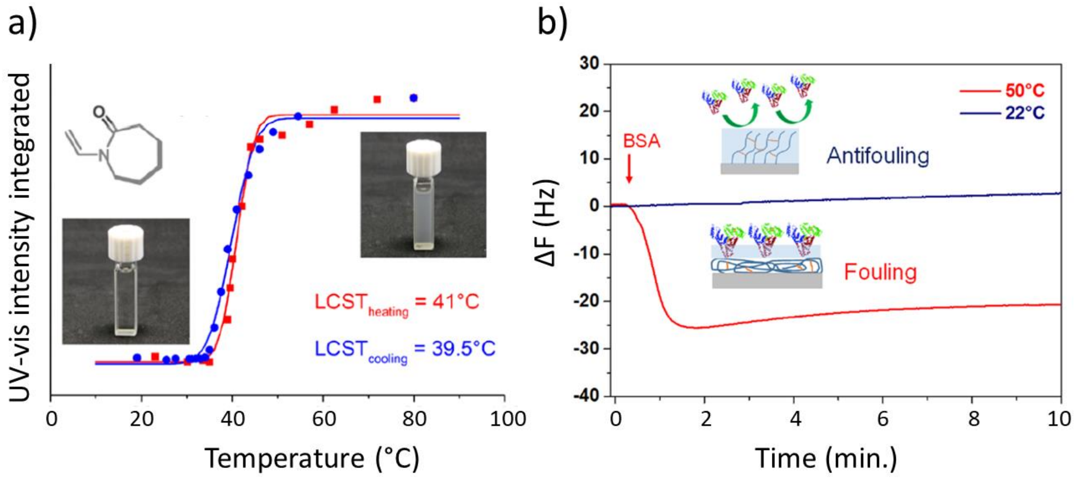

Figure I-3-4: a) UV−vis absorbance spectra of the AP-PiCVD PNVCL homopolymer layer performed at different temperatures. Data adapted from Loyer *et al*.[73] b) Changes in frequency of QCM-D sensors coated with p(NVCL-co-EGDMA)- after a bovine serum albumin (BSA) injection at 22°C and 50°C. The inset schemes depict the BSA-coated surface interactions. Data adapted from Moreno-Couranjou *et al*.[78]

I-3.2 Principle and Important Parameters in AP-PiCVD

The AP-PiCVD principle relies on the combination of ultrashort plasma pulses and long plasma OFF-times to initiate a free-radical polymerisation reaction while minimizing the negative impact of plasma on the resulting polymer thin film chemistry. Therefore, the plasma pulse repetition frequency was identified as an important parameter and thorough investigations were performed to gain insight on its impact on the mechanisms driving the atmospheric-pressure plasma-initiated chemical vapour deposition process. From the analysis of this precedent investigations and the existing knowledge on iCVD and PiCVD, this thesis hypotheses the existence of other parameters, such as the monomer structure or monomer saturation ratio, as important parameters. Hence, this thesis develops a deeper understanding of the structure-property-processing relationship, notably in the perspective to extend the range of applications covered by AP-PiCVD (Table I-3-1).

I-3.2.1 Frequency of the Nanosecond Pulsed Plasma Discharges

Since the ultrashort current discharge, representing the duration of the plasma ON-time (t_{ON}), occurs at the voltage rising and falling edges, the duration of the plasma t_{OFF} is determined by the plasma pulse repetition frequency of the high voltage square-wave pulses (Figure I-3-5).

Optical emission spectroscopy (OES) measurements confirmed that plasma discharges were only created at the high voltage rising and falling edges, giving rise to two current discharges lasting ca. 100 ns. The current oscillations following these two current discharges are attributed to parasitic capacitive coupling from the circuit intensified by the fast voltage variations. Owing to the wide range of frequency covered by the process, a large range of duty cycle (DC = $t_{ON}/(t_{ON} + t_{OFF})$, from 0.0001 % to 0.1 %, can be investigated by tuning the plasma OFF-time (t_{OFF}) from 100 ms to 100 µs, which can be simply achieved by varying the plasma pulse frequency between 10 Hz and 10,000 Hz.

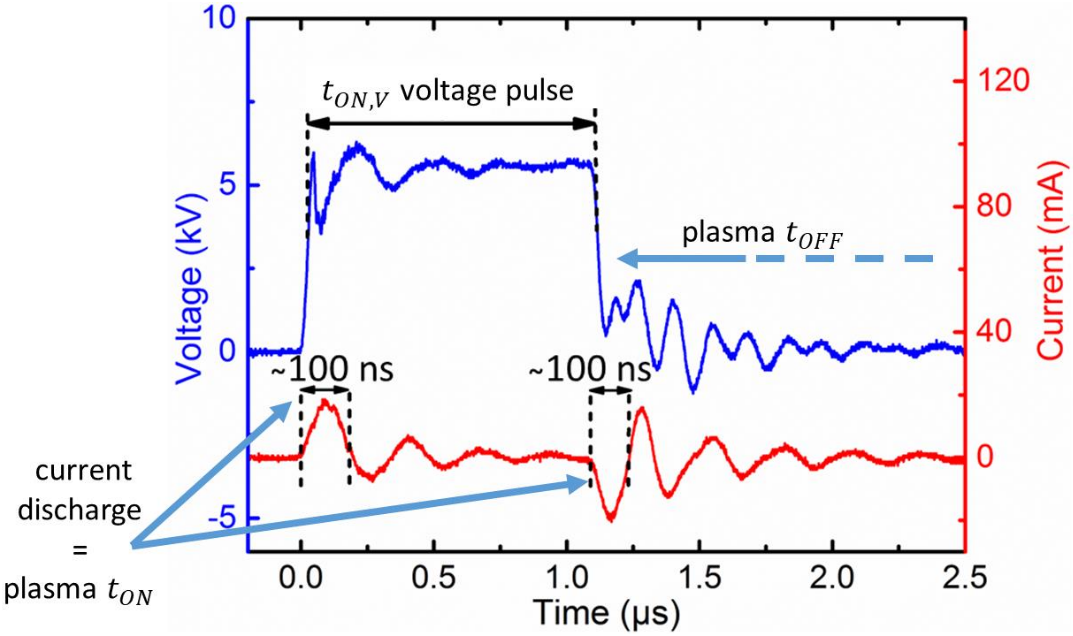

Figure I-3-5: Traces of the I-V curves used for the atmospheric-pressure plasma initiated chemical vapour deposition (AP-PiCVD) of polymer and plasma thin films. The ignition of plasma ultrashort high-voltage square-wave pulse (blue curve) results in the creation of two current discharges lasting ca 100 ns (red curve). These current discharges represent the time when the plasma is ON (t_{ON}).

As such, Loyer *et al*. studied the AP-PECVD reaction of the three methacrylate monomers (MMA, BMA and GMA, Table I-3-1) at different ultrashort plasma pulse frequencies and investigated the impact on the growth rate, morphology and chemistry of the resulting films.[36] One should note that all the methacrylate monomers were investigated using comparable partial pressures (P_M) in spite of their different saturated vapour pressure (P_{sat}) ranked as followed: $P_{sat}^{MMA} > P_{sat}^{BMA} \gg P_{sat}^{GMA}$. Unsurprisingly, an increase of the growth rate with the increase of the plasma pulse frequency was first observed (Figure I-3-6). Indeed, the increase of the frequency is known to lead to the increase of the reactive species that yield an increase of the deposition rate.[68] However, a collapse in the growth rate of films obtained from BMA, GMA and NVCL was observed for the highest plasma pulse frequencies contrary to films obtained from MMA (blue arrows in *Figure I-3-6*).[36,73] This collapse hinted on the occurrence of different growth mechanisms during the AP-PECVD of the methacrylate monomers using ultrashort plasma pulses. This collapse observed in the growth rate of BMA, GMA and NVCL-based thin films was mainly attributed to the different sensitivity of the monomers toward plasma. Nevertheless, the influence of the monomer saturation pressure (P_{sat}), monomer partial pressure (P_M) and thus the monomer saturation ratio (P_M/P_{sat}) on the growth mechanisms, should not be neglected.

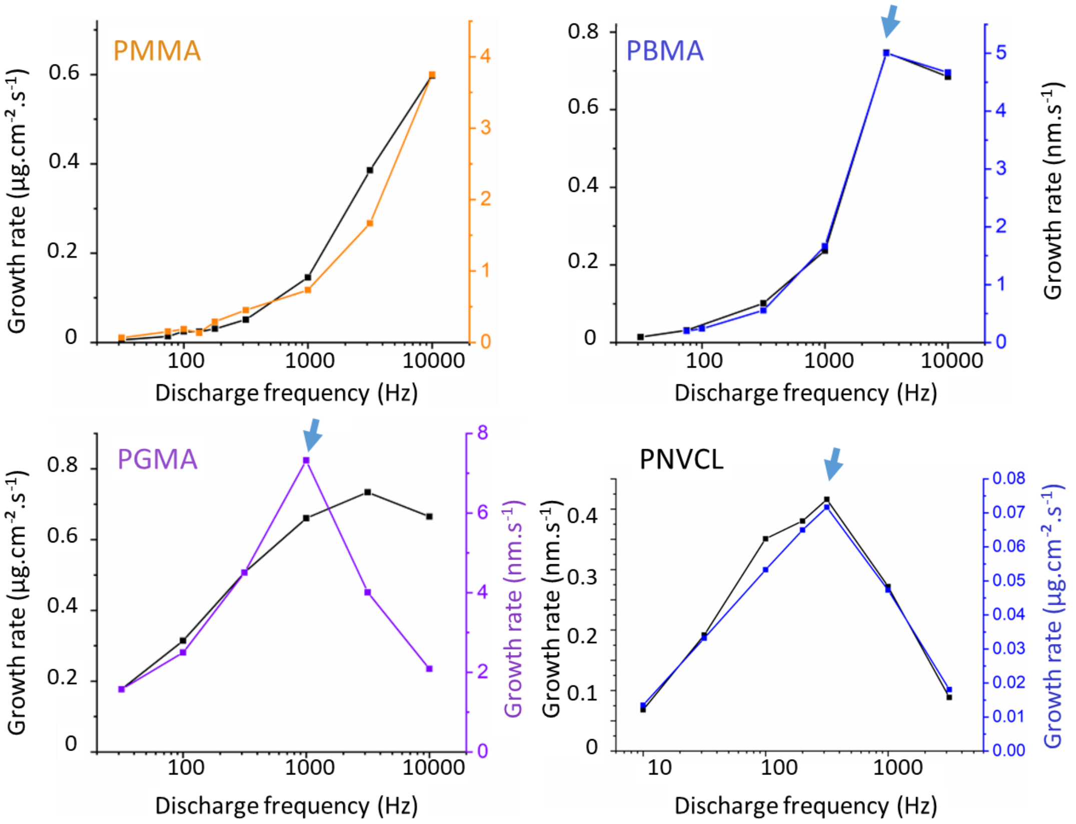

Figure I-3-6: Growth rates per second according to the plasma pulse frequency for the films grown from MMA, BMA GMA and NVCL. The change of the curve's tendency in the case of PGMA is due a change of density for $f \geq$ 1kHz.The blue arrows show the point after which a collapse of the growth rate is observed. Data adapted from Loyer.[79]

To have a clear view on the different mechanisms that were taking place during the nanosecond plasma deposition process, the growth rate was plotted as thickness increment per discharge cycle ($t_{ON} + t_{OFF}$, with t_{ON} being kept constant). As a reminder, the highest frequencies results on the shortest plasma t_{OFF} and hence the shortest cycle duration ($t_{ON} + t_{OFF}$). Irrespective of the methacrylate monomers, higher thickness increments per t_{ON} + t_{OFF} cycle were observed for longer t_{OFF} highlighting the occurrence of deposition reactions during t_{OFF} (Figure I-3-7). For each study, a plateau of the thickness increments per t_{ON} + t_{OFF} cycle was reached for high t_{OFF} times. This plateau, attributed to the termination of the free-radical polymerisation mechanism, was shown dependent on the monomer and deposition conditions. In particular, the termination of the free-radical polymerisation was observed after 15 ms for MMA and BMA based-films and after 100 ms for GMA based-films.[36,68]

Thus, the trend of the poly (alkyl methacrylate)'s thickness increment (progressive increase with the increase of the cycle duration before reaching a plateau) readily indicates the occurrence of different mechanisms. Notably, plasma-induced free-radical polymerisation was identified as prevailing occurring mechanism for long plasma-OFF times (i.e., low plasma pulse frequencies) allowing the maximal growth of the polymeric chain during one cycle pulse duration. On the other hand, plasma-state polymerisation was rather prevalent for short plasma t_{OFF} (i.e. high plasma pulse frequencies) leading to the pronounced fragmentation and dissociation of the monomers' molecule overcoming the conventional growth of the chains and yielding lower thickness increment.[36]

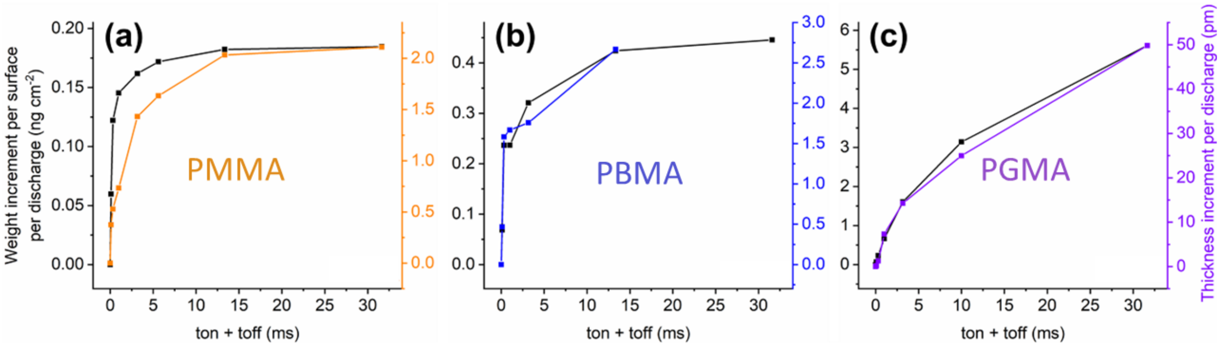

Figure I-3-7: Weight and thickness increment per discharge according to the cycle time (t_{ON} + t_{OFF}) for the thin films elaborated from a) MMA, b) BMA and c) GMA. Data adapted from Loyer *et al.*[36,79]

The mass spectrometry study of the thin films elaborated at low plasma pulse frequencies revealed the formation of true polymeric chains composed of MMA, BMA, GMA, NVCL and DEAP as repeating unit, demonstrating the excellent retention of starting monomer's chemistry during the deposition.[36,69,73] Nevertheless, these mass spectra presented number of species in-between two successive oligomer units, which was even more prominent for PMMA (Figure I-3-8 a & b) compared to PGMA, PDEAP and PNVCL.[36,69,73,80]

Loyer *et al.* demonstrated through a deeper analysis of their mass spectra that the species observed in-between two successive conventional $[(M)_n + H]^+$ oligomer units arose from the plasma-induced monomer single fragmentation used to initiate the free-radical polymerisation.[80] Whereas iCVD involves a labile initiator (e.g., TBPO) cleaved into well-defined radicals by hot filaments to start the free-radical polymerisation of vinylic monomers, AP-PiCVD relies on reactive monomer fragments to initiate the free-radical polymerisation reaction. The high energetic electrons composing plasma have been demonstrated to gain enough energy to break any of the bonds of the studied methacrylate monomers, creating a high number of fragment from each monomers, which can play both the role of initiating (R_i) and terminating group (R_t) leading to $[R_i(M)_nR_t + H]^+$ oligomers (Figure I-3-8 d). Thus, the combination of plasma OFF-times (t_{OFF}) in the range of the free-radical polymerisation lifetime and ultra-short plasma pulses (t_{ON} < 100 ns) afforded by AP-PiCVD allowed the formation of true polymeric chains, which mainly differ from their counterparts synthesized via conventional methods by the variety of their ending groups, i.e. $[R_i(M)_nR_t + H]^+$.[80] Increasing the ultrashort plasma pulses frequency was demonstrated to yield a significant number of alterations such as observed by mass spectrometry.

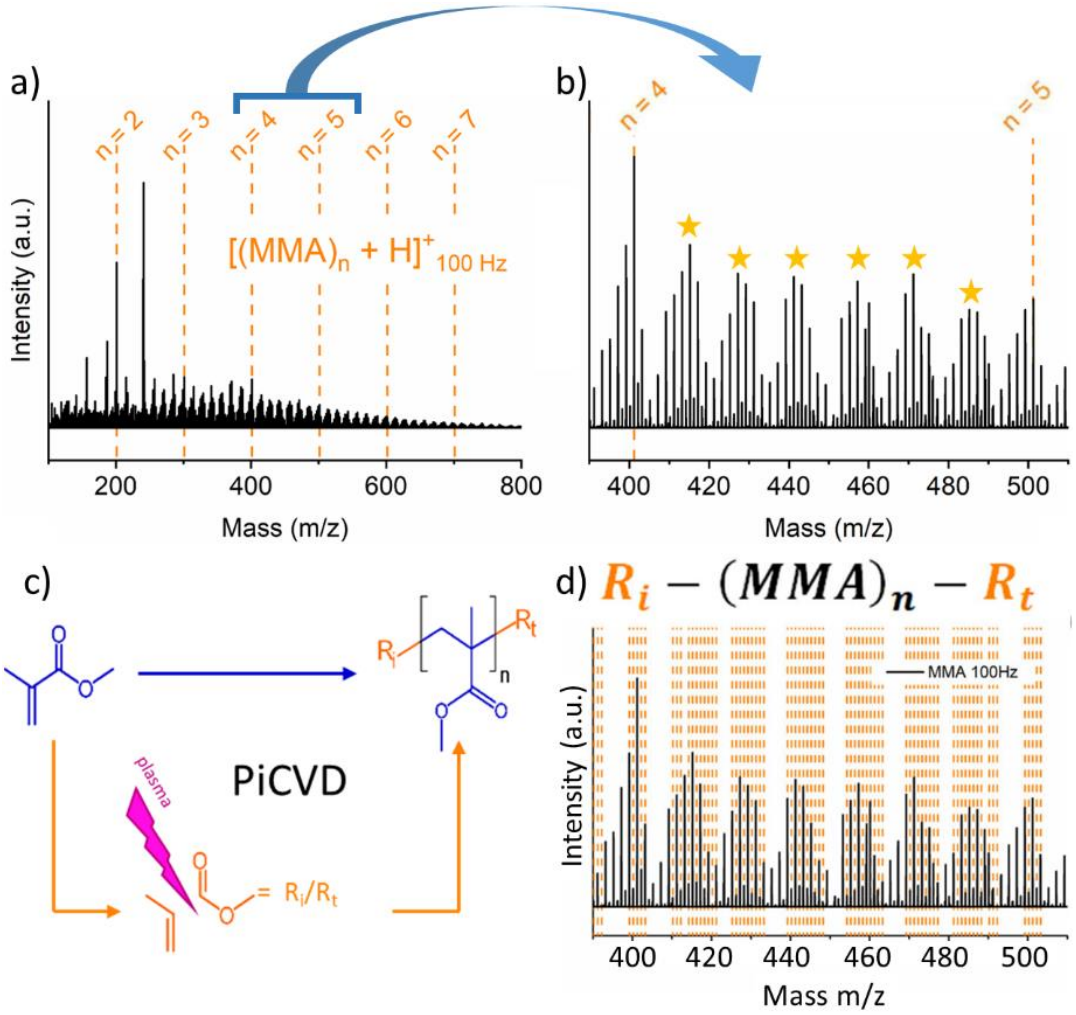

Figure I-3-8: MALDI-HRMS spectra for the thin film elaborated from MMA at a discharge frequency of 100 Hz. a) mass range m/z = 100-800, b & d) mass range m/z = 390–510. The lines displayed on a) show the position related to the MMA oligomers with H as end groups ($[(M)_n + H]^+$). The stars on b) point the different peak distribution that can be observed between two successive conventional $[(M)_n + H]^+$ oligomers. The lines displayed on d) point the mass peaks resulting from the possible $[R_i(MMA)_nR_t + H]^+$ combinations derived from c) the free-radical polymerisation of MMA with the different initiating and terminating groups that can form upon the σ-bond breakdown of MMA when exposed to plasma. Data adapted from Loyer *et al*.[80]

Size exclusion chromatography analysis also evidenced the strong impact of the ultrashort plasma pulse frequencies on the chemical structure of the thin films. To avoid any misinterpretation, these SEC measurements were compared to each other according to the elution time since the weight-average molar mass of the resulting thin film could not be reliably assessed due to the chemistry discrepancies between the low and high pulse's frequency thin films. Hence, they reported the formation of oligomeric chains with weight-average molar mass (M_w) of 2,596 g•mol^{-1} and 4,761 g•mol^{-1} for PMMA and PBMA respectively, and polymeric chain of 94,364 g•mol^{-1} for PGMA, when using a low plasma pulse frequency of 100 Hz.[36] This result was also in good agreement with the ranking of their propagation rate constants which further proved the importance of the monomer kinetic properties at low plasma pulse frequency.[36] On the other hand, with the increase of the plasma pulse frequency, the peak associated to the long polymer chains growth observed at short elution time disappeared (in the case of MMA and BMA) or became less prominent (in the case of GMA) while the overlapping peaks observed at longer elution time remain prevalent. They attributed these overlapping peaks to the formation of several compounds of high degree of cross-linking. Hence, instead of being a complete transition from one mechanism to the other one as one may assume in view of the trend of thickness increment of the different poly(alkyl methacrylate) films, they demonstrated that the AP-PECVD reaction was rather a competition between plasma-induced free-radical polymerisation dominated by the monomer's kinetic at low plasma pulse frequencies and plasma-state polymerisation dominated by plasma polymer regime at high plasma pulse frequencies.[36] Similar observations were made during the AP-PiCVD reaction of NVCL. Indeed, SEC analysis of the NVCL-based films elaborated at low plasma pulse frequency (i.e.10 Hz) showed the formation of longer oligomeric chain with a M_w = 4,100 g•mol^{-1}, providing their observed thermoresponsive properties. However, the increase of the plasma frequency to 1,000 Hz resulted in the formation of shorter chains and a more cross-linked structure showing a M_w = 950 g•mol^{-1}. This highly cross-linked structure did not present any thermoresponsive properties demonstrating the loss of the monomer chemical functionality during the deposition.[73]

Owing to FTIR measurement, they observed that all the thin films elaborated at low plasma pulse frequency confirmed, in good agreement with their MS observation, the retention of the monomer structure during the deposition. This retention of the monomer structure was shown to be ensured thanks to the prevailing occurrence of free-radical polymerisation through the vinyl bond of the different monomers, which bands located at ca. 1,635 cm^{-1} and 1,310 cm^{-1} were shown to disappear in all the poly (alkyl methacrylate) films.

Although the vinyl bond was also absent in the FTIR of the methacrylate based-films obtained at high plasma pulse frequencies, they all presented spectra that strongly differed from those of their starting monomers, which is typical for plasma-polymers. Such alteration was also witnessed by XPS. Curiously, they observed that BMA and MMA based-films showed a decrease of hydroxyl group with the increase of the plasma pulse frequency contrary to GMA based-films which showed a rise of hydroxyl band vibration with the increase of the plasma pulse frequency in good agreement with their MS observations.[36] If the rise of hydroxyl band vibration in the GMA was justified by the opening of the sensitive epoxy function, the opposite observation made with the MMA and BMA based-polymers was not fully understood and was still requiring deeper investigations.[36] The increase of the plasma pulse frequency was similarly observed to lead to the alteration of the monomer structure during the AP-PiCVD reaction of DEAP and NVCL.[69,73] The latter also showed the formation of hydroxyl group.[73]

The ultrashort plasma pulses frequency was also demonstrated to have a strong impact on the morphology of the thin films. Using SEM, they observed a systematic formation of smooth surface morphologies for thin films elaborated at low plasma pulse frequency, irrespective of the starting monomer.[36,68,69,71,73] This demonstrated the preponderance of surface reaction which justify the conformal coverage of unconventional substrate with a high level of conformity (Figure I-3-9 b).[36,68]

On the other hand, the increase of the plasma pulse frequency to f > 1,000 Hz, resulted in the formation of rough surface morphologies and non-conformal coating due to the preponderance of gas phase reaction as usually encounter in plasma-state polymerisation. In addition and to further emphasize the importance of the thickness increment plot according to the cycle duration, they demonstrated that the use of different plasma pulse frequencies (one should remember here that t_{ON} was kept constant in this study) can lead to the growth of thin film with similar growth rate but presenting different features, i.e. different chemistry and morphology (Figure I-3-9). This demonstrated that the film roughening in plasma polymerisation is not related to an excess of deposition rate but rather to an excess of gas phase reaction (Figure I-3-9 a, b & c).[36]

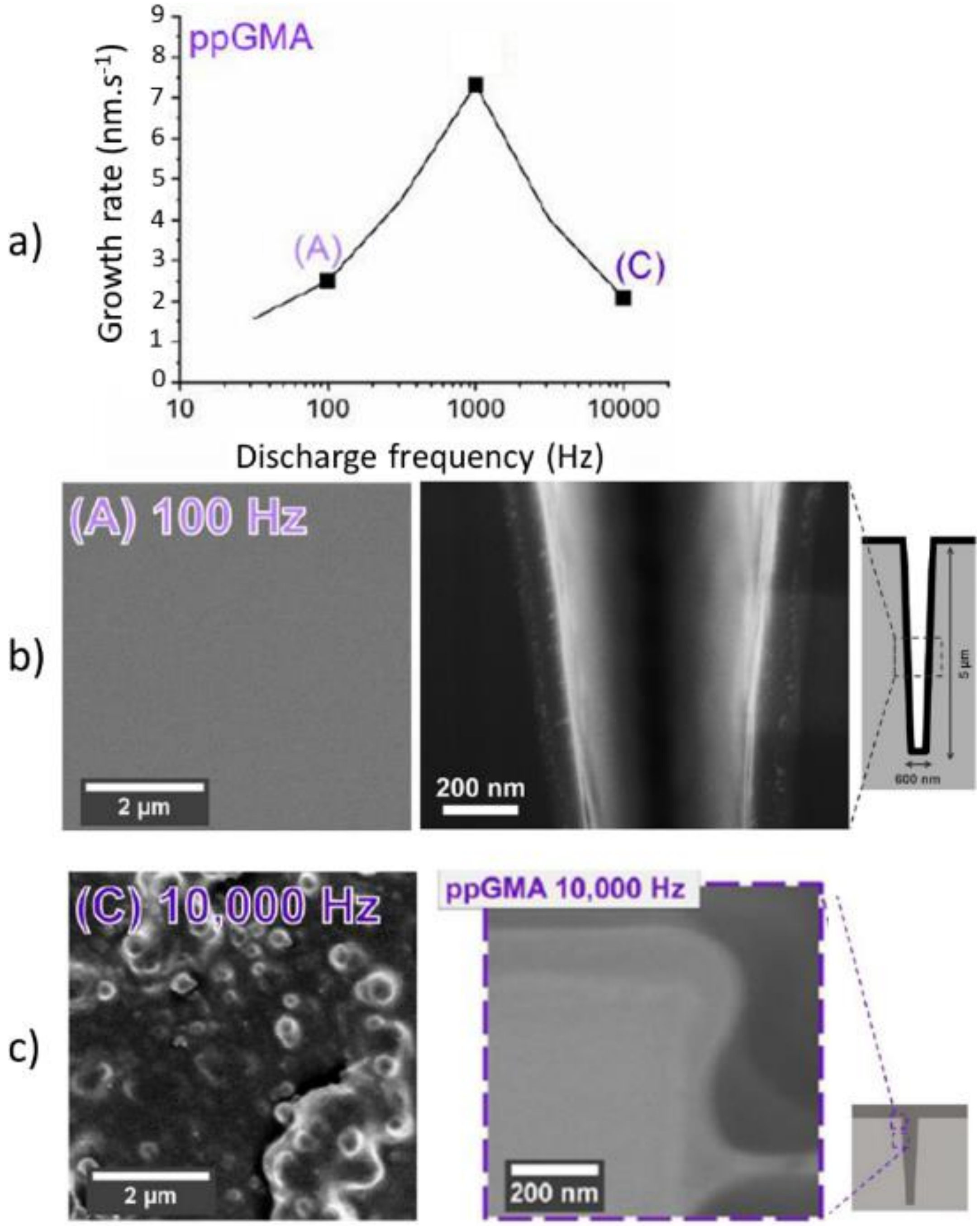

Figure I-3-9: a) Growth rates (nm.s^{-1}) of the films grown from glycidyl methacrylate (GMA) plotted according to the plasma pulse frequency. SEM top view and cross-sectional images of the PGMA elaborated at plasma pulse frequency of (b) 100 Hz and (c) 10,000 Hz. Data adapted from Boscher *et al*.[36,68]

Overall, the plasma pulse frequency has a strong influence on the chemistry and morphology of the resulting thin films, which ultimately have an impact on their properties. The duality of the atmospheric-pressure plasma initiated chemical vapour deposition (AP-PiCVD) process, combining two different regimes, i.e. the plasma-state polymerisation and plasma-induced polymerisation of plasma–polymer and polymer-like moieties, respectively, is highlighted above. Although the two regimes simultaneously occurred when combining plasma and vinylic monomers, surface reaction (i.e. adsorption and subsequent free-radical polymerisation) was identified as prevailing mechanism at low plasma pulse frequencies, leading to unprecedented degree of polymerisation for PECVD processes.[36]

Table I-3-1: List of the polymers and monomers previously investigated by AP-PiCVD and their applications.

Polymers	Monomers	Application	Ref
poly(diethylallylphosphate) PDEAP	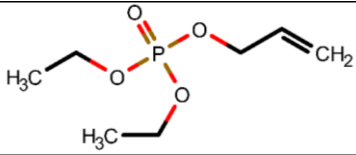	Fire retardant	[69]
poly(N-vinyl caprolactam) PNVCL	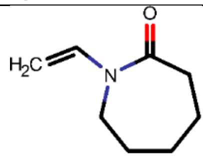	Biomedical	[73]
poly(NVCL-co- ethylene glycol dimethacrylate)	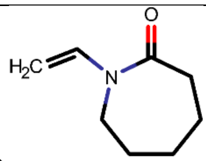 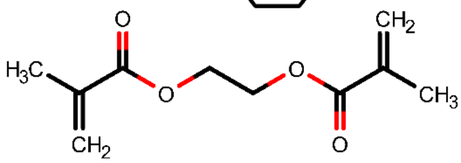	Anti-fouling	[78]
Poly(glycidyl methacrylate) PGMA	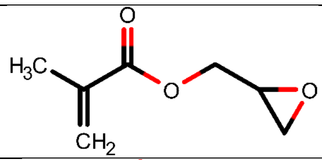	Adhesive coating	[71]
Poly(butyl methacrylate) PBMA	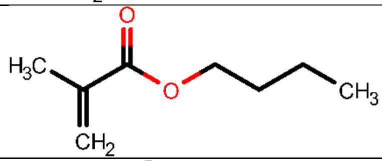	Fundamental studies	[73, 79-81]
Poly(methyl methacrylate) PMMA	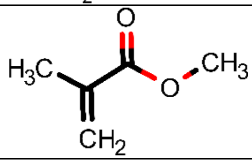	Fundamental studies	

I-3.2.2 Monomer Structure – Vinyl Bonds as a Prerequisite

All the works reported above, involving different vinylic monomers (MMA, BMA, GMA, EGDMA, NVCL, DEAP) demonstrated the different sensitivity of the monomers to the plasma pulse frequency, regarding several of the analysis performed. From the study of the poly(alkyl methacrylate), a clear distinction was systematically noticed between the reactivity and sensitivity of MMA- and GMA-based films while BMA- based films were reported to have an intermediate behaviour.

Notably, the evaluated growth rates obtained at a low plasma pulse frequency of 100 Hz for identical monomer partial pressure (P_M) were reported as followed: DR_{MMA} (0.18 nm•s^{-1}) < DR_{BMA} (0.24 nm•s^{-1}) ≪ DR_{GMA} (2.50 nm•s^{-1}), in good agreement with their propagation rate constant also ranked as: $k_p^{PMMA} \sim k_p^{PBMA} < k_p^{PGMA}$.[73] However, in CVD polymerisation, the rate limiting step may also be related to the adsorption of the reactant to the surface.[45] Hence, at equivalent monomer partial pressures (P_M), the monomer with the lowest vapour pressure (P_{sat}) is expected to remain adsorbed longer on the substrate compared to higher P_{sat} monomers, which are expected to desorb more quickly before reacting and contributing to the film growth. Consequently, the fastest growth observed from GMA-based films synthesised at low plasma pulse frequency was also attributed to the lower P_{sat} combined to the higher k_p of its starting monomer.[36] This result highlighted the importance of both the monomer chemical and physical properties, notably the kinetic property of the monomer hinting on the fact that free-radical polymerisation steps in AP-PiCVD polymerisation is identical to radical polymerisation steps in the bulk phase, and the adsorption of the monomer molecules pointing out similarity with iCVD.[36] Therefore, the deposition rate should be strongly influenced by the concentration of initiating species and active growing chains ([M$^\bullet$]), the concentration of monomer adsorbed on the surface ([M]), and the kinetic rate constant of the different monomers (i.e k_p and k_t). At equivalent monomer's vapour concentration (P_M), the studied vinylic monomers surface concentrations were ranked as $[MMA]_{(ad)} < [BMA]_{(ad)} < [GMA]_{(ad)} \approx [NVCL]_{(ad)}$ suggesting the importance of the monomer saturation ratio (P_M/P_{sat}).[36]

Moreover, contrary to MMA-based films, a collapse in the growth rate of films obtained from BMA, GMA and NVCL was observed with the increase of the frequency. These results highlighted the dependence of the growth rates to the monomer structure and/or concentration at the highest frequencies, with transition in the deposition regime (blue arrows in Figure I-3-6).[36,73]

The sensitivity of the different monomer toward plasma was also noticed through their MS. Indeed, although elaborated at low plasma pulse frequency, the mass spectrum of the MMA based-films was more populated than the ones of GMA and NVCL based-films.[36,73,80] This higher magnitude of species observed in-between two successive oligomer units $[(M)_n + H]^+$ in the case of MMA based-films suggested the strong influence of the monomer itself during the AP-PiCVD reaction. In particular, the mass spectrometry analysis of the thin films elaborated from MMA at low repetition frequency revealed the integration of oxygen to the polymeric chains, responsible for the strong hydroxyl vibration bands detected by FTIR. Such observation was related to the reactivity of oxygen and water available from the surrounding atmosphere. On the other hand, subtraction of oxygen and addition of carbon was detected at higher frequencies, which indicated the alteration of the monomer's chemistry and higher cross-linking degree such as expected for plasma-polymers.[36,80]

The contrast between the high weight-average molecular weight reported for PGMA compared to the PMMA and PBMA was attributed the large difference of their P_{sat} in addition to their propagation constant. With this observation, they emphasised again the importance of the monomer's kinetic and adsorption properties at low plasma pulse frequencies.[36]

To have a deeper insight on the origin of these different polymeric lengths, they used the density functional theoretical (DFT) calculation.[80] The bond dissociation energy (BDE) of the epoxy ring was found to be around 2 eV lower than the other σ-bonds of the GMA molecule. Since presenting the weakest bond in the molecule, the epoxy group was identified as a chemical buffer that effectively protect the molecule from a statistical breakdown while promoting the film's adhesivity through a natural cross-linking.[36,80] Combining this result to the favoured kinetic of GMA monomer conveniently justified the better chemical retention and the longer PGMA polymeric chain formed. On the other hand, MMA molecule was shown to have a difference in BDE as low as 0.5 eV among all its σ-bonds. This highlighted its higher sensitivity to a statistical molecule breakdown implying the generation of a higher amount of fragments. Therefore, this higher amount of fragment formed at low plasma pulse frequency resulted in a higher occurrence of chain termination yielding the formation of shorter PMMA chains which yielded a populated mass spectrum.[36,80] This observations highlighted the importance of the monomer structure or monomer saturation ratio.

Surprisingly, the NVCL-based films were made of shorter oligomeric species despite of the low P_{sat} of NVCL. Even though a statistical fragmentations of the NVCL lactam ring, offering seven different opening pathways, may explain the difference with the GMA case for which a localized fragmentation was able to protect the structure during the deposition, this different behaviour may not be fully explained by the statistical breakdown of NVCL. Indeed, NVCL is in solid state at room temperature making it necessary to melt it to be vapour deposited. In their study,[73,78] in spite of melting the NVCL at 50°C, the PNVCL thin films grown by Loyer *et al.* may still suffer from low monomer partial pressure that yield to the damaging of a higher portion of monomer, which can act as terminating group leading to the formation of short oligomeric chains similarly to MMA, and deposition rates (0.35 nm•s^{-1} at 100 Hz) one order of magnitude lower than the one obtained from GMA (2.50 nm•s^{-1} at 100 Hz).[73]

In addition, the AP-PiCVD films presented extremely different sensitivity to plasma regarding their FTIR although all elaborated at low plasma pulse frequency. Indeed, while MMA and BMA based-films showed an integration of hydroxyl group, GMA and NVCL based- films did not. These observations demonstrated again the importance of the monomer structure or the importance of monomer saturation ratio.

The difference in sensitivity toward plasma was also observed with the SEM of the reported AP-PiCVD films. While MMA and BMA based-films systematically showed a smooth surface morphology when elaborated at plasma pulse frequencies lower or equal to 1,000 Hz, GMA based-films were already showing a rough surface morphology from 1,000 Hz. On the other hand, NVCL-based films showed a rough surface morphology from the low plasma pulse frequency of 100 Hz. This threshold between the preponderance of surface reactions (yielding smooth thin films) and gas phase reactions (yielding rough or powdery thin films) seemed to be monomer structure or monomer saturation ratio dependent.

I-3.2.3 Monomer Saturation Ratio and Substrate Temperature – Monomer Adsorption

To understand this shift from predominant gas phase mechanisms (fragmentation and recombination) to surface mechanisms (initiation, propagation and termination) according to the plasma pulse frequency, a kinetic model called pulsed plasma method (PPM) was developed.[81] This PPM model is based on the same principle as the rotating sector method (RSM) and the pulsed laser polymerisation (PLP) method. Contrary to other plasma-polymerisation model, the PPM integrates the non-steady plasma initiation, the polymerisation propagation and termination, as well as the chain transfer event.[81]

According to the model which take into account the experimental data on the AP-PiCVD reaction of alkyl methacrylate monomers,[36,80] polymeric films in AP-PiCVD are assumed to occur through three following major steps (Figure I-3-10): (1) activated species (radicals) are created intermittently according to the plasma pulse frequency, (2) diffusion and adsorption of primary radicals and monomer from the vapour phase onto a surface where (3) the polymerisation occurs leading to formation of thin films with unprecedented degree of polymerisation and the conformal coatings of 3D structures with high aspect ratio.[36,68,81] Hence showing strong similarities with iCVD.[82,83]

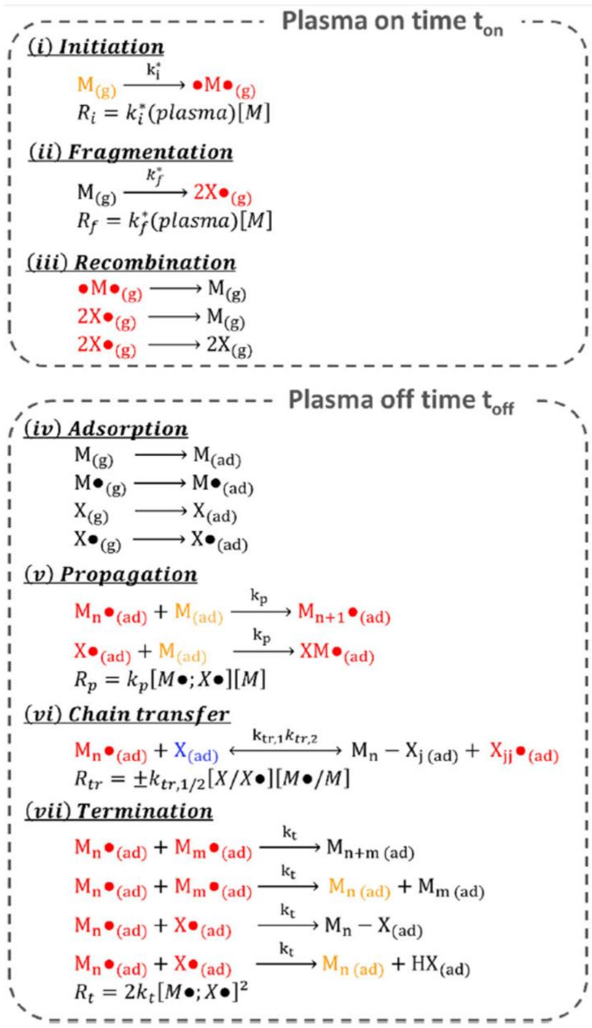

Figure I-3-10: Mechanisms used by Loyer *et al*. in their kinetic model of the AP-PiCVD process. Data adapted from Loyer *et al.*[81]

The PPM model allow estimating the maximum conversion rate of MMA and GMA from monomer to radicals at low plasma pulse frequencies (low DCs). At equivalent P_M (monomer partial pressure), the maximum conversion rates was evaluated to be 5% and 20% for MMA and GMA respectively.[81] This result let assume a higher sensitivity of the GMA's molecules compared to the MMA's ones under the plasma discharge. However, as already mentioned earlier, GMA possesses a chemical buffer group (i.e., the epoxy group) which protects the molecule from a statistical breakdown contrary to MMA, which is more prone to produce a wide range of radicals. Moreover, not all the created radicals participate to the polymerisation reaction since some of them could be deactivate and be flushed away before reaching the substrate. Therefore, for a better understanding of the reactivity of radicals in the reactive volume, the ratio between reacted radicals (that adsorb and polymerise on the surface) and radicals created was plotted according to the ultra-short plasma pulse frequencies. Globally, a linear increase of the radical reactivity was systematically observed with the increase of the plasma pulse frequency before reaching a plateau indicating a saturation, readily visible in the case of GMA. Owing to this result which matched with the variation of their deposition rates and the variation of their SEM morphologies, Loyer *et al*. concluded that the transition from preponderant surface mechanisms to preponderant gas phase mechanisms is a result of the saturation of the reactive species on the substrate surface when reactivity reaches 100%.[81] The early saturation of GMA's reactive species (at ca. 1000 Hz) is attributed to its low vapour pressure implying that the surface substrate would be prone to saturate quickly. On the other hand, the lack of saturation observed in the curve of MMA radical's reactivity is simply linked to the lower adsorption of the monomer's molecule on the substrate, due to the high P_{sat} of MMA. Overall, this study demonstrated the importance of adsorption mechanisms in the PiCVD process and notably de monomer surface concentration which can be related to the non-dimensional parameter given by the ratio of the monomer partial pressure (P_M) and its saturated vapor pressure (P_{sat}).

As a result, few rules were introduced to achieve the AP-PiCVD reactions of vinylic monomers. Notably the use of low repetition frequency of the ultrashort square-wave pulses consistent with the lifetime of the free-radical polymerisation for the selected monomer. Since lower vapour pressure (P_{sat}) adsorption to the surface were shown to be promoted, and both the growth and the conventional polymerisation pathway enhanced, as observed with GMA, they also advised the use of monomer with sufficient vapour pressure to allow its delivery in vapour phase at atmospheric pressure.[36,80]

In addition, free-radical polymerisation prevalent at low plasma pulse frequencies and taking place through the vinyl bond seemed to lead to the retention of the monomer structure. If the use of a vinyl monomer has been set as a prerequisite to allow the simultaneous synthesis and deposition of polymer with various functionalities with AP-PiCVD, the linked between the retention of the monomer structure and the vinyl bond of the monomer was not established or clearly investigated.[36]

Similarities between iCVD and AP-PiCVD are found, notably regarding the emphasized importance of monomer adsorption on the surface which is foreseen as important parameter of the AP-PiCVD process. Indeed, the well-established iCVD process which allows the deposition of various functional polymer thin films that can be synthesized by free-radical polymerisation via surface-growth mechanisms, shows an adsorption-limited kinetic.[82,83] This was notably demonstrated through the iCVD deposition of different n-alkyl acrylate (from ethyl to hexyl) were the relationship between the polymerisation kinetic, such as the deposition rate and the number-average molecular weight (M_n) of the resulting thin films, and the monomer surface concentration was clearly elucidated.[83] Indeed, the studied group of monomers showed an increase of their deposition rates and M_n with the decrease of monomer saturated vapour pressure, although all synthesized in the same conditions similarly to the observations made for the AP-PiCVD reaction of alkyl methacrylate monomers. This provided a hint on the influence of the monomer saturation ratio (P_M/P_{sat}) on the growth mechanism of the resulting thin films. The adsorption-limited kinetic of the process was further demonstrated through the systematic increase of the deposition rate of the main studied monomer, i.e., ethyl acrylate, with the decrease of the substrate temperature irrespective of the investigated conditions (e.g., increase of the filament temperature and substrate temperature).[83]As a result, the saturation ratio (P_M/P_{sat}) was introduced as a measure of the amount of adsorbed monomer, which was related to the adsorbed volume (V_{ad}) of the studied butyl acrylate monomer through BET equation highlighting the formation of multilayers with a coverage c= 2.536.[82,83]

With the aim of developing a mechanistic model for describing the kinetic behaviour in iCVD, Lau *et al.* proposed a theoretical model, based on experimental data. Hence, the reaction mechanism for iCVD was proposed as a series of elementary steps involving gas phase initiator decomposition followed by surface reactions. Overall, this reaction mechanism present the same major steps as in AP-PiCVD (Figure I-3-11).

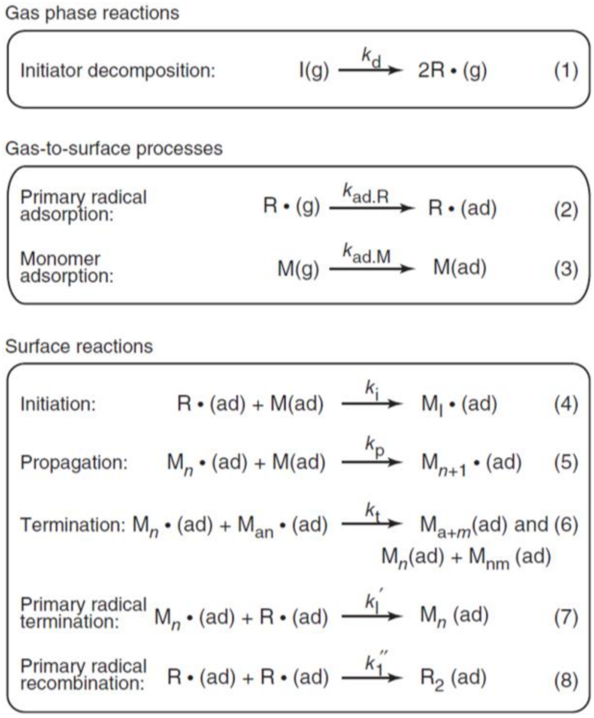

Figure I-3-11: Mechanisms used by Lau *et al*. in their kinetic model of the iCVD process.[45,83]

Owing to the excellent understanding of the structure-property-processing relationships in iCVD process, several types of functional polymers thin films were elaborated for applications as biopassive coating,[29] water-repellent coatings ,dielectric gate for organic microelectronic, etc.[4,21] Many of the monomers used in iCVD are commercially available and have been reported in several reviews.[45,84,85] The highly pure polymers obtained with iCVD resulted in the formation of insulating low dielectric constant polymers from organosiloxane compounds such as 1,3,5-trivinyl-1,3,5-trimethyl cyclotrisiloxane (V3D3) and 1,3,5,7-tetramethyl-1,3,5,7-tetravinylcyclotrisiloxane,[19,21] as well as the formation of insulating high dielectric constant copolymer from di(ethylene glycol) divinyl ether (DEGDVE) and 2-cyanoethyl acrylate (CEA).[4]

Overall, strong similarities with the iCVD regarding the growth mechanisms and the resulting thin films' characteristics were clearly demonstrated, although AP-PiCVD is unlikely to produce pure homo- or copolymers since being a plasma-based process. Notably, the importance of the monomer structure, the monomer saturation ratio or the combination of the two effect is repeatedly pointed out as parameter influencing the growth of the AP-PiCVD films. Yet, their influence cannot yet be discriminate due to the lack of a systematic study of their respective importance. The development of a clear understanding of these parameters, such as in iCVD, would be beneficial for the formation of functional thin films with high potential for entirely new fields of application. The recently developed process has only covered few applications so far, and this thesis aims at extending the library of monomers deposited by AP-PiCVD by targeting the synthesis of low dielectric constant insulating polymer layers for dielectric gate application in organic microelectronic. In addition to their application-driven motivation, the characterisation of the dielectric properties of the films was foreseen to provide an additional dimension for the development of a fundamental understanding of the AP-PiCVD approach.

I-4 Thesis Framework

The objective of this thesis is to gain a deeper understanding on the influence of the monomer structure and monomer saturation ratio through the study of the atmospheric pressure plasma deposition of organosiloxane monomers for the preparation of high-quality and ultrathin polymer layers for dielectric gate application. The study of the dielectric properties of these films (leakage current, k value…) provides a new dimension to the characterization of the films and enables a better comprehension of the growth mechanisms.

I-4.1 Importance of the Monomer Structure on the AP-PiCVD Reaction

The Chapter Two evidences different growth mechanisms of thin films obtained from tetrasiloxane compounds possessing vinyl groups and/or a cyclic structure, i.e. 1,3,5,7-tetramethyltetravinylcyclotetrasiloxane (V4D4) and octamethylcyclotetrasiloxane (D4), and those which don't, i.e. decamethyltetrasiloxane (DMTSO). While ring-opening reaction is observed with the D4 monomer, the free-radical polymerisation reaction through the vinyl bond is preponderant for the AP-PiCVD reaction of V4D4. The characterization methodologies described in this chapter are used extensively in subsequent chapters.

I-4.2 Importance of the Monomer Saturation Ratio on the AP-PiCVD Reaction

In Chapter Three, the saturation ratio (P_M/P_{sat}) is demonstrated as key parameter to promote a free-radical polymerisation pathway and ensure the growth of smooth and dense thin films. Supported by the physico-chemical characterization (FTIR, SEM, growth rate, dielectric constant), and the relationship established between the saturation ratio and the resulting films properties, guidelines are provided to determine the optimal process window for the AP-PiCVD of functional polymer thin films.

I-4.3 Importance of the Monomer Structure on the Dielectric Properties of the AP-PiCVD Thin Films

The Chapter Four reports the atmospheric pressure plasma deposition reaction of cyclic organosiloxane (V3D3 and V4D4) and organosilazane (V3N3 and V4N4) monomers for the preparation of high-quality and ultrathin dielectric polymer layers. The ability to tune the k value ($2.8 \leq k < 4.2$) by carefully selecting the monomer structure is demonstrated. Lower polarizability (organosiloxane) and bigger ring size monomer (V4D4) give the lowest k value. AFM and SEM investigations highlight the atomically smooth, defect-free and conformal nature of the as-deposited polymer thin films, which is desirable for microelectronic applications.

In this cumulative dissertation, each chapter is structured as a journal article. As such, each chapter begins with a brief introduction, followed by the description of the experimental methods used, the presentation of results and discussion, and ending with conclusions. The chapters are arranged in a manner that provides continuity within the thesis. The supporting information of each chapter are provided in the appendix. The thesis concludes with a summary of the work accomplished and outlook for future work.

I-5 References

1) Facchetti, A.; Yoon, M.-H.; Marks, T. J. Gate Dielectrics for Organic Field-Effect Transistors: New Opportunities for Organic Electronics. *Adv. Mater.* **2005**, *17* (14), 1705–1725.

(2) Wang, Y.; Huang, X.; Li, T.; Li, L.; Guo, X.; Jiang, P. Polymer-Based Gate Dielectrics for Organic Field-Effect Transistors. *Chem. Mater.* **2019**, *31* (7), 2212–2240.

(3) Wang, B.; Huang, W.; Chi, L.; Al-Hashimi, M.; Marks, T. J.; Facchetti, A. High- k Gate Dielectrics for Emerging Flexible and Stretchable Electronics. *Chem. Rev.* **2018**, *118* (11), 5690–5754.

(4) Choi, J.; Joo, M.; Seong, H.; Pak, K.; Park, H.; Park, C. W.; Im, S. G. Flexible, Low-Power Thin-Film Transistors Made of Vapor-Phase Synthesized High-k, Ultrathin Polymer Gate Dielectrics. *ACS Appl. Mater. Interfaces* **2017**, *9* (24), 20808–20817.

(5) Yoon, M.-H.; Yan, H.; Facchetti, A.; Marks, T. J. Low-Voltage Organic Field-Effect Transistors and Inverters Enabled by Ultrathin Cross-Linked Polymers as Gate Dielectrics. *J. Am. Chem. Soc.* **2005**, *127* (29), 10388–10395.

(6) Veres, J.; Ogier, S. D.; Leeming, S. W.; Cupertino, D. C.; Khaffaf, S. M. Low-k Insulators as the Choice of Dielectrics in Organic Field-Effect Transistors. *Adv. Funct. Mater.* **2003**, *13* (3), 199-204.

(7) O'Schaughnessy, W. S.; Murthy, S. K.; Edell, D. J.; Gleason, K. K. Stable Biopassive Insulation Synthesized by Initiated Chemical Vapor Deposition of Poly(1,3,5-Trivinyltrimethylcyclotrisiloxane). *Biomacromolecules* **2007**, *8* (8), 2564–2570.

(8) Murthy, S. K.; Gleason, K. K. Fluorocarbon-Organosilicon Copolymer Synthesis by Hot Filament Chemical Vapor Deposition. *Macromolecules* **2002**, *35* (5), 1967–1972.

(9) Boscher, N. D.; Choquet, P.; Duday, D.; Verdier, S. Influence of Cyclic Organosilicon Precursors on the Corrosion of Aluminium Coated Sheet by Atmospheric Pressure Dielectric Barrier Discharge. *Surf. Coatings Technol.* **2011**, *205* (23–24), 5350–5357.

(10) Boscher, N. D.; Choquet, P.; Duday, D.; Verdier, S. Advantages of a Pulsed Electrical Excitation Mode on the Corrosion Performance of Organosilicon Thin Films Deposited

on Aluminium Foil by Atmospheric Pressure Dielectric Barrier Discharge. *Plasma Process. Polym.* **2009**, *7* (2), 163–171.

(11) Lin, Y.; Lai, Y.; Chen, J. Scratch Resistance of Flexible Carbon Fiber-Reinforced Polymer Composites Improved by Atmospheric Pressure Plasma Polymerized-Organosilicon Oxide Films. *Polym. Compos.* **2019**, *40* (S2), E1893–E1902.

(12) Lo, C.-H.; Lin, M.-H.; Liao, K.-S.; De Guzman, M.; Tsai, H.-A.; Rouessac, V.; Wei, T.-C.; Lee, K.-R.; Lai, J.-Y. Control of Pore Structure and Characterization of Plasma-Polymerized SiOCH Films Deposited from Octamethylcyclotetrasiloxane (OMCTS). *J. Memb. Sci.* **2010**, *365* (1–2), 418–425.

(13) Volksen, W.; Miller, R. D.; Dubois, G. Low Dielectric Constant Materials. *Chem. Rev.* **2010**, *110* (1), 56–110.

(14) Jousseaume, V.; El Sabahy, J.; Yeromonahos, C.; Castellan, G.; Bouamrani, A.; Ricoul, F. SiOCH Thin Films Deposited by Chemical Vapor Deposition: From Low-κ to Chemical and Biochemical Sensors. *Microelectron. Eng.* **2017**, *167*, 69–79.

(15) Baklanov, M. R.; de Marneffe, J.-F.; Shamiryan, D.; Urbanowicz, A. M.; Shi, H.; Rakhimova, T. V.; Huang, H.; Ho, P. S. Plasma Processing of Low-k Dielectrics. *J. Appl. Phys.* **2013**, *113* (4), 041101.

(16) Maex, K.; Baklanov, M. R.; Shamiryan, D.; Iacopi, F.; Brongersma, S. H.; Yanovitskaya, Z. S. Low Dielectric Constant Materials for Microelectronics. *J. Appl. Phys.* **2003**, *93* (11), 8793–8841.

(17) Baklanov, M. R.; Maex, K. Porous Low Dielectric Constant Materials for Microelectronics. *Philos. Trans. R. Soc. A Math. Phys. Eng. Sci.* **2006**, *364* (1838), 201–215.

(18) Castex, A.; Favennec, L.; Jousseaume, V.; Bruat, J.; Deval, J.; Remiat, B.; Passemard, G.; Pons, M. Study of Plasma Mechanisms of Hybrid A-SiOC:H Low-k Film Deposition from Decamethylcyclopentasiloxane and Cyclohexene Oxide. *Microelectronic Engineering*; 2005; Vol. 82, 416–421.

(19) Trujillo, N. J.; Wu, Q.; Gleason, K. K. Ultralow Dielectric Constant Tetravinyltetramethylcyclotetrasiloxane Films Deposited by Initiated Chemical Vapor

Deposition (iCVD). *Adv. Funct. Mater.* **2010**, *20* (4), 607–616.

(20) Burkey, D. D.; Gleason, K. K. Structure and Mechanical Properties of Thin Films Deposited from 1,3,5-Trimethyl-1,3,5-Trivinylcyclotrisiloxane and Water. *J. Appl. Phys.* **2003**, *93* (9), 5143–5150.

(21) Moon, H.; Seong, H.; Shin, W. C.; Park, W.-T.; Kim, M.; Lee, S.; Bong, J. H.; Noh, Y.-Y.; Cho, B. J.; Yoo, S.; Im S. G. Synthesis of Ultrathin Polymer Insulating Layers by Initiated Chemical Vapour Deposition for Low-Power Soft Electronics. *Nat. Mater.* **2015**, *14* (6), 628–635.

(22) You, H.; Mennell, P.; Shoudy, M.; Sil, D.; Dorman, D.; Cohen, S.; Liniger, E.; Shaw, T.; Leo, T.-L.; Canaperi, D.; Raymond, M.; Madan, A. Grill, A. Extreme-Low k Porous pSiCOH Dielectrics Prepared by PECVD. *J. Vac. Sci. Technol. B, Nanotechnol. Microelectron. Mater. Process. Meas. Phenom.* **2018**, *36* (1), 012202.

(23) Gourhant, O.; Gerbaud, G.; Zenasni, A.; Favennec, L.; Gonon, P.; Jousseaume, V. Crosslinking of Porous SiOCH Films Involving Si–O–C Bonds: Impact of Deposition and Curing. *J. Appl. Phys.* **2010**, *108* (12), 124105.

(24) Jousseaume, V.; Favennec, L.; Zenasni, A.; Gourhant, O. Porous Ultra Low k Deposited by PECVD: From Deposition to Material Properties. *Surf. Coatings Technol.* **2007**, *201* (22–23), 9248–9251.

(25) El Sabahy, J.; Castellan, G.; Ricoul, F.; Jousseaume, V. Porous SiOCH Thin Films Obtained by Foaming. *J. Phys. Chem. C* **2016**, *120* (17), 9184–9191.

(26) Wróbel, A. M.; Wertheimer, M. R. Plasma-Polymerized Organosilicones and Organometallics. In *Plasma Deposition, Treatment, and Etching of Polymers*; **1990**, 163-268.

(27) Rücker, C.; Kümmerer, K. Environmental Chemistry of Organosiloxanes. *Chem. Rev.* **2015**, *115* (1), 466–524.

(28) Coclite, A. M.; Gleason, K. K. Initiated PECVD of Organosilicon Coatings: A New Strategy to Enhance Monomer Structure Retention. *Plasma Process. Polym.* **2012**, *9* (4), 425–434.

(29) O'Schaughnessy, W. S.; Gao, M.; Gleason, K. K. Initiated Chemical Vapor Deposition

of Trivinyltrimethylcyclotrisiloxane for Biomaterial Coatings. *Langmuir* **2006**, *22* (16), 7021–7026.

(30) Mariotti, D.; Belmonte, T.; Benedikt, J.; Velusamy, T.; Jain, G.; Švrček, V. Low-Temperature Atmospheric Pressure Plasma Processes for “Green” Third Generation Photovoltaics. *Plasma Process. Polym.* **2016**, *13* (1), 70–90.

(31) Bruggeman, P. J.; Iza, F.; Brandenburg, R. Foundations of Atmospheric Pressure Non-Equilibrium Plasmas. *Plasma Sources Sci. Technol.* **2017**, *26* (12), 123002.

(32) Tendero, C.; Tixier, C.; Tristant, P.; Desmaison, J.; Leprince, P. Atmospheric Pressure Plasmas: A Review. *Spectrochimica Acta - Part B Atomic Spectroscopy*. 2006, *61* (1), 2–30.

(33) Knapp, C. E.; Chemin, J.-B.; Douglas, S. P.; Abessolo Ondo, D.; Guillot, J.; Choquet, P.; Boscher, N. D. Room-Temperature Plasma-Assisted Inkjet Printing of Highly Conductive Silver on Paper. *Adv. Mater. Technol.* **2018**, *3* (3), 1700326.

(34) Abessolo Ondo, D.; Loyer, F.; Chemin, J.-B.; Bulou, S.; Choquet, P.; Boscher, N. D. Atmospheric Plasma Oxidative Polymerization of Ethylene Dioxythiophene (EDOT) for the Large-Scale Preparation of Highly Transparent Conducting Thin Films. *Plasma Process. Polym.* **2018**, *15* (4), 1700172.

(35) Feng, L.; Anguita, J. V.; Tang, W.; Zhao, J.; Guo, X.; Silva, S. R. P. Room Temperature Grown High-Quality Polymer-Like Carbon Gate Dielectric for Organic Thin-Film Transistors. *Adv. Electron. Mater.* **2016**, *2* (3), 1500374.

(36) Loyer, F.; Frache, G.; Choquet, P.; Boscher, N. D. Atmospheric Pressure Plasma-Initiated Chemical Vapor Deposition (AP-PiCVD) of Poly(Alkyl Acrylates): An Experimental Study. *Macromolecules* **2017**, *50* (11), 4351–4362.

(37) Boulos, M. I.; Fauchais, P.; Pfender, E. The Plasma State. In *Thermal Plasmas*; Springer US: Boston, MA, **1994**; 1–47.

(38) Friedrich, J. *The Plasma Chemistry of Polymer Surfaces: Advanced Techniques for Surface Design*; **2012**.

(39) Fridman, A. *Plasma Chemistry*; **2008**.

(40) Kong, P.; Myrtle. Atmospheric-Pressure Plasma Process And Applications. *SOHN Int. Symp. Adv. Process. Metals Mater. Technol. Ind. Pract.* **2006**, *6*, 493–506.

(41) Bárdos, L.; Baránková, H. Cold Atmospheric Plasma: Sources, Processes, and Applications. *Thin Solid Films* **2010**, *518* (23), 6705–6713.

(42) Massines, F.; Sarra-Bournet, C.; Fanelli, F.; Naudé, N.; Gherardi, N. Atmospheric Pressure Low Temperature Direct Plasma Technology: Status and Challenges for Thin Film Deposition. *Plasma Process. Polym.* **2012**, *9* (11–12), 1041–1073.

(43) Merche, D.; Vandencasteele, N.; Reniers, F. Atmospheric Plasmas for Thin Film Deposition: A Critical Review. *Thin Solid Films* **2012**, *520* (13), 4219–4236.

(44) Yasuda, H. *Luminous Chemical Vapor Deposition and Interface Engineering*; **2004**.

(45) Gleason, K. K. Overview of Chemically Vapor Deposited (CVD) Polymers; Gleason, K. K., Ed.; Wiley-VCH Verlag GmbH & Co. KGaA, **2015**; *1*, 1–12.

(46) Hamedani, Y.; Macha, P.; Bunning, T. J.; Naik, R. R.; Vasudev, M. C. Plasma-Enhanced Chemical Vapor Deposition: Where We Are and the Outlook for the Future. *Chemical Vapor Deposition - Recent Advances and Applications in Optical, Solar Cells and Solid State Devices*; InTech, **2016**.

(47) Friedrich, J. Mechanisms of Plasma Polymerization - Reviewed from a Chemical Point of View. *Plasma Process. Polym.* **2011**.

(48) Roualdes, S.; Rouessac, V.; Durand, J. Plasma Membranes. *Comprehensive Membrane Science and Engineering*; Elsevier, **2010**; *1*, 159–197.

(49) Nisol, B.; Watson, S.; Lerouge, S.; Wertheimer, M. R. Energetics of Reactions in a Dielectric Barrier Discharge with Argon Carrier Gas: III Esters. *Plasma Process. Polym.* **2016**, *13* (9), 900–907.

(50) Kakaroglou, A.; Nisol, B.; Baert, K.; De Graeve, I.; Reniers, F.; Van Assche, G.; Terryn, H. Evaluation of the Yasuda Parameter for the Atmospheric Plasma Deposition of Allyl Methacrylate. *RSC Adv.* **2015**, *5* (35), 27449–27457.

(51) Short, R. D.; Steele, D. A. Testing the Hypothesis: Comments on Plasma Polymerisation of Acrylic Acid Revisited. *Plasma Process. Polym.* **2010**, *7* (5), 366–370.

(52) Hegemann, D.; Körner, E.; Guimond, S. Reply to: "Testing the Hypothesis: Comments on Plasma Polymerization of Acrylic Acid Revisited." *Plasma Process. Polym.* **2010**, *7* (5), 371–375.

(53) von Keudell, A.; Benedikt, J. A Physicist's Perspective on "Views on Macroscopic Kinetics of Plasma Polymerisation." *Plasma Process. Polym.* **2010**, *7* (5), 376–379.

(54) Gleason, K. K. A Chemical Engineering Perspective on "Views on Macroscopic Kinetics of Plasma Polymerisation." *Plasma Process. Polym.* **2010**, *7* (5), 380–381.

(55) Morent, R.; De Geyter, N.; Jacobs, T.; Van Vlierberghe, S.; Dubruel, P.; Leys, C.; Schacht, E. Plasma-Polymerization of HMDSO Using an Atmospheric Pressure Dielectric Barrier Discharge. *Plasma Process. Polym.*, **2009**, *6*, S537–S542.

(56) Nisol, B.; Gagnon, H.; Lerouge, S.; Wertheimer, M. R. Energy of Reactions in Atmospheric-Pressure Plasma Polymerization with Inert Carrier Gas. *Plasma Process. Polym.* **2016**, *13* (3), 366–374.

(57) Hegemann, D.; Hossain, M. M.; Körner, E.; Balazs, D. J. Macroscopic Description of Plasma Polymerization. *Plasma Process. Polym.* **2007**, *4* (3), 229–238.

(58) Scheltjens, G.; Da Ponte, G.; Paulussen, S.; De Graeve, I.; Terryn, H.; Reniers, F.; Van Assche, G.; Van Mele, B. Deposition Kinetics and Thermal Properties of Atmospheric Plasma Deposited Methacrylate-Like Films. *Plasma Process. Polym.* **2016**, *13* (5), 521–533.

(59) Mertens, J.; Baneton, J.; Ozkan, A.; Pospisilova, E.; Nysten, B.; Delcorte, A.; Reniers, F. Atmospheric Pressure Plasma Polymerization of Organics: Effect of the Presence and Position of Double Bonds on Polymerization Mechanisms, Plasma Stability and Coating Chemistry. *Thin Solid Films* **2019**, *671*, 64–76.

(60) Yasuda, H. Glow Discharge Polymerization. In *Thin Film Processes*; Elsevier, **1978**; *16*, 361–398.

(61) Yasuda, H.; Iriyama, Y. Plasma Polymerization. In *Comprehensive Polymer Science and Supplements*; Elsevier, **1989**; 357–375.

(62) Biederman, H. *Plasma Polymer Films*; Imperial College Press, **2004**.

(63) Kumar, A.; Grant, D.; Alancherry, S.; Al-Jumaili, A.; Bazaka, K.; Jacob, M. V. Plasma Polymerization: Electronics and Biomedical Application. In *Plasma Science and Technology for Emerging Economies*; Springer Singapore, **2017**; 593–657.

(64) Klages, C. P.; Höpfner, K.; Kláke, N.; Thyen, R. Surface Functionalization at Atmospheric Pressure by DBD-Based Pulsed Plasma Polymerization. *Plasmas Polym.* **2000**, *5*, 79–89.

(65) Mackie, N. M.; Dalleska, N. F.; Castner, D. G.; Fisher, E. R. Comparison of Pulsed and Continuous-Wave Deposition of Thin Films from Saturated Fluorocarbon/H2 Inductively Coupled Rf Plasmas. *Chem. Mater.* **1997**, *9* (1), 349–362.

(66) Lefohn, A. E.; Mackie, N. M.; Fisher, E. R. Comparison of Films Deposited from Pulsed and Continuous Wave Acetonitrile and Acrylonitrile Plasmas. *Plasmas Polym.* **1998**, *3*, 197–209.

(67) Batan, A.; Nisol, B.; Kakaroglou, A.; De Graeve, I.; Van Assche, G.; Van Mele, B.; Terryn, H.; Reniers, F. The Impact of Double Bonds in the APPECVD of Acrylate-Like Precursors. *Plasma Process. Polym.* **2013**, *10* (10), 857–863.

(68) Boscher, N. D.; Hilt, F.; Duday, D.; Frache, G.; Fouquet, T.; Choquet, P. Atmospheric Pressure Plasma Initiated Chemical Vapor Deposition Using Ultra-Short Square Pulse Dielectric Barrier Discharge. *Plasma Process. Polym.* **2015**, *12* (1), 66–74.

(69) Hilt, F.; Boscher, N. D.; Duday, D.; Desbenoit, N.; Levalois-Grützmacher, J.; Choquet, P. Atmospheric Pressure Plasma-Initiated Chemical Vapor Deposition (AP-PiCVD) of Poly(Diethylallylphosphate) Coating: A Char-Forming Protective Coating for Cellulosic Textile. *ACS Appl. Mater. Interfaces* **2014**, *6* (21), 18418–18422.

(70) Mauchauffé, R.; Bonot, S.; Moreno-Couranjou, M.; Detrembleur, C.; Boscher, N. D.; Van De Weerdt, C.; Duwez, A. S.; Choquet, P. Fast Atmospheric Plasma Deposition of Bio-Inspired Catechol/Quinone-Rich Nanolayers to Immobilize NDM-1 Enzymes for Water Treatment. *Adv. Mater. Interfaces* **2016**, *3* (8), 1–6.

(71) Bonot, S.; Rodolphe, M.; Boscher, N. D.; Moreno-Couranjou, M.; Cauchie, H. M.; Choquet, P. Self-Defensive Coating for Antibiotics Degradation - Atmospheric Pressure Chemical Vapor Deposition of Functional and Conformal Coatings for the Immobilization of Enzymes. *Adv. Mater. Interfaces* **2015**, *2* (14), 1–11.

(72) Camporeale, G.; Moreno-Couranjou, M.; Bonot, S.; Mauchauffé, R.; Boscher, N. D.; Bebrone, C.; Van de Weerdt, C.; Cauchie, H.-M.; Favia, P.; Choquet, P. Atmospheric-Pressure Plasma Deposited Epoxy-Rich Thin Films as Platforms for Biomolecule Immobilization-Application for Anti-Biofouling and Xenobiotic-Degrading Surfaces. *Plasma Process. Polym.* **2015**, *12* (11), 1208–1219.

(73) Loyer, F.; Combrisson, A.; Omer, K.; Moreno-Couranjou, M.; Choquet, P.; Boscher, N. D. Thermoresponsive Water-Soluble Polymer Layers and Water-Stable Copolymer Layers Synthesized by Atmospheric Plasma Initiated Chemical Vapor Deposition. *ACS Appl. Mater. Interfaces* **2019**, *11* (1), 1335–1343.

(74) Gandhi, A.; Paul, A.; Sen, S. O.; Sen, K. K. Studies on Thermoresponsive Polymers: Phase Behaviour, Drug Delivery and Biomedical Applications. *Asian J. Pharm. Sci.* **2015**, *10* (2), 99–107.

(75) Liu, J.; Debuigne, A.; Detrembleur, C.; Jérôme, C. Poly(N -Vinylcaprolactam): A Thermoresponsive Macromolecule with Promising Future in Biomedical Field. *Adv. Healthc. Mater.* **2014**, *3* (12), 1941–1968.

(76) Lee, B.; Jiao, A.; Yu, S.; You, J. B.; Kim, D.-H.; Im, S. G. Initiated Chemical Vapor Deposition of Thermoresponsive Poly(N-Vinylcaprolactam) Thin Films for Cell Sheet Engineering. *Acta Biomater.* **2013**, *9* (8), 7691–7698.

(77) Beija, M.; Marty, J.-D.; Destarac, M. Thermoresponsive Poly(N-Vinyl Caprolactam)-Coated Gold Nanoparticles: Sharp Reversible Response and Easy Tunability. *Chem. Commun.* **2011**, *47* (10), 2826.

(78) Moreno-Couranjou, M.; Loyer, F.; Grysan, P.; Boscher, N. D.; Choquet, P. Insights into Switchable Thermoresponsive Copolymer Layers by Atmospheric Pressure Plasma-initiated Chemical Vapour Deposition. *Plasma Process. Polym.* **2020**, *17* (3), 1900172.

(79) Loyer, F. Study of Nanopulsed Discharges for Plasma-Polymerization: Experimental Characterization and Theoretical Understanding of Growth Mechanisms in the Deposition of Functional Polymer Thin Films, Luxembourg University, **2019**.

(80) Loyer, F.; Bengasi, G.; Frache, G.; Choquet, P.; Boscher, N. D. Insights in the Initiation and Termination of Poly(Alkyl Acrylates) Synthesized by Atmospheric Pressure Plasma-Initiated Chemical Vapor Deposition (AP-PiCVD). *Plasma Process. Polym.*

2018, *15* (5), 1800027.

(81) Loyer, F.; Bulou, S.; Choquet, P.; Boscher, N. D. Pulsed Plasma Initiated Chemical Vapor Deposition (PiCVD) of Polymer Layers − A Kinetic Model for the Description of Gas Phase to Surface Interactions in Pulsed Plasma Discharges. *Plasma Process. Polym.* **2018**, *15* (12), 1800121.

(82) Wang, M.; Wang, X.; Moni, P.; Liu, A.; Kim, D. H.; Jo, W. J.; Sojoudi, H.; Gleason, K. K. CVD Polymers for Devices and Device Fabrication. *Adv. Mater.* **2017**, *29* (11), 1604606.

(83) Lau, K. K. S.; Gleason, K. K. Initiated Chemical Vapor Deposition (ICVD) of Poly(Alkyl Acrylates): A Kinetic Model. *Macromolecules* **2006**, *39* (10), 3695–3703.

(84) Baxamusa, S. H.; Im, S. G.; Gleason, K. K. Initiated and Oxidative Chemical Vapor Deposition: A Scalable Method for Conformal and Functional Polymer Films on Real Substrates. *Phys. Chem. Chem. Phys.* **2009**, *11* (26), 5227–5240.

(85) Wang, M.; Wang, X.; Moni, P.; Liu, A.; Kim, D. H.; Jo, W. J.; Sojoudi, H.; Gleason, K. K. CVD Polymers for Devices and Device Fabrication. *Adv. Mater.* **2017**, *29* (11), 1604606

CHAPTER II ─ Importance of the Monomer Structure on the AP-PiCVD Reaction

This chapter demonstrates the importance of the monomer structure on the growth mechanisms and performances of low dielectric constant insulating thin films elaborated from the atmospheric-pressure plasma-enhanced chemical vapour deposition (AP-PECVD) reaction of three tetrasiloxane compounds. Through a comprehensive experimental study, the use of vinylic monomers is confirmed as a prerequisite for AP-PiCVD to enable free-radical polymerisation, allowing the retention of the starting monomer's structure, and surface reaction pathways yielding the formation of atomically smooth thin films with excellent insulating properties.

Contents

Article(s) submitted from these results

Abessolo Ondo, D., Loyer, F., Boscher, N. D. (2020). Significance of Double Bonds and Cyclic Structure on the AP-PECVD of Low-k Organosilicon Insulating Layers. Submitted in Plasma Processes and Polymers

Full contribution: experimental work on the synthesis and characterization of the thin films and treatment, analysis and interpretation of the collected data, redaction of the manuscript

Received: 28 October 2020 | Revised: 30 December 2020 | Accepted: 2 January 2021

DOI: 10.1002/ppap.202000222

FULL PAPER

PLASMA PROCESSES AND POLYMERS

Influence of double bonds and cyclic structure on the AP-PECVD of low-*k* organosilicon insulating layers

Dominique Abessolo Ondo[1,2] | **François Loyer**[1] | **Nicolas D. Boscher**[1]

[1]Materials Research and Technology Department, Luxembourg Institute of Science and Technology, Belvaux, Luxembourg

[2]University of Luxembourg, Esch-sur-Alzette, Luxembourg

Correspondence
Nicolas D. Boscher, Materials Research and Technology Department, Luxembourg Institute of Science and Technology, 41 Rue du Brill, L-4422 Belvaux, Luxembourg.
Email: nicolas.boscher@list.lu

Funding information
Luxembourg National Research Fund, Grant/Award Number: PRIDE15/10935404

Abstract

The influence of the monomer's structure on the growth mechanisms and performances of low dielectric constant insulating thin films elaborated from the atmospheric-pressure plasma-enhanced chemical vapour deposition reaction of three different tetrasiloxane compounds is elucidated. The presence of vinyl bonds enables free-radical polymerisation and surface reaction pathways, which is strongly favoured from the combination of ultra-short plasma pulses (ca. 100 ns), as polymerisation initiator, with long plasma off-times (10 ms) to yield the formation of atomically smooth thin films with excellent insulating properties (in the range of 10^{-7} A·cm^{-2}).

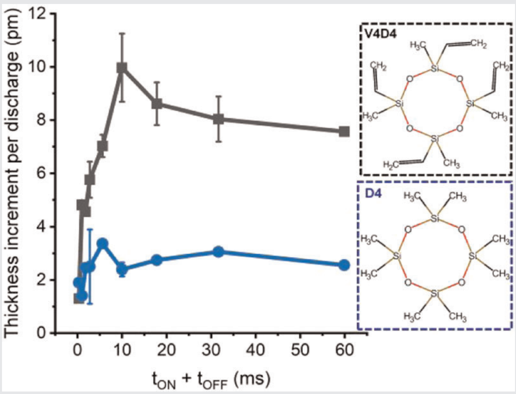

KEYWORDS

atmospheric plasma, dielectric barrier discharge, low-*k* dielectric, nanosecond pulse discharge, plasma-initiated polymerisation

1 | INTRODUCTION

Dielectric polymer thin films are essential materials for organic field effect transistors (OFETs), which are a key element in the emerging field of flexible electronics, owing to their lightweight, insulating properties and mechanical flexibility.[1,2] Irrespective of the OFET configuration, the dielectric layer is always in direct contact with the active layer (i.e., semiconducting layer). Charge transport occurs in the first few molecular layers near the surface of the gate dielectric under the application of an electric field. Consequently, the gate dielectric has a strong influence on the charge transport in OFET devices,[1] and high capacitance densities from the dielectric are essential to lower the power operation of electronic devices. This can theoretically be achieved from high-*k* materials, which, however, suffer from rather high leakage current and dipole disordering that affects the carrier mobility of the underlying semiconductor layer.[2-4] Thus, ultrathin low-*k* and ultralow-*k* layers provide a good alternative as a gate dielectric.

Among the different processing pathways available for the synthesis of gate dielectric polymer thin films, chemical vapour deposition (CVD) processes provide a one-step route for the synthesis, deposition and integration of functional thin films.[5] Moreover, the deposition of the material directly from the gas phase suppresses the need for orthogonal solvents and even allows the processing of insoluble and non-meltable materials on unconventional substrates.[5] Plasma-enhanced chemical vapour deposition (PECVD) processes have been widely used for the elaboration of low-*k* thin films.[6,7] If several strategies (i.e., porogen approach,[8] foaming approach,[9] cyclic precursor approach[10] and carbon-bridging approach[11]) have been proposed to lower the dielectric constant of the materials, the resulting thin films, called "plasma polymers," suffer from moderate-to-poor retention of the precursor structure or/and limited mechanical or insulating properties. In particular, the PECVD of low-*k* dielectric thin films from constitutive porosities (e.g., cyclic precursor approach) is restricted by the disruption of the ring structure of cyclic precursors.[12] However, the low-pressure initiated chemical vapour deposition (iCVD) of vinyl-containing precursors allows the retention of the monomer structure and their polymerisation in a thin film form directly from the gas phase. The iCVD of 1,3,5-trimethyl-1,3,5-trivinyl cyclotrisiloxane (V3D3) was notably reported to yield the formation of low-*k* polymer thin films (i.e., $k = 2.2$) that meet a wide range of requirements for the next generation of electronic devices.[13]

Yet, plasma-assisted deposition approaches possess the significant advantage of being potentially operated under atmospheric-pressure conditions, which is highly desirable to reduce the equipment costs and number of procedures for in-line processing.[14,15] Therefore, huge efforts have been made to improve the selectivity of AP-PECVD processes and notably favour the free-radical polymerisation of vinylic monomers. Proposed strategies include the softening of plasma using various plasma gases,[16,17] discharge configurations[14] and plasma excitation modes.[18] Among all the developed methods, pulsing the plasma discharge is a common approach to promote a better retention of the monomer structure, owing to the predominant occurrence of a plasma-induced free-radical polymerisation pathway, which can persist over several tens of milliseconds during the plasma off-time (t_{OFF}), whereas photons, ions and electrons rapidly disappear.[19] A recent approach called plasma-initiated chemical vapour deposition (PiCVD)[20] combines ultrashort plasma pulses ($t_{ON} < 100$ ns) and plasma off-times in the range of the free-radical polymerisation lifetime (t_{OFF} from 1 to 100 ms) to yield the atmospheric-pressure synthesis and deposition of atomically smooth, conformal ultrathin low-*k* polymer insulating layers.[12,21] This ultrashort square-wave-pulsed plasma process, displaying strong similarities with iCVD, has notably provided thin films with an unprecedented degree of polymerisation for plasma-enhanced or atmospheric-pressure CVD processes.[22] The significance of the ultrashort square-wave pulses frequency[22-24] and monomer saturation ratio, P_M/P_{sat} (with P_M being the partial pressure of the monomer and P_{sat} the saturation pressure of the monomer at the temperature of interest), has recently been demonstrated.[21] The understanding gained on the PiCVD reaction enables the definition of ideal process windows. Yet, if all these studies claim the presence of polymerisable double bonds as a prerequisite to the PiCVD of formation of atomically smooth and conformal polymer layers with an excellent retention of the monomer functionality, none of them have demonstrated this requirement. The present study evidences the significance of vinyl groups and ring structure in ultrashort square-wave-pulsed AP-PECVD from the growth and properties of tetrasiloxane-based thin films. In particular, the selection of vinylic or nonvinylic and linear or cyclic tetrasiloxane compounds (i.e., decamethyltetrasiloxane [DMTSO], 1,3,5,7-tetramethyl-1,3,5,7-tetravinylcyclotetrasiloxane [V4D4] and octamethylcyclotetrasiloxane [D4]) enables to evidence the influence of the monomer structure on the deposition reaction at different plasma pulse frequencies. The cross-comparison of the thin film's deposition rate, chemistry and morphology highlighted the importance of unsaturated vinyl bonds to sustain the free-radical polymerisation during the plasma off-time. The investigation of the thin films' insulating properties confirmed the defect-free and pinhole-free nature of the layer obtained from V4D4, resulting in good insulating properties of 29-nm-thick pV4D4 thin films that exhibit a leakage current density in the range of 10^{-7} A·cm^{-2}.

2 | EXPERIMENTAL SECTION

2.1 | Materials and substrates

The three tetrasiloxane compounds investigated in this study, that is, DMTSO (97%; Sigma-Aldrich); V4D4 (97%; Fluorochem) and D4 (98%; Sigma-Aldrich), were all used as purchased and without any further purification. All the deposition experiments were carried on intrinsic and highly boron-doped ($\rho = 0.01$ Ω·cm) polished silicon wafers (Siltronix). Before each experiment, the silicon wafers were treated during 40 s using a 95%/5% argon/oxygen atmospheric-pressure plasma operated in the dielectric barrier discharge reactor described in the following section.

2.2 | AP-PECVD of polymer layers

The thin films were elaborated in the dynamic mode using an open-air atmospheric-pressure dielectric barrier discharge

(AP-DBD) setup, as previously described.[18,25] Briefly, the AP-DBD setup is composed of two high-voltage electrodes (30-mm width and 300-mm length) covered with an alumina dielectric and a stainless steel moving table (1–3 mm·s^{-1}) as a ground electrode (Figure S1a,b). The plasma was ignited by 1-μs high-voltage square-wave pulses of 6 kV produced by an AHTPB10F generator from EFFITECH, allowing the generation of two ultrashort plasma discharges (i.e., $t_{ON} = 100$ ns) at the voltage rising and falling edges (Figure S2). Plasma pulse frequencies ranging from 16.7 to 3160 Hz were studied, corresponding to plasma off-times (t_{OFF}) ranging from 316 μs to 59.9 ms. The discharge gap was maintained as 1 mm. The tetrasiloxane compounds were directly delivered to the deposition area using a bubbler setup and argon (99.999%; Air Liquid) as a carrier gas. The flow of carrier gas (Ar), fixed to 15 L·min^{-1} ($F_{carrier}$) for all the tetrasiloxane compounds in the first part of the present work (reduced to 4 L·min^{-1} for DMTSO and D4 in Section 3.4), was diluted with a second source of argon to maintain the total gas flow constant to 20 L·min^{-1} (Figure S1c). To prevent contamination from the surrounding atmosphere and more particularly reduce the O_2 and N_2 contamination, argon fluxes were added on both sides of the AP-DBD electrodes.

2.3 | Thin-film characterisation

2.3.1 | Morphology and topography

Scanning electron microscopy (SEM) images were obtained using a Hitachi SU-70 FE-SEM. To avoid distortions due to charge effect, the samples were coated with a 2-nm platinum film before the SEM observations. A Quanta FEG 200 from EDAX Inc. in environmental SEM (ESEM) mode was used to acquire the images of the viscous thin films and measure their thickness. Atomic force microscopy (AFM) topography images were obtained using an Innova instrument operating in a tapping mode. Film thicknesses were measured by a spectroscopic ellipsometer FS-1, a KLA-Tencor P-17 Stylus profiler and SEM cross-sectional observation. The spectrometric ellipsometry measurements were acquired at a single angle of 65° using four different wavelengths (i.e., 465, 525, 590 and 635 nm), and the data were fitted to a Cauchy model. The weight of the films was determined by weighting the substrates before and after the deposition experiments using a Sartorius ME36S scale. For each deposition condition (monomer and frequency), the thickness and mass growth rates were determined from the measured thicknesses and weight of a minimum of two different thin films prepared using different deposition times. The effective deposition time, which is the time effectively spent under the high-voltage electrodes and calculated independently from the plasma pulse frequency, corresponds to the number of runs (1–20) multiplied by the width of the high-voltage electrodes (30 mm) divided by the speed of the moving table (1–3 mm·s^{-1}). For all the experiments reported in this study, the growth rates were shown to be directly proportional to the deposition time, yielding small standard deviations of the growth rates, even though they were evaluated from thin films prepared with different deposition times.

2.3.2 | Chemical characterisation

Fourier-transform infrared spectroscopy (FTIR) analysis of the AP-PECVD thin films was performed in a transmission mode on double-polished silicon wafers using a Bruker Vertex 70 spectrometer equipped with a deuterated triglycine sulphate detector. The spectra were obtained over a range of 4000–400 cm^{-1} with a resolution of 4 cm^{-1}. A 10-min nitrogen purge was performed before each measurement to diminish the contribution of carbon dioxide and moisture. The monomer spectra were acquired with the same FTIR spectrometer using an attenuated total reflection accessory. X-ray photoelectron spectroscopy (XPS) analyses (300 × 700 μm^2) were carried out with a Kratos Axis Ultra DLD spectrometer using a monochromatic Al Kα X-ray source ($h\nu = 1486.6$ eV). A flooding gun was used to reduce the charging effect on the samples' surface. Photoelectron emission was collected at 0° with respect to the surface normal. The surface of the specimen was pre-cleaned by bombardment with Ar^+ ions (2 kV) before the collection of XPS data. CasaXPS software was used for chemical quantification.

2.3.3 | Density functional theory (DFT) calculations

DFT calculations were performed using the 4.2.1 programme suite.[26] The hybrid functional PBE (Perdew–Burke–Ernzerhof) was used for every calculation along with Ahlrichs' basis set def2-TZVP and Weighend's auxiliary basis set def2/J.[27,28] The numerical chain of sphere approximation RIJCOSX and the dispersion correction D3 were also applied in any instance.[29,30] The bond dissociation energies (BDEs) of the investigated monomers were calculated by using a previously reported method.[23] Analytical frequency calculations were performed for each fragment and molecule to obtain their free enthalpy and to ensure the convergence of the calculation. Due to the molecules' symmetry, only a half (for DMTSO) and fourth (for D4 and V4D4) of the BDEs were calculated.

2.4 | Fabrication and electrical characterisation of the metal/insulator/semiconductor (MIS) devices

The AP-PECVD dielectric thin films were sandwiched between a highly doped Si wafer used as a bottom electrode and a patterned Au layer as a top electrode. The patterned Au layer was prepared using a shadow mask of 1 cm^2 by electron beam evaporation with a base pressure below 10^{-6} mbar. Before Au evaporation, a thin layer of Ti (10 nm) was evaporated on top of the dielectric thin film to ensure the adherence of the Au layer (50 nm). The capacitance versus frequency (*C–f*) characteristics of the MIS devices were measured using an IM3570 Hioki impedance analyser. The *C–f* measurement was performed at a frequency range of (100 Hz; 1 MHz) with an excitation level of 0.1 V. The dielectric constant was estimated at 1 kHz using the following relation:

$$\frac{C}{S} = \frac{\varepsilon_0 \varepsilon'_{\mathrm{polymer}}}{d_{\mathrm{polymer}}}, \tag{1}$$

where C is the capacitance of the dielectric thin film, S is the surface of the contact, $\mathcal{E}_0$, $\mathcal{E}'$ and d_{polymer} are the vacuum permittivity, the dielectric constant and the thickness of the thin film, respectively. The current density–voltage (*J–V*) characteristics of the MIS devices were determined at ambient atmosphere using Keithley 2634B instrument.

3 | RESULTS AND DISCUSSION

To demonstrate the influence of vinyl groups and ring structures on the atmospheric-pressure plasma-enhanced chemical vapour deposition of organosilicon insulating layers, we selected three different tetrasiloxane compounds, that is, V4D4, D4 and DMTSO (Figure 1a). DMTSO

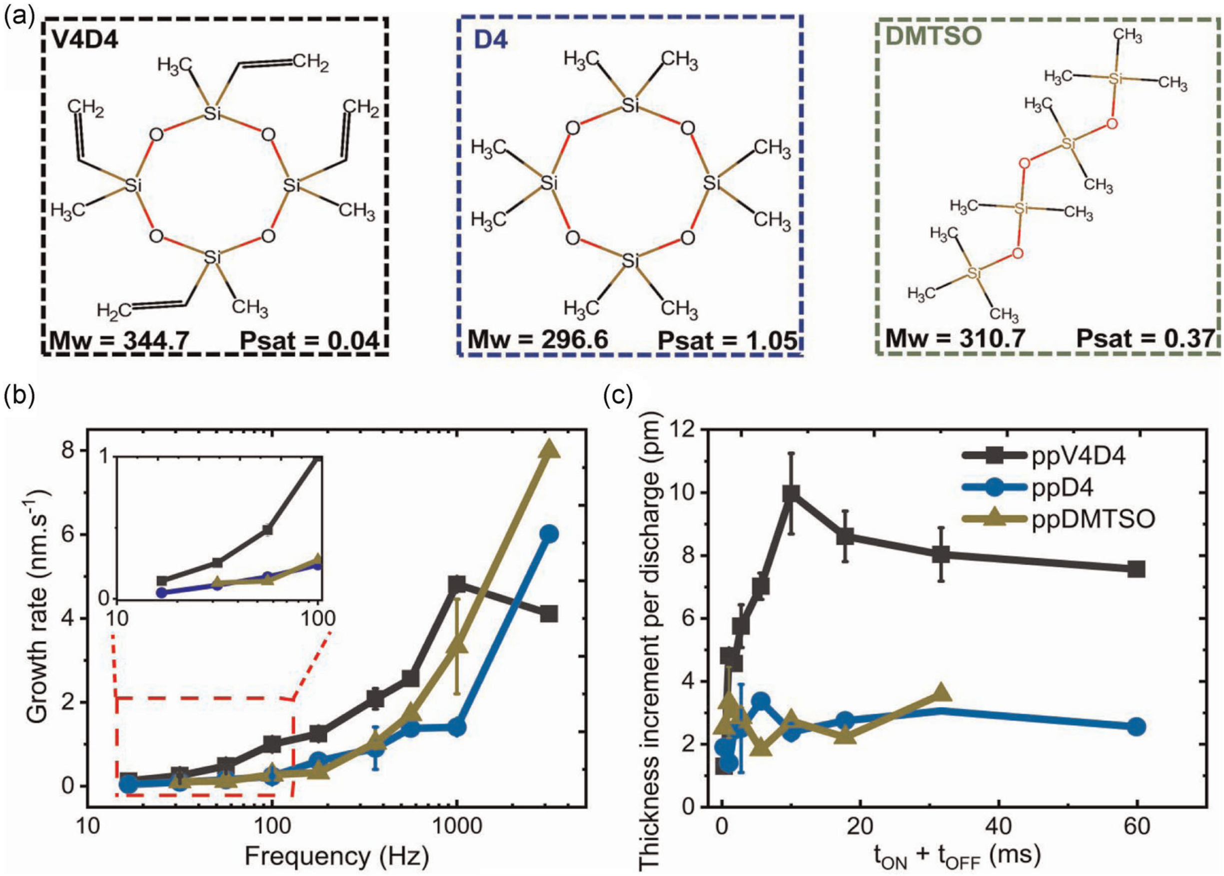

FIGURE 1 (a) The chemical structure, molecular weight (g·mol^{-1}) and the vapour pressure (P_{sat}, mmHg; https://pubchem.ncbi.nlm.nih.gov)[12] of the studied organosiloxane monomers. (b) Growth rates per second according to the plasma pulse frequency (Hz) and (c) thickness increment per $t_{\mathrm{ON}} + t_{\mathrm{OFF}}$ cycle for the thin films grown from 1,3,5,7-tetramethyl-1,3,5,7-tetravinylcyclotetrasiloxane (V4D4), octamethylcyclotetrasiloxane (D4) and decamethyltetrasiloxane (DMTSO)

(also reported as DMTS and MD2M in the literature)[31] is a linear tetrasiloxane substituted with methyl groups, similar to the well-studied hexamethyldisiloxane (HMDSO)[32] but with a longer Si–O–Si backbone. D4 (also reported as OMCTS and OMCATS in the literature)[33,34] and V4D4 are cyclic tetrasiloxanes, with D4 being substituted by only methyl groups and V4D4 possessing four methyl and four vinyl groups. To elucidate the AP-PECVD growth mechanisms of the selected tetrasiloxane compounds, we selected an AP-DBD fed with argon, used as both carrier and plasma gas, and ignited with 1-µs square-wave high-voltage pulses (Figure S2). In this first section, the carrier flow and total flow rate were kept constant to ensure a fair comparison of the tetrasiloxane compounds (Table S1). The assumption that the argon carrier gas was saturated with the monomer vapours and that under such conditions the monomer saturation ratio (P_M/P_{sat}) is approximatively equal to the ratio of the carrier gas flow rate over the total flow rate ($F_{carrier}/F_{total}$) enables the investigation of similar monomer saturation ratios (Figure S1c). Series of thin films were prepared from each of the selected monomers using different square-wave high-voltage pulse frequencies (later called plasma pulse frequencies) to determine the influence of the monomer's structure on the AP-PECVD reaction. Naked eye observations revealed that the physical state of the thin films was strongly influenced by the nature of the tetrasiloxane compound. Whereas macroscopically smooth and adherent thin films were grown from V4D4, viscous and inhomogeneous thin films were obtained from D4 and DMTSO (Figure S3). These morphology discrepancies hint at different chemistries (chain length, degree of reticulation) and suggest a strong influence of the monomer structure on the growth mechanisms.

3.1 | Effect on the growth rate

The mass and the growth rates were evaluated from weight, ellipsometry and profilometry measurements. One should note that irrespective of the plasma pulse frequency, the substrate temperature (known to affect surface adsorption) remained constant at room temperature. In accordance with previous studies[20,22] and irrespective of the monomers, the growth rates (nm·s^{-1}) mainly increase with the increase of the plasma pulse frequency (Figures 1b and S4b, Table S1). This is attributed to the creation of a larger amount of reactive species, owing to the increase of the plasma pulse frequency, which leads to a higher concentration of polymerisation-initiating species [I] responsible for an increase of the deposition rate. Interestingly, a collapse in the growth and mass rates is observed for plasma pulse frequencies higher than 1000 Hz for the thin films obtained from V4D4 (Figures 1b and S4b). This drop of the deposition rate is known to be highly dependent on the monomer; for example, a maximum growth rate was observed around 300 and 1000 Hz for *N*-vinylcaprolactam (NVCL)[35] and glycidyl methacrylate (GMA),[22] respectively. The decay of the deposition rates at higher frequencies is related to an excess of reactive species that induces the depletion of the monomer. It is assumed that this behaviour is more pronounced for the monomer possessing a low vapour pressure (P_{sat}) such as NVCL ($P_{sat,\,NVCL,\,50°C} = 0.355$ mmHg),[35] GMA ($P_{sat,\,GMA,\,20°C} = 0.315$ mmHg)[22] and V4D4 ($P_{sat,\,V4D4,\,20°C} = 0.040$ mmHg).[12] Indeed, low P_{sat} implies a lower concentration of the monomer in the gas phase, which induces a higher probability of interaction between the monomer and the active plasma species that is responsible for significant monomer depletion.

A closer look at the growth rates at low frequencies allowed spotting further differences between the thin films obtained from V4D4 and the ones obtained from D4 and DMTSO (Figure 1b, inset). In particular, higher growth rates are achieved from V4D4 at low plasma pulse frequencies. To have a better insight into these differences, the growth rate data are plotted as thickness increment per $t_{ON} + t_{OFF}$ cycle (with t_{ON} kept constant; Figure 1c and Table S1). Similar to previous studies,[20-22] the thickness increment per $t_{ON} + t_{OFF}$ cycle for the thin films obtained from V4D4 highlights the occurrence of deposition during t_{OFF} with an increase of the thickness for $t_{ON} + t_{OFF}$ cycles of 0.33–10 ms (Figure 1c). A quasi-plateau is reached for t_{OFF} longer than 10 ms. This plateau around 10 pm per $t_{ON} + t_{OFF}$ cycle is attributed to the termination of the free-radical polymerisation of V4D4. Indeed, soon after the end of each plasma pulse (t_{ON}), it is assumed that only the free-radical polymerisation reaction takes place. Previous works reported that the propagation of the free-radical polymerisation reaction can occur for 1–100 ms after t_{ON} under the studied conditions.[20-22,35]

However, no significant increase of the thickness increment per $t_{ON} + t_{OFF}$ cycle is observed for the thin films obtained from D4 and DMTSO (Figure 1c). Irrespective of the t_{OFF} duration, both showed a quasi-constant thickness increment per $t_{ON} + t_{OFF}$ cycle, fluctuating around 3 pm. This observation demonstrated that in the absence of polymerisable bonds, such as for D4 and DMTSO, the growth is not sustained during plasma off-time. Indeed, exposure of monomer to ultrashort plasma pulses produces a range of radicals and neutral fragments that can recombine or act as initiation groups.[23,36] In the case of V4D4, a part of the activated species formed during the plasma on-time can initiate the growth of polymer chains and yield solid and homogeneous thin films. Yet, the lack of polymerisable bonds and insufficient plasma activation in the case of D4 and DMTSO result in the formation of short oligomers and poorly reticulated chains responsible for the formation of viscous and poorly adherent thin films such as that reported above (Figure S3).

3.2 | Effect on the chemistry

The dependence of the growth rate on the monomer structure evidenced the occurrence of different mechanisms, which can also affect the chemistry of the resulting thin films. FTIR was used to characterise the different bonding arrangements in the as-deposited thin films, which were compared with their respective monomers. The absorption bands in the 1250–950 cm^{-1} region are associated with the asymmetric stretching and bending motions of the Si–O–Si groups.[37-39] Interestingly, similarities were observed in the spectra of the linear monomer DMTSO and its corresponding thin films elaborated at low plasma pulse frequencies ($f \leq 100$ Hz), indicating the good retention of the monomer structure during the deposition reaction (Figure S5). Indeed, the band associated with the Si–O–Si group is sharp and split with peaks at 1068 and 1032 cm^{-1}, which represent the contribution of the Si–O–Si network and suboxide stretching forming the structure of the DMTSO monomer.[39] This band is broadened in the thin film elaborated at 100 Hz, showing peaks at 1087 and 1032 cm^{-1} (Figure 2). Although the splitting of this band is typical for long linear siloxane chains,[34,37] the shift and broadening of the Si–O–Si band indicate the heterogeneity of Si–O bonding environment that might include the initial DMTSO arrangement. The increase of the plasma pulse frequency induces a dramatic change in the Si–O bonding environment with a noticeable transition observed when reaching 178 Hz (Figures 2 and S6, Table S2). A further increase of the plasma pulse frequency leads to a clear conversion of the dominant Si–O–Si network structure, whose peak is centred at 1087 cm^{-1}, to a silsesquioxane-like ladder structure showing a peak at 1106 cm^{-1}.[39] Further information is found in the 1290–1230 cm^{-1} region where the peak related to the Si–CH_3 is known to vary in position depending on the degree of cross-linking of the siloxane coatings.[11,32] Indeed, the absorption peak assigned to the siloxy unit O_x–Si–$(CH_3)_{(4-x)}$ ($x = 1, 2, 3$), with x being the number of alkyl substituent, shifts towards higher wavenumbers upon the mono-, di-, or tri-substitution of the silicon atom by oxygen, designated as "M," "D" and "T" configurations, respectively. The position of the band associated with the Si–CH_3 located at 1256 cm^{-1} in the monomer (which is consistent with the equal repartition

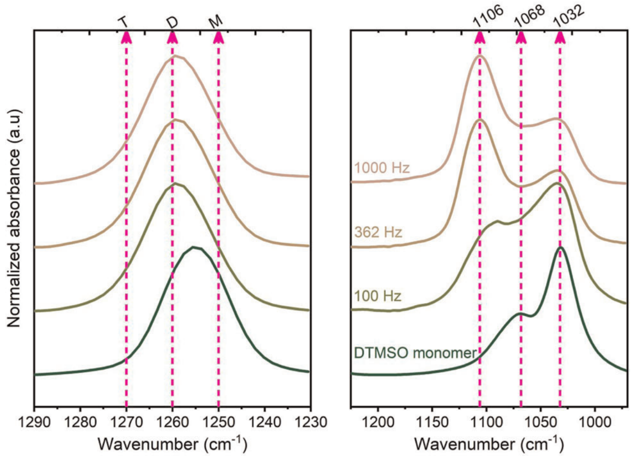

FIGURE 2 Fourier-transform infrared spectra of the 1290–1230 cm^{-1} and the 1225–970 cm^{-1} regions corresponding to (left) the Si–CH_3 bonding region and (right) the Si–O–Si stretching absorption region of the decamethyltetrasiloxane (DMTSO) monomer and the thin films elaborated at different plasma pulse frequencies. The M, D and T groups represent the mono-, di- and tri-substitution of the silicon atom by oxygen, respectively

of the Si atoms between the M and D configurations) is slightly shifted to 1259 cm^{-1} in all the DMTSO-based thin films, irrespective of the plasma pulse frequency. This slight shift is attributed to the preponderant formation of Si^D configuration, which is a chain propagating unit, indicating that the polymerisation of this monomer preferentially occurs through a methyl group subtraction, similar to the plasma polymerisation of HMDSO using low-frequency sinusoidal excitation.[32,40] Indeed, if the energy transfer from excited argon species can provide sufficient energy to break any of the bonds in HMDSO,[41,42] DFT calculations have highlighted that the most probable initial decomposition reaction of HMDSO is to eliminate a CH_3 radical by Si–C bond dissociation.[43] Similarly, DFT calculation of the BDE of DMTSO (Figure S7) points out the methyl groups from Si^M–$(CH_3)_3$ as weakest bonds (ca. 3.9 eV) in the DMTSO monomer, showing a significant difference in energy with the Si^D–O ($\Delta BDE \approx 1.8$ eV) and suggesting their greater sensitivity to plasma breakdown. Thus, justifying that the polymerisation of DMTSO preferentially occurs through the ablation of a methyl group is in good agreement with the FTIR observations.

The absorption band located in the 900–700 cm^{-1} region is attributed to the Si–C stretching and rocking motions.[32,40] The linear tetrasiloxane monomer, DMTSO, contains both Si–$(CH_3)_2$ and Si–$(CH_3)_3$ groups. The band located at 796 cm^{-1}, common to all the studied monomers and attributed to Si–$(CH_3)_2$, which can originate from O_2–Si–$(CH_3)_2$, is also detected in the DMTSO-based thin films and confirms

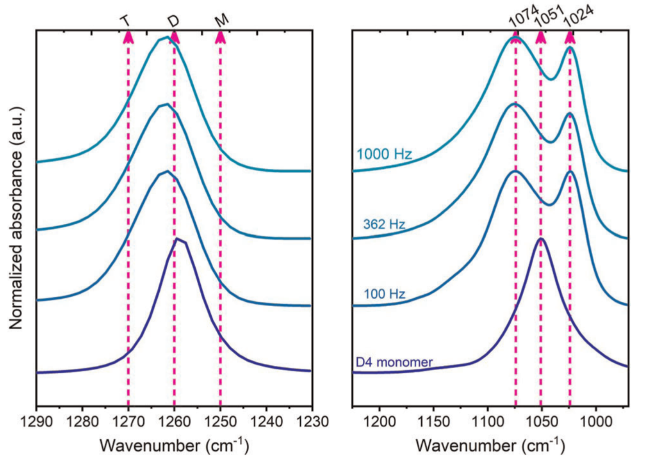

FIGURE 3 Fourier-transform infrared spectra of the 1290–1230 cm^{-1} and the 1225–970 cm^{-1} regions corresponding to (left) the Si–CH_3 bonding region and (right) the Si–O–Si stretching absorption region of the octamethylcyclotetrasiloxane (D4) monomer and the thin films elaborated at different plasma pulse frequencies. The M, D and T groups represent the mono-, di- and tri-substitution of the silicon atom by oxygen, respectively

the retention of the Si configuration to Si^D during the AP-PECVD reaction. However, the band located at around 841 cm^{-1} in the DMTSO monomer and the DMTSO-based thin films is attributed to the Si–$(CH_3)_3$ stretching from O–Si–$(CH_3)_3$ (Figure S8). Even for higher plasma pulse frequencies, the band related to O–Si–$(CH_3)_3$ remains significant and suggests the presence of a large density of end groups that correlates to formation of short oligomers.

Different behaviours were observed for the thin films grown from the two cyclic tetrasiloxane compounds, that is, D4 and V4D4. Although strong similarities are observed at low plasma pulse frequency, that is, 100 Hz, between the V4D4 monomer and its resulting thin film, major discrepancies are already noticed between the D4 monomer and its respective thin films (Figures 3 and S9, Table S3). The asymmetric stretching band associated with the Si–O–Si groups shows a single peak located at 1052 cm^{-1} in the D4 monomer spectrum. This band splits into two peaks located at 1074 and 1024 cm^{-1} in the D4-based thin films. The splitting of this band, already observed for the DMTSO monomer and the DMTSO-based thin films, highlights the preponderant occurrence of a ring-opening reaction, even when using low plasma pulse frequency (e.g., 56.2 Hz; Figure S9). The increase of the plasma pulse frequency up to 1000 Hz neither induced any further broadening of the band related to Si–O–Si nor shifted the Si–CH_3 band from the Si^D configuration. The absence of shifting of the Si–CH_3 band towards higher wavenumbers indicates that the original D configuration of the silicon was retained during the ring-opening reaction undergone by the D4 monomer throughout the deposition process. The band related to Si–$(CH_3)_2$ localised at ca. 798 cm^{-1} is only slightly shifted to 804 cm^{-1} in the spectrum of the D4-based thin films, irrespective of the plasma pulse frequency. Nevertheless, a small shoulder to this peak is observed at around 844 cm^{-1} and indicates the formation of O–Si–$(CH_3)_3$ chain end groups (Figure S10). Combining these results with the retention of the Si^D configuration further confirms that the polymerisation of the D4 monomer predominantly occurs through the cleavage of the Si–O bond of the D4 ring. Indeed, the DFT-calculated BDEs of D4 (Figure S7) reveal moderate differences in energy between the Si^D–$(CH_3)_2$ (ca. 4.3 eV) and Si^D–O (ca. 5.4 eV) bonds, which does not protect the ring from breakdown.

However, the FTIR spectra of the thin films obtained from V4D4 elaborated at low plasma pulse frequency ($f \leq 178$ Hz) display a unique band at ca. 1065 cm^{-1} associated with the Si–O–Si ring (Figures 4, S11 and S12). Such a value is slightly higher than the measured one for V4D4 (1053 cm^{-1}), but it is consistent with the reported ones for iCVD pV4D4 layers (1065 cm^{-1}).[11] The lack of broadening and splitting of this band in the V4D4-based thin films, in contrast to the observations made for D4, is consistent with the hypothesis that the cyclic tetrasiloxane structure of V4D4 is preserved at such low plasma pulse frequency. The increase of the plasma pulse frequency induces a broadening of the Si–O–Si peak, indicating the heterogeneity of Si–O bonding environment that includes the cyclotetrasiloxane ring of V4D4 among other assemblies. Notably, a clear transition occurs when reaching a plasma pulse frequency of 362 Hz

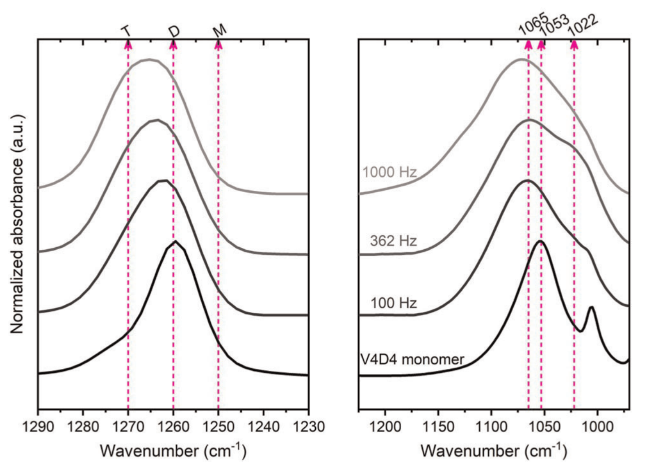

FIGURE 4 Fourier-transform infrared spectra of the 1290–1230 cm^{-1} and the 1225–970 cm^{-1} regions corresponding to (left) the Si–CH_3 bonding region and (right) the Si–O–Si stretching absorption region of the 1,3,5,7-tetramethyl-1,3,5,7-tetravinylcyclotetrasiloxane (V4D4) monomer and the thin films elaborated at different plasma pulse frequencies. The M, D and T groups represent the mono-, di- and tri-substitution of the silicon atom by oxygen, respectively

where the heterogeneous Si–O bonding environment is confirmed by the appearance of a shoulder at 1022 cm^{-1} (Figure 4). This shoulder indicates the ring opening of a part of the V4D4 molecules, similar to what was observed with the D4-based thin films. However, the V4D4 ring structure remains far more preserved than the one of D4, even for high plasma pulse frequency ($f \geq 362$ Hz). The superior retention of the V4D4 ring structure is attributed to (i) the presence of its substituents (Figure S7), among which the weakest π-bond of C=C shows a significant difference in energy with the Si^D–O (ca. $\Delta BDE \approx 3.1$ eV) and Si^D–CH_3 (ca. $\Delta BDE \approx 1.4$ eV), hence, justifying the detection of a preponderant substitution of the methyl group by oxygen with the increase of the plasma pulse frequency, and (ii) the conventional free-radical polymerisation pathway that occurs after the initial breakdown of the monomer.[23]

Despite the noise in the 2000–1400 cm^{-1} region of the V4D4-based thin-film spectra hindering any quantitative analysis relative to the peaks that can be found in this region, some qualitative observations were still possible. Indeed, a reduction of the bands related to the vinyl bond, located at 960, 1600, 3017 and 3057 cm^{-1}, suggests the predominant occurrence of free-radical polymerisation (Figures S11 and S13). Furthermore, the generation of polyethylene-like backbones, resulting from the cleavage of the vinyl group during the AP-PECVD reaction, is indicated through the generation of the symmetric stretching band located at 2878 cm^{-1} (Figure S13).[11,44] It should be noted that the reduction of the vinyl band was observed irrespective of the plasma pulse frequency. The Si–CH_3 band is located at 1261 cm^{-1} in the thin films elaborated at plasma pulse frequency equal to or lower than 178 Hz (Figure S12 and Table S4). The position of this peak is close to the one measured for the V4D4 monomer, that is, 1260 cm^{-1}, highlighting the retention of the Si^D configuration. The combination of this result with the preservation of the monomer's ring demonstrated earlier indicates the good retention of the monomer structure during the deposition of the thin film elaborated using low plasma pulse frequencies ($f \leq 178$ Hz). The increase of the plasma pulse frequency results in the shift of the Si–CH_3 band to 1265 cm^{-1} from the V4D4-based thin films elaborated at 362 Hz. The shift of this band towards higher wavenumbers demonstrates the creation of a large proportion of cross-linking Si^T configuration in the V4D4-based thin films formed at higher plasma pulse frequencies, indicating the alteration of the monomer structure.

The relative atomic composition of all the thin films elaborated at 100 and 1000 Hz was examined by XPS. In accordance with their FTIR spectra, all the thin films elaborated at a plasma pulse frequency of 100 Hz presented a relative atomic composition close to one of their respective monomers (Table S5 and Figure S14). The increase of the plasma pulse frequency to 1000 Hz induced a drastic decrease of carbon content from 60 to 29 at% in the DMTSO-based thin films. This result confirms the selective ablation of methyl groups during the AP-PECVD reaction of DMTSO and indicates the formation of a more inorganic material with the increase of the plasma pulse frequency. In the thin films obtained from V4D4, the carbon content is reduced from 54 to 48 at% upon increase of the plasma pulse frequency, whereas no particular modification in the composition of the D4-based thin films was noticed. This further demonstrates the dependence of different mechanisms on the monomer structure, even for high plasma pulse frequency. The decrease of the carbon content in the V4D4-based thin films is accompanied with the increase of the oxygen content, supporting the assumption of a simultaneous ablation of methyl groups and a ring-opening reaction when using high plasma pulse frequencies.

3.3 | Effect on the morphology

Although thin films are deposited at an equivalent saturation ratio P_M/P_{sat} (75%), morphological discrepancies are observed between the thin films obtained from V4D4 and those obtained with the nonvinylic compounds (i.e., D4 and DMTSO), irrespective of the plasma pulse frequency (Figure 5). Indeed, macroscopic observations of the D4- and DMTSO-based thin films displayed viscous and inhomogeneous morphologies that make high-magnification SEM observations difficult due to sample charging and electron beam damage. Nevertheless, numerous particles were readily observed at their surfaces (Figures S15 and S16). The viscous and inhomogeneous morphology of the D4- and DMTSO-based thin films is attributed to the rather short oligomers and poorly reticulated chains formed during the deposition of these monomers, such as evidenced above, and to a preponderance of the gas-phase reactions. Whereas the V4D4-based thin films elaborated at plasma pulse frequencies equal to or higher than 362 Hz displayed rough surface morphologies (Figures 5 and S17), the V4D4-based thin films elaborated at lower frequencies (i.e., $f < 362$ Hz) exhibit a smooth, pinhole and particle-free surface morphology, demonstrating the preponderance of surface reactions when using V4D4 and low frequencies. Hence, high surface roughness is not related to higher growth rates or higher thicknesses, as the thin films obtained from V4D4 and elaborated at low plasma pulse frequencies (i.e., $f < 362$ Hz) combine both smoother surface and higher growth rate than the thin films obtained from the

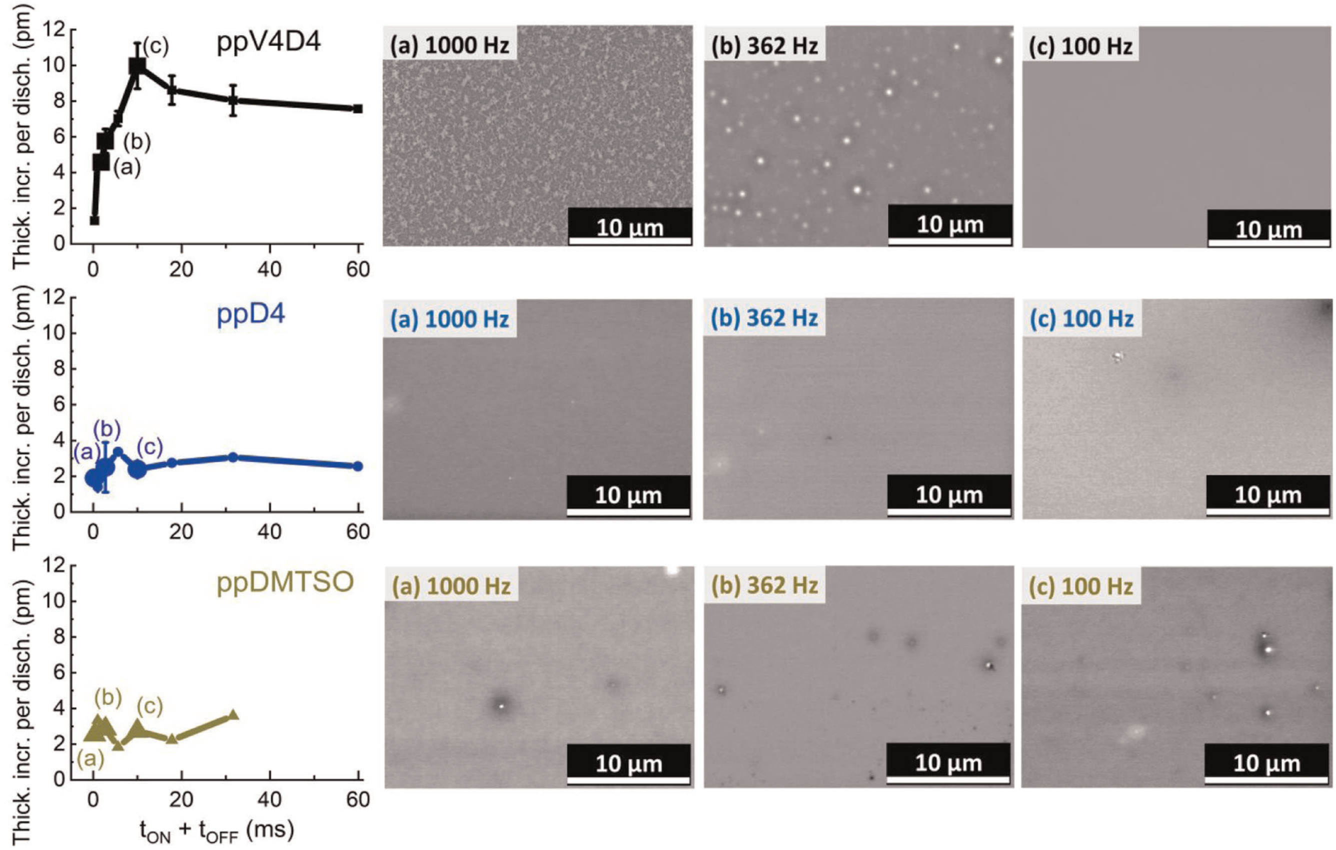

FIGURE 5 (Left) Thickness increment according to the $t_{ON} + t_{OFF}$ cycle duration of the thin films obtained from V4D4, D4 and DMTSO. (Right) Top-view SEM images of the V4D4-based, D4-based and DMTSO-based thin films elaborated at 100, 362 and 1000 Hz. D4, octamethylcyclotetrasiloxane; DMTSO, decamethyltetrasiloxane; V4D4, 1,3,5,7-tetramethyl-1,3,5,7-tetravinylcyclotetrasiloxane

nonvinylic compounds. These results demonstrate the importance of the vinyl bonds to promote the growth of smooth, solid and homogeneous thin films from ultrashort square-wave-pulsed AP-PECVD.

3.4 | Effect on the dielectric properties

The importance of the vinyl bonds is highlighted in the first part of this report as an important parameter for the ultrashort square-wave-pulsed AP-PECVD of smooth and homogeneous polymer thin films. Notably, the use of low ultrashort square-wave pulse repetition frequencies (e.g., 100 Hz) for the deposition of a vinylic monomer (V4D4) results in the prevailing occurrence of surface reactions, especially the free-radical polymerisation reaction, which persists over several tens of millisecond during the long plasma t_{OFF} (Figure 1c). In addition, these V4D4-based thin films display a smooth and particle-free surface morphology across the entire surface of the substrates, including 4-inch silicon wafers (Figures 5 and S3a). This combined with the excellent retention of the monomer structure, highly desirable to form low dielectric constant thin films from a constitutive porosity approach, made these V4D4-based thin films good candidate to assess their dielectric properties. On the contrary, the dielectric properties assessment of the thin films obtained from the nonvinylic compounds could not be possible due to their physical aspect (Figures 5 and S3b,c). To be able to compare and understand the influence of the different tetrasiloxane compounds' structures on the dielectric properties of their resulting thin films, it was essential to determine suitable conditions for the preparation of solid and homogenous thin films with smooth surface from the two nonvinylic compounds, that is, D4 and DMTSO.

Therefore, in this second part, the thin films obtained from the nonvinylic compounds, D4 and DMTSO, were elaborated using a saturation ratio $P_M/P_{sat} = 20\%$, which was identified as a good compromise between the energy-deficient regime (high P_M/P_{sat}) and the monomer-deficient regime.[45,46] Subsequently, series of thin films were prepared at a fix plasma pulse frequency of 100 Hz to fit with the frequency at which the pV4D4 thin films are elaborated and eliminate the influence of the plasma pulse frequency. The thin films obtained from D4 and DMTSO elaborated using a saturation ratio of 20% were solid and macroscopically

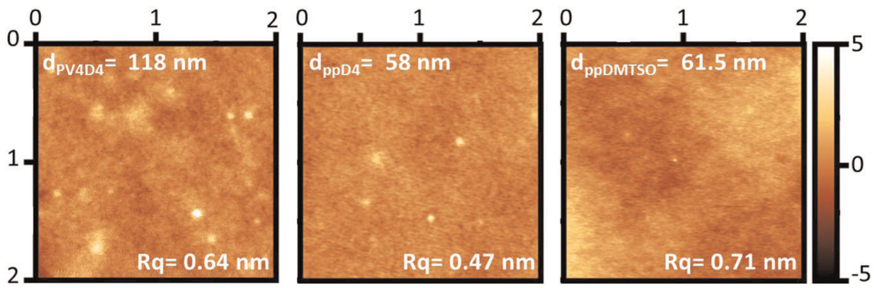

FIGURE 6 Atomic force microscopy images of the as-deposited thin films obtained from V4D4, D4 and DMTSO. The thickness (d_{layers}) and root-mean-square roughness (R_q) values are provided for each of the presented thin films. D4, octamethylcyclotetrasiloxane; DMTSO, decamethyltetrasiloxane; V4D4, 1,3,5,7-tetramethyl-1,3,5,7-tetravinylcyclotetrasiloxane

homogeneous. Their smooth and particulate-free surface morphology was confirmed by SEM (Figure S18). AFM images further witnesses the pinhole-free and defect-free nature of the different thin films (Figure 6). Irrespective of the tetrasiloxane monomer structures and thin film thickness (up to 118 nm), root-mean-square roughness (R_q) were measured below 1 nm. Such low R_q values are desirable for microelectronic applications.[2]

One should note here that if the use of a lower monomer saturation ratio (P_M/P_{sat}) did not significantly altered the chemical composition and bonding arrangement of the D4-based thin films (Figures S19 and S20, Table S6), XPS and FTIR highlighted discrepancies between the DMTSO-based thin films prepared at P_M/P_{sat} of 75% and 20%. Indeed, the DMTSO-based thin film elaborated at $P_M/P_{sat} = 20\%$ shows a main peak located at 1026 cm^{-1} with a weak shoulder at 1068 cm^{-1} that represents the contribution of Si–O–Si suboxide and network (Figures S21 and S22, Table S7). A surge of a small broad peak is noticed at 1137 cm^{-1} that could correspond to the contribution of the silsesquioxane-like cage structure or the O–C vibration in Si–O–C bonds.[8,38,39] This unsurprising result combining with the decrease of the Si–O–Si network band is indicative of the decay of the molecule during the AP-PECVD reaction. However, the band related to the symmetric bending Si–CH_3 is shown to remain located at the same position, that is, 1260 cm^{-1}, demonstrating the existence of an Si–O–Si network, hence confirming a partial retention of the Si^D configuration during the elaboration of the DMTSO-based thin films. Yet, a weak shoulder at 1270 cm^{-1} is also observed in this peak, demonstrating the formation of the cross-linking Si^T configuration. In good agreement with the FTIR observations, XPS analysis revealed that the relative atomic composition of the DMTSO-based thin films elaborated at P_M/P_{sat} of 20% strongly differs from the ones of the monomer and the DMTSO-based thin film elaborated at P_M/P_{sat} of 75% (Table S8). Indeed, DMTSO-based thin films elaborated at P_M/P_{sat} of 20% show a huge increase of the oxygen content from 17.6 to 31 at% measured, confirming the oxidation of silicon during the AP-PECVD reaction. The increase of the oxygen content took place concurrently to a decrease of the carbon content from 60 to 38 at%.

The V4D4-, D4- and DMTSO-based thin films were soaked for 24 h in different common polar solvents (i.e., water, ethanol and acetone) to investigate their chemical stability. Except for the DMTSO-based thin film soaked in water, all the resulting thin films retain their atomically smooth nature with R_q values below 1 nm, regardless of the solvent in which they were soaked (Figures S23 and S24, Table S9). In addition, the thickness of V4D4-based thin films was unaltered, underlying their good chemical stability. This stability is attributed to the highly cross-linked network formed during the low-frequency ultrashort plasma-pulsed AP-PECVD of V4D4 from the polymerisation of the vinyl pendant group of the V4D4 monomer, as confirmed by FTIR (Figures S11 and S13). However, a significant decrease of the thickness was observed for the D4-based (except in water) and DMTSO-based thin films (ca. 37%–57%), assuredly due to the difficulty of these nonvinylic monomers to form highly branched and connected network at low plasma pulse frequencies (ultrashort t_{ON} combined with a long t_{OFF}).

3.4.1 | Ultrathin low-*k* insulating thin films

Measurements on a series of fabricated MIS were performed to quantify the dielectric properties, such as the leakage current and the capacitances as a function of the frequency, of the different thin films. For each of the investigated tetrasiloxane monomer, the areal capacitance (C_i) of their as-deposited thin films was measured for three different thicknesses and plotted according to the frequency (Figure 7). An abrupt drop of the capacitance with vanishing capacitance in the high frequency limit was especially observed for the thin films obtained from D4 and DMTSO,

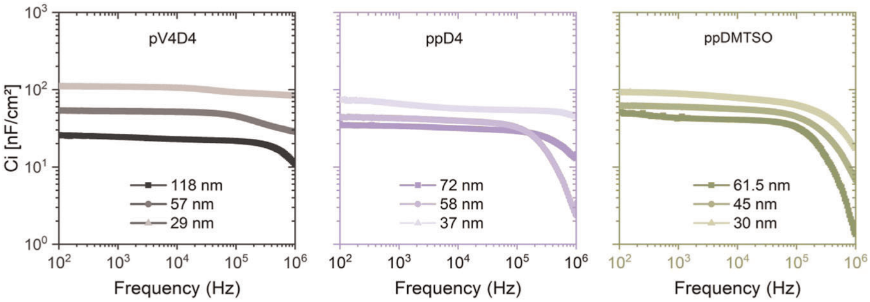

FIGURE 7 C_i versus frequency of all the as-deposited thin films obtained from V4D4, D4 and DMTSO. D4, octamethylcyclotetrasiloxane; DMTSO, decamethyltetrasiloxane; V4D4, 1,3,5,7-tetramethyl-1,3,5,7-tetravinylcyclotetrasiloxane

whereas the V4D4-based thin films showed smaller capacitance steps. Such capacitance steps might, for instance, be related to defects in the films, parasitic capacitances or a dipole orientation lag of the molecule behind the alternating electric field, commonly termed the polarisation effect.[3] The pronounced high-frequency drop of the capacitance is attributed to the series resistance,[47] as the measured capacitance drops below the minimum geometric capacitance, $C_0 = \varepsilon_0/d_{polymer}$.

The real part of the dielectric constant ($\varepsilon' = k$) of each thin film was estimated from a linear fit of C_i versus $1/d$ (Equation 1), where C_i was measured at 1 kHz (Table S10 and Figure S25). All the organosiloxane thin films exhibited a dielectric constant lower than the one of the dense silicon dioxide (SiO_2) which has a $k_{SiO_2} = 4.0 \pm 0.1$.[48] Hence, they are all considered as low dielectric constant materials.[6,39,48] Surprisingly, the thin films obtained from the two nonvinylic compounds displayed a dielectric constant, $k_{ppD4} = 2.72$ and $k_{ppDMTSO} = 3.03$, lower than the one obtained from V4D4 (i.e., $k_{pV4D4} = 3.32$). The dielectric constant depends on the molecular polarizability and density of the molecules, as commonly described by the Clausius–Mossotti equation.[49] Therefore, the observed variations of the k values suggest the influence of the monomer structure as well as probably the density of the resulting thin films. In particular, the methyl groups, which are known to induce a constitutive porosity, detected in the DMTSO-based thin films are partly responsible for the low dielectric constant of the DMTSO-based thin films, ca. $k = 3.03$.

Interestingly, the thin films obtained from V4D4 showed a leakage current density in the range of 10^{-7} A·cm^{-2}. On the contrary, the D4- and DMTSO-based thin films presented a high leakage current density in the range of 10^{-4} A·cm^{-2} (Figure 8 and Table S11), which is three orders of magnitude higher than the leakage current density of the V4D4-based thin films. The low dielectric strength of the D4- and DMTSO-based thin films might be related to their poor cross-linking. Additionally, the pV4D4 thin films demonstrated good down scalability of their insulating properties even for thicknesses as low as 29 nm (Figure S26). These insulating properties further confirm that the low-frequency ultrashort plasma-pulsed AP-PECVD of the vinylic V4D4 monomer results in the formation of compact and highly cross-linked thin films, corroborating the prevalent free-radical polymerisation observed in FTIR. Although a common strategy to enhance the dielectric strength of polymers is by chemical cross-linking,[2,4] using a monomer bearing vinyl bonds allows to readily obtain a good cross-linked material circumventing the need of orthogonal solvent and/or post curing step.

3.5 | Discussion

The present results evidence the significance of polymerisable double bonds for the low-frequency ultrashort plasma-pulsed AP-PECVD of atomically smooth and ultrathin low-k insulating thin films. Indeed, at $P_M/P_{sat} = 75\%$, the energy-deficient regime is observed for the nonvinylic compounds, that is, D4 and DMTSO, due to the use of ultrashort plasma activation (i.e., $t_{ON} = 100$ ns) and the quick depletion of the plasma-activated species during the next plasma off-time. This results in the formation of short and poorly reticulated oligomers (Figure S3). With the aim

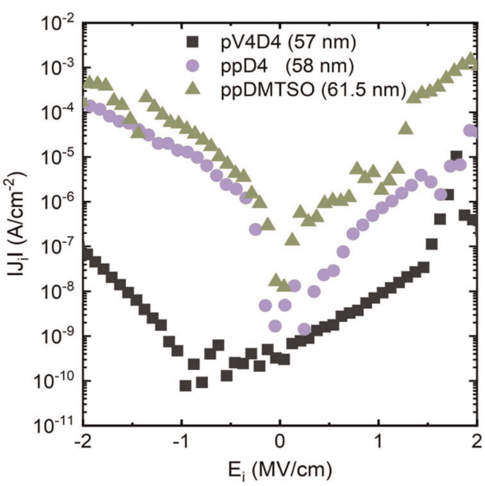

FIGURE 8 J_i versus E_i of the as-deposited thin films obtained from V4D4, D4 and DMTSO. D4, octamethylcyclotetrasiloxane; DMTSO, decamethyltetrasiloxane; V4D4, 1,3,5,7-tetramethyl-1,3,5,7-tetravinylcyclotetrasiloxane

to increase the molecular size and degree of cross-linking in the thin films elaborated from D4 and DMTSO, one could operate in the monomer-deficient regime. However, operating in the monomer-deficient regime, which could be achieved by increasing the input power (W; decreasing the plasma t_{OFF} in the present case) or by decreasing of the monomer saturation ratio (P_M/P_{sat}), would be at the expense of the monomer's chemical structure. Moreover, reaction of the monomer with the activated species is responsible for the formation of a large amount of condensable species that generate particles.[16,50] Under these conditions, particles are generated and defects such as grain boundaries yield low dielectric strengths (Figure 8).

Using a vinylic compound, that is, V4D4, these two regimes are identified, alongside a clear competition between the plasma-induced polymerisation and plasma-state polymerisation, as expected for the PECVD of vinyl monomers.[51] The monomer-deficient regime, dominated by plasma-state polymerisation, is observed at high plasma pulse frequency ($f \geq 362$ Hz) where the high probability of interaction between the monomer and the active plasma species is responsible for the significant monomer dissociation rate (Figures 4 and S12). The excess of gas-phase reaction in this regime is responsible for the granular surfaces and low thickness increment per cycle $t_{ON} + t_{OFF}$ (Figure 5). The shift from the monomer-deficient regime to the energy-deficient regime is ensured by decreasing the plasma pulse frequency ($f < 362$ Hz), which yields to the predominance of the surface adsorption of the monomer and its subsequent plasma-induced polymerisation to form atomically smooth and highly cross-linked low-k polymer thin films.

4 | CONCLUSION

The influence of the monomer structure on the growth, morphology, chemistry and dielectric properties of organosiloxane thin films prepared from ultrashort plasma-pulsed AP-PECVD was elucidated from the study of three tetrasiloxane compounds and different ultrashort plasma pulse frequencies. The predominant plasma-induced polymerisation enabled by the polymerisable double bonds of V4D4 is responsible for the excellent retention of the monomer structure, as highlighted by FTIR and XPS. The highly cross-linked pV4D4 thin films showed excellent insulating properties with a leakage current density in the range 10^{-7} A·cm^{-2}, even for a thickness as low as 29 nm. However, the gentle processing conditions of the low-frequency ultrashort plasma-pulsed AP-PECVD applied to nonvinylic monomers (D4 and DMTSO) resulted in poorly reticulated thin films, which exhibited rather high leakage current densities. These findings will considerably simplify the integration of low-k dielectric polymer thin films for flexible organic electronic application.

ACKNOWLEDGEMENTS

The Luxembourg National Research Fund (FNR) is thanked for financial support through the MASSENA project (PRIDE15/10935404). Dr. J. Guillot, C. Vergne, Dr. S. Girod and Dr. P. Grysan and J.-L. Biagi, all from LIST, are acknowledged for the acquisition of the XPS data, the evaporation of the top electrode for MIS preparation, AFM measurements and the ESEM images, respectively. The authors thank Prof. S. Siebentritt, Prof. P. J. Dale and Dr. M. Guennou from the University of Luxembourg, Prof. M. Creatore from Eindhoven University of Technology and Dr. K. Baba from LIST for insightful discussions.

DATA AVAILABILITY STATEMENT

The data that support the findings of this study are available from the corresponding author upon reasonable request.

ORCID

Dominique Abessolo Ondo http://orcid.org/0000-0002-3324-5229
François Loyer https://orcid.org/0000-0002-5636-3885
Nicolas D. Boscher http://orcid.org/0000-0003-3693-6866

REFERENCES

[1] Y. Wang, X. Huang, T. Li, L. Li, X. Guo, P. Jiang, *Chem. Mater.* **2019**, *31*, 2212.
[2] B. Wang, W. Chi, L. Al-Hashimi, T. J. Marks, A. Facchetti, *Chem. Rev.* **2018**, *118*, 5690.
[3] J. Choi, M. Joo, H. Seong, K. Pak, H. Park, C. W. Park, S. G. Im, *ACS Appl. Mater. Interfaces* **2017**, *9*, 20808.
[4] M.-H. Yoon, H. Yan, A. Facchetti, T. J. Marks, *J. Am. Chem. Soc.* **2005**, *127*, 10388.
[5] M. Wang, X. Wang, P. Moni, A. Liu, D. H. Kim, W. J. Jo, H. Sojoudi, K. K. Gleason, *Adv. Mater.* **2017**, *127*, 1604606.
[6] W. Volksen, R. D. Miller, G. Dubois, *Chem. Rev.* **2010**, *110*, 56.
[7] L. Feng, J. V. Anguita, W. Tang, J. Zhao, X. Guo, S. R. P. Silva, *Adv. Electron. Mater.* **2016**, *2*, 1500374.
[8] V. Jousseaume, L. Favennec, A. Zenasni, O. Gourhant, *Surf. Coat. Technol.* **2007**, *201*, 9248.
[9] J. El Sabahy, G. Castellan, F. Ricoul, V. Jousseaume, *J. Phys. Chem. C* **2016**, *120*, 9184.
[10] A. Castex, L. Favennec, V. Jousseaume, J. Bruat, J. Deval, B. Remiat, G. Passemard, M. Pons, *Microelectron. Eng.* **2005**, *82*, 416.
[11] N. J. Trujillo, Q. Wu, K. K. Gleason, *Adv. Funct. Mater.* **2010**, *20*, 607.
[12] D. Abessolo Ondo, F. Loyer, F. Werner, R. Leturcq, P. J. Dale, N. D. Boscher, *ACS Appl. Polym. Mater.* **2019**, *1*, 3304.

[13] H. Moon, H. Seong, W. C. Shin, W.-T. Park, M. Kim, S. Lee, J. H. Bong, Y.-Y. Noh, B. J. Cho, S. Yoo, S. G. Im, *Nat. Mater.* **2015**, *14*, 628.
[14] D. Mariotti, T. Belmonte, J. Benedikt, T. Velusamy, G. Jain, V. Švrček, *Plasma Processes Polym.* **2016**, *13*, 70.
[15] C. E. Knapp, J.-B. Chemin, S. P. Douglas, D. Abessolo Ondo, J. Guillot, P. Choquet, N. D. Boscher, *Adv. Mater. Technol.* **2018**, *3*, 1700326.
[16] R. Morent, N. De Geyter, S. Van Vlierberghe, P. Dubruel, C. Leys, E. Schacht, *Surf. Coat. Technol.* **2009**, *203*, 1366.
[17] F. Massines, C. Sarra-Bournet, F. Fanelli, N. Naudé, N. Gherardi, *Plasma Processes Polym.* **2012**, *9*, 1041.
[18] G. Camporeale, M. Moreno-Couranjou, S. Bonot, R. Mauchauffé, N. D. Boscher, C. Bebrone, C. Van De Weerdt, H. M. Cauchie, P. Favia, P. Choquet, *Plasma Processes Polym.* **2015**, *12*, 1208.
[19] C. Tendero, C. Tixier, P. Tristant, J. Desmaison, P. Leprince, *Spectrochim. Acta B* **2006**, *61*, 2.
[20] N. D. Boscher, F. Hilt, D. Duday, G. Frache, T. Fouquet, P. Choquet, *Plasma Processes Polym.* **2015**, *12*, 66.
[21] D. Abessolo Ondo, R. Leturcq, N. D. Boscher, *Plasma Processes Polym.* **2020**, *17*, e2000032.
[22] F. Loyer, G. Frache, P. Choquet, N. D. Boscher, *Macromolecules* **2017**, *50*, 4351.
[23] F. Loyer, G. Bengasi, G. Frache, P. Choquet, N. D. Boscher, *Plasma Processes Polym.* **2018**, *15*, e1800027.
[24] F. Loyer, S. Bulou, P. Choquet, N. D. Boscher, *Plasma Processes Polym.* **2018**, *15*, e1800121.
[25] F. Hilt, N. D. Boscher, D. Duday, N. Desbenoit, J. Levalois-Grützmacher, P. Choquet, *ACS Appl. Mater. Interfaces* **2014**, *6*, 18418.
[26] F. Neese, *Wiley Interdiscip. Rev.: Comput. Mol. Sci.* **2012**, *2*, 73.
[27] F. Weigend, *Phys. Chem. Chem. Phys.* **2006**, *8*, 1057.
[28] F. Weigend, R. Ahlrichs, *Phys. Chem. Chem. Phys.* **2005**, *7*, 3297.
[29] S. Grimme, J. Antony, S. Ehrlich, H. Krieg, *J. Chem. Phys.* **2010**, *132*, 154104.
[30] S. Grimme, S. Ehrlich, L. Goerigk, *J. Comput. Chem.* **2011**, *32*, 1456.
[31] M. Borella, M. Plissonnier, T. Belmonte, *Plasma Processes Polym.* **2007**, *4*, S771.
[32] N. D. Boscher, P. Choquet, D. Duday, S. Verdier, *Surf. Coat. Technol.* **2010**, *205*, 2438.
[33] N. D. Boscher, P. Choquet, D. Duday, S. Verdier, *Surf. Coat. Technol.* **2011**, *205*, 5350.
[34] C. Rau, W. Kulisch, *Thin Solid Films* **1994**, *249*, 28.
[35] F. Loyer, A. Combrisson, K. Omer, M. Moreno-Couranjou, P. Choquet, N. D. Boscher, *ACS Appl. Mater. Interfaces* **2019**, *11*, 1335.
[36] D. Abessolo Ondo, F. Loyer, J.-B. Chemin, S. Bulou, P. Choquet, N. D. Boscher, *Plasma Processes Polym.* **2018**, *15*, e1700172.
[37] F. Bernard, D. K. Papanastasiou, V. C. Papadimitriou, J. B. Burkholder, *J. Quant. Spectrosc. Radiat. Transfer* **2017**, *202*, 247.
[38] O. Gourhant, G. Gerbaud, A. Zenasni, L. Favennec, P. Gonon, V. Jousseaume, *J. Appl. Phys.* **2010**, *108*, 124105.
[39] M. R. Baklanov, J.-F. de Marneffe, D. Shamiryan, A. M. Urbanowicz, H. Shi, T. V. Rakhimova, H. Huang, P. S. Ho, *J. Appl. Phys.* **2013**, *113*, 041101.
[40] N. D. Boscher, P. Choquet, D. Duday, S. Verdier, *Plasma Processes Polym.* **2009**, *7*, 163.
[41] J. L. Jauberteau, I. Jauberteau, *J. Phys. Chem. A* **2012**, *116*, 8840.
[42] D. Loffhagen, M. M. Becker, A. K. Czerny, J. Philipp, C.-P. Klages, *Contrib Plasma Phys.* **2018**, *58*, 337.
[43] Y. Huang, Y. Chen, M. Zhou, *Int. J. Quantum Chem.* **2020**, *120*, e26415.
[44] G. Aresta, J. Palmans, M. C. M. van de Sanden, M. Creatore, *J. Vac. Sci. Technol. A* **2012**, *30*, 041503.
[45] S. Roualdes, V. Rouessac, J. Durand, *Compr. Membr. Sci. Eng.* **2010**, *1*, 159.
[46] H. Yasuda, *Luminous Chemical Vapor Deposition and Interface Engineering*, CRC Press, Boca Raton **2004**.
[47] F. Werner, S. Siebentritt, *Phys. Rev. Appl.* **2018**, *9*, 054047.
[48] K. Maex, M. R. Baklanov, D. Shamiryan, F. Iacopi, S. H. Brongersma, Z. S. Yanovitskaya, *J. Appl. Phys.* **2003**, *93*, 8793.
[49] C. C. Ku, R. Liepins, *Electrical Properties of Polymers: Chemical Principles*, Hanser Publishers, New York **1987**.
[50] N. D. Boscher, V. Vaché, P. Carminati, P. Grysan, P. Choquet, *J. Mater. Chem. A* **2014**, *2*, 5744.
[51] H. Yasuda, *J. Polym. Sci. Macromol. Rev.* **1981**, *16*, 199.

SUPPORTING INFORMATION

Additional Supporting Information may be found online in the supporting information tab for this article.

How to cite this article: Abessolo Ondo D, Loyer F, Boscher ND. Influence of double bonds and cyclic structure on the AP-PECVD of low-*k* organosilicon insulating layers. *Plasma Process Polym*. 2021;18:e2000222. https://doi.org/10.1002/ppap.202000222

CHAPTER III ─ Importance of the Monomer Saturation Ratio on the AP-PiCVD Reaction

Following the study on the influence of the monomer structure on the AP-PiCVD, in particular the requirement of the use of vinylic monomer, the present chapter investigates the influence of the monomer saturation ratio on the AP-PiCVD reaction. The investigation of a series of thin film, prepared from the AP-PiCVD reaction of a cyclic vinyl organosiloxane monomer using different monomer saturation ratios (P_M/P_{sat}), is performed. Owing to the relationship established between the saturation ratio and the growth rate together with the chemical composition and dielectric constant of the resulting thin films, highlighting the P_M/P_{sat} as a key parameter of the process, guidelines are provided to determine the optimal process window for the AP-PiCVD of functional polymer thin films.

Contents

Article(s) published from these results

Abessolo Ondo, D., Leturcq, R., Boscher, N. D. (2020). Plasma-initiated chemical vapour deposition of organosiloxane thin films: From the growth mechanisms to ultrathin low-k polymer insulating layers. Plasma Processes and Polymers, e2000032. https://doi.org/10.1002/ppap.202000032

Full contribution: experimental work on the synthesis and characterization of the thin films and treatment, analysis and interpretation of the collected data, redaction of the manuscript

Received: 17 February 2020 | Revised: 20 March 2020 | Accepted: 25 March 2020

DOI: 10.1002/ppap.202000032

FULL PAPER

PLASMA PROCESSES AND POLYMERS

Plasma-initiated chemical vapour deposition of organosiloxane thin films: From the growth mechanisms to ultrathin low-*k* polymer insulating layers

Dominique Abessolo Ondo | **Renaud Leturcq** | **Nicolas D. Boscher**

Materials Research and Technology Department, Luxembourg Institute of Science and Technology, Belvaux, Luxembourg

Correspondence
Nicolas D. Boscher, Materials Research and Technology Department, Luxembourg Institute of Science and Technology, 41, rue du Brill, L-4422 Belvaux, Luxembourg.
Email: nicolas.boscher@list.lu

Funding information
Luxembourg National Research Fund, Grant/Award Number: PRIDE15/10935404

Please note that one sentence was corrected on 15 May 2020 after initial publication. The word “results in” was replaced by “conjugated to” as in the original version from the author.

Abstract

The growth mechanisms of low dielectric constant polymer thin films elaborated from the atmospheric-pressure plasma-initiated chemical vapour deposition (AP-PiCVD) reaction of a cyclic vinyl organosiloxane are experimentally elucidated in this study. The use of ultrashort plasma pulses (ca. 100 ns), as a polymerisation initiator, with long plasma off-times results in the formation of atomically smooth thin films. The increase of the monomer saturation ratio, P_M/P_{sat}, results in an increase in the growth rate and a better retention of the cyclic structure of the monomer, promoting lower dielectric constants. Based on this experimental study, guidelines are provided to determine the optimal process window for the AP-PiCVD of functional polymer thin films.

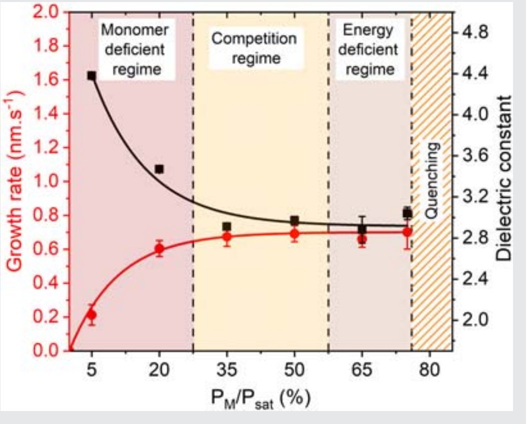

KEYWORDS

atmospheric plasma, low-*k* dielectric, nanosecond pulsed discharges, plasma-initiated chemical vapour deposition, ultrathin polymer film

1 | INTRODUCTION

Flexible electronics is an emerging field requiring materials that can work with unconventional substrates, that is, plastic, paper and textile.[1] Field-effect transistors (FET) are key units of modern electronic devices. FET on flexible or stretchable substrates required components, for example, gate dielectric, electrodes and semiconductors, that can withstand mechanical stress.[1] Among these different components, the dielectric layer plays an important role in the functioning of the device.[2] Yet, high capacitance density is essential to lower the power operation of electronic devices. This can be achieved using high-*k* materials, which, however, suffer from dipole disordering that affects the carrier mobility of the underlying semiconductor layer. Thus, ultrathin low-*k* layers provide a good alternative as a gate dielectric.[2,3] In particular, dielectric polymers have received a lot of attention due to their lightweight, chemical, thermal and mechanical stability,[4–6] as well as their good insulating properties.

In the current context and shift towards more environment-friendly methods, chemical vapour deposition (CVD) processes foster an ever-growing interest over solution-based approaches for the synthesis and integration of functional thin films.[7] Moreover, CVD processes are particularly suitable for the patterning and conformal deposition of thin films. In addition, the simultaneous synthesis and deposition directly from the gas phase avoid the need for orthogonal solvents and even allow the processing of insoluble and nonmeltable materials on unconventional substrates.[7] Plasma-enhanced chemical vapour deposition (PECVD) has been widely used for the elaboration of dielectric thin films.[5,8,9] However, the resulting thin films, called "plasma polymers," suffer from a poor retention of the precursor structure. Thus, the PECVD formation of low-k dielectric thin films from constitutive porosities is restricted by the disruption of the ring structure of cyclic precursors. Unlike PECVD, the low-pressure-initiated chemical vapour deposition (iCVD) of vinyl-containing cyclic precursors can yield the formation of low-k polymer thin films.[4]

Yet, PECVD approaches possess the major advantage of being compatible with atmospheric-pressure operating conditions.[10,11] In particular, the combination ultrashort plasma pulses ($t_{ON} < 100$ ns) and long plasma off-times (t_{OFF}) in the range of the free-radical polymerisation lifetime can yield the atmospheric-pressure synthesis and deposition of atomically smooth, conformal and ultrathin low-k polymer insulating layers.[12] The approach, called plasma-initiated chemical vapour deposition (PiCVD), displays strong similarities with iCVD.[13] Indeed, the polymerisation and deposition mechanisms in AP-PiCVD are assumed to occur through three major steps: (a) activated species (radicals) are created intermittently according to the plasma pulse frequency, (b) diffusion and adsorption of primary radicals and monomer from the vapour phase on a surface where (c) the polymerisation occurs.[14] Although the influence of the plasma pulse frequency has been thoroughly studied,[13–15] the influence of the monomer saturation ratio, P_M/P_{sat} (with P_M being the partial pressure of the monomer and P_{sat} the saturation pressure of the monomer at the temperature of interest), still needs to be understood. The present work elucidates for the first time the influence of the P_M/P_{sat} ratio on the growth mechanisms in AP-PiCVD. The influence of the monomer saturation ratio on the polymerisation initiation is investigated for different plasma pulse frequencies, highlighting the dependence of the gas phase and surface reaction kinetics on the initiating and monomer species concentrations. The studies concerning a series of atomically smooth ultrathin polymer insulating thin films prepared from an organosiloxane monomer, that is, 1,3,5-trimethyl-1,3,5-trivinylcyclotrisiloxane (V3D3), at a plasma pulse frequency of 100 Hz further evidenced the impact of the P_M/P_{sat} ratio on the thin-film chemistry and morphology, which ultimately influence the functional properties (dielectric constant and leakage current in the present study). Indeed, a decrease of the dielectric constant from ca. 4.4 to ca. 2.9 is simply achieved by the increase of the P_M/P_{sat} ratio. On the basis of this experimental study, guidelines are provided for the atmospheric-pressure PiCVD of polymer thin films with an optimal retention of the structure and functional group of the selected monomers.

2 | EXPERIMENTAL SECTION

2.1 | Materials and AP-PiCVD

Thin films were elaborated in an open-air atmospheric-pressure dielectric barrier discharge (AP-DBD) setup, as previously described.[10] In short, the AP-DBD setup is composed of two high-voltage electrodes covered with alumina dielectric and a stainless steel moving table as a ground electrode. The plasma was ignited by 1-μs square pulses of 6 kV produced by an AHTPB10F generator from EFFITECH (Gif-sur-Yvette, France), allowing the generation of two ultrashort plasma discharges (i.e., $t_{ON} = 100$ ns) at the voltage rising and falling edges. Plasma pulse frequencies ranging from 31.6 to 3,000 Hz were studied, corresponding to plasma off-times (t_{OFF}) ranging from 333 μs to 31.6 ms. The discharge gap was maintained at 1 mm. The monomer, that is, V3D3 was purchased from Fluorochem and used without any purification. The monomer was directly delivered to the deposition area using a bubbler setup and argon (air liquid, 99.999%) as a carrier and plasma gas. The flow rate of the carrier gas (Ar) was varied from 1 to 15 L/min ($F_{carrier}$), whereas the total gas flow (F_{total}) was maintained constant at 20 L/min using another Ar source. This allowed to investigate different monomer saturation ratios, from 5% to 75%. It was not possible to go beyond 75%, as high monomer partial pressures (P_M) induce quenching of the plasma discharges.[16] Such irregularity of the plasma discharges could be circumvented by increasing the input energy, but it would assuredly lead to the alteration of the monomer's structure during the deposition.[16,17] To prevent contamination from the surrounding atmosphere and more particularly reduce the O_2 and N_2 contamination, argon fluxes were added on both sides of the AP-DBD electrode. All depositions were carried on intrinsic and highly boron-doped ($\rho = 0.01$ ohm/cm) polished silicon wafers (Sil'tronix, Archamps, France). Before each deposition experiment, the substrates were treated using a 95%/5% argon/oxygen plasma for 40 s.

2.2 | Thin-film characterisation

2.2.1 | Morphology and topography

Scanning electron microscope (SEM) images were obtained using a Hitachi SU-70 FE-SEM (Tokyo, Japan). To avoid distortions due to charge effect, the samples were coated with a 10-nm platinum film before the SEM observations. Atomic force microscopy (AFM) images were obtained using Innova instrument operating in a tapping mode. The mechanical properties of the samples were investigated by the mean of an MFP-3D Infinity AFM (Asylum Research/Oxford Instruments, Santa Barbara, CA) working in bimodal AM–FM (amplitude modulation–frequency modulation). The second eigenmode (ca. 1.7 MHz) is used to detect resonance frequency shift via a phase lock loop set at 90°. These frequency shifts are proportional to the elastic modulus of the sample. The AFM tip (AC160TS; Olympus, Japan) cantilever stiffness and inverse optical sensitivity are calibrated before the measurements by a Sadler noncontact method. A Hertz punch model is chosen to reflect the supposed Hertzian interactions between the tip and the surface. From theory, the only free parameter to be determined is the AFM tip radius. This value is obtained by analysing a reference sample of polystyrene/polycaprolactone. The elastic modulus of the polystyrene phase is known at 2.7 GPa and the tip radius is then extracted. Film thicknesses were measured by a spectroscopic ellipsometer FS-1 and a KLA-Tencor P-17 Stylus profiler (Milpitas, CA). The spectrometric ellipsometry measurements were acquired at a single angle of 65° using four different wavelengths, that is, 465, 525, 590 and 635 nm, and the data were fitted to a Cauchy model. For each deposition condition (frequency, P_M/P_{sat}), the growth rate was determined from the measured thicknesses of minimum three different thin films prepared using different deposition times and the effective deposition time, which correspond to the time spent under the high-voltage electrodes, given by the number of runs multiplied by the width of the high-voltage electrodes (30 mm) and divided by the speed of the moving table. For all the experiments reported in this study, the film thickness was shown directly proportional to the deposition time, yielding small standard deviations of the growth rates, even though they were evaluated from thin films prepared with different deposition times.

2.2.2 | Chemical characterisations

Fourier-transform infrared spectroscopy (FTIR) analysis of the AP-PiCVD thin films was performed in a transmission mode on double-polished silicon wafers using a Bruker Hyperion 2000 spectrometer equipped with a mercury cadmium telluride detector. The spectra were obtained over a range of 4,000–400 cm^{-1} with a resolution of 4 cm^{-1}. A 10-min nitrogen purge was performed for each measurement to diminish the contribution of carbon dioxide and moisture. The monomer spectrum was acquired with the same FTIR spectrometer using an attenuated total reflection accessory. X-ray photoelectron spectroscopy (XPS) analyses (300 × 700 μm^2) were carried out with a Kratos Axis Ultra DLD spectrometer using a monochromatic Al Kα X-ray source ($h\nu = 1{,}486.6$ eV). A flooding gun was used to reduce the charging effect on the samples' surface. Photoelectron emission was collected at 0°. The surface of the specimen was precleaned by bombardment with Ar^+ ions (2 kV) before the collection of XPS data. Casa XPS software was used for chemical quantification.

2.2.3 | Fabrication and characterisation of the metal insulator semiconductor

The AP-PiCVD dielectric thin films were sandwiched between a highly doped Si wafer used as a bottom electrode and a patterned Au layer as a top electrode. The patterned Au layer was prepared using a shadow mask of 1 cm^2 by electron beam evaporation with a base pressure below 10^{-6} mbar. Before Au evaporation, a thin layer of Ti (10 nm) was evaporated on top of the dielectric thin film to ensure the adherence of the Au layer (50 nm). Capacitance versus frequency characteristics of the metal insulator semiconductor (MIS) devices were measured using an impedance analyser, IM3570 Hioki. The C–f measurement was performed in a frequency range of (100 Hz; 1 MHz) with an excitation level of 0.1 V. The dielectric constant was measured at 1 kHz and estimated from the relation:

$$\frac{C}{S} = \frac{\varepsilon_0 \varepsilon'_{polymer}}{d_{polymer}}. \tag{1}$$

The J–V characteristic measurements of the MIS devices were performed at ambient atmosphere using Keithley 2634B instrument.

3 | RESULTS AND DISCUSSION

3.1 | Influence of the plasma pulse frequency

To gain insight into the influence of the monomer saturation ratio (P_M/P_{sat}) on the growth mechanisms of the thin films deposited using ultrashort plasma pulses, we selected a cyclic vinyl organosilicon monomer, that is, V3D3, which was previously demonstrated to form smooth and ultrathin low-*k* polymer insulating layers via AP-PiCVD.[12] The monomer was fed to an AP-DBD reactor using a bubbler system and argon as a carrier and plasma gas (Figure S1). Making the assumption that the argon carrier gas was saturated with V3D3 vapour, its dilution in the overall argon gas flow allowed to investigate different P_M/P_{sat} ratios (approximated to be equal to the ratio of the carrier gas flow rate to the total flow rate, $F_{carrier}/F_{total}$; Figure S1b). The AP-DBD was ignited using ultrashort high-voltage square pulses of 1 μs, creating two distinct current discharges at the rising and falling edges of the high-voltage pulses (Figure S2), as previously reported.[12] In this first section, two monomer saturation ratios, P_M/P_{sat} (20% and 75%), were studied for different plasma pulse frequencies (Table S1) to determine their influence on the initiation and lifetime of the free-radical polymerisation of the selected monomer. Irrespective of the monomer saturation ratio and plasma pulse frequency, the substrate temperature remained constant at room temperature. For all the investigated conditions, solid thin films were obtained. However, obvious growth rate and morphology discrepancies were readily noticeable from a naked-eye observation.

3.1.1 | Effect on the growth rate

Unsurprisingly, the growth rate (nm/s) was shown to increase with the increase in the plasma pulse frequency (Figure 1a). Indeed, the increase of the plasma pulse frequency leads to the formation of a larger amount of reactive species and therefore a higher concentration of polymerisation-initiating species [I] that yield an increase in the deposition rate. Reasonably, the increase of the monomer saturation ratio, P_M/P_{sat}, yields an increase in the growth rate for all the studied frequencies (Table S1). This difference in the growth rate, more obviously noticeable from 1,000 Hz plasma pulse frequency (Figure 1a), assuredly correlates with the higher concentration of monomer [M].

To extract information on the lifetime of the free-radical polymerisation step for each of the investigated monomer saturation ratio, P_M/P_{sat}, the growth rate data (Table S1) are plotted as thickness increment per cycle ($t_{ON} + t_{OFF}$, with t_{ON} being kept constant). In accordance to previous studies,[13,15] the thickness increment per cycle for the thin films elaborated using a 20% monomer saturation ratio highlights the occurrence of deposition reactions during t_{OFF}, with an increase of thickness for $t_{ON} + t_{OFF}$ cycles, between 0.33 and 3 ms (Figure 1b). A quasi-plateau of 6 picometre (pm) per cycle is reached above t_{OFF} longer than 3 ms, indicating the termination of the free-radical polymerisation of V3D3 under these conditions ($P_M/P_{sat} = 20\%$). Curiously, and in contrast to the previous observations, the thickness increment per cycle of the thin films elaborated using a 75% monomer saturation ratio was shown to first decrease with the increase of the cycle duration before reaching a plateau for $t_{ON} + t_{OFF}$ longer than 3 ms. The plateau of thickness

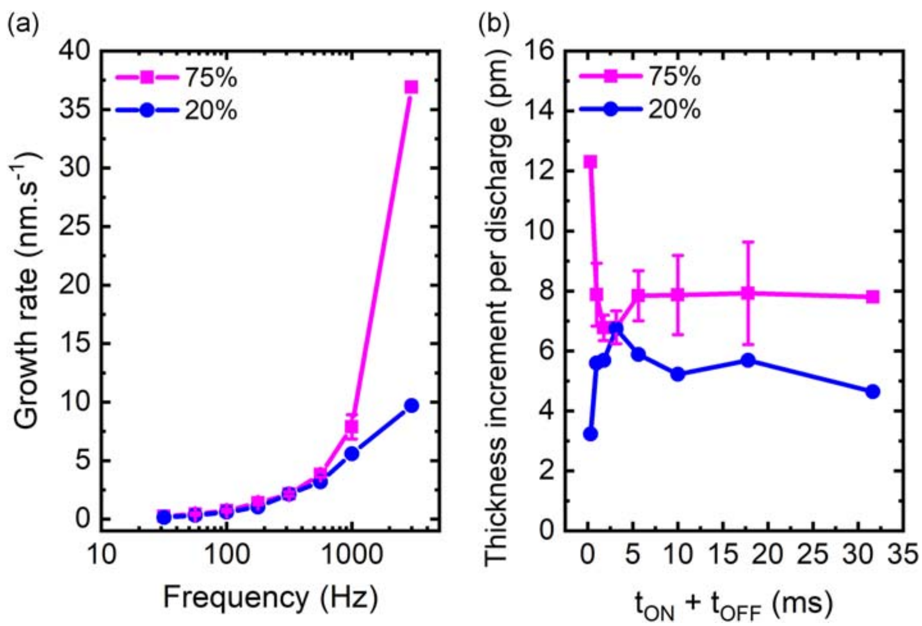

FIGURE 1 (a) Growth rate per second according to the plasma pulse frequency. (b) Thickness increment per cycle duration (t_{ON}+t_{OFF})

increment per cycle for the thin films elaborated using a $P_M/P_{sat} = 75\%$ was slightly higher (8 pm per cycle) than the one for the thin films elaborated using a $P_M/P_{sat} = 20\%$ (6 pm per cycle). This slight difference is attributed to the larger concentration of monomer [M] and its higher adsorption rate at high P_M/P_{sat}. However, the opposite behaviour of the thickness increment per cycle for the thin films elaborated from the shortest t_{OFF} may be related to the creation of a much larger number of polymerisation-initiating species for high P_M/P_{sat}. Indeed, a previous study has highlighted that the exposure of the monomer to ultrashort plasma pulses produces a range of radicals and neutral fragments that can act as initiation groups.[14] Therefore, for high monomer saturation ratio, the large concentration of monomer [M] coupled to an increase in the plasma pulse frequency likely yields a high concentration of initiating species [I], which conjugated to high [M]; thus, high adsorption rates yield high deposition rates. Overall, this difference in the thickness increment per cycle trend is indicative of the occurrence of different competing mechanisms, which are known to also have an influence on the chemistry and morphology of the resulting thin films.

3.1.2 | Effect on the chemistry

FTIR was used to characterise the different bonding arrangements in the as-deposited thin films (Figures 2 and S3). Irrespective of P_M/P_{sat}, the FTIR spectra of the thin films elaborated at a plasma pulse frequency of 100 Hz display the peak associated to the Si–O–Si ring at ca. 1,012 cm^{-1} (Figure S4). Such value is slightly higher than the measured one for the V3D3 monomer (997 cm^{-1}), but it is consistent with the reported ones for iCVD PV3D3 layers (995–1,020 cm^{-1}).[4,18] The small shoulder observed at higher wavenumbers is attributed to the minor side reactions related to the plasma initiation of the polymerisation reaction. The increase of the plasma pulse frequency induces a broadening and shift of the Si–O–Si peak, indicating the heterogeneity of Si–O bonding environment that includes cyclotrisiloxane ring among other assemblies.[19] Notably, the heterogeneous Si–O bonding environment of the thin films elaborated using a 20% monomer saturation ratio at 1,000 and 3,000 Hz is confirmed by the appearance of a shoulder centred at around 1,090 and 1,130 cm^{-1}, attributed to the formation of a linear Si–O–Si and silsesquioxane ring structure, respectively (Figures 2, S4 and Table S2).[6,18,20] The presence of a broad absorbance peak centred at around 3,250 cm^{-1} is attributed to the incorporation of –OH groups, which further evidenced the alteration of the monomer structure during the deposition at high plasma pulse frequency. Meanwhile, the absorbance peak related to the Si–O in the silanol group (Si–OH) is also detected at around 900 cm^{-1}, allowing to assume that the previously mentioned –OH groups are bonded to silicon (Figure S5). Interestingly, the Si–CH_3 peak located at

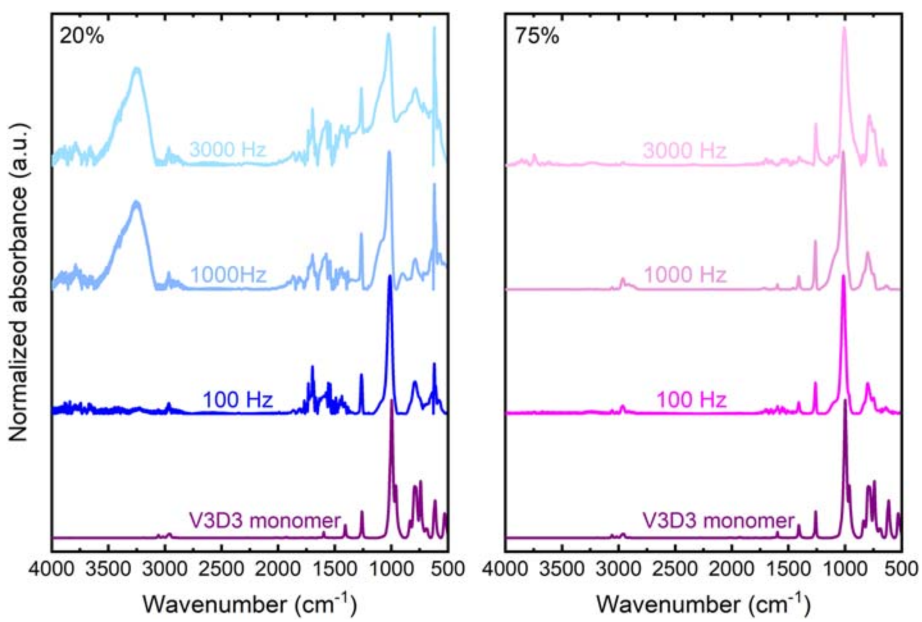

FIGURE 2 Fourier-transform infrared spectra of the thin films elaborated at different plasma pulse frequencies, that is, 100, 1,000 and 3,000Hz, using 20% and 75% monomer saturation ratio (P_M/P_{sat}). The spectra of both the monomer and the resulting thin films are normalised according to the Si–O–Si absorbance peak located at ca. 1,000cm^{-1}

1,259 cm^{-1} is shifted to 1,263 cm^{-1} for the thin films elaborated using a 20% monomer saturation ratio, even for the thin film elaborated at 100 Hz, indicating a slight alteration of the monomer structure during the synthesis using such low P_M/P_{sat} (Figure S6).

Regarding the thin films elaborated using a 75% monomer saturation ratio at 1,000 Hz, a broad shoulder is observed between 1,074 and 1,163 cm^{-1}, whereas different bonding arrangement is observed at 3,000 Hz (Figures 2, S4 and Table S3). Indeed, the absorbance peak located at 1,004 cm^{-1} is assigned to the asymmetric stretching of the Si–O–Si ring in short polymeric chains.[18] In addition, instead of being observed as a shoulder, there is a clear distinction between the peaks related to the formation of linear Si–O–Si, the cage structures and the preservation of the Si–O–Si ring, suggesting a competition between a free-radical polymerisation pathway and the formation of new Si–O–Si bonds. Nevertheless, the position of the Si–CH_3 peak is at 1,260 cm^{-1} for the thin films elaborated at 75% P_M/P_{sat} ratio, irrespective of the plasma pulse frequency (Figure S6), demonstrating the retention of the Si configuration and suggesting a limited formation of new Si–O–Si bonds. The different behaviour at high plasma pulse frequency (≥1,000 Hz) for the two studied P_M/P_{sat} ratios correlates well with the trend observed for the thickness increment per cycle. In addition, in contrast to the thin films elaborated using a 20% monomer saturation ratio, no incorporation of silanol groups was detected for the thin films elaborated at 75% P_M/P_{sat} ratio, irrespective of the plasma pulse frequency (Figure S5).

3.1.3 | Effect on the morphology

If the thin films elaborated at plasma pulse frequencies lower than 1,000 Hz systematically show a smooth surface morphology irrespective of the P_M/P_{sat} ratio (Figure 3), strong morphology discrepancies are observed above 1,000 Hz. In particular, rough surface morphologies are observed for the thin films elaborated using a 20% monomer saturation ratio at 1,000 Hz. This demonstrates the preponderance of gas phase reactions due to the high concentration of initiating species [I] produced at such high frequency (i.e., 1,000 Hz). Nevertheless, this statement is apparently in contradiction to the smooth surface morphologies observed for the thin films elaborated using a much higher monomer saturation ratio (75%) at 1,000 Hz. Indeed, at identical plasma pulse frequency (1,000 Hz), higher partial pressures of the monomer (P_M) yield a higher concentration of initiated species ($[I]^{75\%}_{1000\,Hz} > [I]^{20\%}_{1000\,Hz}$). However, higher P_M/P_{sat} ratios are also responsible for higher surface adsorption of the monomer on the surface, and they counterbalance the system reactivity in favour of surface reactions. Hence, higher surface roughnesses are not related to higher growth rates or higher thicknesses, as the thin films elaborated at 1,000 Hz for a P_M/P_{sat} ratio = 75% combine both smoother surface and higher growth rate. Thus, the threshold between the preponderance of surface reactions (yielding smooth thin films) and gas phase reactions (yielding rough or powdery thin films) in AP-PiCVD is not only dependent on the plasma pulse frequency but also on the P_M/P_{sat} ratio.

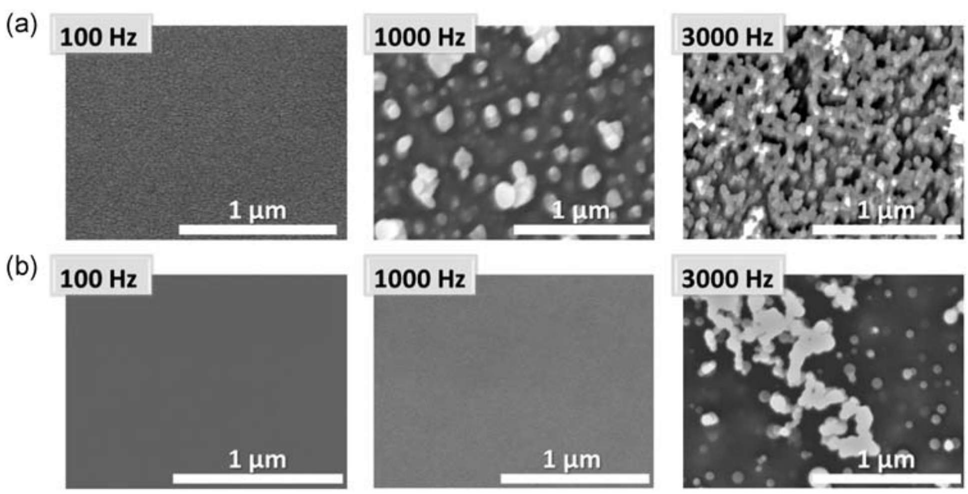

FIGURE 3 Scanning electron microscope top view images of the as-deposited PV3D3 elaborated at different plasma pulse frequencies using a monomer saturation ratio (P_M/P_{sat}) of (a) 20% and (b) 75%

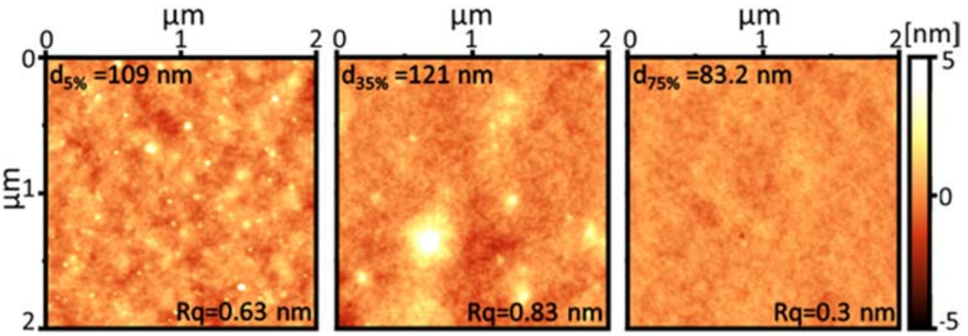

FIGURE 4 Atomic force microscopy images of the as-deposited thin films elaborated using different P_M/P_{sat} ratios: 5%, 35% and 75%. The thickness ($d_{P_M/P_{sat\%}}$) and root mean square roughness (R_q) values are provided for each of the presented thin films

3.2 | Influence of the P_M/P_{sat}

In the first part of this report, the monomer saturation ratio, P_M/P_{sat}, is highlighted as an important parameter in AP-PiCVD. Notably, the increase of the P_M/P_{sat} ratio led to a better retention of the monomer structure, which is highly desirable to form low dielectric constant thin films from a constitutive porosity approach. To gain further understanding on the influence of the monomer saturation ratio on thin film's growth mechanism and the properties, a series of thin films was prepared from different P_M/P_{sat} ratios at a plasma pulse frequency fixed at 100 Hz. The studied monomer saturation ratios ranged from 5% to 75%, as for this specific monomer, that is, V3D3, P_M/P_{sat} ratio beyond 75% induces a quenching of the plasma discharges. It is worth reminding here that irrespective of the monomer saturation ratio and at a plasma pulse frequency of 100 Hz, the substrate temperature (known to influence the monomer adsorption) remained constant at room temperature. In accordance with the previous SEM observation (Figure 3), all the thin films elaborated at a plasma pulse frequency of 100 Hz display a smooth and particle-free surface across the entire surface of the substrates, including 4-inch silicon wafers (Figure S7). AFM images confirm the pinhole-free and defect-free nature of the thin films (Figures 4 and S8). Irrespective of the P_M/P_{sat} ratio and thin film thickness (up to 120 nm), root mean square roughnesses (R_q) below 1 nm were measured. Such low R_q values are desirable for microelectronic applications.[1]

3.2.1 | Effect on the growth rate

Interestingly, in the perspective of practical applications and integration into electronic devices, for all the investigated monomer saturation ratios, highly homogeneous thicknesses were measured (with a standard deviation lower than 1 nm for thicknesses exceeding 100 nm) across the entire surface of 4-inch silicon wafers (Figure S7a). Unsurprisingly, higher growth rates are achieved from higher monomer partial pressures (P_M). Notably, the increase of the monomer saturation ratio, P_M/P_{sat}, from 5% to 35% results in an increase in the growth rate, from ca. 0.2 nm/s to a maximum of ca. 0.7 nm/s (Figure 5 and Table S4). Any further increase of the monomer saturation ratio above 35% leads to a plateau at 0.7 nm/s. Although the P_M/P_{sat} range cannot be investigated up to 100% due to discharge quenching above P_M/P_{sat} ratio of 75%, the shape of the growth rate curve resembles that of a type I adsorption isotherm, commonly referred as Langmuir isotherm,[21] which occurs when adsorption is limited to a complete monolayer.

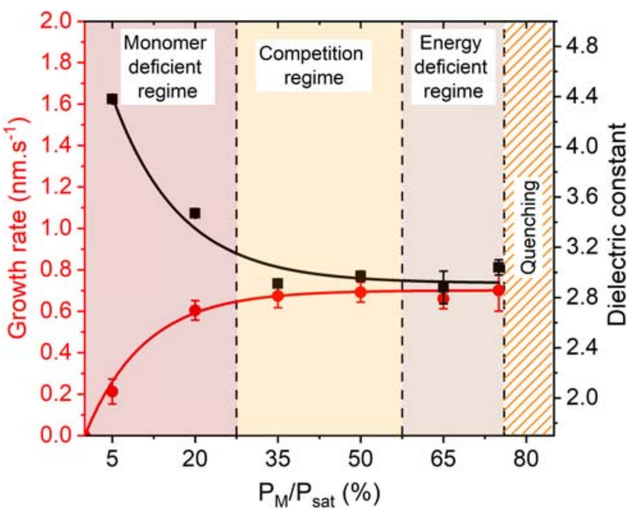

FIGURE 5 Growth rate and dielectric constant of the as-deposited thin films are plotted according to the monomer saturation ratio, P_M/P_{sat}, at which they were elaborated. The red and black lines show the trend of the growth rate and the dielectric constant, respectively

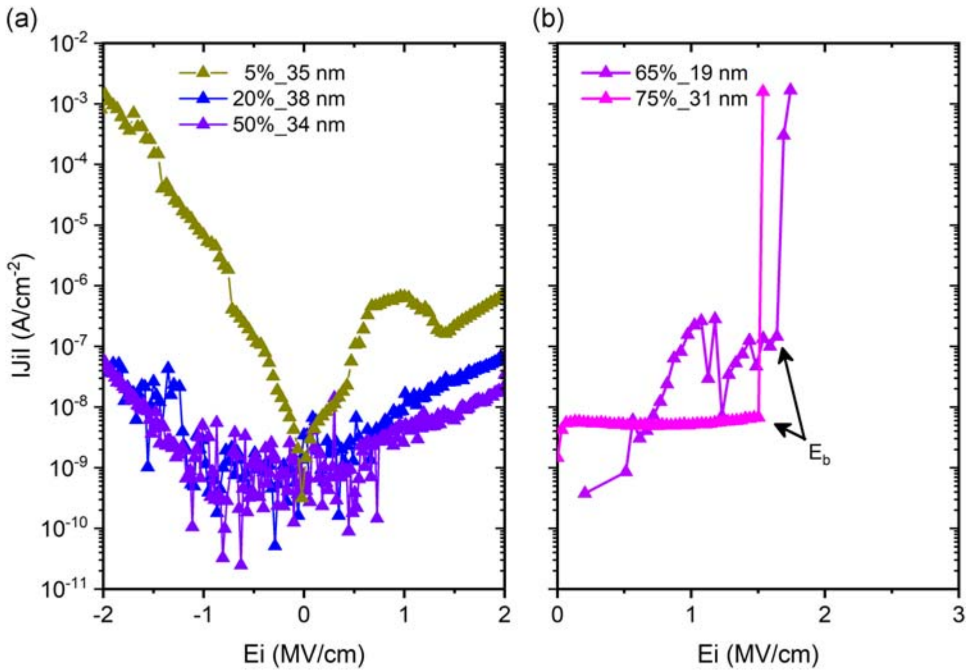

FIGURE 6 (a) Ji versus Ei of the as-deposited thin films elaborated using a monomer saturation ratio, P_M/P_{sat}, ≤50%. (b) Breakdown electric field (Ei) of the thin films elaborated using a monomer saturation ratio, P_M/P_{sat}, >50%. The results are presented with the following notation: $X\% - d$ nm, where X represents the P_M/P_{sat} ratio and d is the thickness of the thin film

3.2.2 | Effect on the dielectric properties

To evaluate the dielectric properties of the as-deposited thin films, a series of MIS structures was fabricated (Table S5). Particular attention was paid to the influence of the monomer saturation ratio, P_M/P_{sat}, on the insulating properties of the thin films, as the as-deposited PV3D3 thin films elaborated at P_M/P_{sat} ratio of 75% have shown a breakdown electric field at 1.5 MV/cm in our previous study.[12] The breakdown electric field is determined as the electric field (E) at which the leakage current density (Ji) increases abruptly. Interestingly, the thin films elaborated at a P_M/P_{sat} ratio ≤50% showed a leakage current density lower than 10^{-6} A/cm^2 at 2 MV/cm for thicknesses in the range of several tens of nanometres (Figure 6a,b and Table S6). No clear breakdown electric field has been observed in these thin films even at a higher applied electric field. In addition, a fair down scalability of thin films' insulating properties is observed for the thin films elaborated using a P_M/P_{sat} ratio ≤50% (Figure S9). However, a breakdown electric field is observed for the thin films elaborated at a P_M/P_{sat} ratio >50%. The decrease of the dielectric strength in the thin films elaborated at P_M/P_{sat} ratio >50% might be related to unreacted monomer molecules trapped in the layer.

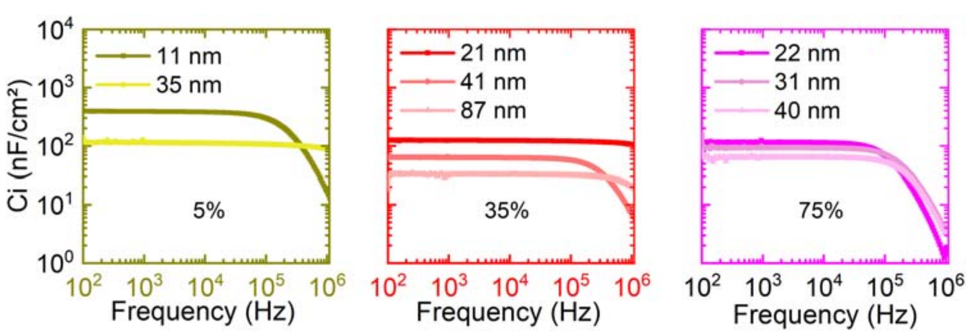

FIGURE 7 Ci versus frequency of all the as-deposited thin films elaborated using a monomer saturation ratio, P_M/P_{sat}, of 5%, 35% and 75%

For each of the investigated monomer saturation ratio, P_M/P_{sat}, the areal capacitance (Ci) of all the as-deposited thin films was measured for different thicknesses and plotted according to the frequency (Figures 7, S10 and Table S5). A decrease in the capacitance to almost zero at high frequencies is often observed, especially for the thin films elaborated at a P_M/P_{sat} ratio >50%. This pronounced high-frequency drop of the capacitance is attributed to the series resistance,[22] as the measured capacitance drops below the minimum geometric capacitance, $C_0 = \varepsilon_0/d_{polymer}$.

The areal capacitance of each thin film was measured on three different thicknesses (Table S5).[12] Subsequently, the dielectric constant (k) of each thin film was estimated from a linear fit of Ci versus $1/d$ (Equation 1) and plotted according to the P_M/P_{sat} ratio at which they were elaborated. The increase of the monomer saturation ratio from 5% to 35% resulted in the decrease of the k value from ca. 4.4 to 2.9, respectively (Figure 5 and Table S5). It is noteworthy that the thin films obtained using a monomer saturation ratio higher or equal to 20% exhibit a dielectric constant lower than $k = 4.0 \pm 0.1$, and they are all considered as low dielectric constant materials.[6,8] Interestingly, the variation of the dielectric constant as a function of the monomer saturation ratio is the mirror of the $f(P_M/P_{sat})$ = growth rate curve (Figure 5), with a plateau reached for monomer saturation ratio higher than 35%. The dielectric constant of material made up of nonpermanent dipole moment is commonly described by the Clausius–Mossotti equation, expressing the dependence of the dielectric constant on the molecular polarizability and density of the molecules.[23] Therefore, the variations of the k value, in addition to the changes in the growth rate, suggest an impact of the monomer saturation ratio on the chemistry and the density of the deposited thin films.

3.2.3 | Effect on the chemistry

FTIR and XPS were used to characterise the bonding environment and the composition of the thin films. The FTIR spectra of all the thin films elaborated using a monomer saturation ratio $P_M/P_{sat} \geq 20\%$ appear identical (Figure S11), with a sharp asymmetric Si–O–Si stretching peak located at 1,012 cm^{-1} (Table S7). As mentioned earlier in this report, such value is consistent with the reported ones for iCVD PV3D3 layers.[4,24] The lack of broadening in this peak is indicative of the preservation of the original cyclic siloxane ring. Further information is found in the 1,290–1,230 cm^{-1} region where the position of the peak related to the Si–CH_3 is known to vary in position, depending on the number of oxygen bonds with

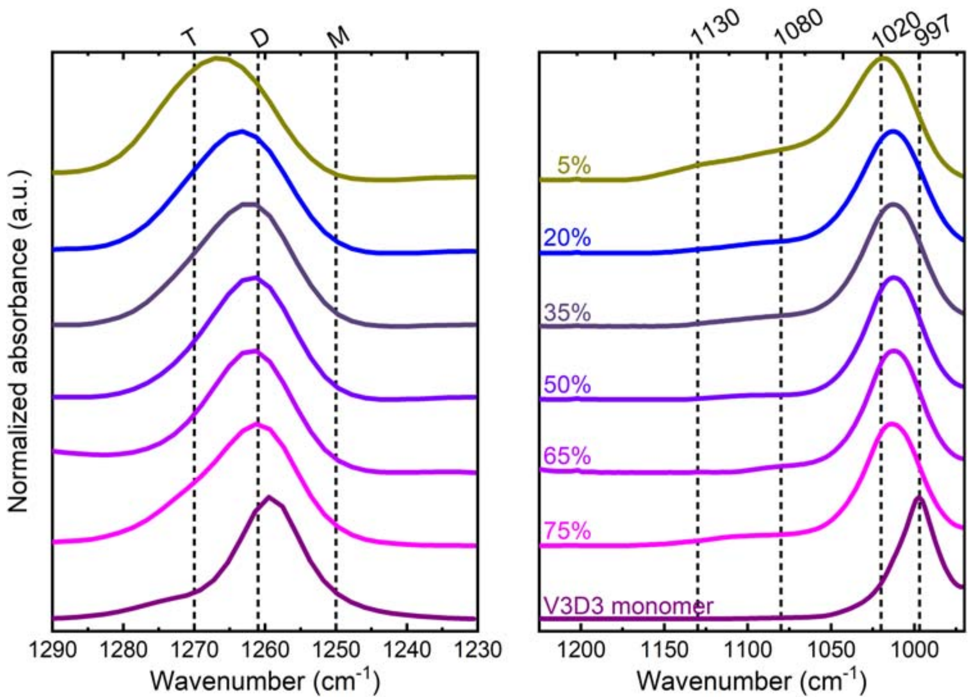

FIGURE 8 Fourier-transform infrared spectra of the 1,290–1,230 and the 1,225–970 cm^{-1} regions, corresponding, respectively, to the Si–CH_3 bonding region and the Si–O–Si stretching of the V3D3 monomer and the thin films elaborated using various P_M/P_{sat}. The M, D and T groups represent the mono-, di- and trisubstitution of the silicon atom by oxygen, respectively

Si (Figure 8). Indeed, the absorption peak assigned to O_x–Si–$(CH_3)_{(4-x)}$ ($x = 1$, 2 and 3) shifts towards high wavenumbers upon the mono-, di- or trisubstitution of the silicon atom by oxygen, designated as "M", "D" and "T" configurations, respectively.[25,26] Interestingly, all the thin films elaborated using P_M/P_{sat} ratio ≥35% have a Si–CH_3 peak located 1,261 cm^{-1}. Such a value, close to the one measured for the monomer, that is, 1,259 cm^{-1}, demonstrates the retention of the Si^D configuration. This result, also related to the preservation of the monomer's ring, indicates the good retention of the monomer structure for all thin films elaborated using a P_M/P_{sat} ratio ≥35%. Also, this observation correlates with the similar k values observed for the thin films elaborated using P_M/P_{sat} ratio ≥35%.

However, the Si–CH_3 peak is observed to shift to higher wavenumbers (Figure 8), that is, 1,263 cm^{-1} and 1,267 cm^{-1}, for the thin films elaborated using monomer saturation ratios of 20% and 5%, respectively. This blue shift is attributed to the formation of Si^T configuration, which even becomes dominant for $P_M/P_{sat} = 5\%$. Moreover, a monomer saturation ratio of 5% results in the broadening and blue shift of the asymmetric Si–O–Si stretching peak to 1,018 cm^{-1} (Figure 8 and Table S7), confirming the alteration of the monomer structure for low P_M/P_{sat} ratio. The broad shoulder on the Si–O–Si peak presents two peaks centred at 1,130 and 1,080 cm^{-1}, which correspond to the contribution of the silsesquioxane-like cage structure and linear Si–O–Si, respectively.[6] One should note that no infrared activity of Si^M configuration was observed, whose peak would be located at 1,250 cm^{-1}.[25–27] According to the monomer alteration observed for low monomer saturation ratios, the formation of Si–OH groups was observed with a peak located at 907 cm^{-1} for the thin film elaborated using a P_M/P_{sat} ratio of 5% (Figure S11). This observation also justifies a much higher dielectric constant value observed for this film compared with the others, owing to the high polarizability of –OH groups.

The relative atomic composition of the thin films was examined by XPS. Although all the prepared thin films display silicon concentrations (ca. 18–19%) close to the expected one for PV3D3 (Table S8 and Figure S12), strong discrepancies were observed for the oxygen and carbon elements. Unsurprisingly, the thin films elaborated from the highest P_M/P_{sat} ratio (75%) display a relative atomic concentration (Si, 19%; O, 22% and C, 59%) very close to the one expected for PV3D3 (Si, 20%; O, 20% and C, 60%). However, for the thin films elaborated using a monomer saturation ratio of 5%, lower carbon content (ca. 43%) and higher oxygen content (ca. 38%) are measured, coinciding with the oxidation of the silicon atom as previously observed in FTIR.

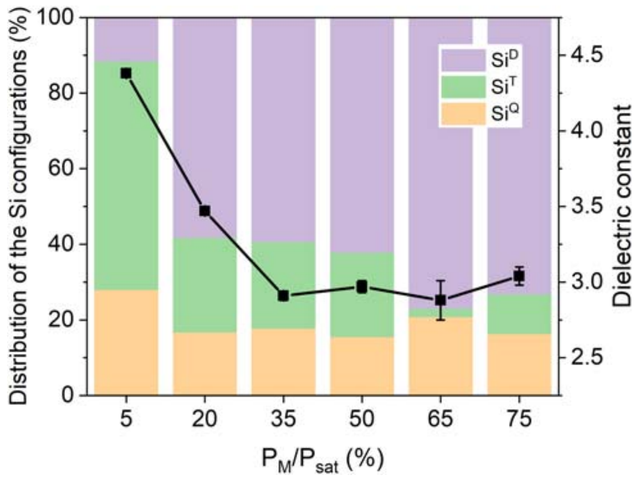

FIGURE 9 Distribution of the Si^D, Si^T and Si^Q configurations of the Si element estimated from the simultaneous X-ray photoelectron spectroscopy curve fitting of the Si 2p, C 1s and O 1s core levels for the thin films synthesised at different P_M/P_{sat} ratios. The variation of the dielectric constant as a function of the P_M/P_{sat} is plotted to highlight its correlation with the evolution of the Si configurations

To gain a deeper understanding on the influence of P_M/P_{sat} ratio on the chemical composition of the films, the environment of the silicon-based units was determined from the simultaneous XPS curve fitting of the Si 2p, C 1s and O 1s core levels, as described elsewhere.[27,28] Particularly, the Si 2p peak was fitted with a sum of three components, considering three different silicon environments: (a) Si^D that corresponds to the silicon-based unit present in the monomer, that is, $[(CH_2{=}CH)(CH_3)SiO_{2/2}]$, which can be further crosslinked or not through its vinyl group, and (b) Si^T for $[R_1SiO_{3/2}]$ and Si^Q for $[SiO_{4/2}]$ that could arise from the alteration of the monomer structure and where R is more likely to be methyl or vinyl groups already present in the starting monomer. Unsurprisingly, in view of the previous observations, the film prepared from the lowest monomer saturation ratio (5%) shows the lowest retention of the Si^D configuration, with only 11% of the original Si configuration retained (Figure 9 and Table S9). Such an alteration of the monomer structure is coupled to the creation of a large proportion of crosslinking Si^T configuration (60%), and in a lesser extent to the formation of crosslinking Si^Q configuration (28%), responsible for the higher dielectric constant of this film, that is, $k_{5\%} = 4.4$. The increase in the monomer saturation ratio to 20% results in a significant increase in the Si^D configuration to 58%, coupled with a decrease in the Si^T configuration to 25% as well as a decrease in the dielectric constant to 3.5. A further increase in the monomer saturation ratio results in even better retention of the Si^D configuration up to 77% and lower dielectric constants, ca. 2.9. However, similar to what was observed for the dielectric constant and growth rate evolution, the distribution of the Si configurations is not significantly varied above a monomer saturation ratio of 35%.

The variation of the Si configurations and notably the creation of crosslinking units (Si^T and Si^Q) are known to affect the elastic modulus of organosiloxane thin films. In the present work, a decrease in the Young modulus is observed when P_M/P_{sat} ratio is increased (Figure S13). The relationship between the composition and mechanical properties of our AP-PiCVD thin films is interpreted through the concepts of continuous random network theory and percolation of rigidity.[20,26] As a key parameter to these concepts, the average connectivity number, which is the ratio of network forming bonds to network forming atoms in a polymeric thin film, is calculated from the XPS curve-fitting data.[20] Following the same rationale as Trujillo et al.,[20] the Si^D, Si^T and Si^Q configurations are ascribed to 2.20, 2.40 and 2.67 connectivity numbers, respectively. The connectivity number of the different thin films is calculated by summing the weighted contribution of each configuration, that is, multiplied by their relative abundance determined from the XPS curve fitting:

$$<r> = 2.2 \times Si^D\% + 2.4 \times Si^T\% + 2.67 \times Si^Q\%.$$

Expectedly, the connectivity number exhibits a trend close to the evolution observed for the Young modulus, and all the thin films elaborated using a P_M/P_{sat} ratio ≥20% show an $<r>$ value of approximately 2.3 (obviously close to the percolation threshold value of the Si^D group that constitutes the main Si configuration in these films). The thin films elaborated using a 5% monomer saturation ratio demonstrates the highest connectivity number, ca. 2.4, which corresponds to the threshold value at which the material becomes rigid and amorphous. It is interesting to note that the thin films elaborated at $P_M/P_{sat} \geq 20\%$ possess a connectivity number below the percolation threshold (2.4) and can, therefore, be considered as nonrigid materials.

3.3 | Operating regime in PiCVD

Monomers bearing polymerisable vinyl groups and low plasma pulse frequencies are essential for the AP-PiCVD of regular polymer thin films.[13,14] In addition to these two prerequisites, the present work highlights the influence of the monomer saturation ratio on the chemical and physical properties of the thin films formed using ultrashort plasma pulses ($t_{ON} < 100$ ns) and long plasma off-times (t_{OFF}). This is not surprising, as Yasuda widely demonstrated that the energy density per monomer strongly influences the chemical composition and structure of plasma polymer thin films.[29] However, when vinyl compounds are used in PECVD, plasma-induced polymerisation and plasma-state polymerisation both occur simultaneously,[30] and the Yasuda factor, that is, $Y = W/FM$, where W is the deposition power (J/s), F is the monomer flow rate (mol/s) and M is the monomer molecular weight (g/mol), becomes insufficient to describe or predict the PECVD of vinyl compounds, notably when operating under atmospheric pressure conditions.[31]

Nevertheless, the present investigations evidence the different regimes of PECVD[32]: (a) the monomer-deficient regime, (b) the competition regime and (c) the energy-deficient regime. In the present case, the monomer-deficient regime is observed for monomer saturation ratios lower than 20% (Figure 5), notably at higher plasma pulse frequency ($f \geq 1{,}000$ Hz) where the high probability of interaction between the monomer and the active plasma species is responsible for the significant monomer dissociation rate (Figure 2a). Under such conditions, the high concentration of condensable vapours quickly yields small-to-large clusters that are responsible for low growth rates (Figure 1b) and granular surfaces (Figure 3a), respectively. If the monomer-deficient regime can be attenuated from a decrease of the plasma pulse frequency, the minimum plasma pulse frequency, that is, maximum plasma off-time, is limited by the lifetime of the free-radical polymerisation propagation step. This limitation is illustrated by the altered chemical structure (Figure 8), lower growth rate and higher k value (Figure 5) of the thin films grown from a P_M/P_{sat} ratio of 5% and for which further decrease of the plasma pulse frequency below 100 Hz does not yield any improvement.

On the other hand, the energy-deficient regime is observed for high monomer saturation ratio, typically for $P_M/P_{sat} \geq 65\%$, and low plasma pulse frequency. Under these conditions, if high monomer structure retention is ensured (Figure 8), lower levels of crosslinking are most probably obtained, resulting in lower dielectric strengths (Figure 6). If the energy-deficient regime may not be readily identified from the growth rate variation (Figure 5) or macroscopic features for crosslinking monomers such as V3D3, it might result in the formation of low molecular weight species for monomers possessing a single vinyl group. The formation of short oligomers can result in the formation of viscous thin films, as reported for the AP-PiCVD reaction of butyl methacrylate for P_M/P_{sat} of 20%,[13] or thin films that suffer from leaching of low molecular weight species.[33]

The present study highlighted an ideal process window ($35\% \leq P_M/P_{sat} < 65\%$) for which no changes are detected in the deposition rate (Figure 5), the chemical structure (Figures 8 and 9) and the functional properties of the thin films (Figures 5 and 6). This region, known as the competition regime, provides a rather large operating window for the dry and atmospheric-pressure deposition of atomically smooth and ultrathin low-*k* polymer insulating layers. The competition region is strongly dependent on the kinetic properties and saturation pressure (P_{sat}) of the studied monomer, and it needs to be determined for each case, bearing in mind that if high P_{sat} allows high monomer partial pressure (P_M), high P_M can quench the plasma, and low monomer saturation ratios (P_M/P_{sat}) will yield low adsorption rates. However, monomer possessing low P_{sat} can be heated up to ensure high monomer partial pressure required to grow polymer thin films with optimal functional properties.[34] In the perspective of applications where the length of the polymer chain is crucial to grant functional properties to a thin film, for example, thermoresponsive polymer layers,[34] or prevent leaching of low molecular species, for example, biomedical coatings,[33,34] it is essential to understand and determine the influence of the monomer saturation ratio (P_M/P_{sat}) on the growth mechanism of the thin films to define the optimal process window of AP-PiCVD.

4 | CONCLUSION

The importance of the monomer saturation ratio (P_M/P_{sat}) for the AP-PiCVD of low dielectric constant thin films was demonstrated in this study. FTIR and XPS highlighted the better retention of the monomer structure with the increase of the P_M/P_{sat} ratio, resulting in a decrease of the dielectric constant from 4.4 to 2.9. Nevertheless, the increase of the monomer saturation ratio above 50% is responsible for the early breakdown electric field of the polymer thin films. Thus, an ideal process window was defined for the AP-PiCVD of atomically smooth, conformal and ultrathin low-*k* polymer insulating layers from V3D3. The PV3D3 thin films elaborated using a P_M/P_{sat} ratio in the range of 20–50% showed excellent insulating properties with a leakage current density of 10^{-8} A/cm^2, even for a thickness as low as 21 nm. In addition, the investigation of different monomer saturation ratios at various plasma pulse frequencies allowed a better description of the competition between the various mechanisms implied in the growth of thin films using ultrashort plasma pulses. The strong correlations established between the monomer saturation ratio and the growth rate, the chemistry and the resulting properties of the thin films could be beneficial for the synthesis of other functional thin films elaborated by AP-PiCVD.

ACKNOWLEDGEMENTS

The authors thank Dr. J. Guillot, Dr. S. Girod and P. Grysan, all from LIST, for the acquisition of the XPS data, the MIS preparation and Young modulus measurements, respectively. Prof. M. Creatore from Eindhoven University of Technology, Prof. P. Dale from the University of Luxembourg and Dr. F. Loyer, Dr. K. Baba from LIST are acknowledged for insightful discussions. The Luxembourg National Research Fund (FNR) is thanked for financial support through the MASSENA project (PRIDE15/10935404).

ORCID

Dominique Abessolo Ondo http://orcid.org/0000-0002-3324-5229
Nicolas D. Boscher http://orcid.org/0000-0003-3693-6866

REFERENCES

[1] B. Wang, W. Chi, L. Al-Hashimi, T. J. Marks, A. Facchetti, *Chem. Rev.* **2018**, *118*, 5690.
[2] Y. Wang, X. Huang, T. Li, L. Li, X. Guo, P. Jiang, *Chem. Mater.* **2019**, *31*, 2212.
[3] J. Veres, S. D. Ogier, S. W. Leeming, D. C. Cupertino, S. M. Khaffaf, *Adv. Funct. Mater.* **2003**, *13*, 199.
[4] H. Moon, H. Seong, W. C. Shin, W.-T. Park, M. Kim, S. Lee, J. H. Bong, Y.-Y. Noh, B. J. Cho, S. Yoo, S. G. Im, *Nat. Mater.* **2015**, *14*, 628.
[5] V. Jousseaume, J. El Sabahy, C. Yeromonahos, G. Castellan, A. Bouamrani, F. Ricoul, *Microelectron. Eng.* **2017**, *167*, 69.
[6] K. Maex, M. R. Baklanov, D. Shamiryan, F. Iacopi, S. H. Brongersma, Z. S. Yanovitskaya, *J. Appl. Phys.* **2003**, *93*, 8793.
[7] M. Wang, X. Wang, P. Moni, A. Liu, D. H. Kim, W. J. Jo, H. S., K. K. Gleason, *Adv. Mater.* **2017**, *29*, 1604606.
[8] W. Volksen, R. D. Miller, G. Dubois, *Chem. Rev.* **2010**, *110*, 56.
[9] M. R. Baklanov, J.-F. de Marneffe, D. Shamiryan, A. M. Urbanowicz, H. Shi, T. V. Rakhimova, H. Huang, P. S. Ho, *J. Appl. Phys.* **2013**, *113*, 041101.
[10] D. Abessolo Ondo, F. Loyer, J.-B. Chemin, S. Bulou, P. Choquet, N. D. Boscher, *Plasma Process. Polym.* **2018**, *15*, e1700172.
[11] D. Mariotti, T. Belmonte, J. Benedikt, T. Velusamy, G. Jain, V. Švrček, *Plasma Process. Polym.* **2016**, *13*, 70.
[12] D. Abessolo Ondo, F. Loyer, F. Werner, R. Leturcq, P. J. Dale, N. D. Boscher, *ACS Appl. Polym. Mater.* **2019**, *1*, 3304.
[13] F. Loyer, G. Frache, P. Choquet, N. D. Boscher, *Macromolecules* **2017**, *50*, 4351.
[14] F. Loyer, S. Bulou, P. Choquet, N. D. Boscher, *Plasma Process. Polym.* **2018**, *15*, e1800121.
[15] N. D. Boscher, F. Hilt, D. Duday, G. Frache, T. Fouquet, P. Choquet, *Plasma Process. Polym.* **2015**, *12*, 66.
[16] A. Kumar, D. Grant, S. Alancherry, A. Al-Jumaili, K. Bazaka, M. V. Jacob *Plasma Science and Technology for Emerging Economies* (Eds: Rawat, R.), Springer, Singapore **2017**.
[17] J. Friedrich, *Plasma Process. Polym.* **2011**, *8*, 783.
[18] G. Aresta, J. Palmans, M. C. M. van de Sanden, M. Creatore, *J. Vac. Sci. Technol. A* **2012**, *30*, 041503.
[19] J. Lubguban Jr., T. Rajagopalan, N. Mehta, B. Lahlouh, S. L. Simon, S. Gangopadhyay, *J. Appl. Phys.* **2002**, *92*, 1033.
[20] N. J. Trujillo, Q. Wu, K. K. Gleason, *Adv. Funct. Mater.* **2010**, *20*, 607.

[21] S. Lowell, J. E. Shields, *Powder Surface Area and Porosity*, Springer Science+Business Media BV, the Netherlands **1984**.
[22] F. Werner, S. Siebentritt, *Phys. Rev. Appl.* **2018**, *9*, 054047.
[23] C. C. Ku, R. Liepins, *Electrical Properties of Polymers: Chemical Principles*, Hanser Publishers, Munich **1987**.
[24] W. S. O'Shaughnessy, M. Gao, K. K. Gleason, *Langmuir* **2006**, *22*, 7021.
[25] N. D. Boscher, P. Choquet, D. Duday, S. Verdier, *Surf. Coat. Technol.* **2010**, *205*, 2438.
[26] D. D. Burkey, K. K. Gleason, *J. Appl. Phys.* **2003**, *93*, 5143.
[27] N. D. Boscher, P. Choquet, S. Verdier, *Surf. Coat. Technol.* **2011**, *205*, 5350.
[28] L.-A. O'Hare, A. Hynes, M. R. Alexander, *Surf. Interface Anal.* **2007**, *39*, 926.
[29] H. Yasuda, T. Hirotsu, *J. Polym. Sci., Part A: Polym. Chem.* **1978**, *16*, 743.
[30] H. Yasuda, *J. Polym. Sci. Macromol. Rev.* **1981**, *16*, 199.
[31] A. Kakaroglou, B. Nisol, K. Baert, I. De Graeve, F. Reniers, G. Van Asschec, H. Terryna, *RSC Adv.* **2015**, *5*, 27449.
[32] H. Yasuda, *Luminous Chemical Vapor Deposition and Interface Engineering*, CRC Press, Boca Raton **2004**.
[33] P. Cools, N. De Geyter, R. Morent, *Int. J. Nanotechnol.* **2016**, *13*, 695.
[34] F. Loyer, A. Combrisson, K. Omer, M. Moreno-Couranjou, P. Choquet, N. D. Boscher, *ACS Appl. Mater. Interfaces* **2019**, *11*, 1335.

SUPPORTING INFORMATION

Additional supporting information may be found online in the Supporting Information section.

How to cite this article: Abessolo Ondo D, Leturcq R, Boscher ND. Plasma-initiated chemical vapour deposition of organosiloxane thin films: From the growth mechanisms to ultrathin low-*k* polymer insulating layers. *Plasma Process Polym*. 2020;e2000032. https://doi.org/10.1002/ppap.202000032

CHAPTER IV─ Importance of the Monomer Structure on the Dielectric Properties of the AP-PiCVD Thin Films

The previous chapters highlight the importance of the vinyl group on the atmospheric-pressure chemical vapour deposition of polymeric thin films using low nanosecond plasma pulses as polymerisation initiator. In addition, the significance of the monomer saturation ratio (P_M/P_{sat}), impacting the retention of the monomer structure and thus the functional properties of the films, is demonstrated. Insight into the growth mechanisms is provided. The present chapter aims at exploiting the versatility of the AP-PiCVD approach to investigate the dielectric properties of thin films elaborated from two cyclic organosiloxane (V3D3 and V4D4) and two organosilazane (V3N3 and V4N4) monomers. The dielectric constant of as-deposited polymer layers is shown to vary (i.e. $2.8 \leq k < 4.2$) by varying the monomer bonds, i.e., siloxane and silazane, as well as their ring size, demonstrating the importance of the monomer structure (functionality). Low leakage current densities measured in the range of 10^{-9} A/cm^2 for a thickness as low as 12 nm exhibit the good insulating properties of the resulting layers.

Contents

Article(s) published from these results

Dominique Abessolo Ondo, François Loyer, Florian Werner, Renaud Leturcq, Phillip J. Dale, Nicolas D. Boscher (2019). Atmospheric-Pressure Synthesis of Atomically Smooth, Conformal, and Ultrathin Low-k Polymer Insulating Layers by Plasma-Initiated Chemical Vapor Deposition. https://doi.org/10.1021/acsapm.9b00759

Full contribution: experimental work on the synthesis and characterization of the thin films and treatment, analysis and interpretation of the collected data, redaction of the manuscript

ACS APPLIED POLYMER MATERIALS

Article

Cite This: ACS Appl. Polym. Mater. 2019, 1, 3304−3312

pubs.acs.org/acsapm

Atmospheric-Pressure Synthesis of Atomically Smooth, Conformal, and Ultrathin Low-*k* Polymer Insulating Layers by Plasma-Initiated Chemical Vapor Deposition

Dominique Abessolo Ondo,[†] François Loyer,[†] Florian Werner,[‡] Renaud Leturcq,[†] Phillip J. Dale,[‡] and Nicolas D. Boscher*[,†]

[†]Materials Research and Technology Department, Luxembourg Institute of Science and Technology, 41, rue du Brill, L-4422 Belvaux, Luxembourg

[‡]Physics and Materials Science Research Unit, University of Luxembourg, 41, rue du Brill, L-4422 Belvaux, Luxembourg

Supporting Information

ABSTRACT: The straightforward synthesis of ultrathin low dielectric constant insulating polymer layers from four cyclic organosilicon monomers (i.e., two organocyclosiloxanes and two organocyclosilazanes) by atmospheric pressure plasma-initiated chemical vapor deposition (AP-PiCVD) is demonstrated. The combination of ultrashort plasma pulses (ca. 100 ns), as polymerization initiator, with long plasma off-times (10 ms), yields the formation of atomically smooth and conformal polymer layers with excellent insulating properties. Leakage current densities of 10^{-9} A cm^{-2} are measured for film thicknesses as low as 12 nm. Low dielectric constants are obtained because of the retention of the cyclic structure of the monomers during the deposition. The polymer layers prepared from 1,3,5,7-tetramethyl-1,3,5,7-tetravinylcyclotrisiloxane display the lowest dielectric constant (k = 2.8). The present study demonstrates the ability to vary the dielectric constant of as-deposited polymer layers by varying the monomer bonds, i.e., siloxane and silazane, as well as their ring size.

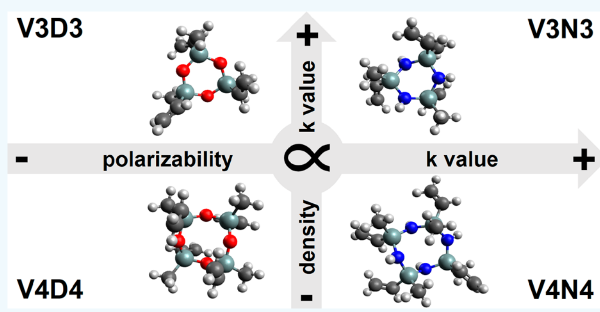

KEYWORDS: *low dielectric constant polymer, polymer dielectric, polymer thin film, atmospheric plasma CVD, plasma-initiated chemical vapor deposition (PiCVD)*

■ INTRODUCTION

Dielectric polymers are lightweight materials that have attracted a huge interest in electrical and electronic applications because of their insulating properties, chemical resistance, and mechanical flexibility.[1] In particular, dielectric polymer layers have been integrated into various microelectronic devices, including flexible displays[2] and sensors.[2] Integrated into organic field-effect transistors (OFETs) as a gate dielectric, the capacitance (C_i) of these dielectric polymer layers must be kept high enough to ensure a low power operation of the devices.[2] This requirement can be addressed by using polymers with high dielectric constant (denoted ε_r or k). High-k polymers have a low dielectric strength, and thick layers are typically required to prevent high leakage current, ultimately leading to an increase of the power consumption.[3,4] Another strategy is to downscale the thickness of low-k polymer layers.[5,6] The Clausius−Mossotti relation states[7]

$$\frac{\varepsilon_r - 1}{\varepsilon_r + 2} = \frac{N}{3\varepsilon_0}\alpha \tag{1}$$

where ε_r is the material dielectric constant, N is the number of molecules (dipoles) per unit volume (density), and α is the polarizability, which is the sum of the electronic, ionic (also referred to as the distortion[8] or atomic[7] polarization), and orientation (or dipolar[8]) polarizations. Thus, the dielectric constant of polymers can be lowered by doping silicon dioxide using less polarizable bonds, e.g., Si−CH or silicon oxycarbides,[8] and/or decreasing the density (N) via subtractive or constitutive porosities.[8,9]

Solution-based deposition methods, e.g., spin-coating, are broadly employed to deposit low-k polymers in thin film form and are often combined with a thermal curing step to remove the residual solvent.[1,3] Complications appear with the solubility of these polymer layers requiring the use of a cross-linker to prevent a detrimental swelling and implying the use of an orthogonal solvent with underlying layers. Plasma-based processes, broadly used in the microelectronics industry,[9] provide an excellent alternative for the deposition of a wide variety of thin films at both low temperature[10] and atmospheric pressure (AP).[10] A plethora of studies have already reported the plasma-enhanced chemical vapor

Received: August 15, 2019
Accepted: October 25, 2019
Published: October 25, 2019

deposition (PECVD) of low-k thin films.[10,11] The PECVD of low-k thin films relies on four strategies, i.e., porogen approach,[12] foaming approach,[13] cyclic precursor approach,[14] and carbon-bridging approach,[15] that can be used separately or combined.[14] The two first approaches aim at forming subtractive porosities by thermal,[11] UV, or plasma post-treatments.[16] In addition to the multiplication of the processing steps, subtractive porosity strategies are detrimental to the mechanical properties of the films.[16] On the other hand, constitutive porosity approaches mainly rely on the use of cyclic precursors, e.g., decamethylcyclopentasiloxane (D5),[14] for which a high degree of retention of the ring structure is ensured under mild or pulsed plasma conditions.[15] Nevertheless, minimizing the highly reactive and nonspecific nature of plasma to protect the ring structure of cyclic siloxanes also implies a lower degree of cross-linking of the films.[17] The network connectivity of the films can be increased by introducing carbon-bridging groups.[9] Notably, the use of cyclic siloxanes bearing polymerizable pendant groups, e.g., 1,3,5-trimethyl-1,3,5-trivinylcyclotrisiloxane (V3D3)[15] and 1,3,5,7-tetramethyl-1,3,5,7-tetravinylcyclotrisiloxane (V4D4),[18] promotes a better retention of the ring structure while ensuring the formation of highly cross-linked networks.[15,18] In recent years, the low-pressure-initiated chemical vapor deposition (iCVD) of vinyl-containing cyclosiloxanes has been reported as a convenient alternative to the PECVD approach.[19] iCVD, which can produce ultrathin and conformal polymer insulating layers,[19] is particularly suitable for the preparation of flexible field-effect transistors for low-power soft electronics.[4,5]

However, plasma-based processes still possess significant advantages over iCVD since PECVD can be operated at atmospheric pressure.[10] Moreover, atmospheric plasmas can be implemented as a microplasma torch for the localized deposition and patterning of functional thin films,[10,20] which is particularly relevant to the preparation of semitransparent micro solar cells. Among the developed materials, transparent conductive thin films,[21] crystalline oxide semiconductor thin films,[10,22] and metallic contacts[10,23] can all be formed at low temperature on paper[23] or polymers substrates by using atmospheric plasmas.[21,22] Dielectric layers can also be prepared by using atmospheric plasmas;[24] however, the preparation of ultrathin organic layers with good insulating properties remains a challenge due to the reactivity of plasmas that alters the chemical structure of the monomers and induces particle formation.[14,15] Very recently, the combination of ultrashort plasma pulses (ca. 100 ns) with plasma off-times in the range of the free-radical polymerization lifetime (e.g., 1−100 ms) was demonstrated to yield conformal conventional polymer layers under atmospheric pressure conditions.[25,26] The method, called plasma-initiated chemical vapor deposition, has already been exploited for the atmospheric-pressure deposition of conformal fire-retardant polymer layers on textile,[27] thermoresponsive copolymer layers,[28] and functional polymer layers on 3D substrates for immobilization of biomolecules.[29] The present work aims at investigating further the capabilities of AP-PiCVD in the perspective to extend its range of applications to microelectronics. In particular, this work investigates the ability to form polymer layers with tunable k value by AP-PiCVD. With the objective to decrease of the power consumption of future microelectronic devices, the down-scalability of the dielectric properties of the AP-PiCVD layers is assessed. For the first time, we report the atmospheric-pressure deposition of atomically smooth, conformal, and ultrathin low-k polymer insulating layers from a dry process. The excellent down-scalability of the AP-PiCVD approach is highlighted by the low-leakage current (ca. 10^{-9} A cm^{-2}) measured for a film thickness as low as 12 nm. The high retention of the monomer structure in AP-PiCVD allowed the easy tuning of the k value from the careful selection of the polarizability and ring size of the monomer.

■ EXPERIMENTAL METHODS

Materials and Substrates. The four investigated monomers, i.e., 1,3,5-trimethyl-1,3,5-trivinylcyclotrisilazane (V3N3), 1,3,5,7-tetravinyl-1,3,5,7-tetramethylcyclotetrasilazane (V4N4), 1,3,5-trivinyl-1,3,5-trimethylcyclotrisiloxane (V3D3), and 1,3,5,7-tetravinyl-1,3,5,7-tetramethylcyclotetrasiloxane (V4D4), were all purchased from Fluorochem and used without any purification. All depositions were carried on intrinsic and highly boron doped (ρ = 0.01 ohm·cm) polished silicon wafers (Siltronix, Archamps, France). Prior to each experiment, the silicon wafers were treated using a 95%/5% argon/oxygen plasma for 40 s. A high-resolution stationary manometer 424-10 (Dwyer, IN) was used to determine the vapor pressure of V3D3, V3N3, V4D4, and V4N4 at 20 °C.

AP-PiCVD of Polymer Layers. The thin films were deposited by using an open-air atmospheric-pressure dielectric barrier discharge setup as previously described.[25] The nanosecond discharges used to initiate the free-radical polymerization of the selected vinylic monomers were ignited by 1 μs square pulses of 6 kV produced by an AHTPB10F generator from EFFITECH, allowing the generation of ultrashort plasma discharges (ca. t_{on} = 100 ns) at a discharge frequency of 100 Hz (i.e., t_{off} = 10 ms). The discharge gap was maintained to 1 mm. Each monomer was directly delivered to the deposition area by using a bubbler setup and argon (Air Liquide, 99.999%) as carrier gas. The flow rate of the argon carrier gas was set to 15 L min^{-1}. The total gas flow was maintained constant to 20 L min^{-1} by using another argon source. To avoid O_2 and N_2 contamination, argon fluxes were added on both sides of the electrodes.

Thin Film Characterizations. Scanning electron microscopy (SEM) images were obtained by using a Hitachi SU-70 FE-SEM. To avoid distortions due to the charge effect, the samples were coated with a 10 nm platinum film prior to the SEM observations. Atomic force microscopy (AFM) images were obtained by using an Innova instrument operating in tapping mode.

Chemical Characterizations. FTIR analyses of the resulting films were performed in reflection mode on Si wafers by using a Bruker Hyperion 2000 spectrometer equipped with an ATR objective. The spectra were obtained over a range of 650−4000 cm^{-1} with a resolution of 4 cm^{-1}. The monomer spectra were acquired with the same FTIR spectrometer. XPS analyses (300 × 700 μm^2) were performed with a Kratos Axis Ultra DLD spectrometer using a monochromatic Al Kα X-ray source ($h\nu$ = 1486.6 eV). A flooding gun was used to reduce charging effect on the samples surface. Photoelectrons emission were collected at 0° angle with respect to the normal. The surface of the samples was precleaned by bombardment with Ar$^+$ ions (2 kV) and etched for 300 s, prior to the collection of XPS data. Casa XPS software was used for chemical quantification and identification.

Fabrication and Electrical Characterization of the Metal/Insulator/Semiconductor Devices. The synthesized dielectric polymer layers were sandwiched between a highly doped Si wafer used as bottom electrode and a patterned gold layer as top electrode. The patterned gold layers were formed by using shadow masks by electron beam evaporation at a base pressure lower than 10^{-6} mbar. Prior to gold evaporation, a thin layer of titanium (10 nm) was evaporated on top of the AP-PiCVD layers to ensure the adhesion of the gold layer (50 nm). Capacitance versus frequency (C−f) characteristics of the metal/insulator/semiconductor (MIS) devices were measured by using an impedance analyzer (IM 3570 HIOKI). The C−f measurements were performed in a range of frequencies

DOI: 10.1021/acsapm.9b00759
ACS Appl. Polym. Mater. 2019, 1, 3304−3312

from 100 Hz to 1 MHz with an excitation level of 0.1 V. The J−V characteristic measurements of the MIS devices were performed at ambient atmosphere by using a Keithley 2614B instrument while the voltage was from −20 to 20 V.

Density Functional Theory (DFT) Calculations. DFT calculations were performed by using the 4.0.1 program suite using the HPC facilities of the University of Luxembourg.[30,31] The hybrid functional B3LYP was used for every calculation along with Ahlrichs' basis set def2-TZVP and Weighend's auxiliary basis set def2/J.[32,33] The numerical chain of sphere approximation RIJCOSX and the dispersion correction D3 were also applied in any instance.[34,35] The bond dissociation energies (BDE) of the investigated monomers were calculated by using a previously reported method.[26] Analytical frequency calculations were performed for each fragment and molecule to obtain their free enthalpy and to ensure the convergence of the calculation. Because of the molecules' symmetry, only a third (for V3N3 and V3D3) and fourth (for V4N4 and V4D4) of the BDE were calculated and reported.

RESULTS AND DISCUSSION

AP-PiCVD of Atomically Smooth and Conformal Ultrathin Polymer Layers. To demonstrate our atmospheric-pressure chemical vapor deposition approach toward the simultaneous synthesis and deposition of atomically smooth, conformal, and ultrathin insulating polymer layers with tunable dielectric properties, four different cyclic monomers were selected, i.e., two silazanes (1,3,5-trimethyl-1,3,5-trivinylcyclotrisilazane (V3N3) and 1,3,5,7-tetravinyl-1,3,5,7-tetramethylcyclotetrasilazane (V4N4)) as well as two siloxanes (1,3,5-trivinyl-1,3,5-trimethylcyclotrisiloxane (V3D3) and 1,3,5,7-tetravinyl-1,3,5,7-tetramethylcyclotetrasiloxane (V4D4)). Briefly, they are six- to eight-member silazane or siloxane rings with three to four vinyl pendant groups, respectively (Figure 1). The vinyl groups are a prerequisite in AP-PiCVD, which relies on the free-radical polymerization reaction.[26,36] The cyclic structure of the selected monomers is foreseen to provide a constitutive porosity to the polymer layers and therefore yield a low dielectric constant according to the Clausius−Mossotti equation (eq 1).[7] Thus, the four monomers, which differ by their polarizability, i.e., different chemical bonds between the silazanes and siloxanes, and/or their ring sizes (Figure 1), should yield different dielectric constants. The pore surface area of each siloxane and silazane rings was determined in their most stable geometry by DFT calculations. The silazane's pores are roughly 6% larger than the siloxane's ones due to longer Si−N (174 pm) bonds in comparison to Si−O (166 pm) bonds and lower Si−N−Si (106−110° and 122−128°) angles in comparison to the Si−O−Si (109−110° and 131−143°) angles. In a general manner, the pore surface area increases by 40% when increasing the ring members from six (i.e., V3D3 and V3N3) to eight (i.e., V4D4 and V4N4).

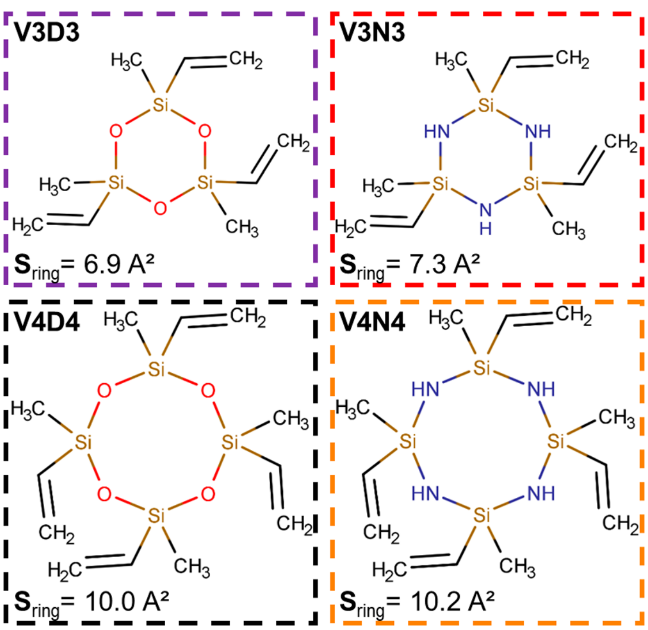

Figure 1. Chemical structure of the V3D3, V3N3, V4D4, and V4N4 monomers. The DFT calculated ring size of these cyclic monomers ranges from 6.9 Å^2 to 7.3, 10.0, and 10.2 Å^2 for V3D3, V3N3, V4D4, and V4N4, respectively.

To initiate the free-radical polymerization of the selected monomers, we employed 1 μs square-wave high-voltage pulses (6 kV) to ignite an atmospheric-pressure dielectric barrier discharge in argon (Figure 2a). Each high-voltage pulse generates two distinct current discharges (ca. 100 ns) at the voltage rising and falling edges (Figure 2b). The repetition frequency of the high-voltage pulses was set to 100 Hz. This corresponds to a 10 ms plasma off-time, which is consistent with the lifetime of the free-radical polymerization reaction of vinyl compounds in AP-PiCVD.[25,27,28,36]

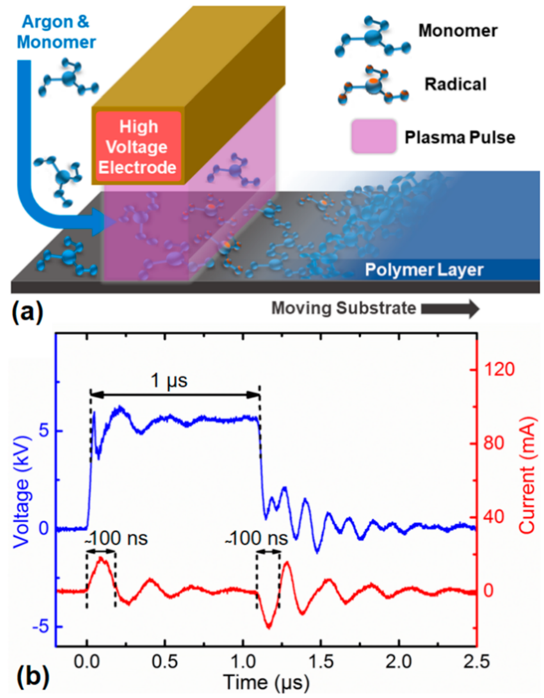

Figure 2. (a) Scheme of the atmospheric-pressure plasma-initiated chemical vapor deposition used for the preparation of atomically smooth, conformal, and ultrathin low-k polymer insulating layers. (b) Traces of the high-voltage pulse and current discharges.

The AP-PiCVD reaction of the selected monomers leads to the deposition of macroscopically smooth and defect-free thin films across the entire surface of the substrates, including 4 in. silicon wafers. Scanning electron microscopy (SEM) observations confirmed that, irrespective of the monomers, smooth and particle-free thin films are formed over the whole surface of the substrate (Supporting Information Figure S1). The pinhole-free nature and low particulate density of the AP-

DOI: 10.1021/acsapm.9b00759
ACS Appl. Polym. Mater. 2019, 1, 3304−3312

PiCVD thin films are further confirmed through atomic force microscopy (AFM) investigations (Figure 3). More importantly, AFM highlights the atomically smooth nature of the AP-PiCVD thin films with a root-mean-squared roughness (R_q) measured below 7 Å, even for thicknesses higher than 300 nm (Figure 3). Such low R_q values, similar to the ones measured for the thin films grown by low-pressure iCVD,[37] make the proposed AP-PiCVD approach highly suitable for OTFT applications.[2]

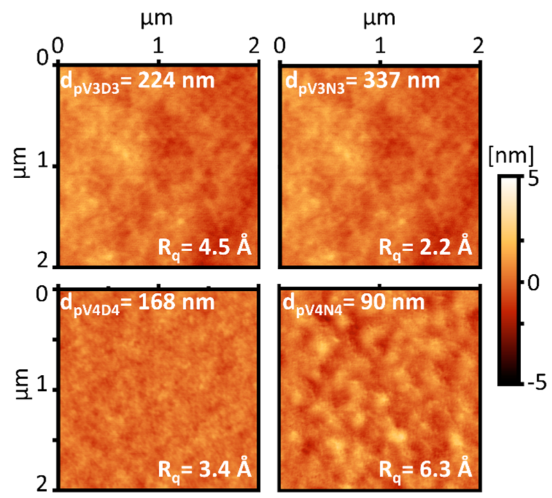

Figure 3. Atomic force microscopy (AFM) images and root-mean-square roughness (R_q) of pV3D3 (d = 224 nm), pV4D4 (d = 168 nm), pV3N3 (d = 377 nm), and pV4N4 (d = 126.7 nm) coatings prepared by AP-PiCVD. d is the thickness of the thin films.

SEM cross-sectional observation of the AP-PiCVD thin films deposited on a trenched wafer highlights their excellent conformality with a d_{bottom}/d_{top} and a $d_{sidewall}/d_{top}$ ratio close to 100% and 63%, respectively (Figure 4). d_{top}, $d_{sidewall}$, and d_{bottom} are the thicknesses at the top, sidewall, and bottom of the trench, respectively. The conformal coverage of 3-dimensional structures, which is very difficult to achieve by classical wet methods, is also highly desirable for the preparation of functional devices, e.g., sensors[38] and transistors.[5]

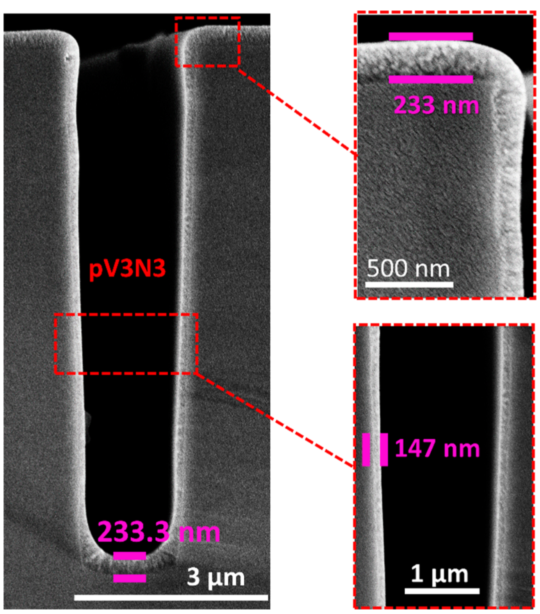

Figure 4. SEM cross-sectional image of 233 nm thick pV3N3 coating on a 9 μm deep and 1.5 μm wide silicon trench structure.

In addition to the atomically smooth and conformal nature of the as-deposited layers, the AP-PiCVD process allowed their rather fast and uniform deposition. Ellipsometry measurements confirmed that uniform thicknesses were achieved across the whole length of the silicon substrates. The deposition rates were evaluated to be 0.68, 0.70, 0.96, and 0.42 nm s^{-1} for the V3D3, V3N3, V4D4, and V4N4 monomers, respectively (Table 1). The monomer carrier gas flow (15 slm), in which the monomer partial pressure (P_M) is approximately its vapor pressure (P_{sat}), and dilution flow (5 slm) being identical for the four monomers, the P_M/P_{sat} ratio was constant for all monomers (in spite of their different P_{sat}).[39] This approach ensures comparable adsorption mechanisms that are known to have a strong influence on the growth mechanisms in the AP-PiCVD process.[26,36] The slight growth rate differences can be attributed to different polymerization rate parameters.[36] First, the different P_{sat} of the monomers (Table 1) for a constant P_M/P_{sat} ratio implies different monomer gas phase concentrations that directly affect the amount of initiating species [$M^•$] and the initiation rate R_i. One can also assume that the four monomers possess different propagation constants (k_p) that yield different propagation rates (R_p). In other words, in a process driven by surface reactions where a comparable amount of monomer adsorbs $[M]_{ad}$ on the surface, the growth rates are determined by the ability of the adsorbed monomer to polymerize prior to its desorption.

Table 1. Vapor Pressure (P_{sat}), Deposition Rate (DR), Pore Size, and k Value of the V3D3, V3N3, V4D4, and V4N4 Monomers and Their Respective As-Deposited AP-PiCVD Layers

monomer	P_{sat} (Torr)	DR (nm s^{-1})	pore size (Å^2)	k
V3D3	3.33	0.69 ± 0.09	6.9	3.6 ± 0.1
V3N3	>18	0.70 ± 0.04	7.3	4.2 ± 0.1
V4D4	0.04	0.96 ± 0.04	10.0	2.8 ± 0.1
V4N4	0.29	0.42 ± 0.04	10.2	3.7 ± 0.1

The AP-PiCVD thin films were soaked for 24 h in different solvents to investigate their chemical stability. After 24 h immersion in common polar solvents, i.e., acetone and ethanol, the thickness of the layers was unaltered for the pV4D4 and pV4N4 layers and only slightly reduced (ca. 8 to 20%) for the pV3D3 and pV3N3 layers (Table S1 and Figure S2). More interestingly, the organosilicon layers retain their atomically smooth nature with a Rq measured below 10 Å, which is desirable for application in microelectronic. These observations underline the excellent chemical stability of the organosilicon layers and suggest the successful polymerization of the vinyl pendant groups of studied monomers, yielding highly cross-linked organosilicon networks.

Ultrathin Low-k Polymer Insulating Layer. A series of metal/insulator/semiconductor (MIS) structures were fabricated to evaluate the dielectric properties of the as-deposited polymer layers (Table S2). All the polymer layers deposited from V3N3, V4D4, and V4N4 (pV3N3, pV4D4, and pV4N4) were able to sustain a voltage up to 20 V without any occurrence of an electrical breakdown, even for thicknesses as low as 12 nm (Figure 5). Additional measurements performed

DOI: 10.1021/acsapm.9b00759
ACS Appl. Polym. Mater. 2019, 1, 3304−3312

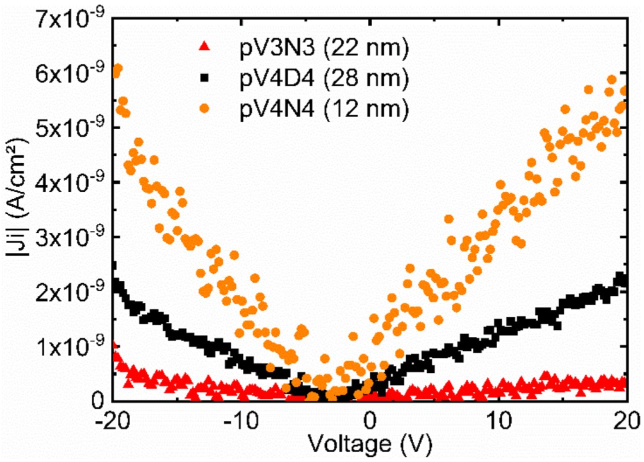

Figure 5. Voltage dependence of the absolute leakage current density $|J_i(V)|$ of the MIS devices with the ultrathin (d < 30 nm) AP-PiCVD layers grown from V3N3, V4D4, and V4N4.

on thicker polymer layers are available in Figure S3. For all the presented polymers layers, the experimental current−voltage characteristics show a linear behavior indicating an ohmic leakage current. The apparent increase of the measured current around −20 V was attributed to a transient response when abruptly applying the bias voltage at the beginning of the measurement. Thus, the initial data points ($V < -17$ V) have been disregarded for the analysis. The linear fits of the experimental current−voltage characteristics (solid lines in Figure S3) reveal resistance values in a range of approximately 4−55 GΩ cm^2 for different pV3N3, pV4D4, and pV4N4 layers. Taking into account the thickness of the polymer layers, these effective resistance values correspond to specific resistivities of $\rho = (4 \pm 2) \times 10^{15}$ Ω cm for pV4D4 and pV4N4 and slighly higher values of 10^{16} Ω cm and more for pV3N3. Such excellent insulation properties highlight the ability of our low-frequency ultrashort plasma pulses approach, i.e., AP-PiCVD, to produce insulating ultrathin dielectric layers under atmospheric pressure conditions in an open-air reactor. These excellent insulating properties were confirmed with leakage current densities (J_i) below 10^{-8} A cm^{-2} for the AP-PiCVD layers grown from V3N3, V4D4, and V4N4 (Figure S3), making them attractive as gate dielectric polymers. Surprisingly, an electrical breakdown, which is defined as an exponential increase of the leakage current density,[2] was observed for rather low electrical field for the pV3D3 layers (Figure S4). Indeed, for 23 nm thick pV3D3 layer, a voltage of 4.6 V yields to an abrupt increase of J_i, corresponding to a breakdown electric field (E_b) of 1.5 MV cm^{-1}. This early dielectric breakdown observed for the pV3D3 layers may find its origin in the much higher saturation pressure (P_{sat}) of the V3D3 monomer (Table 1). Indeed, with the aim of making fair comparisons between the four monomers selected, identical argon carrier gas flows (15 L min^{-1}) have been used with the aim to investigate a similar P_M/P_{sat} ratio (approximated to be equal to the ratio of the carrier gas flow rate over the total flow rate). Therefore, the much higher P_{sat} of V3D3 implies a much higher partial pressure (P_M) of this monomer that may either be responsible of a partial quenching of the nanosecond

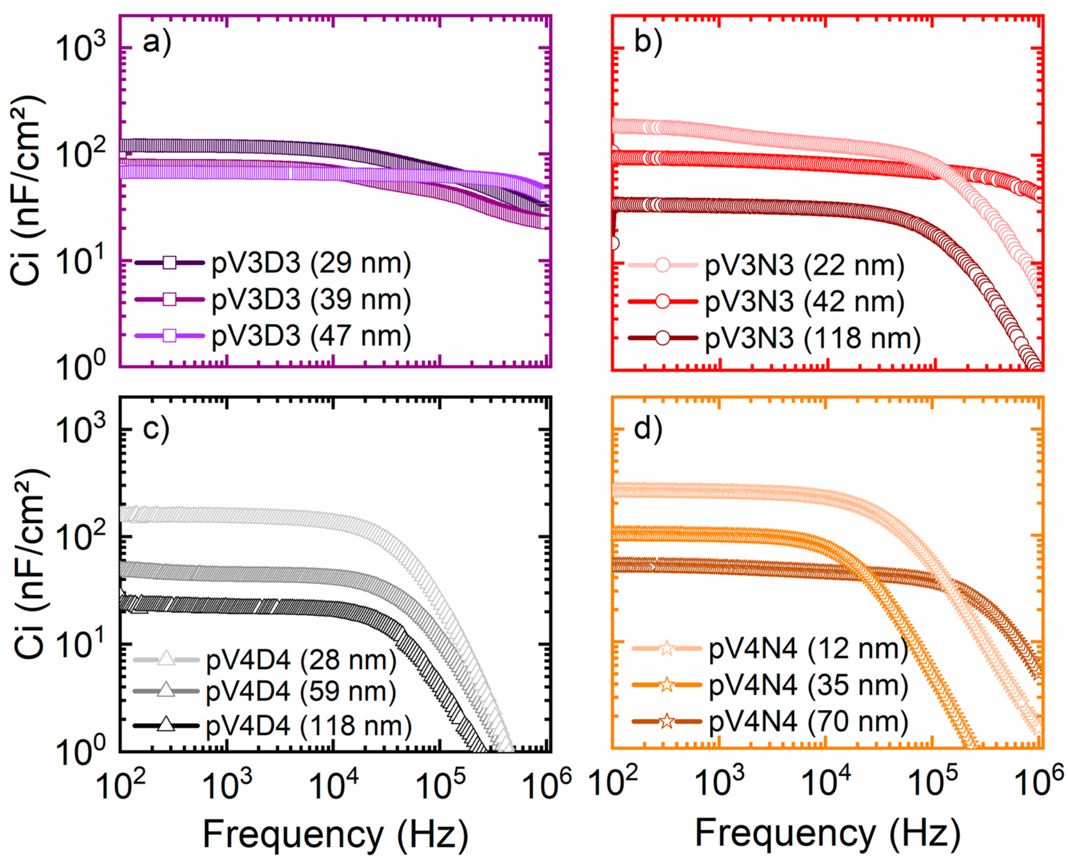

Figure 6. C_i versus frequency of all the as-deposited (a) pV3D3, (b) pV3N3, (c) pV4D4, and (d) pV4N4 layers with various thicknesses.

DOI: 10.1021/acsapm.9b00759
ACS Appl. Polym. Mater. 2019, 1, 3304−3312

discharges or promote the formation of smaller oligomers[25] that could altered the dielectric resistance of the films.

For each of the investigated monomers, the areal capacitance (C_i) of all the as-deposited polymer layers was systematically measured on three samples of different thickness and plotted with respect to the frequency (Figure 6). An abrupt drop of the capacitance with vanishing capacitance in the high frequency limit was observed for the pV3N3, pV4D4, and pV4N4 layers, while the pV3D3 and pV3N3 (42 nm) layers show smaller capacitance steps. Such capacitance steps might, for example, be related to defects in the films, parasitic capacitances, or a dipole orientation lag of the molecule behind the alternating electric field, commonly termed the polarization effect.[4] The pronounced high frequency drop of the capacitance down to zero is instead attributed to the series resistance of the MIS structure[40] because the measured capacitance drops below the minimum geometric capacitance $C_0 = \varepsilon_0/d_{\text{polymer}}$.

The real part of the dielectric constant ($\varepsilon' = k$) of each polymer layer was estimated from the relation

$$C_i = \frac{\varepsilon_0 \varepsilon'_{\text{polymer}}}{d_{\text{polymer}}} \quad (2)$$

where C_i was measured at 1 kHz for different layer thicknesses (Figure 7). It is noteworthy to underline that the C_i of all the synthesized layers was stable in the studied frequency range, i.e., low frequencies. The siloxane layers exhibited the lowest dielectric constant compared to the silazane ones, i.e., $k_{\text{pV3D3}} = 3.6 \pm 0.1$ and $k_{\text{pV4D4}} = 2.8 \pm 0.1$. It should be highlighted here that the k_{pV4D4} value (2.8) is in accordance with the values reported for the pV4D4 layers prepared from the low-pressure-initiated chemical vapor deposition method, i.e., $k = 2.8 \pm 0.1$.[41] On the other hand, the k values of the pV3N3 and pV4N4 layers were evaluated to 4.2 ± 0.1 and 3.7 ± 0.1, respectively. While the dense silicon dioxide (SiO_2) has a $k_{SiO_2} = 4.0 \pm 0.1$,[8] the silicon carbonitride (SiC_xN_y) has a $k_{SiC_xN_y} = 4.5{-}5.5$.[42] Consequently, the low dielectric constant ($k < 4$)[39] of the pV3D3, pV4D4, and pV4N4 must stem from the ability of the AP-PiCVD process to preserve the ring's structure of the selected monomers.

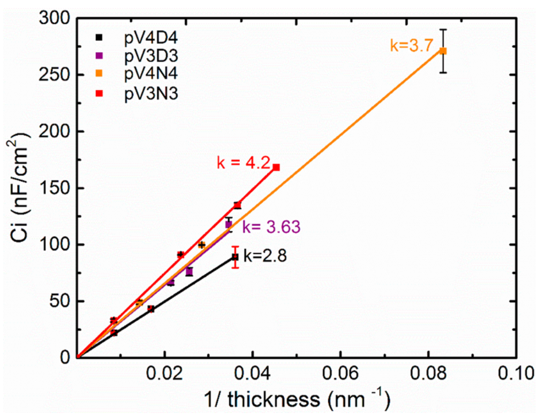

Figure 7. Estimation of the dielectric constant of the as-deposited pV3D3, pV3N3, pV4D4, and pV4N4 layers.

The FTIR spectra of the as-deposited polymer layers (Figure 8) confirmed the assumption of the preservation of the ring's structure responsible for the low dielectric constants measured. Indeed, all the polymer layers exhibit strong similarities with their respective monomer (Tables S3–S6), whereas the qualitative reduction (pV3D3 and pV3N3) or full disappearance (pV4D4 and pV4N4) of the absorbance peaks of vinyl bond located at ca. 1600 cm^{-1} and ca. 3050 cm^{-1} suggests the predominance of the free-radical polymerization pathway (Figure 8 and Figure S5).

The strong absorbance peak corresponding to the cyclic siloxane ring of V4D4 located at 1053 cm^{-1} is present in both the spectra of the monomer and the polymer layer (Figure 8c). The absence of broadening of this peak for the polymer layer is consistent with the hypothesis that the AP-PiCVD process has preserved the original cyclic siloxane ring of V4D4. Similarly, the strong absorption peak observed in the both spectra of V3D3 and the as-deposited pV3D3 layers at 997 cm^{-1} (corresponding to the Si–O—Si tricyclosiloxane ring) points out a fair retention of the tricyclosiloxane ring during the deposition. However, the presence of a weak peak that can be attributed to Si——O open cycle moieties can also be observed around 1080 cm^{-1}.[41] Ring-opening of cyclic monomers is not surprising and can be attributed to plasma-induced side reactions. This can justify the higher dielectric constant of the formed pV3D3 layers (3.6) compared to the one synthesized by iCVD, i.e., $k^{\text{iCVD}}_{\text{pV3D3}} = 2.2$.[5] On the other hand, FTIR suggests a retention of the other groups in the pV3D3 layers, notably the methyl and ethyl groups bonded to silicon (Figure S6). The mono-, di-, or trisubstitution of the silicon atom with oxygen, designated as "M", "D", and "T" configurations, respectively, can be easily monitored from the Si–CH_3 symmetric bending peak observed in the 1300–1240 cm^{-1} region (Figure S6). Shifting of this absorption peak toward higher wavenumbers is indicative of a higher substitution of carbon by oxygen atoms (O_x–Si–$(CH_3)_{4-x}$ with x = 1, 2, 3).[15,43] Despite the possible ring-opening of V3D3 during the deposition process, the original D configuration of the silicon was retained. This result further confirms the prevalence of the free-radical polymerization reaction over the opening of the V3D3 ring. To understand the reactivity difference between the V3D3 and V4D4 in AP-PiCVD, DFT calculation of their bond dissociation energies (BDE) was performed and pointed out the weaker stability of the Si–O bonds of V3D3 (4.0 eV) compared those of V4D4 (5.5 eV) (Figure S7). Thus, the differences in energy of the Si–O bonds with the other single σ-bonds in V4D4 are significant (ΔBDE $\approx$ 1.5 eV) and suggest a much lower sensitivity of the cyclotetrasiloxane ring to plasma breakdown, while the cyclotrisiloxane ring is not granted any protection due to the rather small differences in energy with the other single σ-bonds present in V3D3 (ΔBDE < 0.2 eV).

The FTIR spectra of the layers elaborated from V3N3 and V4N4 both exhibit a broad peak between 930 and 1140 cm^{-1} (Figure 8b,d), which differs from the sharp Si–N–Si peaks of the silazane rings of their respective monomers observed at ca. 930–910 and 1005 cm^{-1} (Tables S4 and S6).[37,44] Moreover, the peaks related to the stretching and deformation of N–H at 3399 and 1155 cm^{-1}, respectively, disappear. Such a broadening or disappearance of the peaks is consistent with the observation made for the pV3N3 and pV4N4 coatings elaborated by iCVD.[37] Moreover, these observations contrast with the ones made for PECVD coatings where N–H bands increase due to the disruption of the silazane rings.[44] Nevertheless, the FTIR spectra of the layers elaborated from V3N3 and V4N4 also strongly resemble the ones obtained for pV3D3 and pV4D4 (Figure 8), and the enlargement of the Si–

DOI: 10.1021/acsapm.9b00759
ACS Appl. Polym. Mater. 2019, 1, 3304–3312

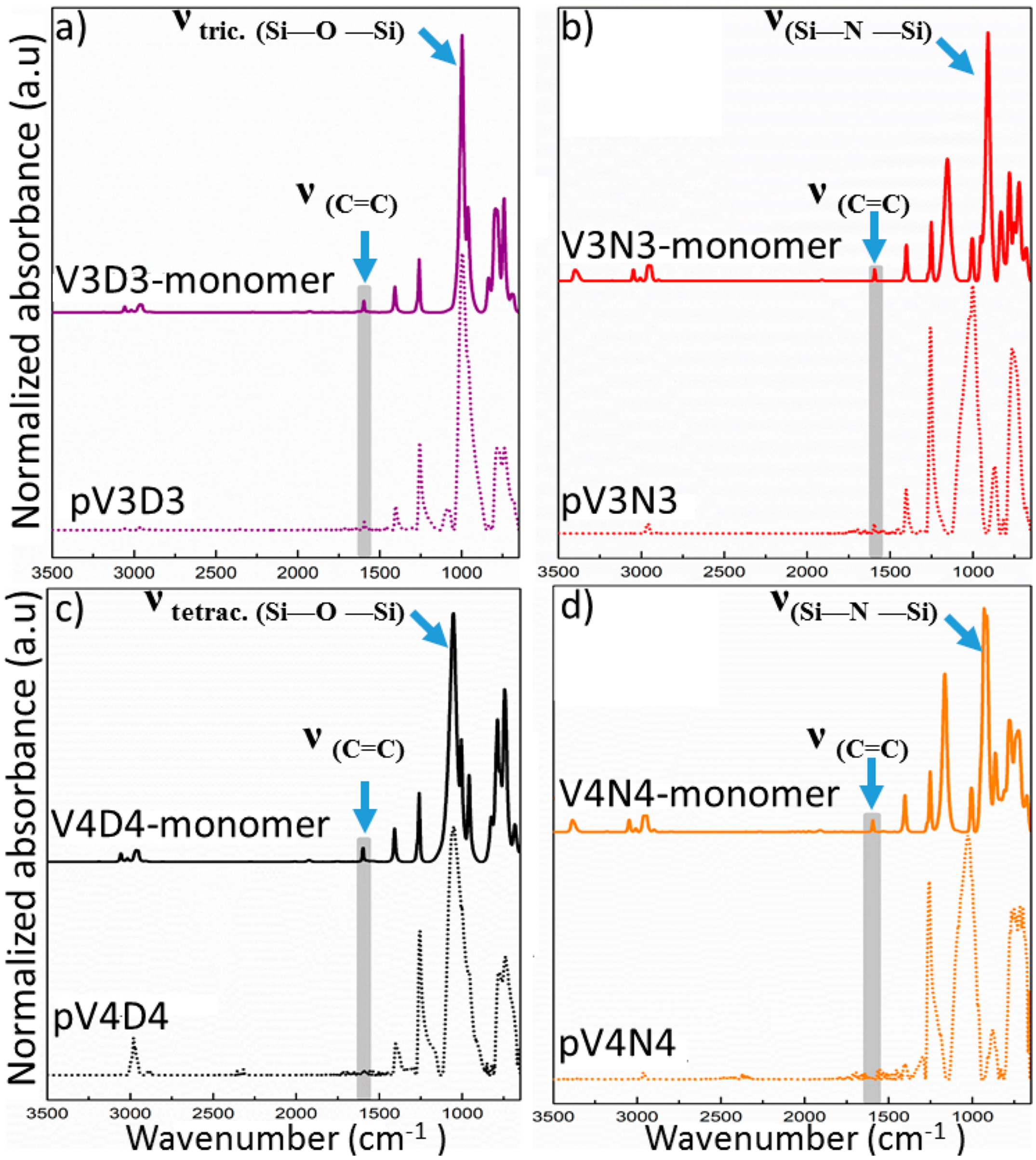

Figure 8. FTIR spectra of the AP-PiCVD layers synthesized from (a) V3D3, (b) V3N3, (c) V4D4, and (d) V4N4 and their respective monomers.

N−Si peaks between 930 and 1140 cm^{-1} could be related to the formation of Si−O−Si bonds when operating under open-atmosphere conditions. One should also mention the shift of the $Si-CH_3$ peak of the silazane-based coatings to higher wavenumbers, i.e., from 1252 to 1257 cm^{-1}, indicative of a partial oxidation of silicon (Figure S6). Therefore, a quantitative XPS analysis of the chemical composition of the AP-PiCVD coatings was undertaken to evidence any discrepancy between the expected and actual chemical compositions of the films. Unsurprisingly in view of their FTIR spectra, the pV3D3 and pV4D4 layers exhibit an almost perfect match with their expected chemical composition (Table S7). On the other hand, XPS analysis of the layers obtained from V3N3 and V4N4 reveals a drastic decrease of the nitrogen content, from 20% expected to ca. 0.6−10% measured, coupled with the incorporation of oxygen, ca. 19% (Table S7). Hence, the broadening of the Si−N−Si peaks observed in the FTIR spectra of the layers obtained from the silazane monomers can be attributed to the oxidation of silicon and the formation of Si−O bonds, in accordance with previous PECVD studies.[45]

It is noteworthy to highlight that for all the investigated monomers the formation and incorporation of −OH groups was not detected in the AP-PiCVD coatings. Indeed, the presence of a hydroxyl group was not observed by FTIR, neither at 3500 cm^{-1} nor at 920−830 cm^{-1}.[15] This aspect is important for the targeted application since the sorption of water in the dielectric layer should be avoided because the inclusion of such highly polarizable bonds −OH would lead to an increase in the resulting k value. Overall, the lower bond polarizability of the siloxane compounds and the larger and more stable ring of V4D4 make it the monomer of choice to grow ultrathin low-k polymer insulating layers by AP-PiCVD. Such findings could considerably simplify the elaboration of microelectronic devices.

DOI: 10.1021/acsapm.9b00759
ACS Appl. Polym. Mater. 2019, 1, 3304−3312

CONCLUSION

Atomically smooth, conformal, and ultrathin low-*k* polymer insulating layers were successfully deposited from a straightforward atmospheric-pressure gas phase approach based on ultrashort plasma pulses. The polymer layers, prepared from various cyclic organosilicon monomers (V3N3, V4D4, and V4N4), showed excellent insulating properties with a leakage current density of 10^{-9} A cm^{-2} for layers as thin as 12 nm. These excellent insulating properties have been attributed to the pinhole and defect-free nature of the organosilicon films. The ability to vary the dielectric constant of the resulting polymer layers was achieved by varying the polarizability of the monomer bonds, i.e., siloxane and silazane, as well as the monomer ring size. Particularly, the cyclic siloxane layers exhibited lower dielectric constant values (k_{pV3D3} = 3.6 and k_{pV4D4} = 2.8) compared to the cyclic silazane layers (k_{pV3N3} = 4.2 and k_{pV4N4} = 3.7) due to the lower polarizability of the siloxane bonds. The retention of the ring structure in AP-PiCVD allowed the synthesis of polymer layers bearing a constitutive porosity, with the layers elaborated from the larger siloxane ring (V4D4) possessing the lowest dielectric constant values (k_{pV4D4} = 2.8).

ASSOCIATED CONTENT

Supporting Information

The Supporting Information is available free of charge on the ACS Publications website at DOI: 10.1021/acsapm.9b00759.

SEM of the organosilicon-based coatings, thickness, and roughness variation of the organosilicon-based coatings after soaking in common solvents, list and characteristics of the organosilicon-based coatings integrated in MIS devices, voltage dependence of the leakage current density for the organosilicon-based coatings, assignation of the FTIR peaks for the organosilicon-based coatings and their respective monomer, enlargement of the main FTIR peaks of interest, bond dissociation energies for the investigated monomers and XPS quantification of the organosilicon-based coatings (PDF)

AUTHOR INFORMATION

Corresponding Author

*Phone: +352 275 888 578. E-mail: nicolas.boscher@list.lu.

ORCID

Florian Werner: 0000-0001-6901-8901

Renaud Leturcq: 0000-0001-7115-9172

Nicolas D. Boscher: 0000-0003-3693-6866

Notes

The authors declare no competing financial interest.

ACKNOWLEDGMENTS

The Luxembourg National Research Fund (FNR) is thanked for financial support through the MASSENA project (PRIDE15/10935404). We thank Dr. J. Guillot, Dr. S. Girod, and P. Grysan for the acquisition of the XPS data, the MIS preparation, and AFM measurements. Dr. M. Guennou, Dr. K. Baba, G Bengasi, and P. Baustert are acknowledged for insightful discussions. The DFT calculations presented in this paper were performed using the HPC facilities of the University of Luxembourg.

REFERENCES

(1) Maier, G. Low Dielectric Constant Polymers for Microelectronics. *Prog. Polym. Sci.* **2001**, *26*, 3−65.

(2) Wang, B.; Huang, W.; Chi, L.; Al-Hashimi, M.; Marks, T. J.; Facchetti, A. High- k Gate Dielectrics for Emerging Flexible and Stretchable Electronics. *Chem. Rev.* **2018**, *118*, 5690−5754.

(3) Yoon, M. H.; Yan, H.; Facchetti, A.; Marks, T. J. Low-Voltage Organic Field-Effect Transistors and Inverters Enabled by Ultrathin Cross-Linked Polymers as Gate Dielectrics. *J. Am. Chem. Soc.* **2005**, *127*, 10388−10395.

(4) Choi, J.; Joo, M.; Seong, H.; Pak, K.; Park, H.; Park, C. W.; Im, S. G. Flexible, Low-Power Thin-Film Transistors Made of Vapor-Phase Synthesized High-k, Ultrathin Polymer Gate Dielectrics. *ACS Appl. Mater. Interfaces* **2017**, *9*, 20808−20817.

(5) Moon, H.; Seong, H.; Shin, W. C.; Park, W.-T.; Kim, M.; Lee, S.; Bong, J. H.; Noh, Y.-Y.; Cho, B. J.; Yoo, S.; Im, S. G. Synthesis of Ultrathin Polymer Insulating Layers by Initiated Chemical Vapour Deposition for Low-Power Soft Electronics. *Nat. Mater.* **2015**, *14*, 628−635.

(6) Ortiz, P.; Facchetti, A.; Marks, T. J. High- k Organic, Inorganic, and Hybrid Dielectrics for Low-Voltage Organic Field-Effect Transistors. *Chem. Rev.* **2010**, *110*, 205−239.

(7) Ku, C. C.; Liepins, R. *Electrical Properties of Polymers: Chemical Principles*; Hanser Gardner Publications: 1987.

(8) Maex, K.; Baklanov, M. R.; Shamiryan, D.; Iacopi, F.; Brongersma, S. H.; Yanovitskaya, Z. S. Low Dielectric Constant Materials for Microelectronics. *J. Appl. Phys.* **2003**, *93*, 8793−8841.

(9) Volksen, W.; Miller, R. D.; Dubois, G. Low Dielectric Constant Materials. *Chem. Rev.* **2010**, *110*, 56−110.

(10) Mariotti, D.; Belmonte, T.; Benedikt, J.; Velusamy, T.; Jain, G.; Švrček, V. Low-Temperature Atmospheric Pressure Plasma Processes for "Green" Third Generation Photovoltaics. *Plasma Processes Polym.* **2016**, *13*, 70−90.

(11) You, H.; Mennell, P.; Shoudy, M.; Sil, D.; Dorman, D.; Cohen, S.; Liniger, E.; Shaw, T.; Leo, T.-L.; Canaperi, D.; Raymond, M.; Madan, A.; Grill, A. Extreme-Low k Porous PSiCOH Dielectrics Prepared by PECVD. *J. Vac. Sci. Technol., B: Nanotechnol. Microelectron.: Mater., Process., Meas., Phenom.* **2018**, *36*, 012202.

(12) Jousseaume, V.; Favennec, L.; Zenasni, A.; Gourhant, O. Porous Ultra Low k Deposited by PECVD: From Deposition to Material Properties. *Surf. Coat. Technol.* **2007**, *201*, 9248−9251.

(13) El Sabahy, J.; Castellan, G.; Ricoul, F.; Jousseaume, V. Porous SiOCH Thin Films Obtained by Foaming. *J. Phys. Chem. C* **2016**, *120*, 9184−9191.

(14) Castex, A.; Favennec, L.; Jousseaume, V.; Bruat, J.; Deval, J.; Remiat, B.; Passemard, G.; Pons, M. Study of Plasma Mechanisms of Hybrid A-SiOC:H Low-k Film Deposition from Decamethylcyclopentasiloxane and Cyclohexene Oxide. *Microelectron. Eng.* **2005**, *82*, 416−421.

(15) Burkey, D. D.; Gleason, K. K. Structure and Mechanical Properties of Thin Films Deposited from 1,3,5-Trimethyl-1,3,5-Trivinylcyclotrisiloxane and Water. *J. Appl. Phys.* **2003**, *93*, 5143−5150.

(16) Gourhant, O.; Gerbaud, G.; Zenasni, A.; Favennec, L.; Gonon, P.; Jousseaume, V. Crosslinking of Porous SiOCH Films Involving Si-O-C Bonds: Impact of Deposition and Curing. *J. Appl. Phys.* **2010**, *108*, 124105.

(17) Jousseaume, V.; El Sabahy, J.; Yeromonahos, C.; Castellan, G.; Bouamrani, A.; Ricoul, F. SiOCH Thin Films Deposited by Chemical Vapor Deposition: From Low-k to Chemical and Biochemical Sensors. *Microelectron. Eng.* **2017**, *167*, 69−79.

(18) Lubguban, J.; Rajagopalan, T.; Mehta, N.; Lahlouh, B.; Simon, S. L.; Gangopadhyay, S. Low-k organosilicate films prepared by tetravinyltetramethylcyclotetrasiloxane. *J. Appl. Phys.* **2002**, *92*, 1033−1038.

(19) Wang, M.; Wang, X.; Moni, P.; Liu, A.; Kim, D. H.; Jo, W. J.; Sojoudi, H.; Gleason, K. K. CVD Polymers for Devices and Device Fabrication. *Adv. Mater.* **2017**, *29*, 1604606.

(20) Belmonte, T.; Henrion, G.; Gries, T. Nonequilibrium Atmospheric Plasma Deposition. *J. Therm. Spray Technol.* **2011**, *20*, 744–759.
(21) Abessolo Ondo, D.; Loyer, F.; Chemin, J. B.; Bulou, S.; Choquet, P.; Boscher, N. D. Atmospheric Plasma Oxidative Polymerization of Ethylene Dioxythiophene (EDOT) for the Large-Scale Preparation of Highly Transparent Conducting Thin Films. *Plasma Processes Polym.* **2018**, *15*, 1700172.
(22) Quesada-González, M.; Baba, K.; Sotelo-Vázquez, C.; Choquet, P.; Carmalt, C. J.; Parkin, I. P.; Boscher, N. D. Interstitial boron-doped anatase TiO_2 thin-films on optical fibres: atmospheric pressure-plasma enhanced chemical vapour deposition as the key for functional oxide coatings on temperature-sensitive substrates. *J. Mater. Chem. A* **2017**, *5*, 10836–10842.
(23) Knapp, C. E.; Chemin, J.-B.; Douglas, S. P.; Abessolo Ondo, D.; Guillot, J.; Choquet, P.; Boscher, N. D. Room-Temperature Plasma-Assisted Inkjet Printing of Highly Conductive Silver on Paper. *Adv. Mater. Technol.* **2018**, *3*, 1700326.
(24) Park, J.; Cho, N.-K.; Lee, S.-E.; Lee, E. G.; Lee, J.; Im, C.; Na, H.-J.; Kim, Y. S. Atmospheric-pressure plasma treatment toward high-quality solution-processed aluminum oxide gate dielectric films in thin-film transistors. *Nanotechnology* **2019**, *30*, 495702.
(25) Loyer, F.; Frache, G.; Choquet, P.; Boscher, N. D. Atmospheric Pressure Plasma-Initiated Chemical Vapor Deposition (AP-PiCVD) of Poly(Alkyl Acrylates): An Experimental Study. *Macromolecules* **2017**, *50*, 4351–4362.
(26) Loyer, F.; Bengasi, G.; Frache, G.; Choquet, P.; Boscher, N. D. Insights in the Initiation and Termination of Poly(Alkyl Acrylates) Synthesized by Atmospheric Pressure Plasma-Initiated Chemical Vapor Deposition (AP-PiCVD). *Plasma Processes Polym.* **2018**, *15*, 1800027.
(27) Hilt, F.; Boscher, N. D.; Duday, D.; Desbenoit, N.; Levalois-Grützmacher, J.; Choquet, P. Atmospheric pressure plasma-initiated chemical vapor deposition (AP-PiCVD) of poly(diethylallylphosphate) coating: A char-forming protective coating for cellulosic textile. *ACS Appl. Mater. Interfaces* **2014**, *6*, 18418–18422.
(28) Loyer, F.; Combrisson, A.; Omer, K.; Moreno-Couranjou, M.; Choquet, P.; Boscher, N. D. Thermoresponsive Water-Soluble Polymer Layers and Water-Stable Copolymer Layers Synthesized by Atmospheric Plasma Initiated Chemical Vapor Deposition. *ACS Appl. Mater. Interfaces* **2019**, *11*, 1335–1343.
(29) Bonot, S.; Mauchauffé, R.; Boscher, N. D.; Moreno-Couranjou, M.; Cauchie, H.-M.; Choquet, P. Self-Defensive Coating for Antibiotics Degradation - Atmospheric Pressure Chemical Vapor Deposition of Functional and Conformal Coatings for the Immobilization of Enzymes. *Adv. Mater. Interfaces* **2015**, *2*, 1500253.
(30) Neese, F. The ORCA Program System. *WIREs Comput. Mol. Sci.* **2012**, *2*, 73–78.
(31) Varrette, S.; Bouvry, P.; Cartiaux, H.; Georgatos, F. Management of an Academic HPC Cluster: The UL Experience. *Proceedings of the 2014 Intl. Conf. on High Performance Computing & Simulation (HPCS 2014), Bologna, Italy, July 2014*; 2014; pp 959–967.
(32) Weigend, F.; Ahlrichs, R. Balanced Basis Sets of Split Valence, Triple Zeta Valence and Quadruple Zeta Valence Quality for H to Rn: Design and Assessment of Accuracy. *Phys. Chem. Chem. Phys.* **2005**, *7*, 3297–3305.
(33) Weigend, F. Accurate Coulomb-Fitting Basis Sets for H to Rn. *Phys. Chem. Chem. Phys.* **2006**, *8*, 1057–1065.
(34) Grimme, S.; Ehrlich, S.; Goerigk, L. Effect of the Damping Function in Dispersion Corrected Density Functional Theory. *J. Comput. Chem.* **2011**, *32*, 1456–1465.
(35) Grimme, S.; Antony, J.; Ehrlich, S.; Krieg, H. A Consistent and Accurate Ab Initio Parametrization of Density Functional Dispersion Correction (DFT-D) for the 94 Elements H-Pu. *J. Chem. Phys.* **2010**, *132*, 154104.
(36) Loyer, F.; Bulou, S.; Choquet, P.; Boscher, N. D. Pulsed Plasma Initiated Chemical Vapor Deposition (PiCVD) of Polymer Layers– A Kinetic Model for the Description of Gas Phase to Surface Interactions in Pulsed Plasma Discharges. *Plasma Processes Polym.* **2018**, *15*, 1800121.
(37) Chen, N.; Reeja-Jayan, B.; Liu, A.; Lau, J.; Dunn, B.; Gleason, K. K. iCVD Cyclic Polysiloxane and Polysilazane as Nanoscale Thin-Film Electrolyte: Synthesis and Properties. *Macromol. Rapid Commun.* **2016**, *37*, 446–452.
(38) Kaltenbrunner, M.; Sekitani, T.; Reeder, J.; Yokota, T.; Kuribara, K.; Tokuhara, T.; Drack, M.; Schwödiauer, R.; Graz, I.; Bauer-Gogonea, S.; Bauer, S.; Someya, T. An Ultra-Lightweight Design for Imperceptible Plastic Electronics. *Nature* **2013**, *499*, 458–465.
(39) Atkins, P.; De Paula, J.; Keeler, J. *Atkins' Physical Chemistry*; Oxford University Press: 2018; p 908.
(40) Werner, F.; Siebentritt, S. Buffer Layers, Defects, and the Capacitance Step in the Admittance Spectrum of a Thin-Film Solar Cell. *Phys. Rev. Appl.* **2018**, *9*, 057047.
(41) Trujillo, N. J.; Wu, Q.; Gleason, K. K. Ultralow Dielectric Constant Tetravinyltetramethylcyclotetrasiloxane Films Deposited by Initiated Chemical Vapor Deposition (iCVD). *Adv. Funct. Mater.* **2010**, *20*, 607–616.
(42) Tu, H. E.; Su, C. J.; Jeng, U. S.; Leu, J. Pore Morphology of Low-k SiCxNy Films Prepared with a Cyclic Silazane Precursor Using Plasma-Enhanced Chemical Vapor Deposition. *Thin Solid Films* **2015**, *590*, 1–6.
(43) Boscher, N. D.; Choquet, P.; Duday, D.; Verdier, S. Chemical compositions of organosilicon thin films deposited on aluminium foil by atmospheric pressure dielectric barrier discharge and their electrochemical behavior. *Surf. Coat. Technol.* **2010**, *205*, 2438–2448.
(44) Tu, H.-E.; Chen, Y.-H.; Leu, J. Low-k SiCxNy Films Prepared by Plasma-Enhanced Chemical Vapor Deposition Using 1,3,5-trimethyl-1,3,5-trivinylcyclotrisilazane Precursor. *J. Electrochem. Soc.* **2012**, *159*, G56.
(45) Bulou, S.; Le Brizoual, L.; Miska, P.; de Poucques, L.; Hugon, R.; Belmahi, M.; Bougdira, J. The influence of CH4 addition on composition, structure and optical characteristics of SiCN thin films deposited in a CH_4/N_2/Ar/hexamethyldisilazane microwave plasma. *Thin Solid Films* **2011**, *520*, 245–250.

DOI: 10.1021/acsapm.9b00759
ACS Appl. Polym. Mater. 2019, 1, 3304–3312

CHAPTER V ─ Summary and Outlook

V-1 Summary

This PhD dissertation provides an in-depth understanding on the growth mechanisms driving the formation of organosilicon thin films in a nanosecond pulsed AP-PECVD process. In particular, the influence of the monomer structure and monomer saturation ratio on the growth rate, morphology, chemistry and dielectric properties of the resulting thin films is elucidated here for the first time. In addition to expand the range of application of the process, the investigation of the thin films' dielectric properties (leakage current, k value…) performed in this thesis provides a deeper understanding of the structure-property-processing relationships. As such, guidelines are drawn for the nanosecond pulsed AP-PECVD formation of functional polymer thin films.

The importance of the monomer structure is demonstrated through the nanosecond pulsed AP-PECVD reaction of different siloxane compounds. Irrespective of their cyclic or linear structure, the low-frequency nanosecond pulsed AP-PECVD reaction (combination of ultra-short plasma pulses, i.e. 100 ns, with very long OFF-time, i.e. 10 ms) of non-vinylic siloxane compounds yields poorly reticulated thin films exhibiting high leakage current densities. The same AP-PECVD conditions being applied to siloxane compounds bearing vinyl bonds, such as the 1,3,5,6-tetramethyltetravinylcyclotetrasiloxane (V4D4) or the 1,3,5-trimethyltrivinylcyclotrisiloxane (V3D3), promotes the preponderance of plasma-induced free-radical polymerisation enabling the excellent retention of the monomer structure and the formation of atomically smooth, dense and highly cross-linked thin films. The superior insulating properties of the thin films elaborated from vinylic siloxane compounds, afforded by their highly crosslinked structure, allowed to conclude that monomer with polymerisable bonds are essential to promote the growth of high quality insulating thin films.

Unsurprisingly, two growth mechanisms were readily identified from the variation of the plasma pulse frequency (variation of t_{OFF} duration) and the variation of the monomer saturation ratio (P_M/P_{sat}) from the nanosecond pulsed AP-PECVD reaction of the vinylic cyclic siloxane compounds, i.e. V3D3 and V4D4. Gas phase reactions are preponderant in the monomer deficient regime (low P_M/P_{sat} or high plasma pulse frequencies). The combination of ultra-short plasma pulses with very long OFF-time (low plasma pulse frequency) is essential to ensure the prevalence of surface reactions (adsorption and subsequent free-radical polymerisation) falling in the competition regime (or energy-deficient regime for high P_M/P_{sat}) and resulting in the formation of smooth and conformal insulating thin films. For excessively high P_M/P_{sat}, the energy-deficient regime is reached, and the thin films become leaky. The strong influence of the monomer structure on the growth mechanisms is well observed in the energy-deficient regime where non-vinylic siloxane compounds yield the formation of viscous thin films composed of short oligomers.

Therefore, using low plasma pulse frequencies, the insulating properties of the thin films elaborated from vinylic compounds displayed a strong dependence on the monomer saturation ratio (P_M/P_{sat}). Optimisation of the monomer saturation ratio is required for each vinylic compound to yields the formation of thin films with excellent insulating properties and low-k values owing to the better retention of the monomer structure.

To summarize, monomers with polymerisable bonds, high monomer saturation ratio and low plasma pulse frequency are essential to promote the plasma-induced free-radical polymerisation of atomically smooth and highly crosslinked insulating low-k thin films. Taking into account the understanding gained, the versatility of the approach was exploited to grow low dielectric constant insulating layers from four organosilicon compounds, i.e. two silazane (V3N3 and V4N4) and two siloxane (V3D3 and V4D4). The ability to tune the k value ($2.8 \leq k \leq 4.2$) from the careful selection of the monomer structure highlighted the importance of the starting monomer chemistry. The lowest dielectric constant value was obtained from the monomer with lower polarizability (organosiloxane) and larger ring size, i.e. the V4D4, which showed a k-value as low as 2.8. Low leakage current densities, in the range of 10^{-9} A/cm^2 at 20 V for thicknesses as low as 12 nm, are measured, confirming the excellent down scalability of the insulating properties of the thin films elaborated using this nanosecond pulsed AP-PECVD process.

V-2 Outlook

This PhD dissertation provides a deep understanding of the growth mechanisms of low dielectric constant insulating thin films elaborated by nanosecond pulsed PECVD operated at atmospheric pressure. In particular, the straightforward synthesis of tuneable insulating organosilicon thin films by the atmospheric pressure plasma-initiated chemical vapor deposition (AP-PiCVD) could simplify the integration of low-k dielectric polymer thin films for flexible organic electronic application. The chemical stability of the low dielectric constant insulating thin films obtained in the framework of this thesis offers the possibility to combine the nanosecond pulsed AP-PECVD process to wet chemistry methods for the fabrication of an organic field effect transistor device.

The knowledge generated in this work, highly complementary to a previous PhD work undertaken at LIST, provides solid guidelines for simultaneous synthesis and deposition of new functional thin films from a dry and atmospheric-pressure process. Further works could notably investigate the influence of the P_M/P_{sat} on the length of the polymer chains grown from the AP-PiCVD reaction of alkyl methacrylate monomer. The determination of optimal process window, optimisation of the monomer saturation ratio (P_M/P_{sat}), is particularly important when investigating new monomers in the perspective to extend the field of applications of thin films synthesised by the AP-PiCVD. When targeting applications where the length of the polymer chain is crucial to grant functional properties to a thin film, such as thermoresponsive polymer layers, or prevent leaching of low molecular species, the understanding and determination of monomer saturation ratio (P_M/P_{sat}) influence on the growth mechanism of the thin films is essential.

Appendix

Appendix 1: definitions

This appendix provides the definitions of some keywords used in thesis. For more physical relationships of all these terms, I refer the reader to literature.[1,2]

1) Structure and working principle of organic field-effect transistors

Organic field-effect transistors (OFET), also referred as organic thin film transistors (OTFT) since assembled from a thin-film stack (Figure 1), are composed of three fundamental components: the contacts (source, drain and gate), the organic semiconductor (active layer) and the dielectric layer. The drain and the source electrodes which are in direct contact with the active layer, are used to inject and collect charge carriers, while the gate is isolated from the active layer by a dielectric layer.[3-5]

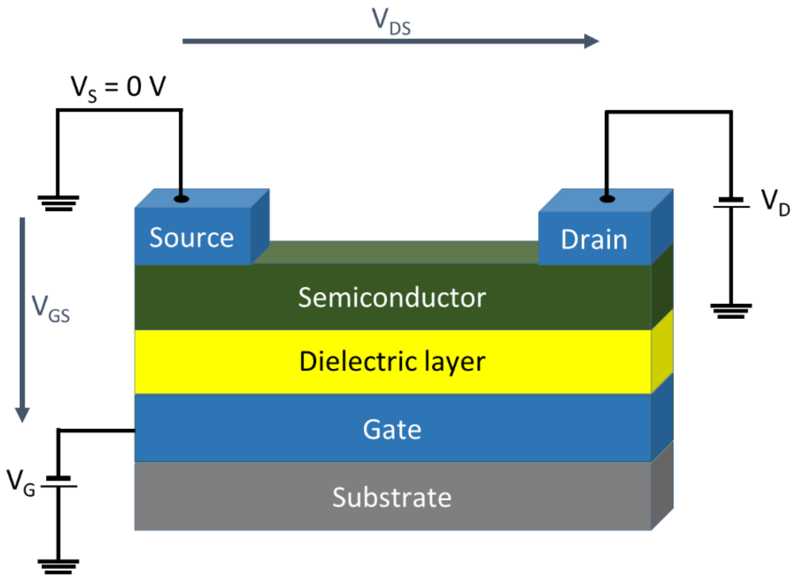

Figure 1: Structure of an organic thin film transistor (OFET) in bottom gate/top contact (BGTC) configuration.

OFET operates under the application of two voltages: one between the source and the gate (V_{GS}) and the second one between the source and the drain (V_{DS}). Without the application of a gate voltage (V_{GS}), the current (I_D) between the drain and the source is very low (no charge accumulation) and the transistor is off. The application of a gate voltage polarises the dielectric resulting in the accumulation of charge carriers at the semiconductor-dielectric interface. The electric field applied at the gate electrode determines the density of the charge carriers accumulated at this interface. Hence, the current flow between the drain and source electrodes is modulated by the applied gate voltage. The transistor turns on when the voltage V_{DS} is applied, inducing the transport of the accumulated charge carriers from the source to the drain electrode, through the semiconductor, where a source-drain current (I_{DS}) is generated.[3,6-8] As such, the transport of the charge carriers occurs in the first few monolayers of the organic semiconductor, near the surface of the gate dielectric. Thus, the interface between the dielectric and the active layer plays a major role in the device performances.

2) Dielectric properties

Dielectric materials are electrical insulators that can be polarized by the application of an electric field. The crucial parameters of a dielectric material are the maximum possible electric displacement (D_{max}) the dielectric can sustain:

$$D_{max} = \varepsilon_0 \varepsilon_r E_B \quad (1)$$

where ε_0 is the vacuum permittivity ($\varepsilon_0 = 8.854 \times 10^{-12}$ F.m^{-1}), ε_r (ε_r = k) is the dielectric constant (also called relative permittivity) and E_B is the dielectric breakdown field.

- **Capacitance & relation between C and k**

The capacitance per unit of area, C_i, which in the two-parallel-plate model can be represented using the following equation:

$$C_i = \varepsilon_0 \frac{\varepsilon_r}{d} \quad (2)$$

where d is the thickness of the dielectric. The magnitude of the capacitance C_i is monitored by the k value and the thickness (d) of the dielectric. The capacitance density, which is the ability of a material to store electrical charges at a given voltage, must be high to lower the operation voltage in OFET.

- **Dielectric constant**

The capacitance is directly proportional to the dielectric constant (2 & *3*) which represents the potential amount of electric energy, in the form of induced polarisation, that can be stored in a material under the application of an electric field. Indeed, placed in an electrical field, the dielectric's electrical charges shift from their average equilibrium positions toward the electric field direction causing dielectric polarisation (*Figure 1*).

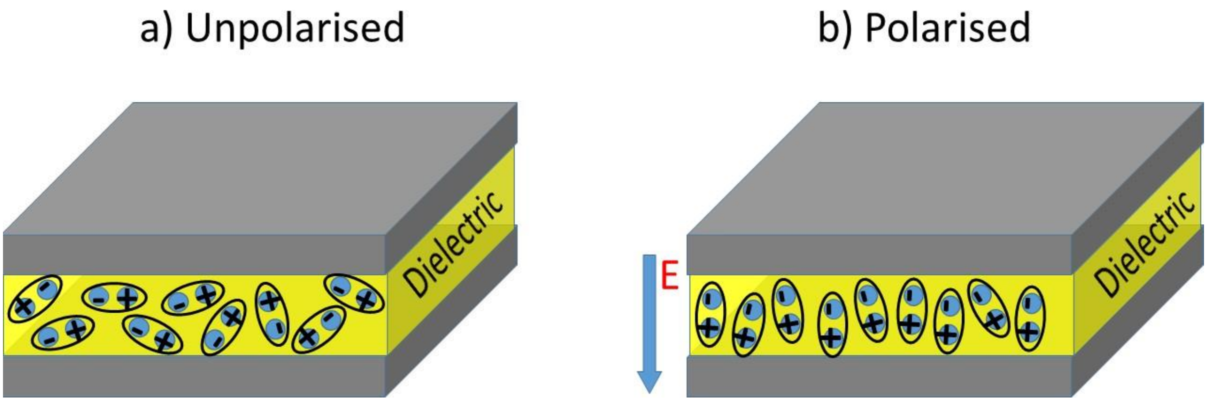

Figure 1: Schematic of a parallel-plate metal−insulator−metal (MIM) capacitor where a) in the absence of an applied electric field, the charge distribution is at equilibrium in the dielectric. b) Applying an electric field leads to the shift of the charge from their average equilibrium positions toward the electric field direction.

- **Dielectric polarisation**

This effect is related to the polarizability which is the ability of the molecule's electron cloud to be distorted under the application of an electric field, hence resulting in the acquiring of an electric dipole moment. This induced electric dipole moment, which is not permanent, can be induced by two polarisation phenomena, i.e., distortion polarisation and electronic polarisation.

The electronic polarisation, α_e, describes the modification of the cloud of bound electrons around the positive atomic nuclei under the application of an electric field. The electronic polarisation operates at frequencies up to ~10^{15} Hz. The distortion polarisation, α_d, also referred as ionic polarisation, relates the distortion of cations and anions in opposite direction under the application of an electric field. It responds to field frequencies up to $\sim 10^{12}$ Hz. In the case of polar molecules, their existing permanent dipole moment is rearranged under the application of the electric field giving rise to the orientation polarisation.

The physical relation between the dielectric constant and the properties of the molecule is given by the Debye equation:

$$\frac{\varepsilon_r - 1}{\varepsilon_r + 2} = \frac{N}{3\varepsilon_0}\left(\alpha_e + \alpha_d + \frac{\mu^2}{3kbT}\right) \quad (3)$$

where N is the number of molecules per m^3, μ is the orientation polarizability, k the Boltzmann constant, and T the temperature in K. The term $\mu^2/3kT$ stems from the thermal averaging of the permanent electric dipole moments of the molecule in the presence of an applied field. Hence, the dielectric constant of a material depends on the polarity of the molecule. Indeed, the dielectric constant of a material is high if the molecule is polar, thus highly polarisable. To obtain a low dielectric constant material, one can reduce the density N of the material by introducing pores or reduce the polarizabilities α_e and α_d.

The same expression without the permanent dipole moment contribution, is called the Clausius–Mossotti equation:

$$\frac{\varepsilon_r - 1}{\varepsilon_r + 2} = \frac{N}{3\varepsilon_0}(\alpha_e + \alpha_d) \quad (4)$$

Due to all these microscopic mechanisms, the polarisation of the dielectric does not occur instantaneously in response to the electric field (E). The delay of polarisation observed when changing the electric field in the dielectric medium is called dielectric relaxation and gives rise to a dielectric loss (tan δ).[1,2,8]This dielectric loss can be viewed as the energy dissipation coming from the dipole relaxation or the leakage current.[2]

- **Leakage current density**

Ideally, dielectric materials should totally prevent the flow of the electrical current. Yet, a certain amount of current defined as leakage current (or leakage current per unit area, Ji), flows through the dielectric in practice when submitted to an electric field. The amount of the leakage depends on the electric field. The electrical breakdown corresponds to the process in which the dielectric start to conduct electricity resulting in the exponential increase of the leakage current density (Ji). The key parameters associated with it are the breakdown voltage (V_B) and breakdown electric field (E_B, Figure 2).

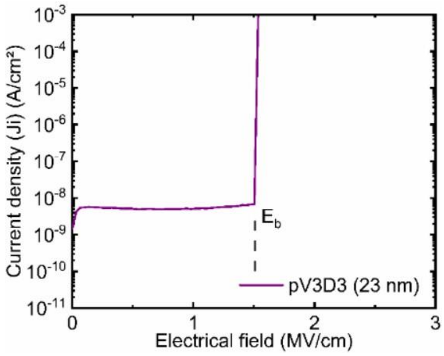

Figure 2: Representative curve of current density (Ji) vs. electric field of pV3D3 layer. The breakdown field (Eb) is observed when the current density (Ji) increases abruptly.

References

(1) Maex, K.; Baklanov, M. R.; Shamiryan, D.; Iacopi, F.; Brongersma, S. H.; Yanovitskaya, Z. S. Low Dielectric Constant Materials for Microelectronics. *J. Appl. Phys.* **2003**, *93* (11), 8793–8841.

(2) Wang, B.; Huang, W.; Chi, L.; Al-Hashimi, M.; Marks, T. J.; Facchetti, A. High- k Gate Dielectrics for Emerging Flexible and Stretchable Electronics. *Chem. Rev.* **2018**, *118* (11), 5690–5754.

(3) Houin, G. Développement d'amplificateurs Sur Substrats Flexibles à Partir de Transistors Organiques à Effet de Champ, Université de Bordeaux, **2017**.

(4) Facchetti, A.; Yoon, M. H.; Marks, T. J. Gate Dielectrics for Organic Field-Effect Transistors: New Opportunities for Organic Electronics. *Adv. Mater.* **2005**, *17* (14), 1705–1725.

(5) Torsi, L.; Magliulo, M.; Manoli, K.; Palazzo, G. Organic Field-Effect Transistor Sensors: A Tutorial Review. *Chem. Soc. Rev.* **2013**, *42* (22), 8612.

(6) Lamport, Z. A.; Haneef, H. F.; Anand, S.; Waldrip, M.; Jurchescu, O. D. Tutorial: Organic Field-Effect Transistors: Materials, Structure and Operation. *J. Appl. Phys.* **2018**, *124* (7), 071101.

(7) Malo, R. Développement de Transistors à Effet de Champ Organiques et de Matériaux Luminescents à Base de Nanoclusters Par Impression à Jet d'Encre, Université de Rennes 1, **2018**.

(8) Wang, Y.; Huang, X.; Li, T.; Li, L.; Guo, X.; Jiang, P. Polymer-Based Gate Dielectrics for Organic Field-Effect Transistors. *Chem. Mater.* **2019**, *31* (7), 2212–2240.

Supporting Information

Significance of Double Bonds and Cyclic Structure on the AP-PECVD of Low-k Organosilicon Insulating Layers

Dominique Abessolo Ondo, François Loyer, Nicolas D. Boscher

D. Abessolo Ondo, Dr. N. D. Boscher
Luxembourg Institute of Science and Technology, Materials Research and Technology Department, 41 Rue du Brill, L-4422 Belvaux, Luxembourg
E-mail: nicolas.boscher@list.lu
D. Abessolo Ondo
University of Luxembourg, 2 Avenue de l'Université, L-4365 Esch-sur-Alzette, Luxembourg
Dr. F. Loyer
IMEC, Kapeldreef 75, 3001 Leuven, Belgium; performed outside of IMEC programs

---

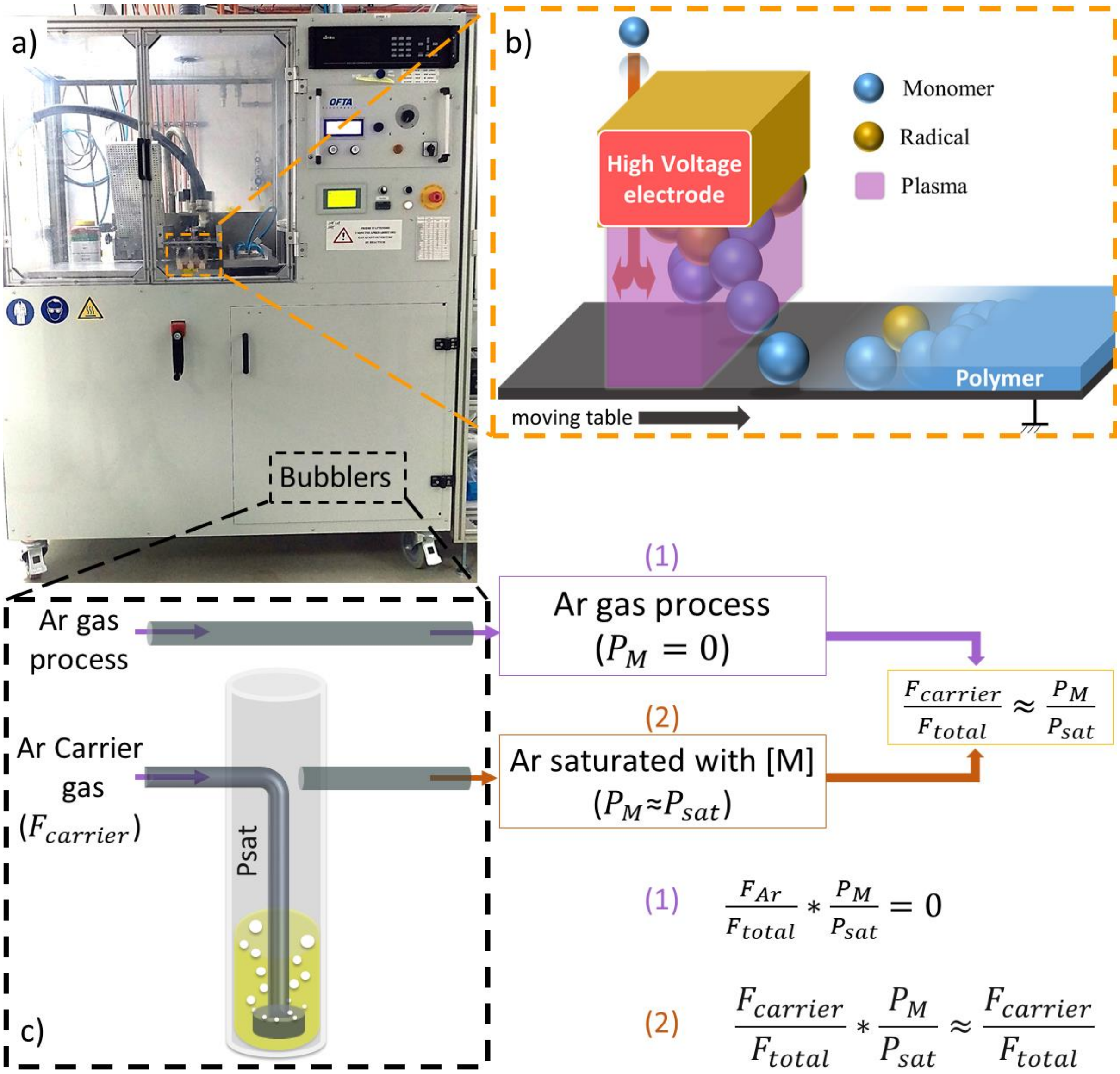

Figure S1: a) Photograph of the AP-PDBD reactor setup that affords the dry, single-step, and up-scalable solution for the deposition of functional thin films. b) Schematic of the dielectric barrier discharge displaying one upper electrode and a moving grounded electrode (represented as a table) on which the substrate is stuck. The radicals are created during the plasma ON time (purple area) in the gap between the upper and the grounded electrode. c) The monomer to deposit is held in a bubbler and the vapours of the studied monomers are directed toward the reactor chamber using argon (Ar), which was playing the role of carrier and the plasma gas.

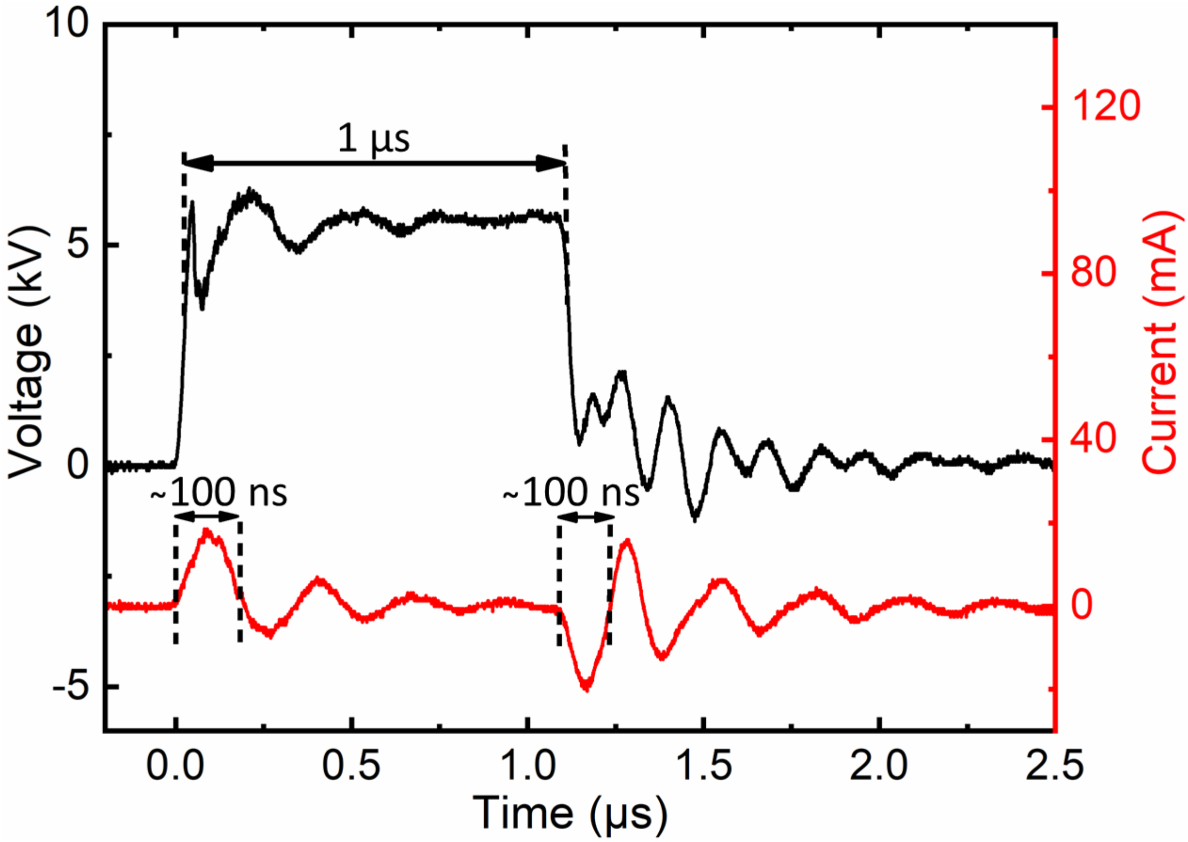

Figure S2: Traces of the I-V curves used for the atmospheric-pressure plasma enhanced chemical vapour deposition (AP-PECVD) of polymer and plasma thin films. The plasma was ignited with a 1µs ultrashort high-voltage square pulse (black curve) resulting in the creation of two current discharges lasting ca 100 ns (red curve). These current discharges represents the time when the plasma is actually ON.

Table S1: Experimental condition for the deposition performed to determine the impact of plasma pulse frequencies on the initiation and lifetime of the free-radical polymerisation of V4D4, D4 and DMTSO. The deposition rate (DR) and the thickness increment per cycle (thick. incr.) are provided.

Monomer	Frequency (Hz)	$F_{Ar,\ carrier}$ (SLM)	$F_{Ar,\ total}$ (SLM)	Pressure (bar)	t_{ON} (µs)	t_{OFF} (µs))	DR (nm/s)	Thick. incr. (pm)
V4D4	16.7	15	5	1	1	59879	0.126	7.57
	31.6	15	5	1	1	31645	0.254	8.03
	56.2	15	5	1	1	17793	0.484	8.61
	100	15	5	1	1	9999	0.981	9.95
	178	15	5	1	1	5617	1.25	7.02
	362	15	5	1	1	2761	2.08	5.76
	562	15	5	1	1	1778	2.56	4.56
	1000	15	5	1	1	999	4.82	4.82
	3160	15	5	1	1	315	4.11	1.30
D4	16.7	15	5	1	1	59879	0.0427	2.56
	31.6	15	5	1	1	31645	0.0967	3.06
	56.2	15	5	1	1	17793	0.154	2.75
	100	15	5	1	1	9999	0.239	2.39
	178	15	5	1	1	5617	0.600	3.37
	362	15	5	1	1	2761	0.906	2.50
	562	15	5	1	1	1778	1.38	2.46
	1000	15	5	1	1	999	1.41	1.41
	3160	15	5	1	1	315	6.02	1.90
DMTSO	31.6	15	5	1	1	31645	0.113	3.58
	56.2	15	5	1	1	17793	0.125	2.22
	100	15	5	1	1	9999	0.274	2.74
	178	15	5	1	1	5617	0.327	1.84
	362	15	5	1	1	2761	1.03	2.86
	562	15	5	1	1	1778	1.71	3.05
	1000	15	5	1	1	999	3.33	3.33
	3160	15	5	1	1	315	7.99	2.53

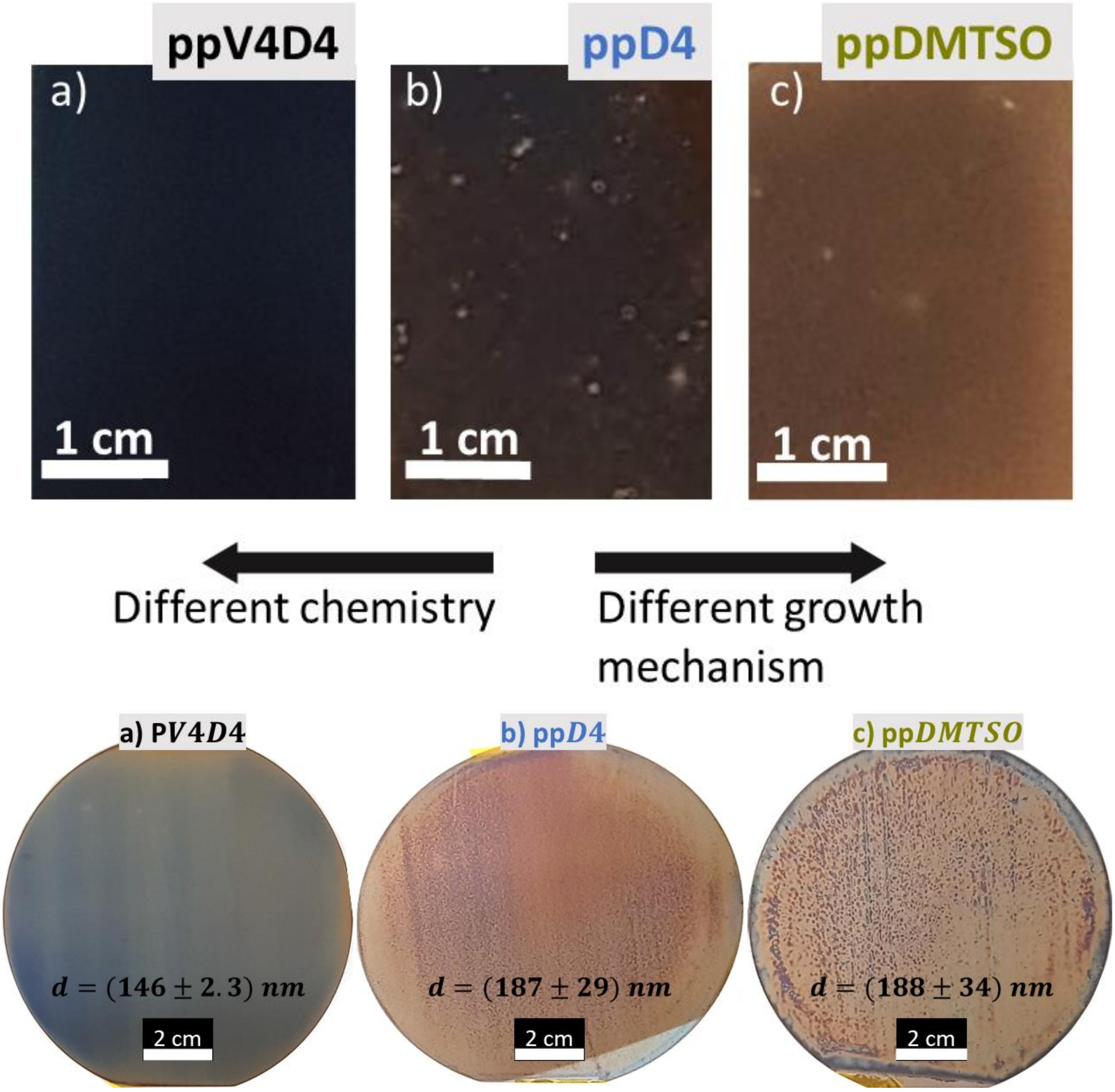

Figure S3: Optical images of the thin films grown on silicon wafer from (a) V4D4, (b) D4 and (c) DMTSO at identical deposition condition (*f* = 100 Hz; P_M/P_{sat} = 75%).

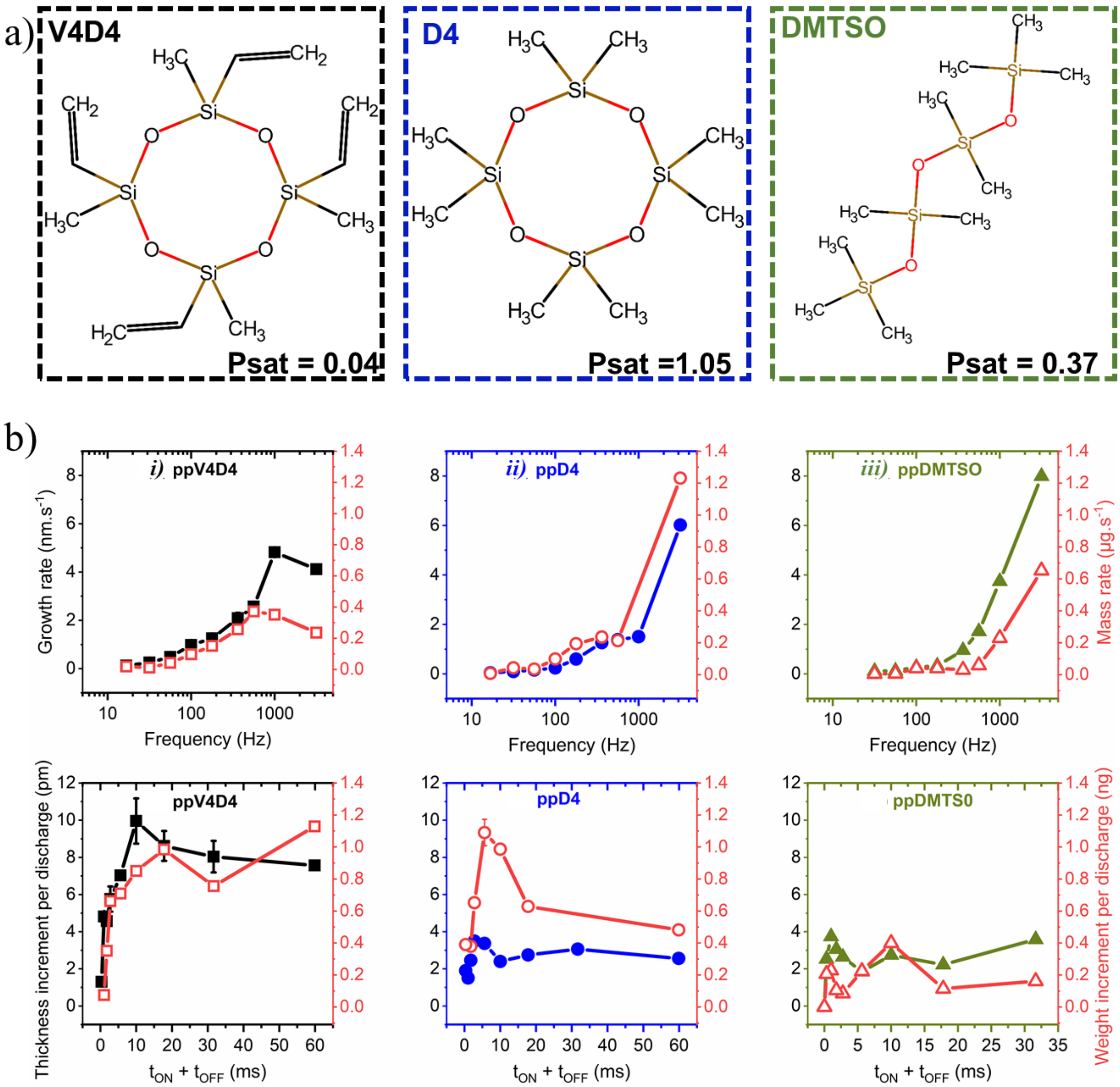

Figure S4: a) Vapour pressure (P_{sat}) in mmHg and chemical structure of all the studied organosiloxane compounds. b) Growth and mass rates per second plotted according to the plasma pulse frequency as well as the thickness and weight increment per cycle duration (t_{ON} + t_{OFF}) of the thin films grown from *i)* V4D4; *ii)* D4 and *iii)* DMTSO.

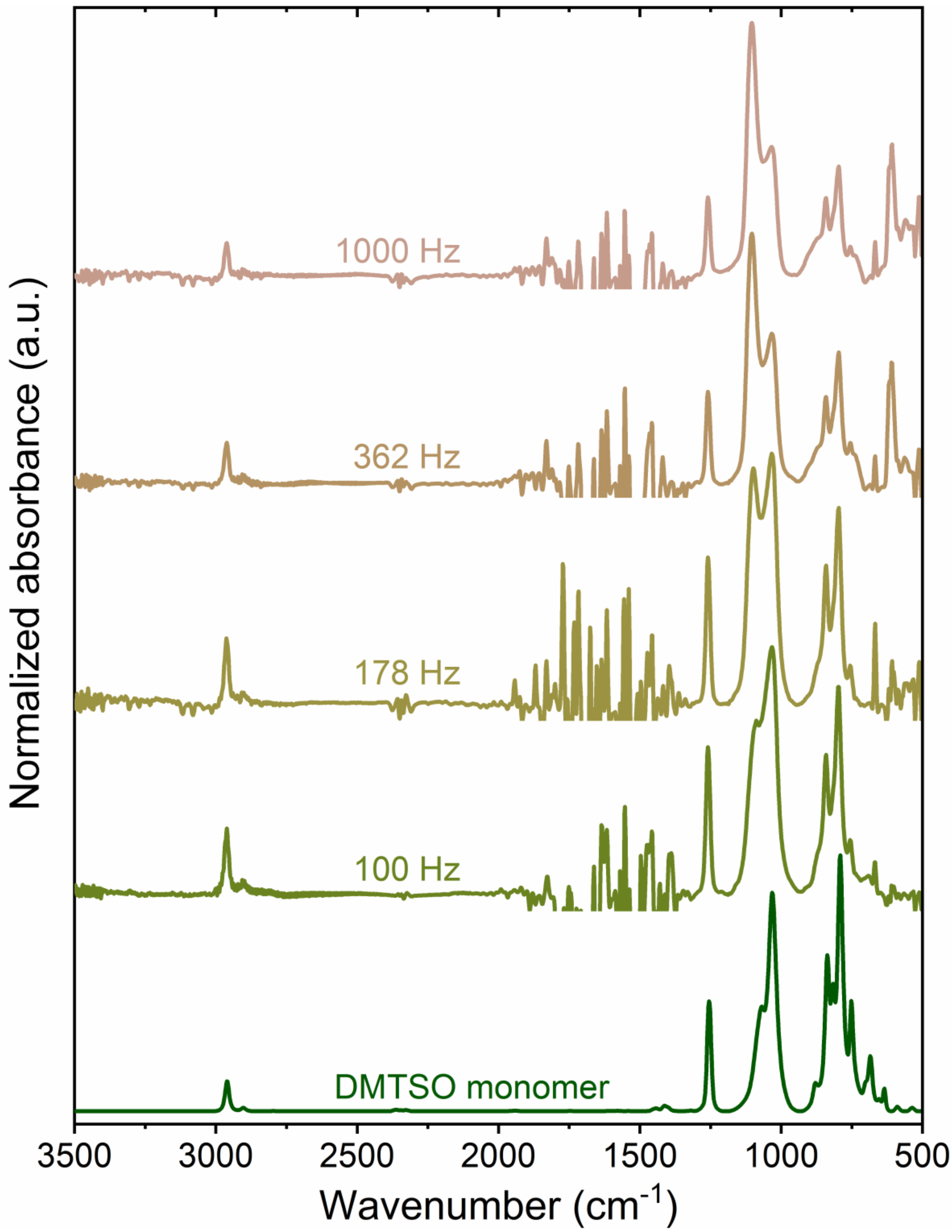

Figure S5: FTIR spectrum of the ppDMTSO thin films elaborated using a 75% saturation ratio at different plasma pulse frequencies.

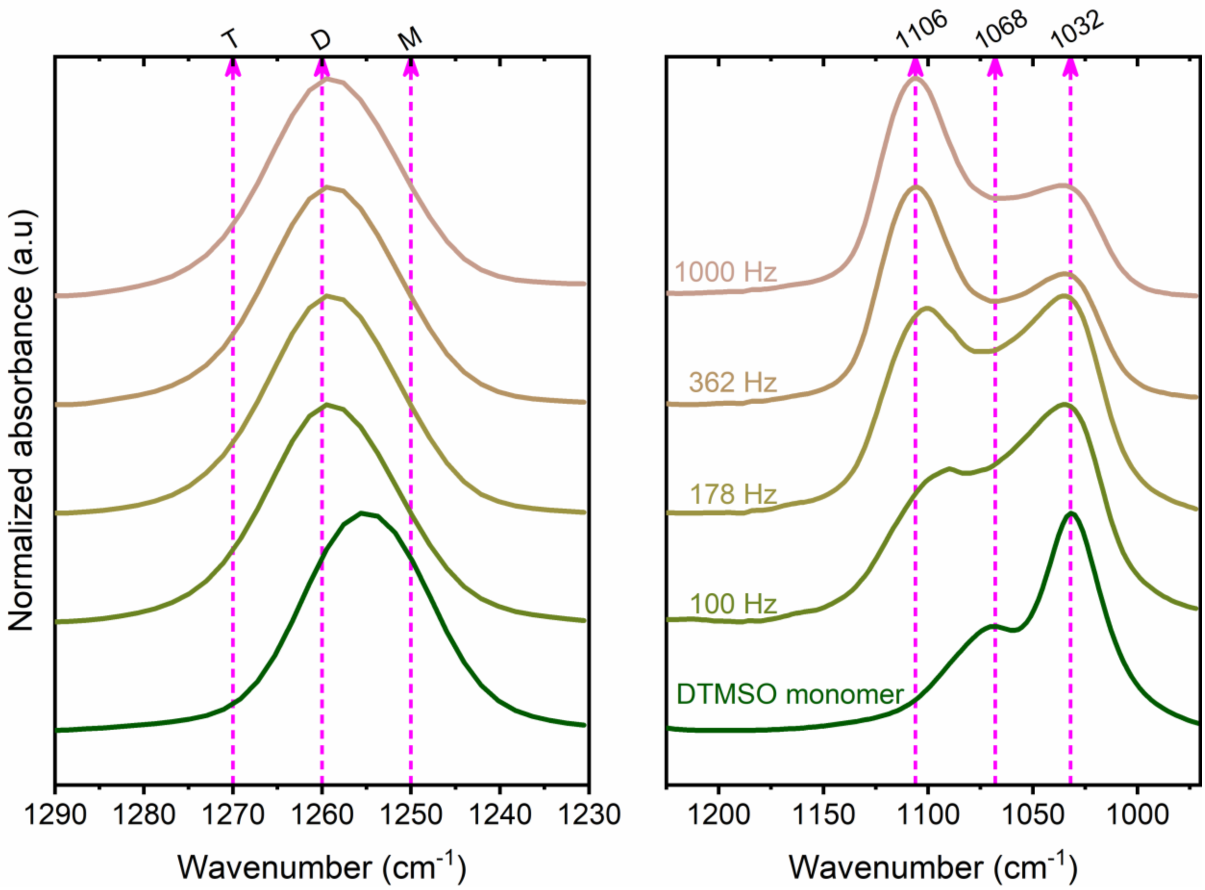

Figure S6: FTIR spectra of the 1290-1230 cm^{-1} and the 1225-970 cm^{-1} regions corresponding respectively to the Si─CH$_3$ and the Si─O─Si stretching absorption region of the DMTSO monomer and the thin films elaborated at different plasma pulse frequencies. The M, D and T group represent the mono-, di-, and tri-substitution of the silicon atom by oxygen, respectively.

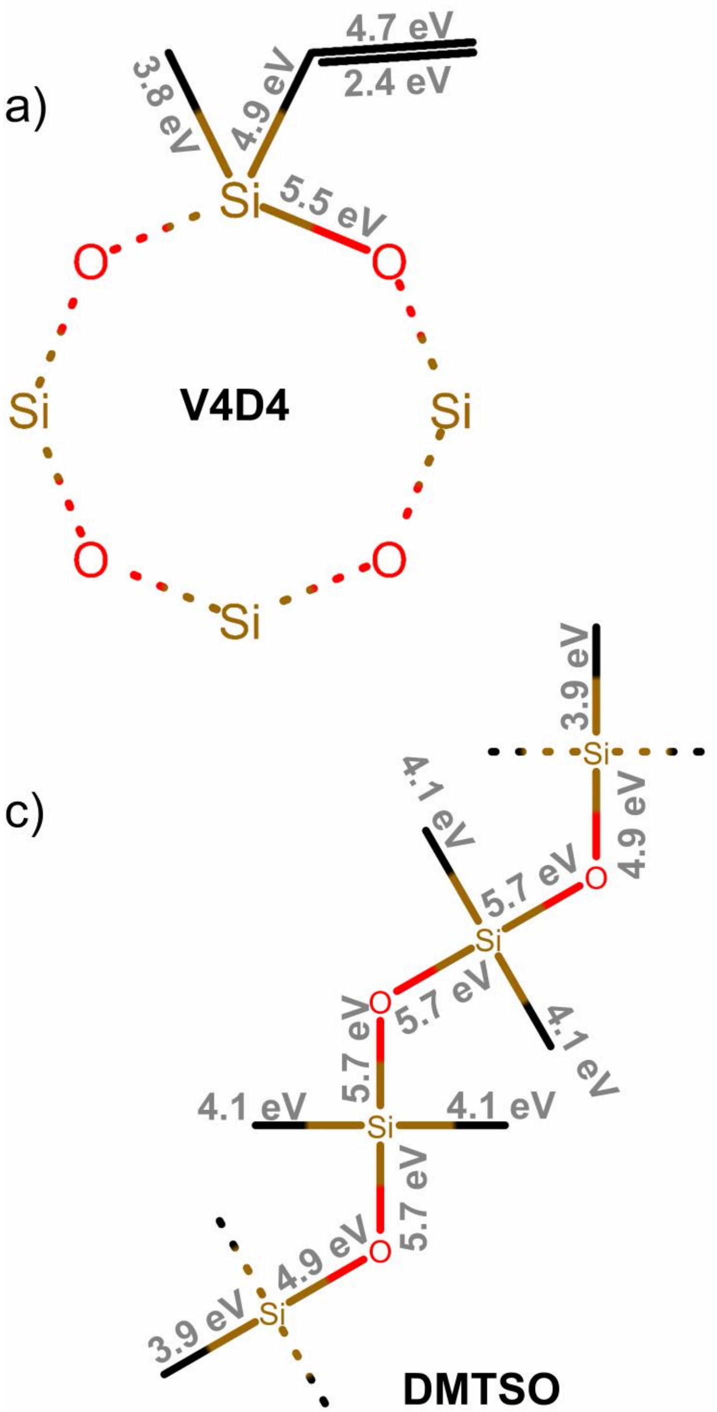

Figure S7: Bond dissociation energies (BDE) of (a) V4D4, (b) D4 and (c) DMTSO.

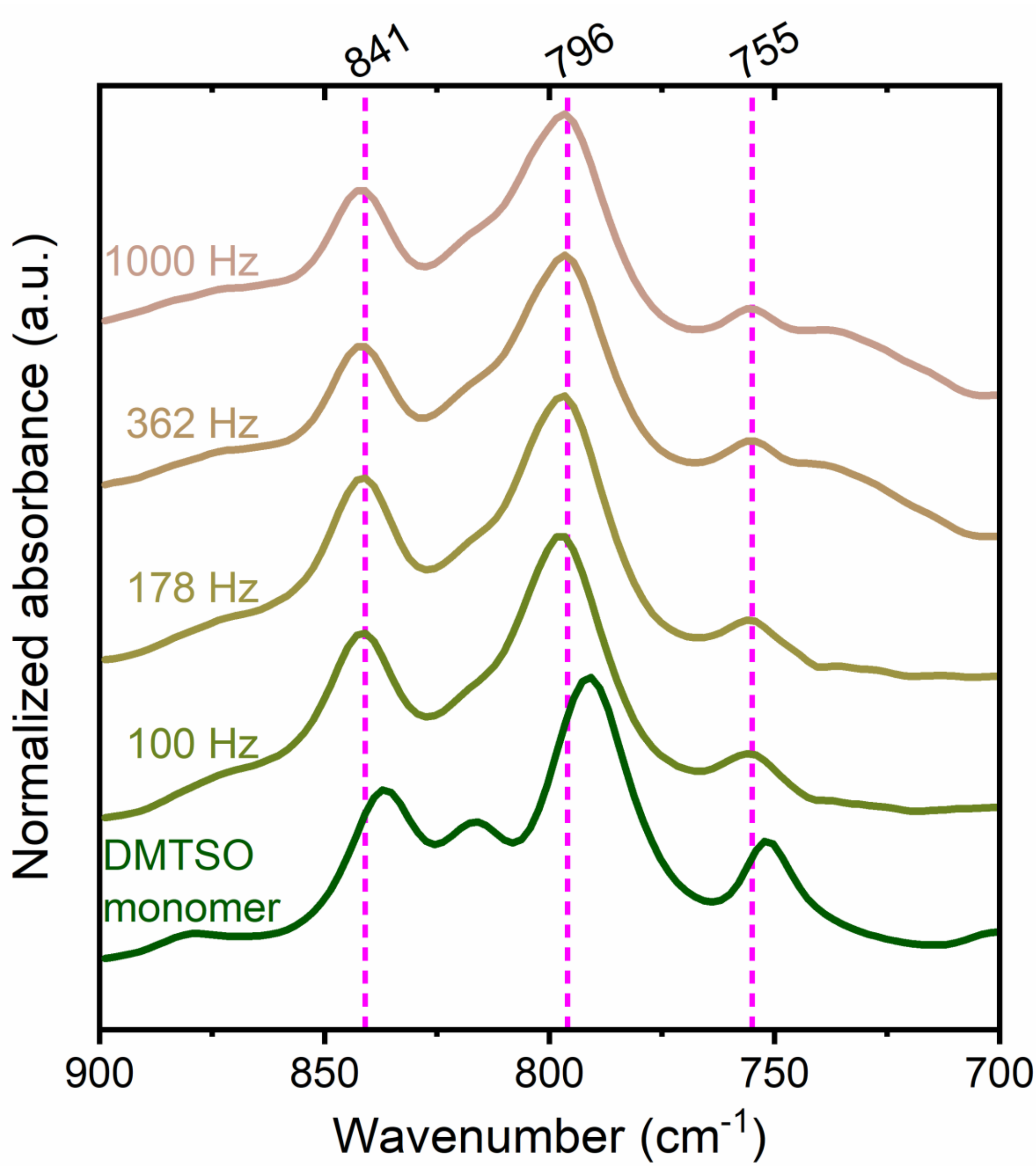

Figure S8: FTIR spectra of the 900-700 cm^{-1} region corresponding to the Si─C stretching absorption region of the DMTSO monomer and the thin films elaborated at different plasma pulse frequencies.

Table S2: FTIR absorption assignments of DMTSO monomer and the resulting thin films elaborated at different plasma pulse frequencies, i.e. 100 Hz, 362 Hz and 1,000 Hz.

Chemical bond	DMTSO (nm^{-1})	ppDMTSO (cm^{-1})		
		100 Hz	362 Hz	1,000 Hz
CH_3 antisymmetric stretching	2960	2960	2961	2961
CH_3 symmetric stretching	2902	2901	-	-
CH_3 sym. deformation from Si-CH_3	1256	1259	1259	1259
Si-O asymmetric stretching in ladder	-	-	1103	1106
Si-O asymmetric stretching	-	1087	-	-
Si-O-Si asymmetric stretching in linear network	1068	-	-	-
Si-O-Si asymmetric stretching in suboxide	1032	1032	1034	1034
$Si(CH_3)_3$ rocking	837	840	841	841
$Si(CH_3)_2$ rocking	791	796	796	796
Si-C stretch	752	755	755	-

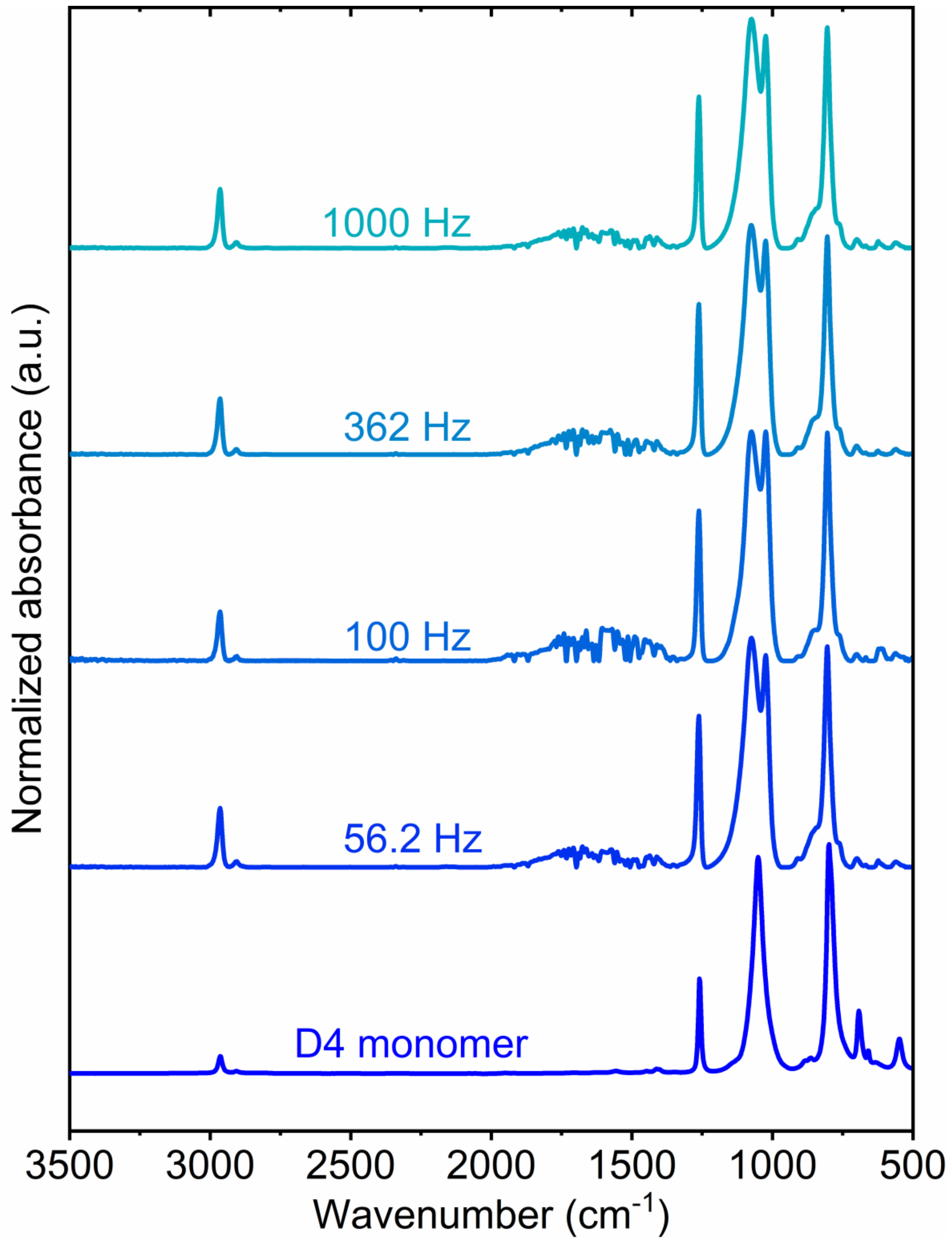

Figure S9: FTIR spectra of the ppD4 thin films elaborated using a 75% saturation ratio at different plasma pulse frequencies.

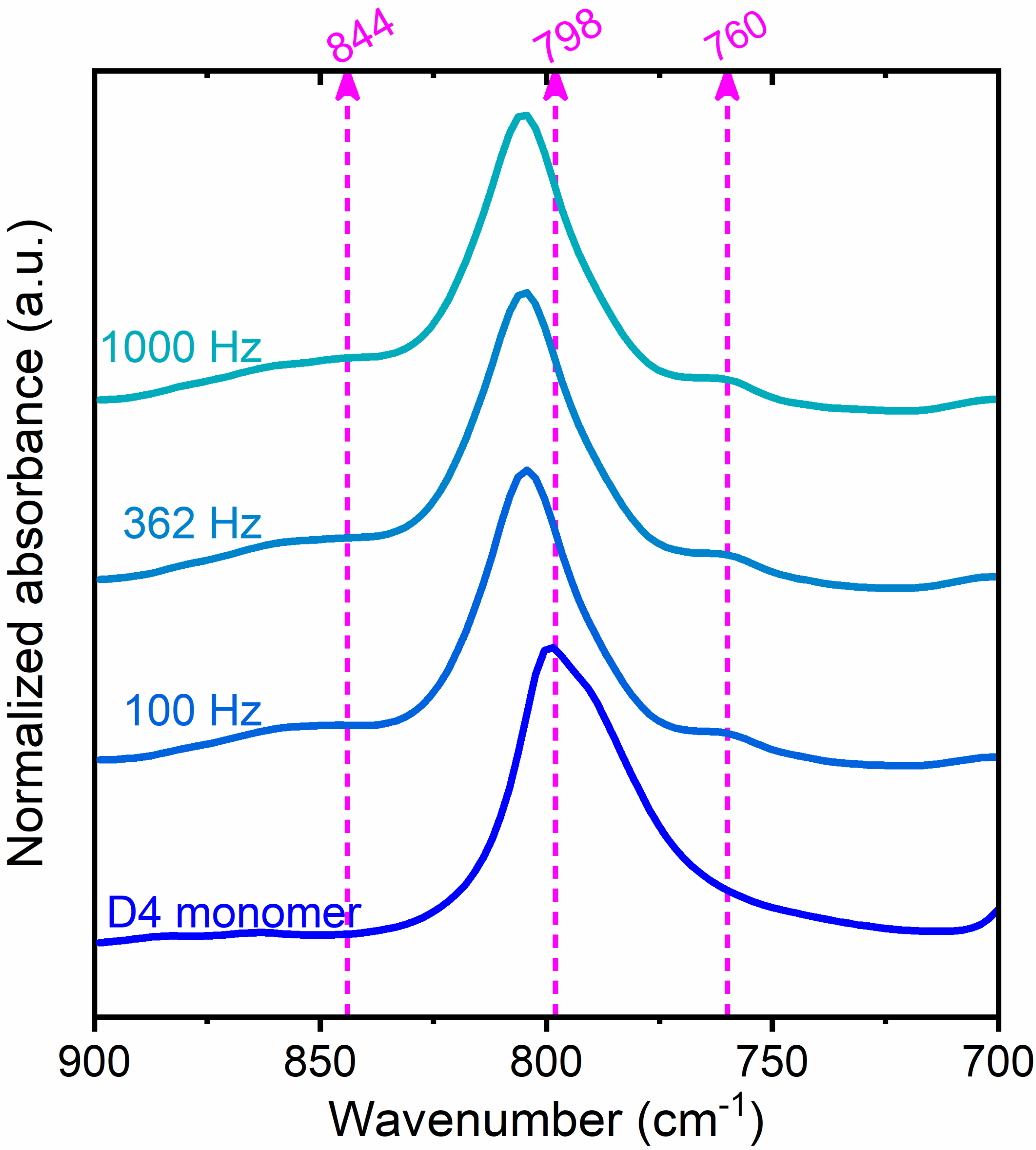

Figure S10 FTIR spectra of the 900-700 cm^{-1} region corresponding to the Si─C stretching absorption region of the D4 monomer and the thin films elaborated at different plasma pulse frequencies.

Table S3: FTIR absorption assignments of D4 monomer and the resulting thin films elaborated at different plasma pulse frequencies, i.e. 100 Hz, 362 Hz, and 1,000 Hz.

Chemical bond	**D4 (nm^{-1})**	**ppD4 (cm^{-1})**		
		100 Hz	**362 Hz**	**1,000 Hz**
CH_3 antisymmetric stretching	2964	2961	2961	2961
CH_3 symmetric stretching	2906	2913	2913	2913
CH_3 sym. deformation from Si-CH_3	1259	1257	1259	1259
Si—O asymmetric stretching from linear network	-	1074	1074	1074
(Si—O)$_3$ asymmetric stretching from the ring	1051	-	-	-
Si—O asymmetric stretching in suboxide	-	1024	1024	1024
Si(CH_3)$_2$ rocking	798	804	804	804

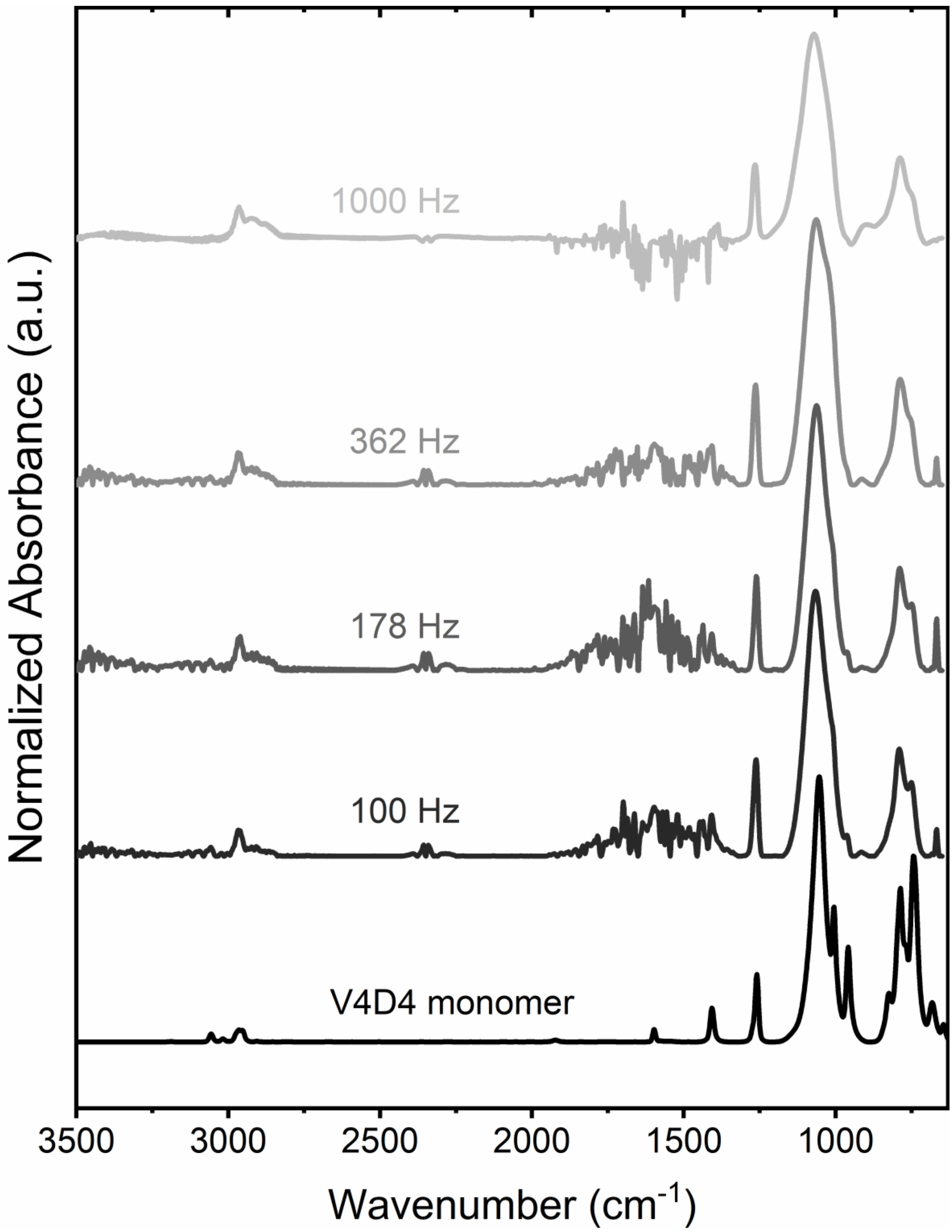

Figure S11: FTIR spectra of the pV4D4 thin films obtained from V4D4 elaborated using a 75% saturation ratio and deposited at different plasma pulse frequencies.

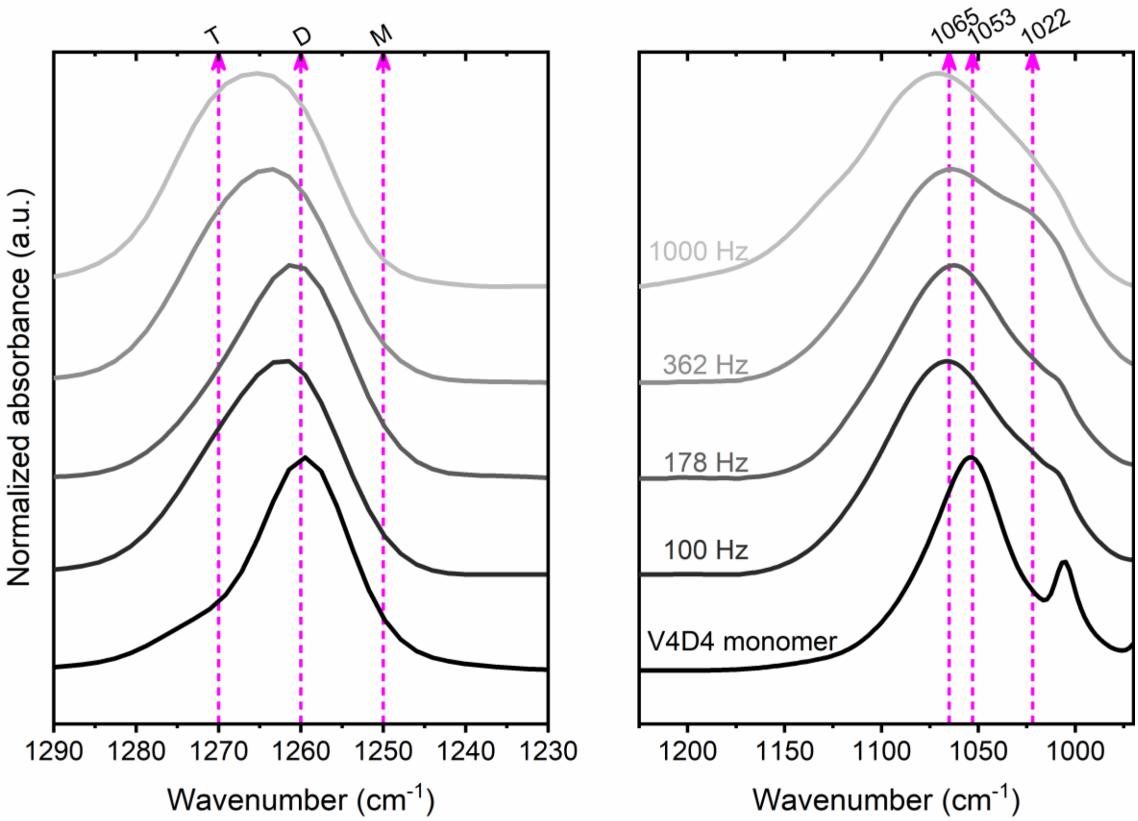

Figure S12: FTIR spectra of the 1,290-1,230 cm^{-1} and the 1,225-970 cm^{-1} regions corresponding respectively to the Si─CH_3 and the Si─O─Si stretching absorption region of the V4D4 monomer and the thin films elaborated at different plasma pulse frequencies. The M, D and T group represent the mono-, di-, and tri-substitution of the silicon atom by oxygen, respectively.

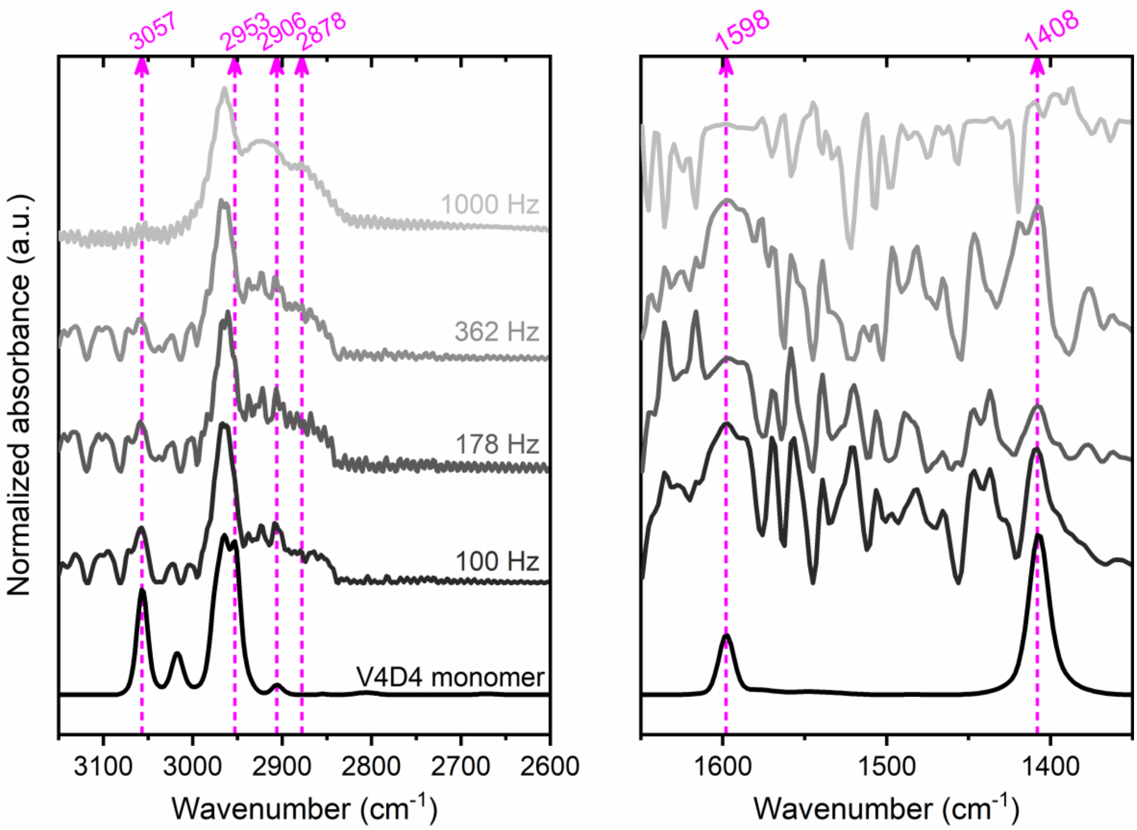

Figure S13: FTIR spectra of the 3,150-2,600 cm^{-1} and the 1,650-1,350 cm^{-1} regions corresponding respectively to the C─H absorption region of the V4D4 monomer and the thin films elaborated at different plasma pulse frequencies.

Table S4: FTIR absorption assignments of V4D4 monomer and the resulting thin films elaborated at different plasma pulse frequencies, i.e. 100 Hz, 362 Hz, 1000 Hz.

Chemical bond	V4D4 (nm^{-1})	ppV4D4 (cm^{-1})			
		100 Hz	178 Hz	362 Hz	1000 Hz
$=CH_2$ antisymmetric stretching	3057	3057	3057	3057	-
C–H stretching of vinyl bond	3017	3017	3017	3017	-
CH_3 antisymmetric stretching	2964	2964	2965	2965	2964
CH_3 symmetric stretching	2905	2906	2906	2906	2924
CH3 symmetric stretching	-	2978	2978	2978	2978
C=C stretching from $Si–CH=CH_2$	1598	-	-	-	-
$=CH_2$ deformation from $Si–CH=CH_2$	1406	-	-	-	-
CH_3 sym. deformation from $Si-CH_3$	1259	1261	1261	1263	1265
$(Si—O)_3$ asymmetric stretching from the ring	1053	1064	1062	1065	1070
Si—O asymmetric stretching in suboxide	-	-	-	1022	-
$=CH_2$ waging from $Si–CH=CH_2$	958	963	963	-	-
$Si(CH_3)_2$ rocking	787	791	788	788	788

Table S5: Theoretical and experimental atomic composition of the thin films obtained from the AP-PECVD reaction of V4D4, D4 and DMTSO (P_M/P_{sat} = 75 %).

		Atomic %			
		Si	N	O	C
V4D4	1000 Hz	23	0	30	48
	100 Hz	22	0	25	54
	Theory	20	0	20	60
D4	1000 Hz	27	0	27	46
	100 Hz	27	0	29	44
	Theory	25	0	25	50
DTMSO	1000 Hz	28	0	43	29
	100 Hz	17	0	22	60
	Theory	23.5	0	17.6	59

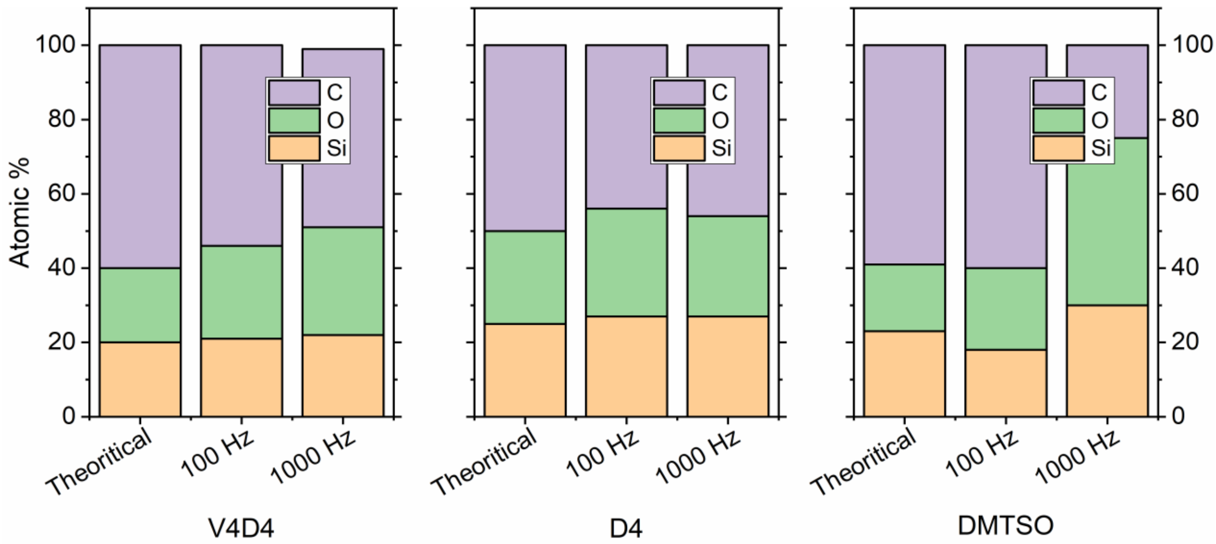

Figure S14: Distribution of the atomic compositions of the thin films obtained from the AP-PECVD reaction of V4D4, D4 and DMTSO calculated from the XPS survey scans.

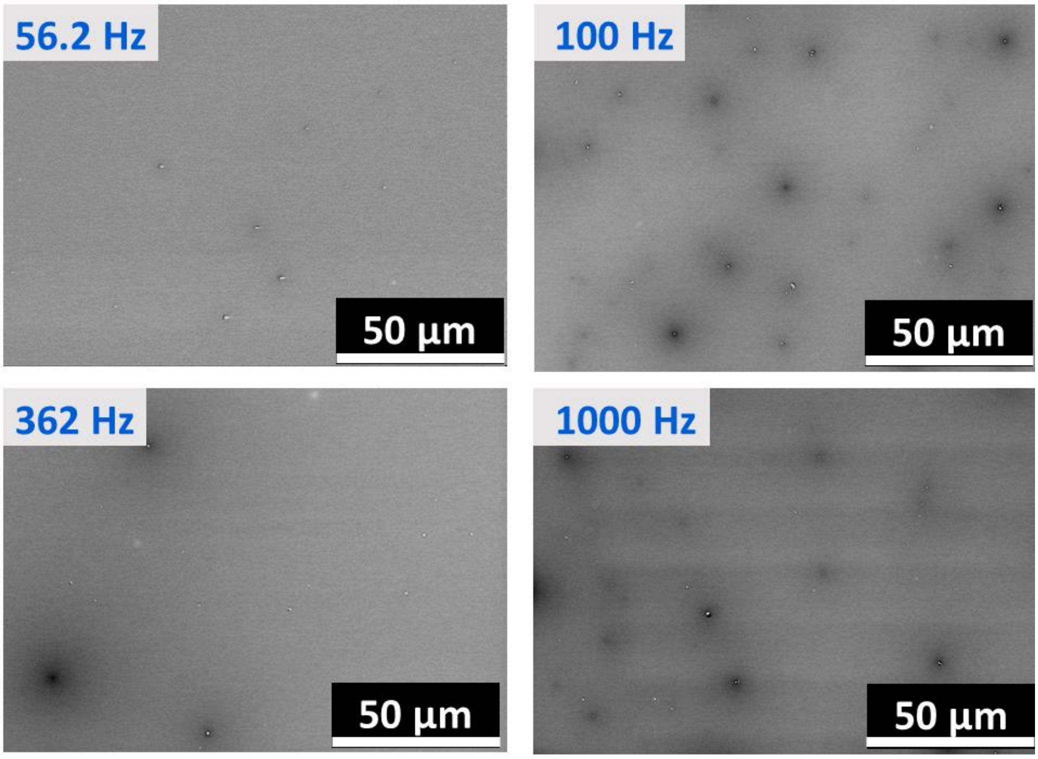

Figure S15: SEM top view images of the thin film obtained from D4 and elaborated at different plasma pulses frequency using a 75% monomer saturation ratio.

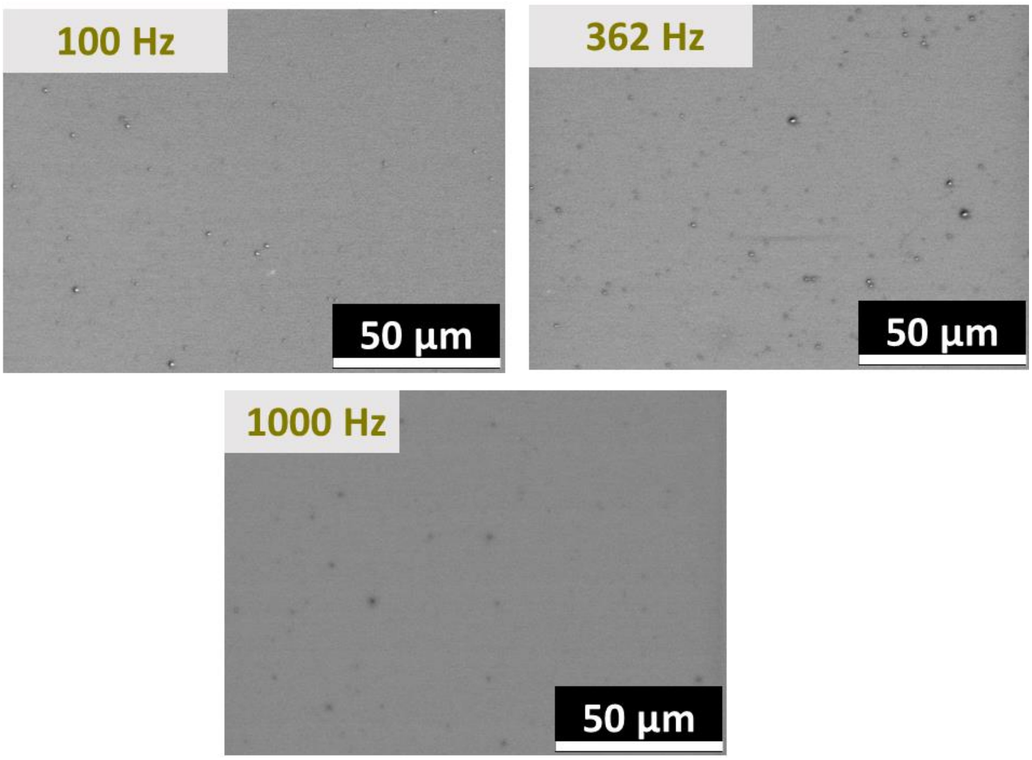

Figure S16: SEM top view images of the thin film obtained from DMTSO and elaborated at different plasma pulses frequency using a 75% monomer saturation ratio.

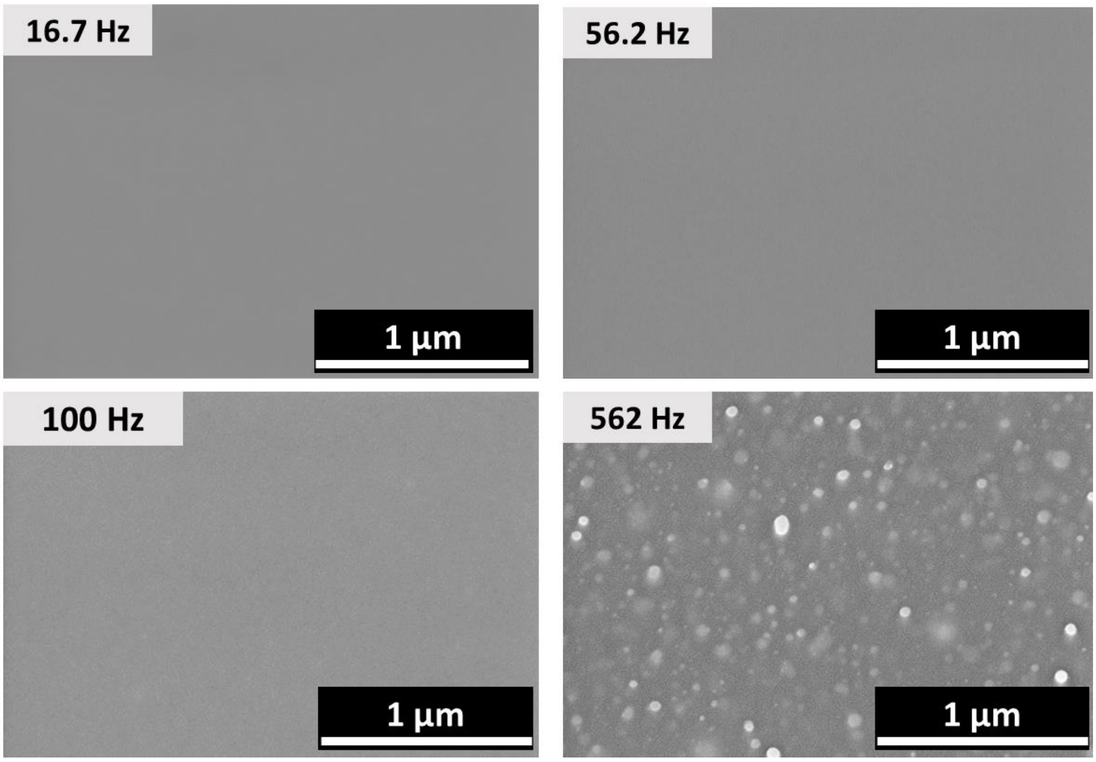

Figure S17: SEM top view images of the thin film obtained from V4D4 and elaborated at different plasma pulses frequency using a 75% monomer saturation ratio.

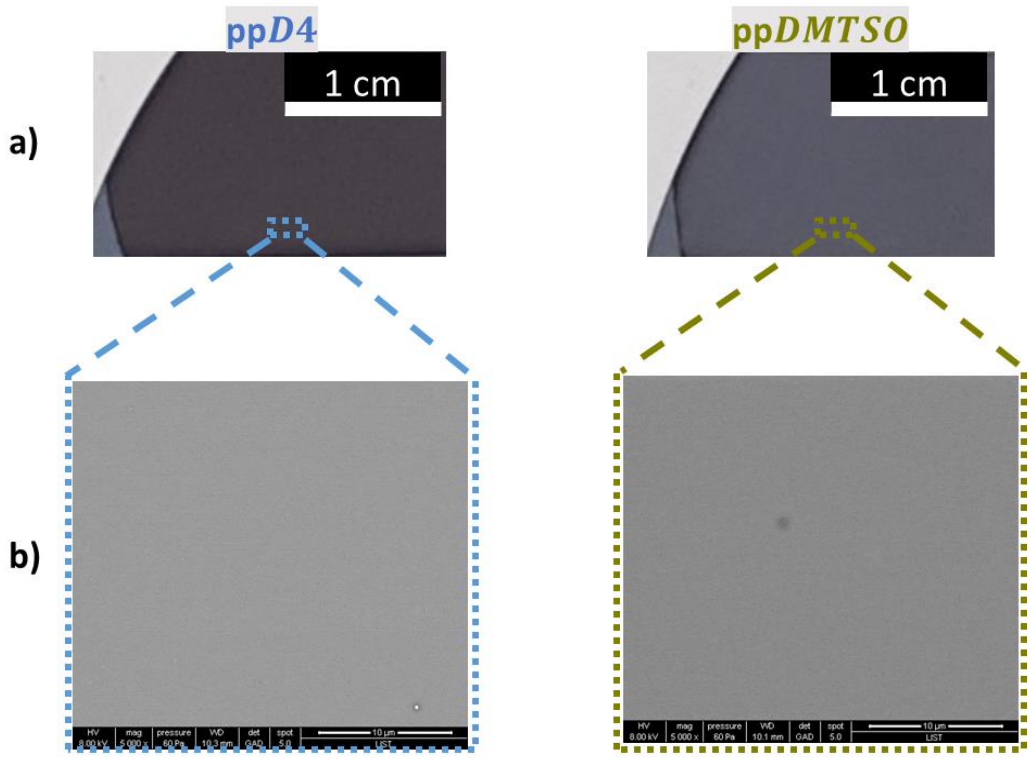

Figure S18: a) Optical images and b) top view SEM images of the thin films obtained from D4 and DMTSO elaborated using a monomer saturation ratio P_M/P_{sat} of 20%. The plasma pulse frequency was fixed to 100 Hz. The variation of the thin films colours are due to their difference of thickness.

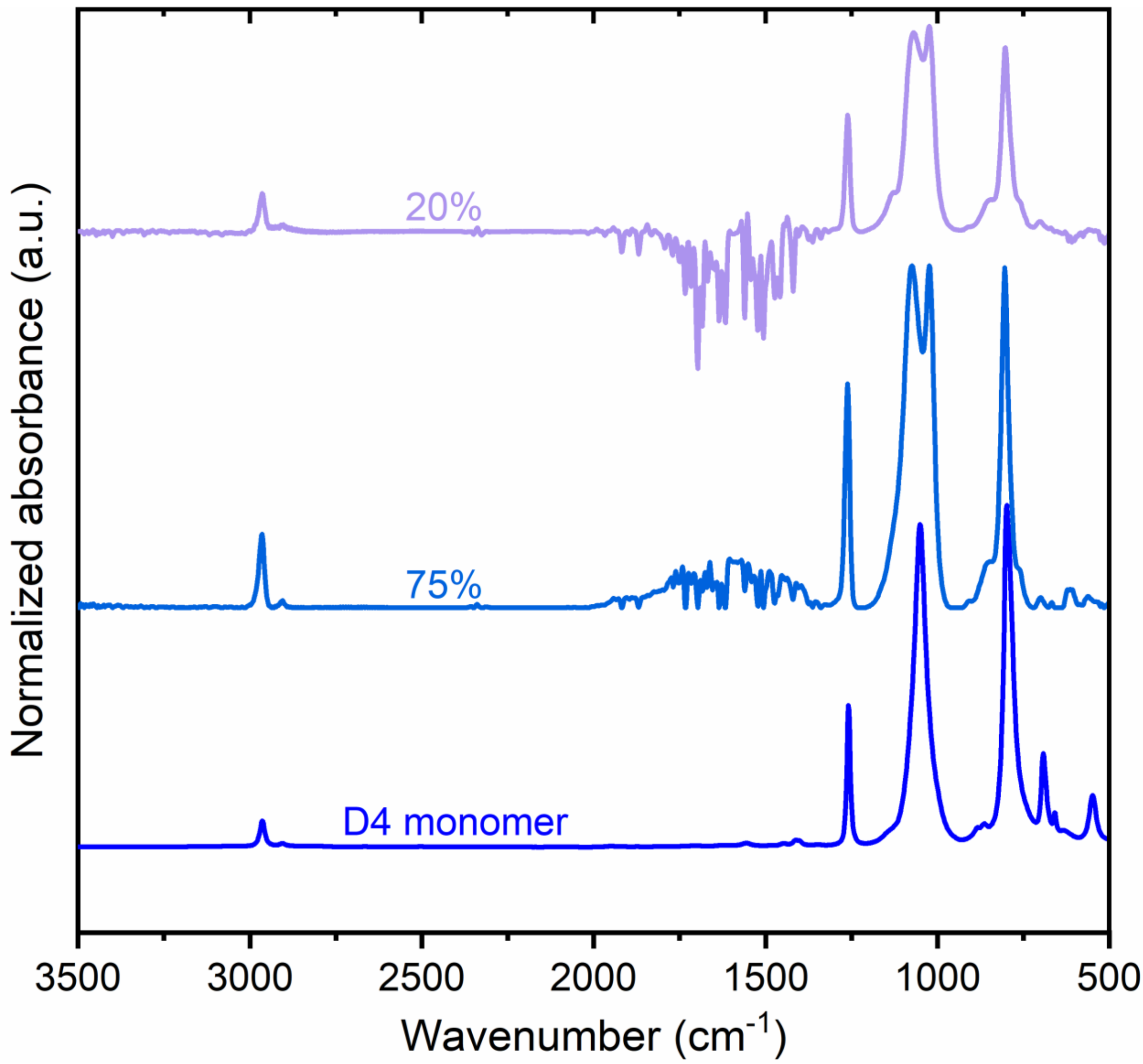

Figure S19: FTIR spectra of the D4 monomer and the as-deposited thin films elaborated at a fix plasma pulse frequency, i.e. 100 Hz, using different saturation ratio P_M/P_{sat} 75 % and 20 %. The thin films obtained from D4 and elaborated using a saturation ratio P_M/P_{sat} of 20 % shows a similar FTIR spectrum than the thin films elaborated using a saturation ratio of 75 %. Indeed, the single peak located at 1,052 cm^{-1} in the D4 monomer spectrum, attributed to the asymmetric stretching band associated to the Si─O─Si group, is split into two peaks located at 1,074 cm^{-1} and 1,024 cm^{-1} in the resulting thin films. The splitting of this band is typical for long linear siloxane chain and consequently highlights the occurrence of a ring-opening reaction during the AP-PECVD reaction of this D4 monomer.

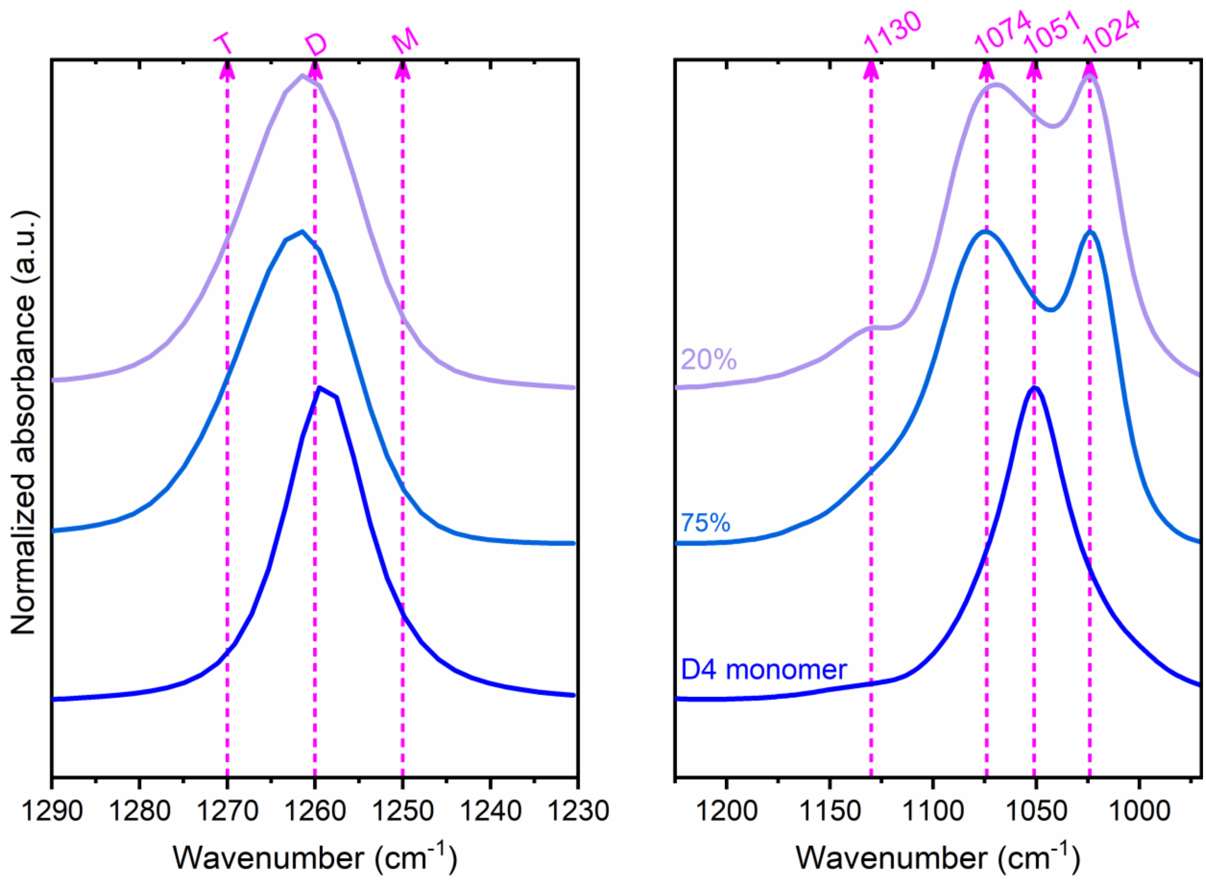

Figure S20: FTIR spectra of the 1290-1230 cm^{-1} and the 1225-970 cm^{-1} regions corresponding respectively to the Si─CH_3 bonding region and the Si─O─Si stretching of the D4 monomer and the thin films elaborated at fix plasma pulse frequency of 100 Hz using saturation ratios of 75 % and 20 %. The M, D and T group represent the mono-, di-, and trisubstitution of the silicon atom by oxygen, respectively. A small peak is noticed at 1,130 cm^{-1} that corresponds to the contribution of the silsesquioxane-like cage structure. Interestingly, the band related to Si─CH_3 located at 1,259 cm^{-1} did not show any shift, indicating that the original D configuration of silicon is retained during the ring-opening reaction.

Table S6: FTIR absorption assignments of the D4 monomer and the thin films elaborated at a fix plasma pulse of 100 Hz using different saturation ratio P_M/P_{sat} of 20 % and 75 %.

Chemical bond	**D4 monomer (nm^{-1})**	**ppD4 (cm^{-1})**	
		75 %	**20 %**
CH_3 antisymmetric stretching	2964	2961	2964
	2906	2913	2913
CH_3 sym. deformation from Si-CH_3	1259	1257	1261
	-	-	1129
Si—O asymmetric stretching from linear network	-	1074	1068
$(Si—O)_3$ asymmetric stretching from the ring	1051	-	-
Si—O asymmetric stretching in suboxide	-	1024	1024
$Si(CH_3)_3$ rocking	--	--	844
$Si(CH_3)_2$ rocking	798	804	802

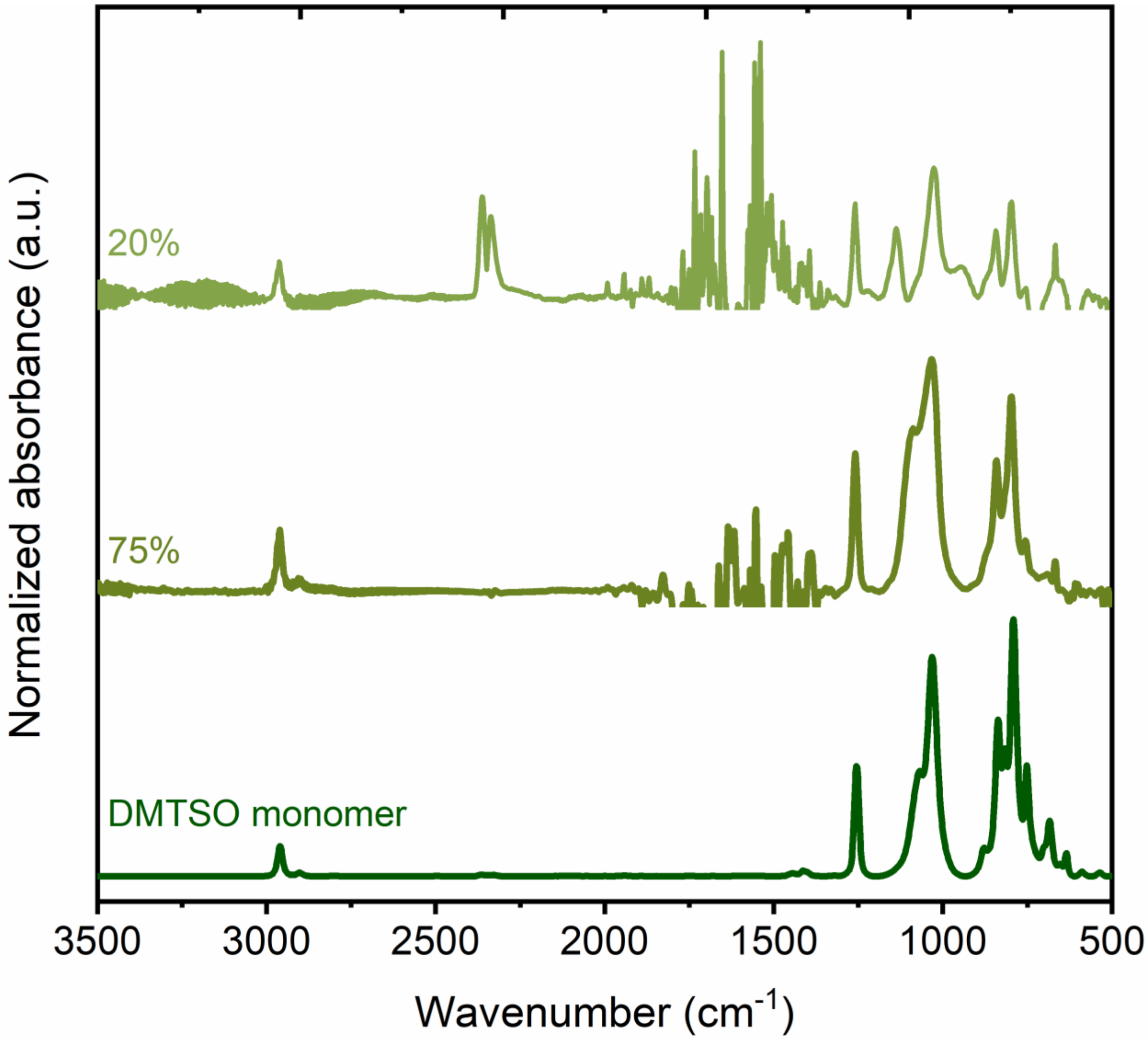

Figure S21: FTIR spectra of the DMTSO monomer and the as-deposited thin films elaborated at a fix plasma pulse frequency, i.e. 100 Hz, using different saturation ratio P_M/P_{sat} of 75 % and 20 %.

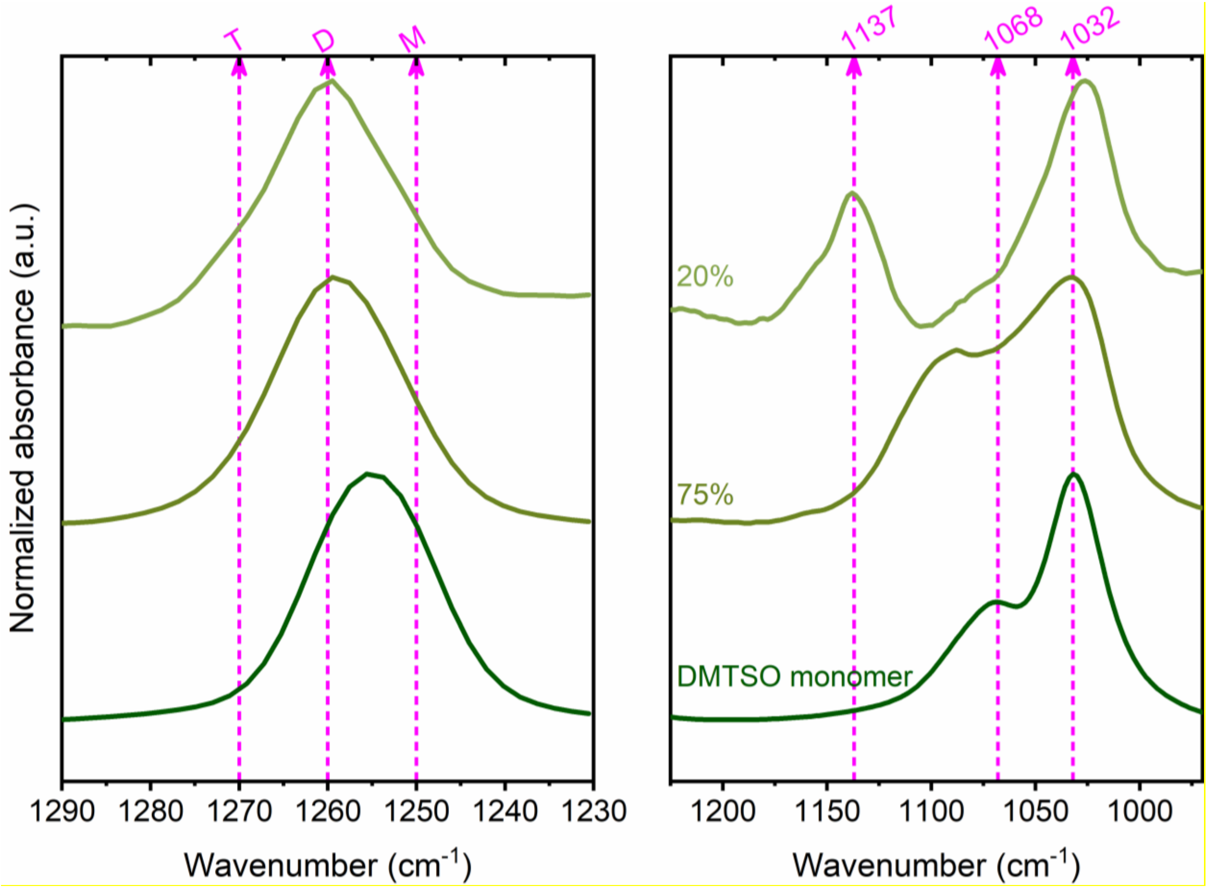

Figure S22: FTIR spectra of the 1,290-1,230 cm^{-1} and the 1,225-970 cm^{-1} regions corresponding respectively to the Si─CH$_3$ bonding region and the Si─O─Si stretching of the DMTSO monomer and the thin films elaborated at fix plasma pulse frequency of 100 Hz using saturation ratios of 75 % and 20 %. The M, D and T group represent the mono-, di-, and trisubstitution of the silicon atom by oxygen, respectively.

Table S7: FTIR absorption assignments of the DMTSO monomer and the thin films elaborated at a fix plasma pulse of 100 Hz using different saturation ratio P_M/P_{sat} of 20 % and 75 %.

Chemical bond	**DMTSO (nm^{-1})**	**ppDMTSO (cm^{-1})**	
		75%	**20%**
CH_3 antisymmetric stretching	2960	2960	2962
CH_3 symmetric stretching	2902	2901	-
CH_3 sym. deformation from Si^T-CH_3	-	-	1270
CH_3 sym. deformation from Si^D-CH_3	1256	1259	1259
Si-O asymmetric stretching in ladder	-	-	1137
Si-O asymmetric stretching	-	1087	1137
Si-O-Si asymmetric stretching in linear network	1068	-	-
Si-O-Si asymmetric stretching in suboxide	1032	1032	1026
$Si(CH_3)_3$ rocking	837	840	842
$Si(CH_3)_2$ rocking	791	796	796

Table S8: Theoretical and experimental atomic composition of the thin films obtained from the AP-PECVD reaction of D4 and DMTSO elaborated at a saturation ratio P_M/P_{sat} = 20 % and 75 % using a plasma pulse frequency of 100 Hz.

		Atomic %			
		Si	N	O	C
D4	As-deposited at P_M/P_{sat} = 20 %	28	0	28	44
	As-deposited at P_M/P_{sat} = 75 %	27	0	27	46
	Theory	25	0	25	50
DTMSO	As-deposited at P_M/P_{sat} = 20 %	31	0	31	38
	As-deposited at P_M/P_{sat} = 75 %	17	0	22	60
	Theory	23.5	0	17.6	59

Table S9: Chemical resistance of the thin films obtained from V4D4, D4 and DMTSO towards water, ethanol and acetone. The root-mean-square roughness (Rq) and thickness (d) were measured before and after 24 hours of soaking. D4- and DMTSO-based thin films were elaborated using a saturation ratio P_M/P_{sat} of 20 % and V4D4-based thin films using a P_M/P_{sat} of 75 %.

	PV4D4		**ppD4**		**ppDMTSO**	
	Rq (nm)	d (nm)	Rq (nm)	d (nm)	Rq (nm)	d (nm)
As-deposited	0.64	118	0.47	58	0.71	61.4
Water-treated	0.41	122.3	0.6	52.5	1.4	43.2
Ethanol-treated	0.53	111.7	0.7	40.5	0.48	28.9
Acetone-treated	0.48	117.4	0.7	36.5	0.61	29.3

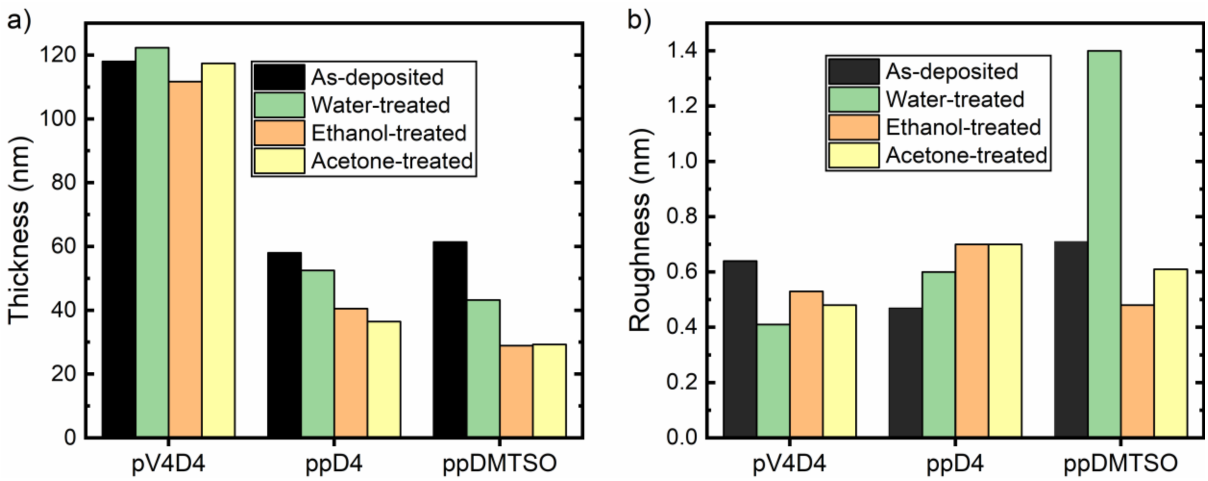

Figure S23: (a) Thickness and (b) root-mean-square roughness of the thin films obtained from V4D4, D4 and DMTSO before and after 24 hours immersion in ethanol and acetone. D4- and DMTSO-based thin films were elaborated using a saturation ratio P_M/P_{sat} of 20 % and V4D4-based thin films using a P_M/P_{sat} of 75 %.

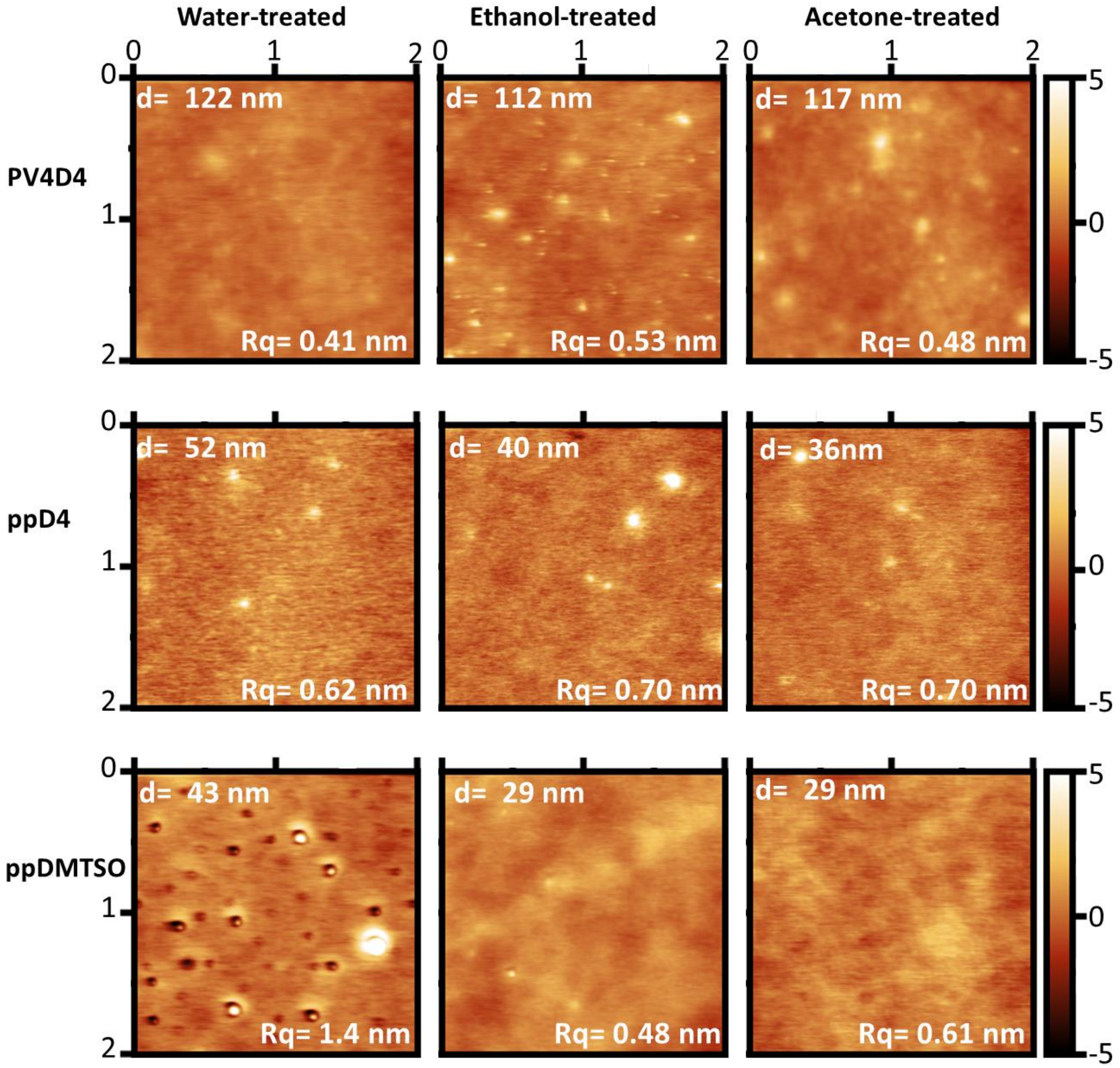

Figure S24: AFM images of the as-deposited thin films obtained V4D4, D4 and DMTSO after the 24-hours of soaking in water, ethanol and acetone. D4- and DMTSO-based thin films were elaborated using a saturation ratio P_M/P_{sat} of 20 % and V4D4-based thin films using a P_M/P_{sat} of 75 %.

Table S10: List of the V4D4, D4 and DTMOS based-thin films integrated in metal/insulator/semiconductor (MIS) structures and their respective areal capacitance (Ci) measured at 1 kHz. Their respective k values are provided.

Monomer	***P_M/P_{sat} (%)***	***Thickness (nm)***	***Ci (nF·cm^{-2})***	***k***
V4D4	75	118 57 29	24.3 52.5 106	3.32
D4	20	72 58 37	33.5 41.5 64	2.72
DTMOS	20	61.5 45 30	44.9 59.8 86.4	3.03

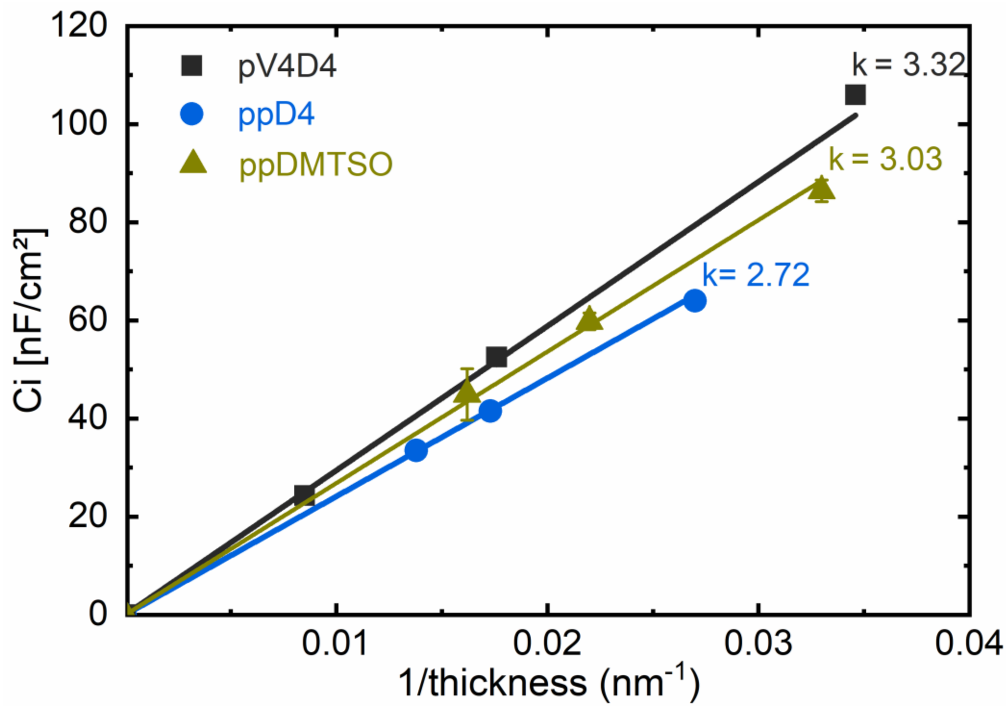

Figure S25: Estimation of the dielectric constant of the thin films obtained from V4D4, D4 and DMTSO. D4- and DMTSO-based thin films were elaborated using a saturation ratio P_M/P_{sat} of 20 % and V4D4-based thin films using a P_M/P_{sat} of 75 %.

Table S11: Leakage current values at ±2 MV/cm of the thin films obtained from V4D4, D4 and DMTSO. D4- and DMTSO-based thin films were elaborated using a saturation ratio P_M/P_{sat} of 20 % and V4D4-based thin films using a P_M/P_{sat} of 75 %.

Thin films	Thickness (nm)	Ji (MV/cm)	
		-2	2
pV4D4	57	9.7E-8	2.2E-7
	29	2.1E-7	7.8E-7
ppD4_	58	1.7E-4	3.4E-5
ppDMTSO	61.5	1.7E-4	1.1 E-3

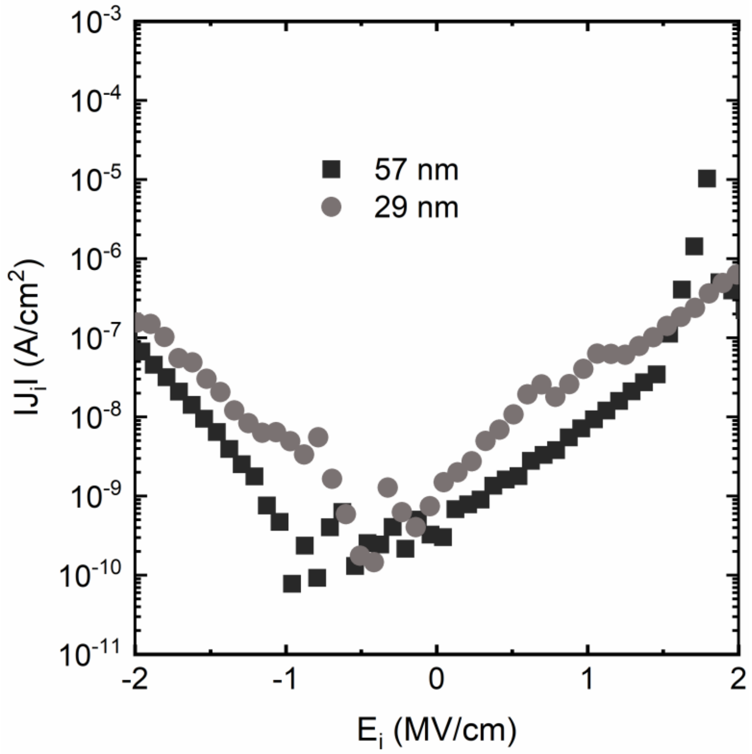

Figure S26: Leakage current density versus electric field (Ji-Ei) characteristics of MIS structures with the thin films obtained from V4D4 measured on a 57 nm and a 29 nm thick layer.

Supporting Information

Plasma initiated chemical vapour deposition of organosiloxane thin films - from the growth mechanisms to ultrathin low-k polymer insulating layers

Dominique Abessolo Ondo, Renaud Leturcq, Nicolas D. Boscher*

Luxembourg Institute of Science and Technology, Materials Research and Technology Department, 41, rue du Brill, L-4422 Belvaux, Luxembourg
E-mail: nicolas.boscher@list.lu

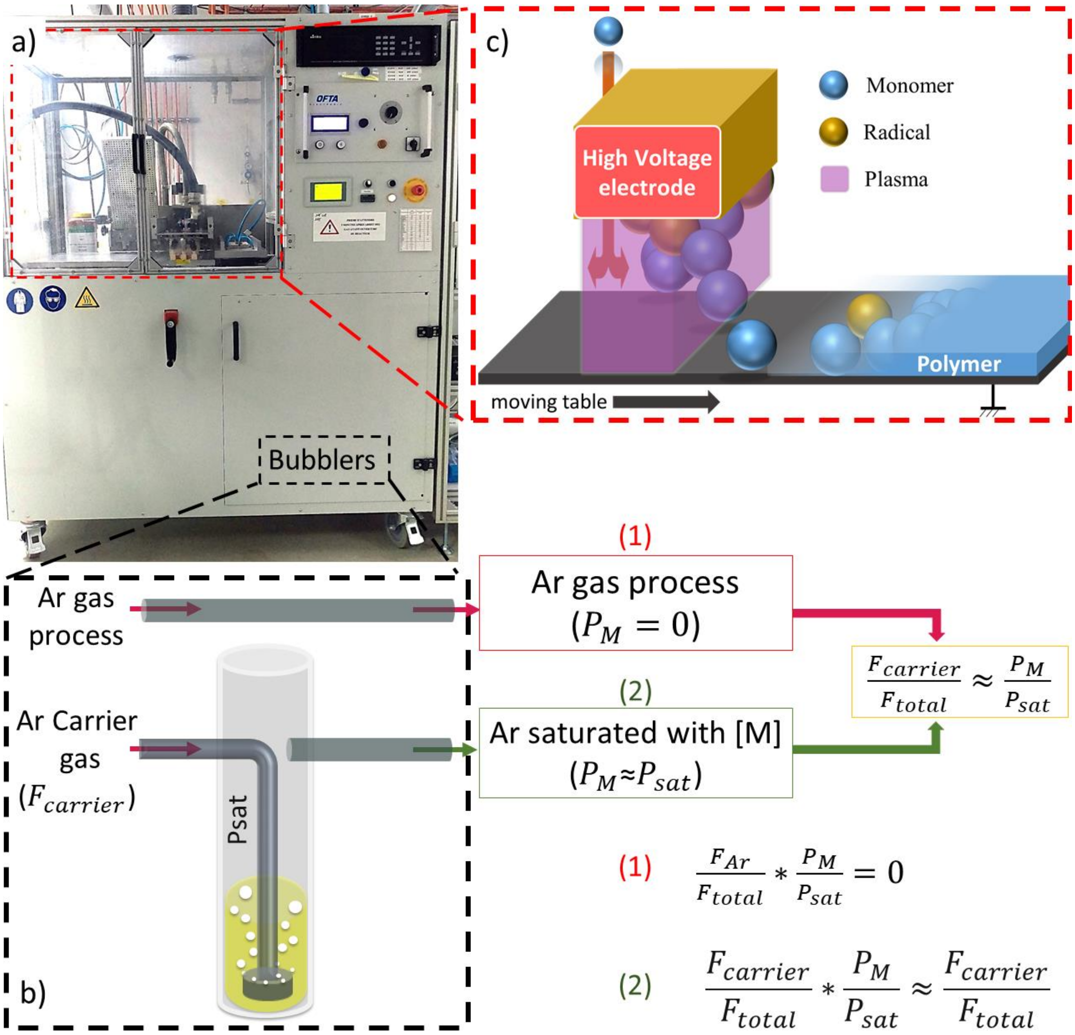

Figure S1. a) Photograph of the AP-PiCVD reactor setup that affords a dry, single-step, and up-scalable solution for the deposition of functional thin films. b) The monomer to deposit is held in a bubbler. Vapours of the V3D3 monomer are directed toward the reactor chamber using argon (Ar), which was playing the role of carrier and the plasma gas. c) Schematic of the dielectric barrier discharge displaying one upper electrode and a moving grounded electrode (represented as a table) on which the substrate is stuck. The radicals are created during the plasma ON time (purple area).

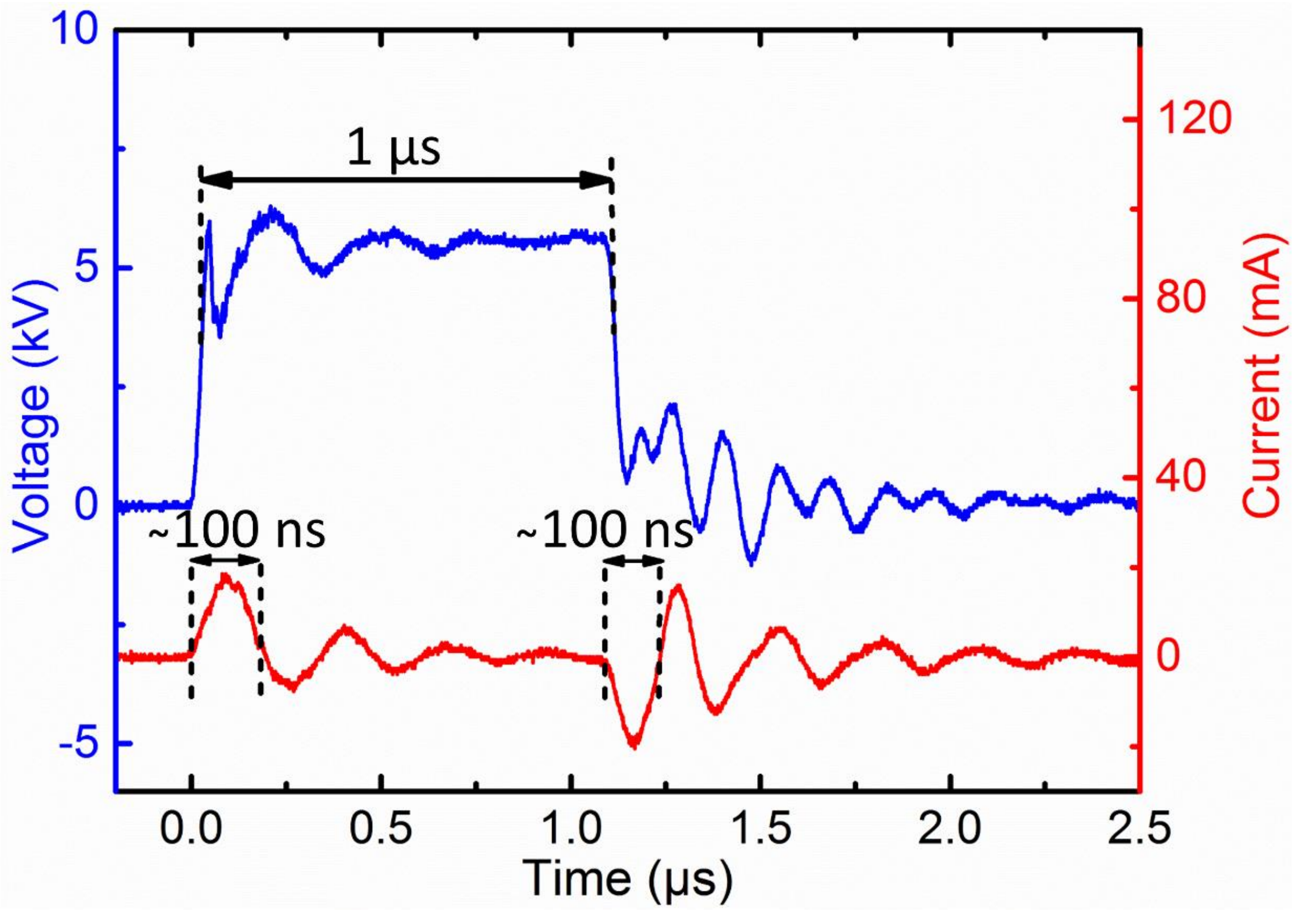

Figure S2. Traces of the I-V curves used for the atmospheric-pressure plasma initiated chemical vapour deposition (AP-PiCVD) of polymer and plasma thin films. The plasma was ignited with a 1µs ultrashort high-voltage square pulse (blue curve) resulting in the creation of two current discharges lasting *ca* 100 ns (red curve). These current discharges represents the time when the plasma is ON.

Table S1. Experimental condition for the deposition performed to determine the impact of plasma pulse frequencies on the initiation and lifetime of the free-radical polymerisation of V3D3. The deposition rate (DR) and the thickness increment per cycle (thick. incr.) are provided.

P_M/P_{sat} (%)	Frequency (Hz)	$F_{Ar, carrier}$ (SLM)	$F_{Ar, total}$ (SLM)	Pressure (bar)	t_{ON} (1µs)	DR (nm/s)	Thick. incr. (pm)
20	31.6	4	20	1	1	0.150	4.64
	56.2	4	20	1	1	0.320	5.68
	100	4	20	1	1	0.604	5.22
	178	4	20	1	1	1.05	5.88
	316	4	20	1	1	2.13	6.74
	562	4	20	1	1	3.19	5.68
	1000	4	20	1	1	5.59	5.59
	3000	4	20	1	1	9.7	3.23
75	31.6	15	20	1	1	0.246	7.80
	56.2	15	20	1	1	0.445	7.92
	100	15	20	1	1	0.724	7.86
	178	15	20	1	1	1.40	7.84
	316	15	20	1	1	2.14	6.78
	562	15	20	1	1	3.80	6.77
	1000	15	20	1	1	7.88	7.88
	3000	15	20	1	1	36.9	12.3

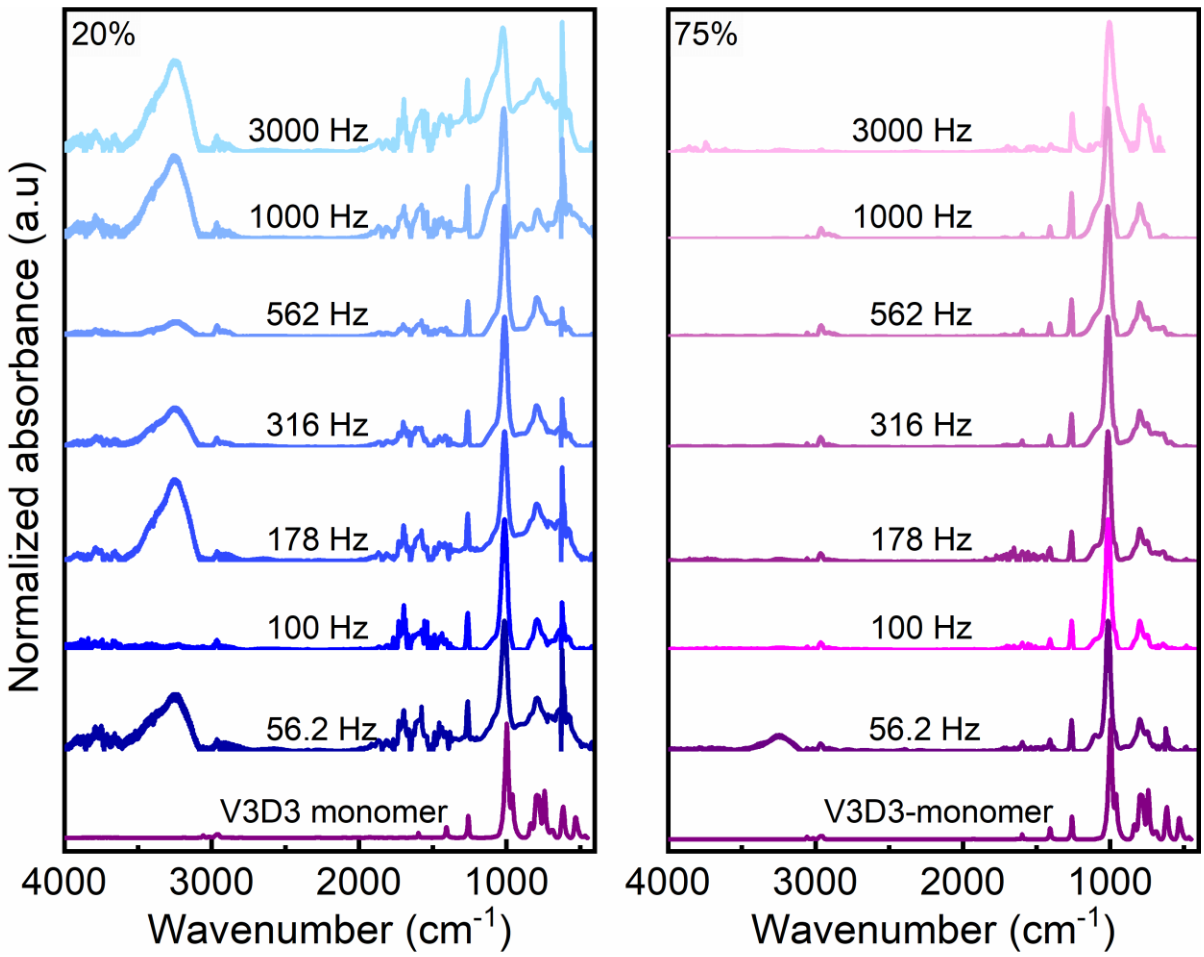

Figure S3. FTIR spectrum of the thin films elaborated using a 20 % and 75 % saturation ratio deposited at different plasma pulse frequencies.

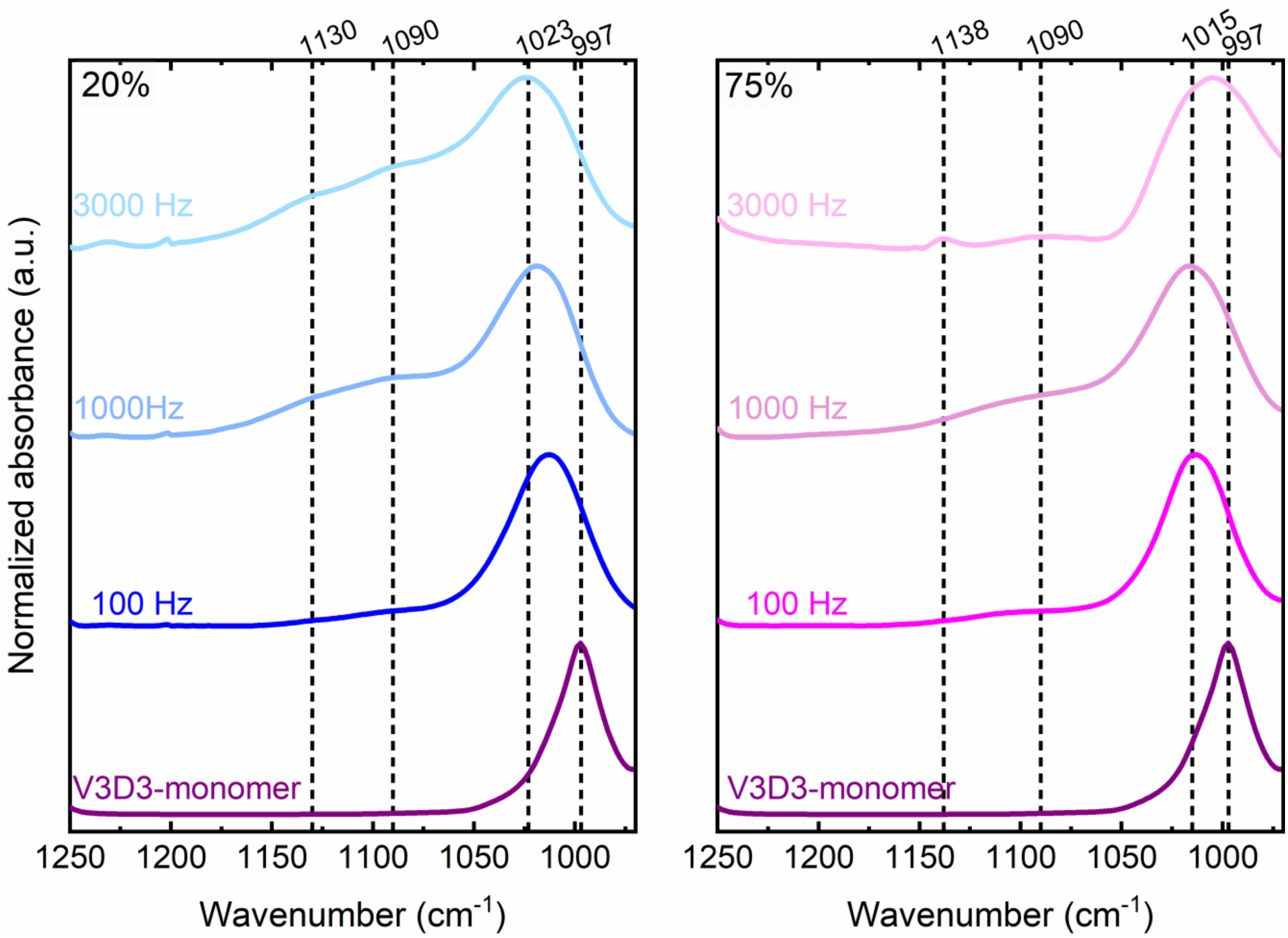

Figure S4. FTIR spectra of the 1250-970 cm^{-1} region of V3D3 monomer and the resulting thin films elaborated using a P_M/P_{sat} of 20 % and 75 % and deposited at different plasma pulse frequencies, i.e. 100 Hz, 1000 Hz and 3000 Hz. Irrespective of the P_M/P_{sat}, the broadening of the peak associated to the Si-O-Si ring is observed with the increase of the pulse plasma frequency.

Table S2. FTIR absorption assignments of V3D3 monomer and the resulting thin films elaborated using a P_M/P_{sat} of 20 % and deposited at different plasma pulse frequencies, i.e. 100 Hz, 1000 Hz and 3000 Hz.

Chemical bond	**Monomer (nm^{-1})**	**Polymers (cm^{-1})**		
		100 Hz	**1000 Hz**	**3000 Hz**
-OH	-	-	3250	3246
=CH_2 stretching	3057	3059	-	-
=CH stretch of vinyl bond	3017	-	-	-
CH_3 antisymmetric stretching	2960	2963	2963	-
C=C stretch from (Si—CH=CH_2)	1597	-	-	-
CH_2 in Si—$(CH_2)_x$—Si and vinyl	1407	-	-	-
CH_3 sym. deformation from Si-CH_3	1259	1263	1265	1265
Silesquioxane cage structure	-	-	-	1130
Linear Si—O	-	-	1090	1090
$(Si—O)_3$ from the ring	997	1012	1018	1024
Si-O in Si-OH group	-	-	900	900

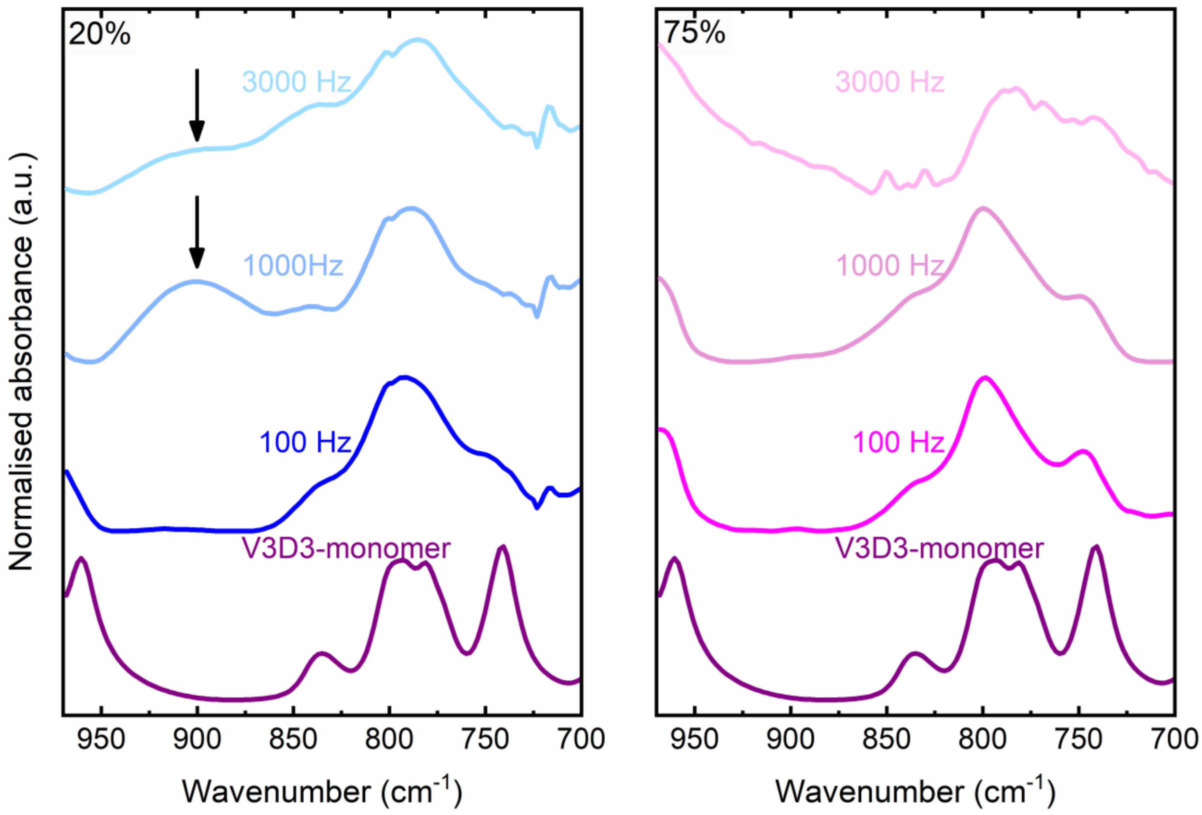

Figure S5. FTIR spectra of the 970-700 cm^{-1} region of V3D3 monomer and the resulting thin films elaborated using a P_M/P_{sat} of 20 % and 75 % and deposited at different plasma pulse frequencies, i.e. 100 Hz, 1000 Hz and 3000 Hz. Note that, the Si-O stretch from the silanol group (Si-OH) gives rise to an absorbance peak located at 900 cm^{-1} for the polymer layers synthesized using a P_M/P_{sat}= 20 % (black arrows).

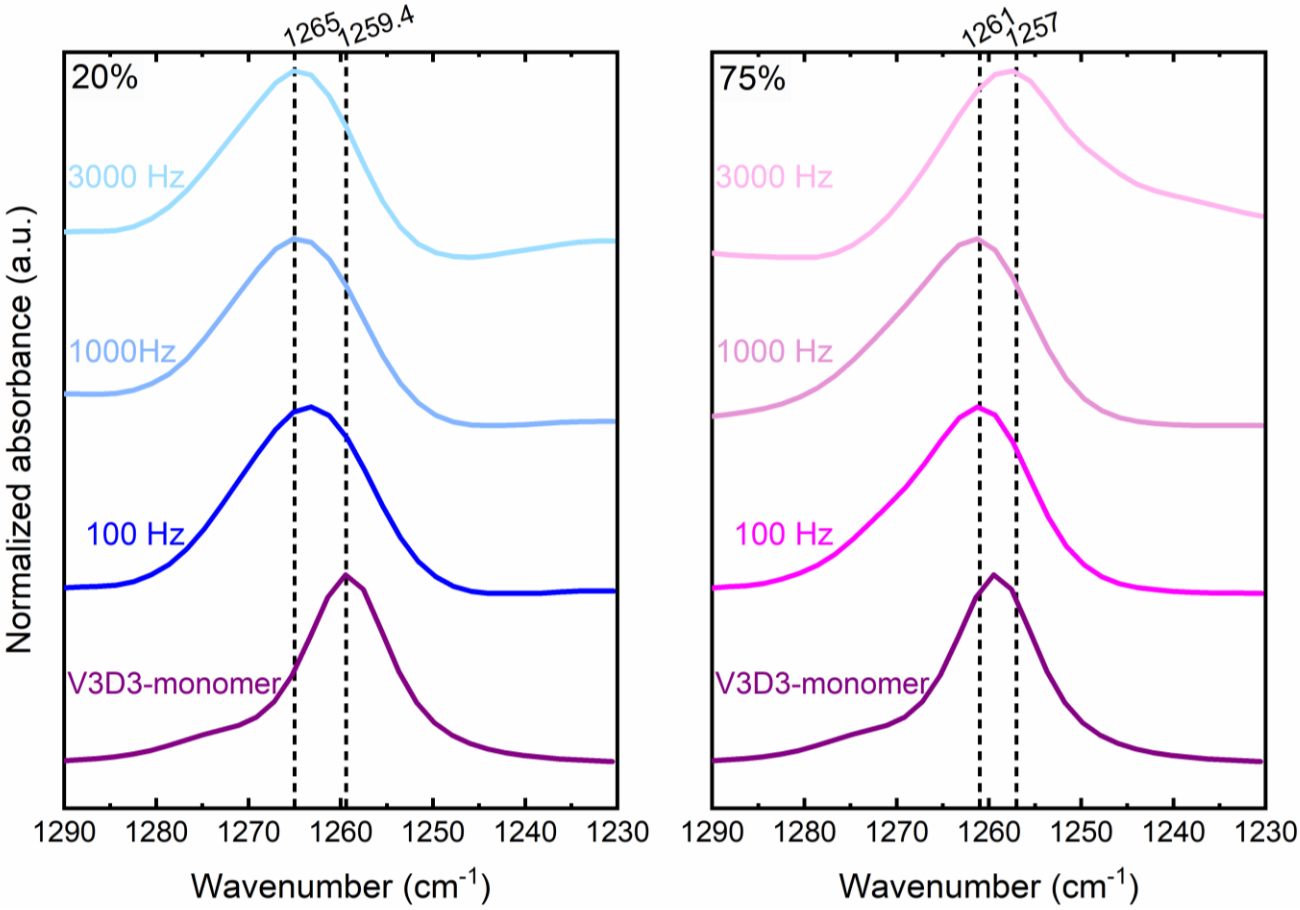

Figure S6. FTIR spectra of the 1290-1230 cm^{-1} region of V3D3 monomer and the resulting thin films elaborated using a P_M/P_{sat} of 20 % and 75 % deposited at different plasma pulse frequencies, i.e. 100 Hz, 1000 Hz and 3000 Hz.

Table S3. FTIR absorption assignments of V3D3 monomer and the resulting thin films elaborated using a P_M/P_{sat} of 75% and deposited at different plasma pulse frequencies, i.e. 100 Hz, 1000Hz and 3000Hz.

Chemical bond	Monomer (nm^{-1})	Polymers (cm^{-1})		
		100 Hz	1000 Hz	3000 Hz
$=CH_2$ stretching	3057	3055	3055	-
=CH stretch of vinyl bond	3017	--	3017	-
CH_3 antisymmetric stretching	2960	2966	2963	2958
CH_3 symmetric stretching	-	-	2908	-
CH_2 symmetric stretching	-	-	2874	-
C=C stretch from ($Si—CH=CH_2$)	1597	1596	1596	-
CH2 in Si—$(CH_2)_x$—Si and vinyl	1407	1407	1407	1402
CH_3 sym. deformation from O_2—Si—CH_3	1259	1261	1261	1257
Silesquioxane cage structure	-	-	-	1137
Linear Si—O	-	-	1090	1086
$(Si—O)_3$	997	1012	1016	1004

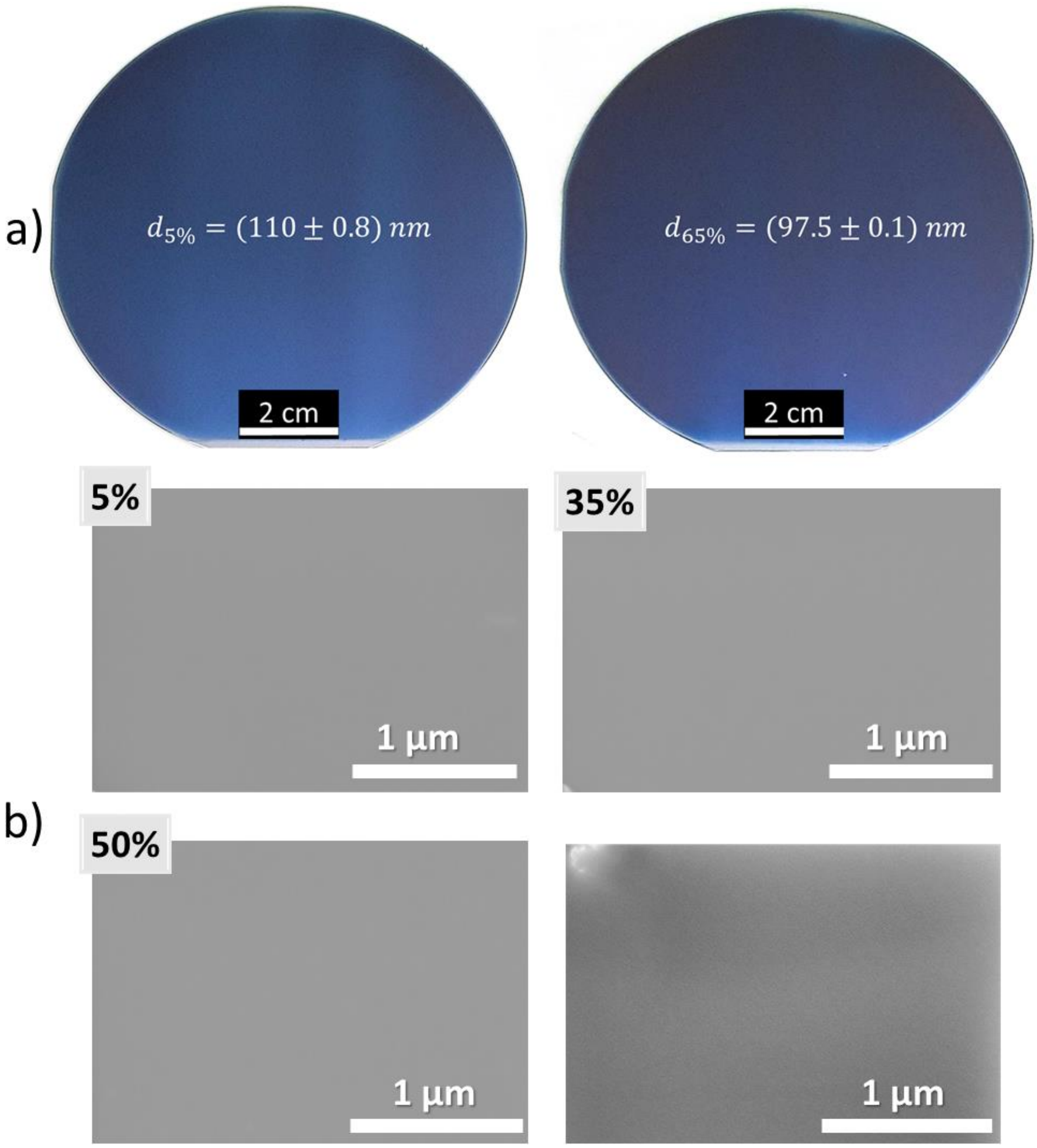

Figure S7. a) Optical images and b) top view SEM images of the as-deposited PV3D3 thin film elaborated using different monomer saturation ratio (P_M/P_{sat}). The plasma pulse frequency was fixed to 100 Hz. The reported thicknesses, $d_{x\%}$ with x% being the P_M/P_{sat} at which the thin films were elaborated, is the average of four measurements randomly performed across the entire substrate surface.

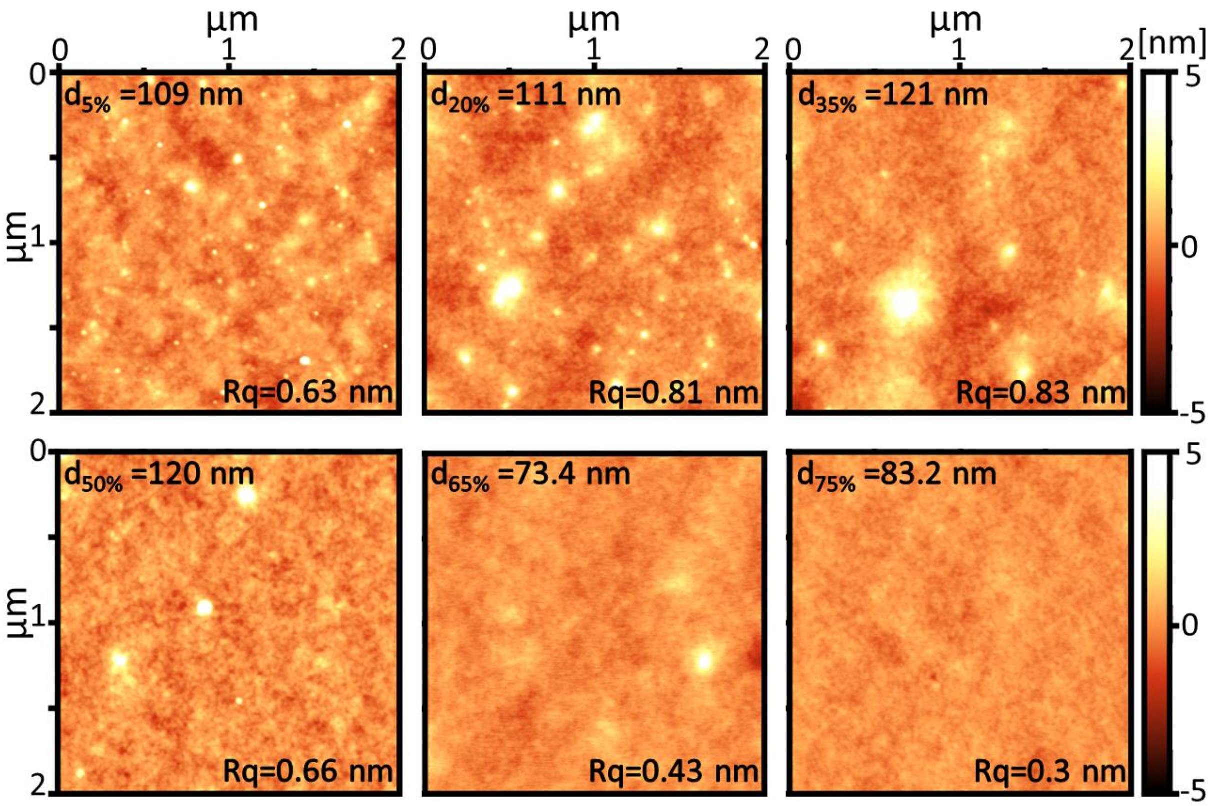

Figure S8. AFM images of the as-deposited PV3D3 thin films elaborated using different P_M/P_{sat} ratios. The thickness ($d_{PM/Psat\,\%}$) and root mean square roughness (Rq) are provided for each of the presented thin films.

Table S4. Experimental condition of the deposition performed to determine the influence of the monomer saturation ratio P_M/P_{sat} on the resulting thin films features. The deposition rates (DR) are provided.

***P_M/P_{sat}* (%)**	***Frequency* (Hz)**	***$F_{Ar,\ carrier}$* (SLM)**	***$F_{Ar,\ total}$* (SLM)**	***Pressure* (bar)**	***t_{ON}* (1µs)**	***DR* (nm/s)**
5	100	1	20	1	1	0.21
20	100	4	20	1	1	0.604
35	100	7	20	1	1	0.67
50	100	10	20	1	1	0.69
65	100	13	20	1	1	0.66
75	100	15	20	1	1	0.724

Table S5. List of the PV3D3 thin films integrated in metal/insulator/semiconductor (MIS) structures and their respective areal capacitance (Ci) measured at 1 kHz employed. Their respective k values are provided.

P_M/P_{sat} (%)	***Thickness (nm)***	***Ci ($nF\cdot cm^{-2}$)***	***k***
5	34.6 21.6 10	116 184 387	4.38±0.02
20	56.8 37.7 18.5	56.1 81.6 165	3.47±0.02
35	87.7 41.3 21.1	31.6 62.5 121	2.91±0.03
50	43.8 34.1 19.6	57 79.6 134	2.97±0.04
65	44.2 29.5 19.5	68.1 77.1 133	2.88±0.13
75	40.5 30.6 22.6	64.5 93.7 119	3.04±0.06

Table S6. Leakage current value of the as-deposited PV3D3 thin films presented below

Samples	5 %	20 %	35 %	50 %
J (à -2 MV/cm)	1.1E-6	5.6E-8	1.9E-9	5.9E-8
J (à 2 MV/cm)	9.4E-7	6.4E-8	1.4E-8	3.4E-8

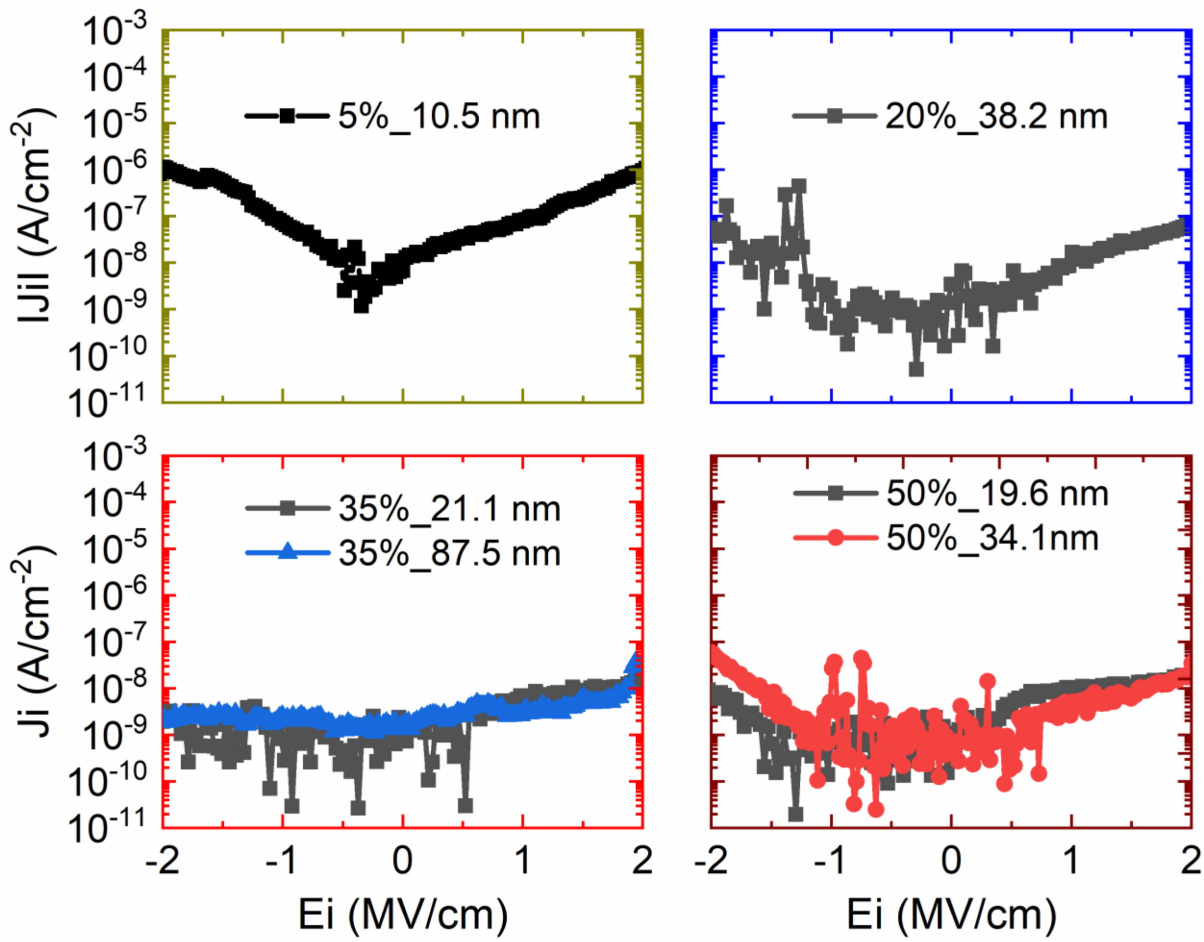

Figure S9. Current density versus electric field (Ji-E) characteristics of MIS structures with PV3D3 thin films elaborated using different P_M/P_{sat} ratio.

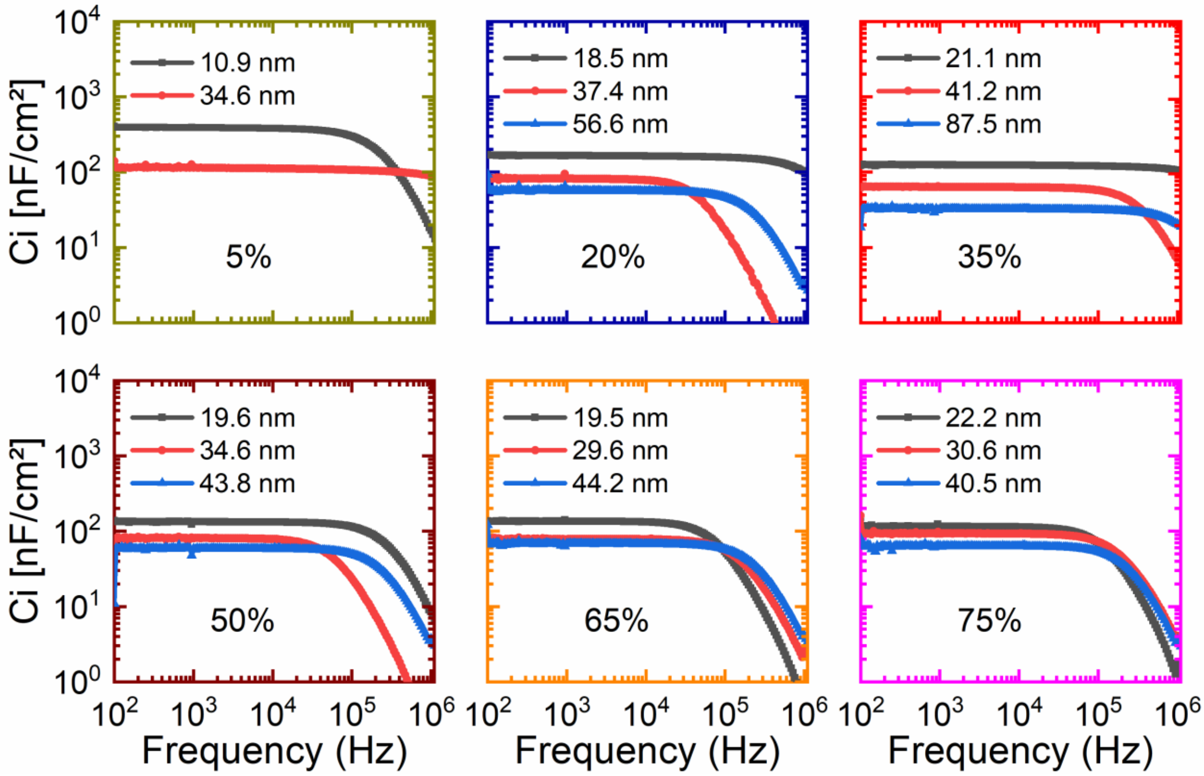

Figure S10. Ci versus frequency of all the as-deposited thin films elaborated using different saturation ratio P_M/P_{sat}.

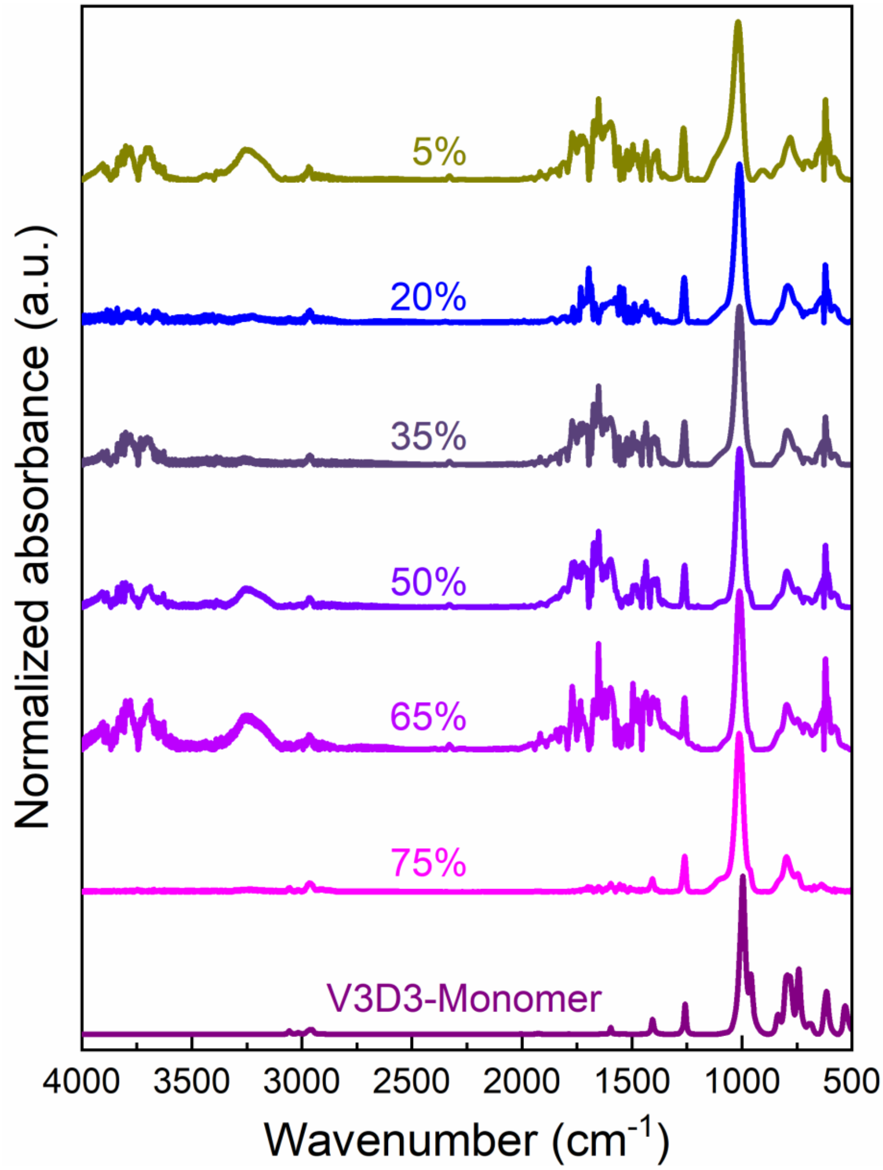

Figure S11. FTIR spectra of the V3D3 monomer and the as-deposited thin films elaborated at a fix plasma pulse frequency, i.e. 100 Hz, using different saturation ratio.

Table S7. FTIR absorption assignments of the V3D3 monomer and the thin films elaborated at a fix plasma pulse, i.e. 100 Hz, using different saturation ratio P_M/P_{sat}: 5 %; 20 %; 35 %; 50 %; 65 % and 75 %.

Chemical bond	**Monomer (nm^{-1})**	**Polymers (cm^{-1})**					
		75 %	**65 %**	**50 %**	**35 %**	**20 %**	**5 %**
-OH	-	-	-	-	-	-	3252
$=CH_2$ stretching	3057	3055		-	-	-	-
=CH stretch of vinyl bond	3017	-	-	-	-	-	-
CH_3 antisymmetric stretch	2960	2966	2964	2964	2964	2963	2965
C=C stretch from (Si—$CH=CH_2$)	1597	1596	1598	1598	1598	-	1598
CH_2 in Si—$(CH_2)_x$—Si and vinyl	1407	1407	-	-	-	-	-
CH_3 sym. deformation in Si^D conf.	1259	1261	1261	1261	1263	1263	-
CH_3 sym. deformation in Si^T conf	-	-	-	-	-	-	1267
Silesquioxane cage structure	-	-	-	-	-	-	1130
Linear Si—O	-	-	-	-	-	-	-
$(Si—O)_3$	997	1012	1012	1012	1012	1012	1018
Si-O in Si-OH group	-	-	-	-	-	-	907

Table S8. Atomic compositions calculated from XPS survey scan of the PV3D3 thin films elaborated using different saturation P_M/P_{sat}, i.e. 5 %; 20 %; 35 %; 50 %; 65 %; and 75 %.

Element	Atomic %						
	pp-5%	pp-20%	pp-35%	pp-50%	pp-65%	pp75%	Theoretical
Si	19	18	18	18.4	19	19	20
O	38	27	27	25.2	23	22	20
C	43	55	55	56.4	58	59	60
C:O:Si	*2.3:2:1*	*3:1.5:1*	*3:1.5:1*	*3:1.4:1*	*3:1.2:1*	*3:1.2:1*	*3:1:1*

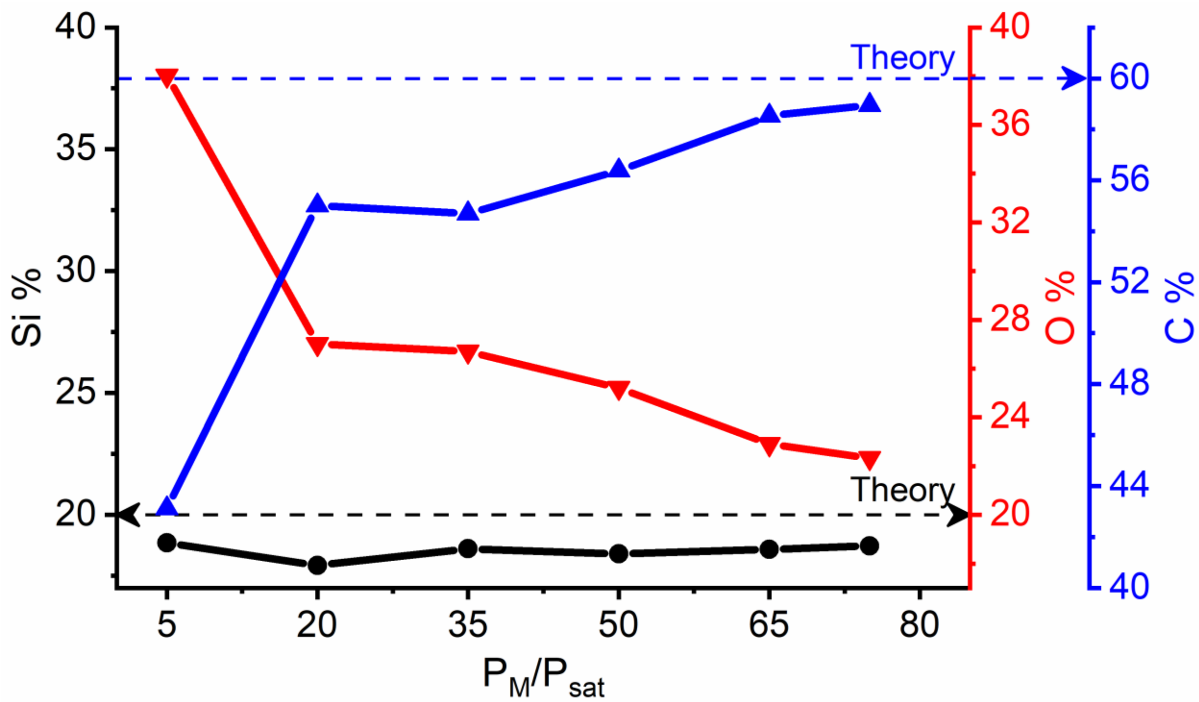

Figure S12. Atomic percentage of silicon (Si), carbon (C) and oxygen in the as-deposited thin films vs. the saturation ratio P_M/P_{sat} at which there were synthesized.

Table S9. Concentration of the different configuration of Si in the different as-deposited PV3D3 thin films elaborated using various saturation ratio P_M/P_{sat}. Their respective average connecting numbers are provided.

Si configuration	Atomic %					
	pp-5%	pp-20%	pp-35%	pp-50%	pp-65%	pp75%
D	11.5	58	59	62.1	77	73.1
T	60.5	25	23	22.2	2.2	10.5
Q	28.0	17	18	15.7	20.8	16.4
$< r >$	2.6	2.3	2.3	2.3	2.3	2.3

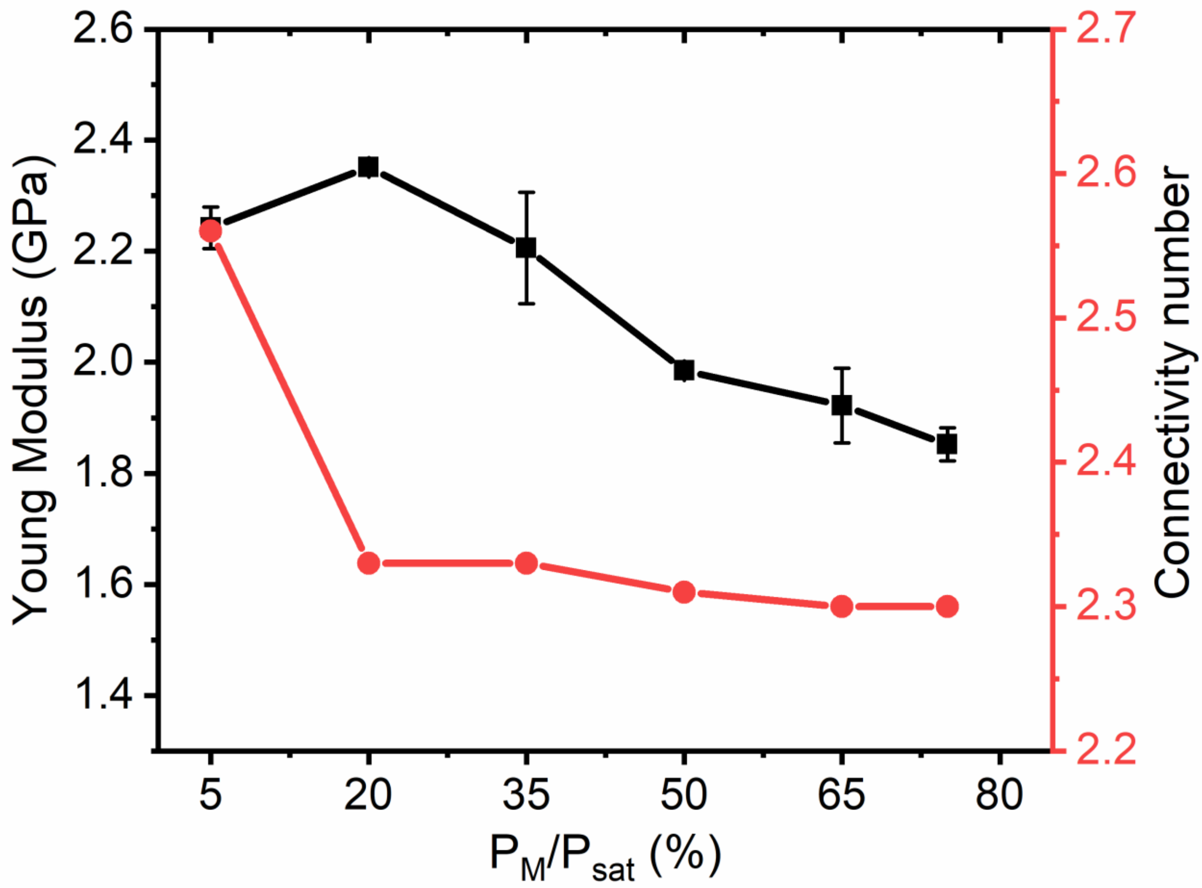

Figure S13. Evolution of the Young modulus and connectivity number of the as-deposited PV3D3 thin films vs. the saturation ratio P_M/P_{sat} at which they were synthesized.

Supporting Information

Atmospheric-Pressure Synthesis of Atomically Smooth, Conformal and Ultrathin Low-k Polymer Insulating Layers by Plasma-Initiated Chemical Vapour Deposition

Dominique Abessolo Ondo,[1] François Loyer,[1] Florian Werner,[2] Renaud Leturcq,[1] Phillip J. Dale,[2] Nicolas D. Boscher[1,*]

[1] *Luxembourg Institute of Science and Technology, Materials Research and Technology Department, 41, rue du Brill, L-4422 Belvaux, Luxembourg*

[2] *University of Luxembourg, Physics and Materials Science Research Unit, 41, rue du Brill, L-4422 Belvaux, Luxembourg*

* Corresponding author: nicolas.boscher@list.lu

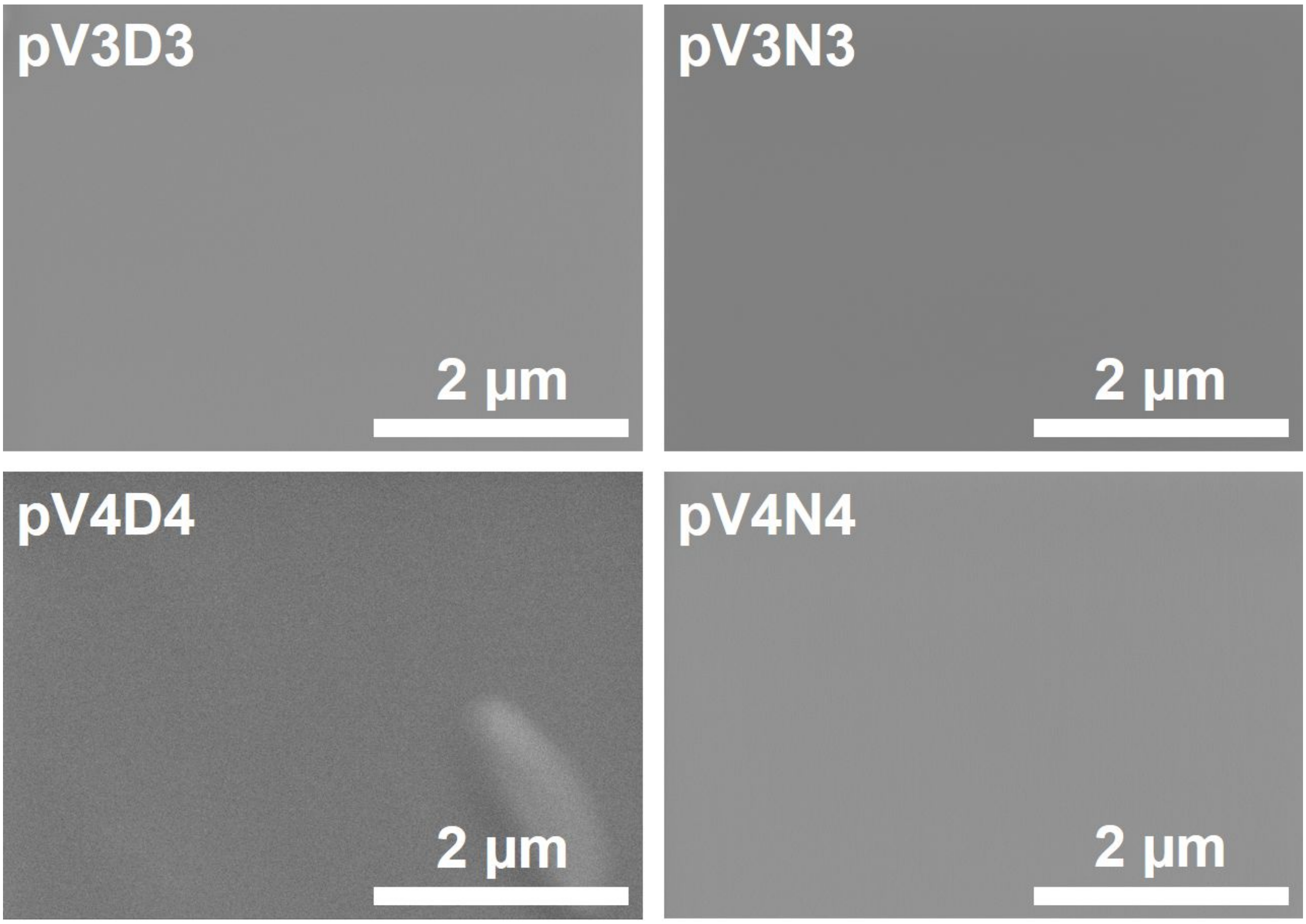

Figure S1. SEM top-view images of the as-deposited AP-PiCVD organosilicon thin films grown from V3D3, V3N3, V4D4 and V4D4 on silicon wafers at an ultrashort plasma pulse frequency of 100 Hz. Irrespective of their thickness, up to 337 nm for the thicker layer investigated, all films are smooth and particle-free. Due to the atomically smooth surface of the AP-PiCVD layers reported in this work, the focus had to be performed on the few dust particles present at the samples surface (cf. SEM micrograph of sample pV4D4).

Table S1. Chemical resistance of the pV3D3, pV3N3, pV4D4 and pV4N4 layers towards ethanol, acetone. The root-mean-square roughness (Rq) and thickness (d) were measured before and after 24 hours of soaking.

	pV3D3 layer		**pV3N3 layer**		**pV4D4 layer**		**pV4N4 layer**	
	Rq (nm)	d (nm)	Rq (nm)	d (nm)	Rq (nm)	d (nm)	Rq (nm)	d (nm)
As-deposited	0.5	224	0.2	361	0.5	90	0.6	127
Ethanol-treated	0.5	181	1.0	360	0.3	85	0.6	122
Acetone-treated	0.4	202	0.3	333	0.4	81	1.0	127

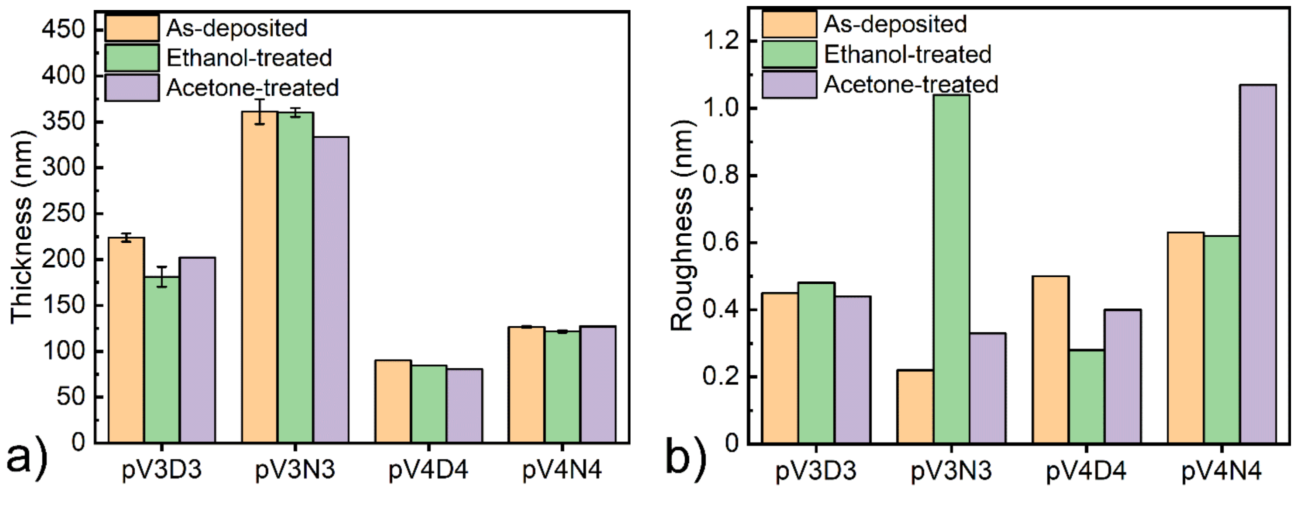

Figure S2. (a) Thickness and (b) root-mean-square roughness of the pV3D3, pV3N3, pV4D4 and pV4N4 layers before and after 24 hours immersion in ethanol and acetone.

Table S2. List of the poly(organosilicon) layers integrated in metal/insulator/semiconductor (MIS) structures and their respective areal capacitance (Ci) at 1 kHz employed to estimate their k values.

	Thickness (nm)	**Ci at 1 kHz ($nF\cdot cm^{-2}$)**
pV3D3 layers	29	117.6
	39	76.1
	47	66.3
pV3N3 layers	22	168.3
	42	91.0
	119	33.0
pV4D4 layers	28	88.9
	59	43.1
	118	22.1
pV4N4 layers	12	271.0
	35	99.8
	70	48.9

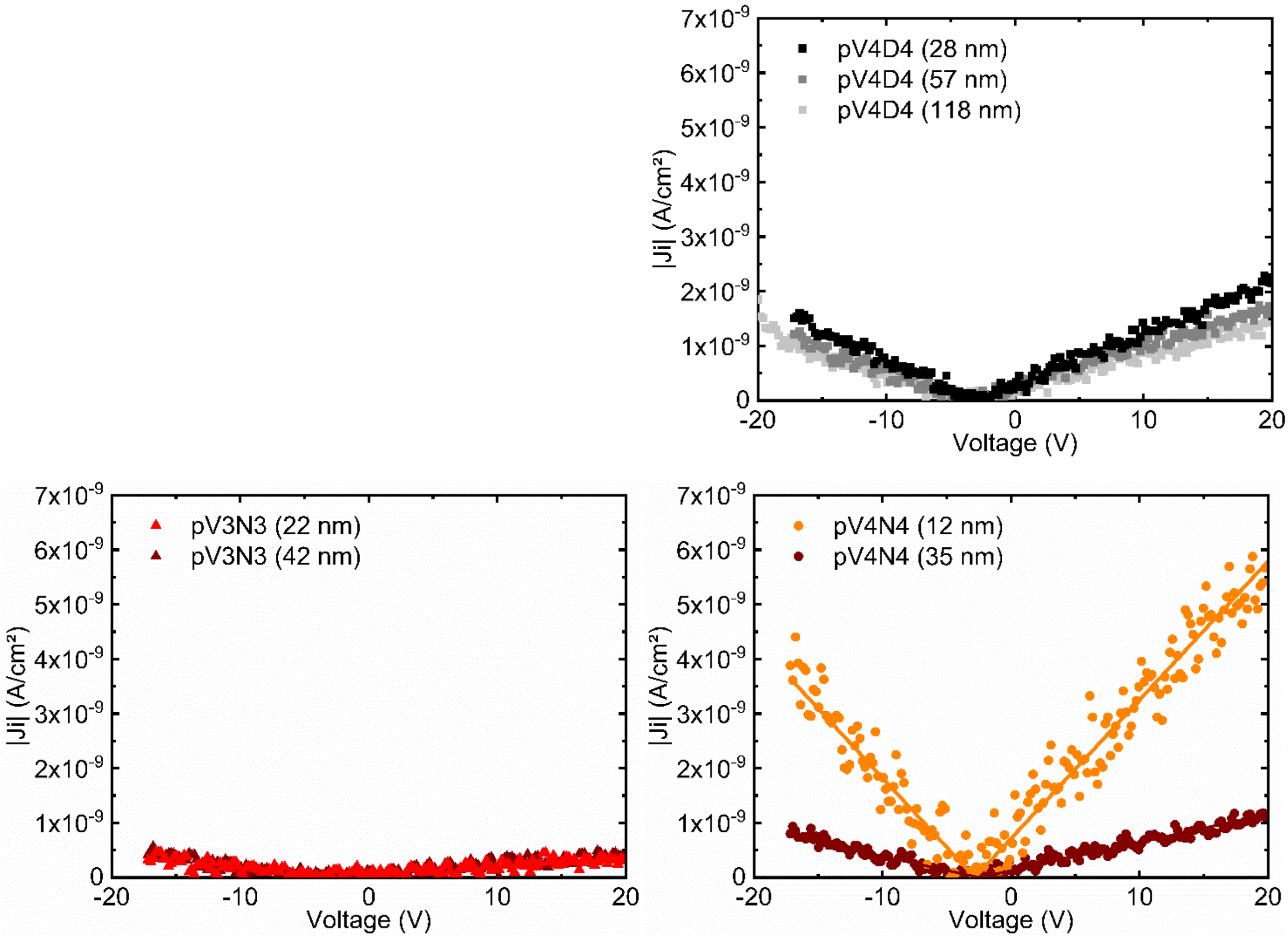

Figure S3. Voltage-dependence of the leakage current density of the pV3N3, pV4D4 and pV4N4 layers (for different thicknesses) assembled in MIS devices.

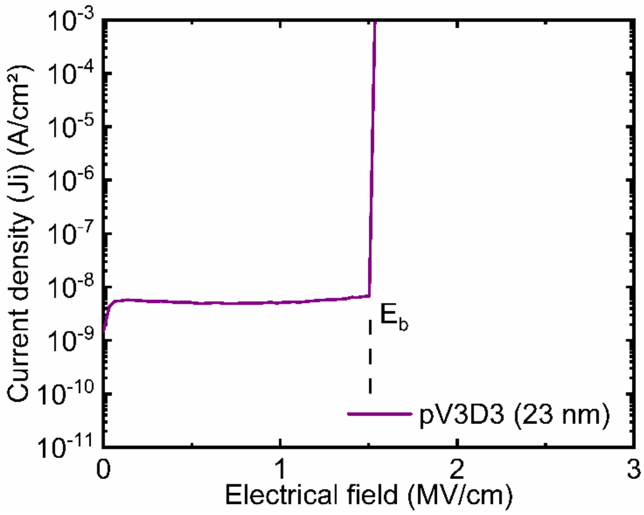

Figure S4. Current density (Ji) vs. electric field of pV3D3 layer. The breakdown field (Eb), observed when the current density (Ji) increase abruptly, occurs at around 1.5 MV·cm^{-1} corresponding to a voltage of 4.6 V for a 23 nm thick layer.

Table S3. FTIR band assignments of V3D3 and the pV3D3 layers deposited by AP-PiCVD.

Vibration (cm^{-1})	**V3D3**	**pV3D3**	**References**
$=CH_2$ asymmetric stretching	3057	3054	3058[1]
CH_2 symmetric stretching in vinyl bond	3017	3017	3016[2]
CH_3 asymmetric stretching	2960	2960	2969-2965[3]
CH_3 symmetric stretching	2900	2900	2905-2878[1]
CH_2 symmetric stretching	-	2866	2861[1]
C=C stretching from Si–CH=CH_2	1597	1594	1615-1590[3]
CH_2 in Si–$(CH_2)_x$–Si and vinyl	1407	1403	1410-1390[3]
CH_3 symmetric deformation from Si–CH_3	1259	1255	1290-1240[4]
Open cycle Si–O	-	1083	1080[1]
$(Si–O)_3$ long polymer chains	997	995	995[1]
–O–Si–CH_3 in cyclic compounds	831, 792, 781	831, 783	820-780[5]
CH_3 rocking from Si–CH_3 Si–C stretching interaction	740	737	870-750[3]

Table S4. FTIR band assignments of V3N3 and the pV3N3 layers deposited by AP-PiCVD.

Vibration (cm^{-1})	**V3N3**	**pV3N3**	**References**
N–H stretching from Si–NH–Si	3399	-	3400[4], 3370[6]
=CH_2 asymmetric stretching	3048	3053	3055[6]
CH_2 symmetric stretching in vinyl bond	3006	-	3017[1]
CH_3 asymmetric stretching	2957	2960	2956[6]
CH_3 symmetric stretching	2900	2900	2905-2878[1]
CH_2 symmetric stretching	-	2866	2861[1]
C=C stretching from Si–CH=CH_2	1593	1597	1615-1590[3]
=CH_2 deformation from Si–CH=CH_2	1402	1403	1410-1390[3]
CH_3 symmetric deformation from Si–CH_3	1252	1257	1290-1240[4]
N–H deformation vibration	1155	-	1150[4]
Suboxide Si-O_2 (shoulder)	-	1027	1035[6]
Si–N–Si stretching	1005, 910	1002	1048[5]-1005[7], 920[5,7]
CH_3 rocking from Si—CH_3	831, 781	871	870-750[3]

Table S5. FTIR band assignments of the V4D4 and the pV4D4 layers deposited by AP-PiCVD.

Vibration (cm^{-1})	**V4D4**	**pV4D4**	**References**
=CH_2 antisymmetric stretching	3056	3052	3090-3075[3]
C–H stretching of vinyl bond	3017	-	3016[2]
CH symmetric stretching in vinyl	-	2981	2976[1]
=CH	2970	2970	2976-2974[1]
CH_3 asymmetric stretching	2960	2960	2956[6]
CH_3 stretching	2905	2885	2887[6]
CH_3 antisymmetric stretching	2964	2969	2969-2965[3]
C=C stretching from Si–CH=CH_2	1598	1594	1615-1590[3]
=CH_2 deformation from Si–CH=CH_2	1407	1401	1410-1390[3]
CH_3 symmetric deformation from Si-CH_3	1259	1255	1290-1240[4]
Si–O–Si stretching from cyclosiloxane ring	1053	1051	1080[3], 1075-1065[6,8]
=CH_2 waging from Si–CH=CH_2	958	958	980-950[3]
–O–Si–CH_3 in cyclic compounds	787	781	820-780[4]

Table S6. FTIR band assignments of the V4N4 and the pV4N4 layers deposited by AP-PiCVD.

Vibration (cm^{-1})	**V4N4**	**pV4N4**	**References**
NH stretching from Si–NH–Si	3385	-	3400[4]
=CH_2 stretching	3047	3047	3055[6]
CH_3 antisymmetric stretching	2960	2960	2956[5]
CH_2 symmetric stretching in vinyl bond	3006	-	3017[1]
CH_2 symmetric stretching	-	2866	2861[1]
C=C stretching from Si–CH=CH_2	1593	-	1615-1590[3]
=CH_2 deformation from Si–CH=CH_2	1402	1397	1410-1390[3]
CH_3 symmetric deformation from Si–CH_3	1252	1257	1290-1240[4]
N–H deformation vibration	1165	-	1150[4]
Suboxide Si-O_2 (shoulder)	-	1029	1035[6]
NH stretching from Si–NH–Si	1005, 929	1002 (shoulder)	1048[5]-1005[7], 920[5,7]
CH_3 rocking from Si–CH_3 (plus Si–C stretching interaction)	864, 779	879	870-750[3]
CH_3 in Me-Si-Me	725	775, 698	730-650[3]

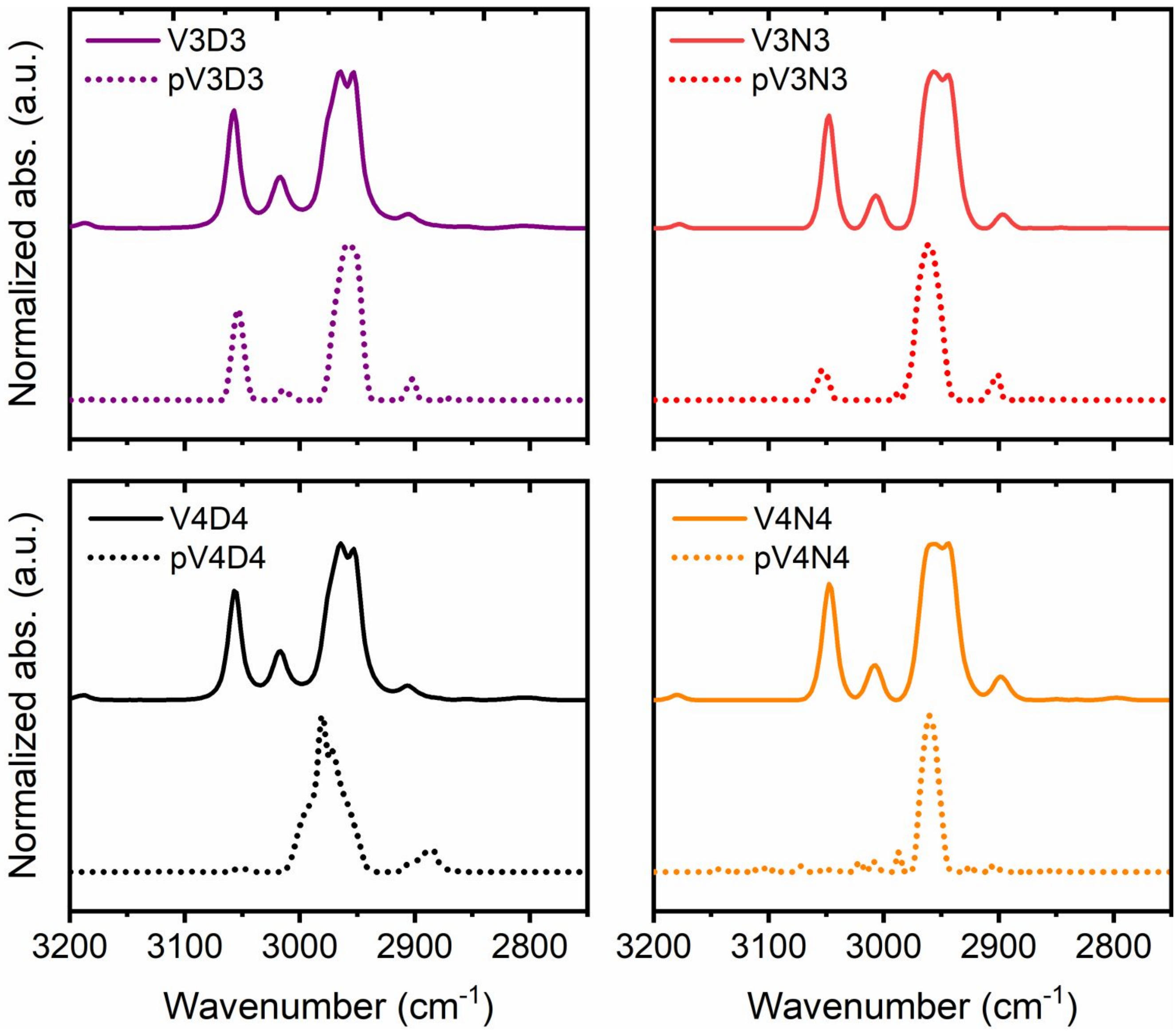

Figure S5. Enlargement of the 3200-2750 cm^{-1} region of the FTIR spectra of the as-deposited AP-PiCVD layers and their respective monomers.

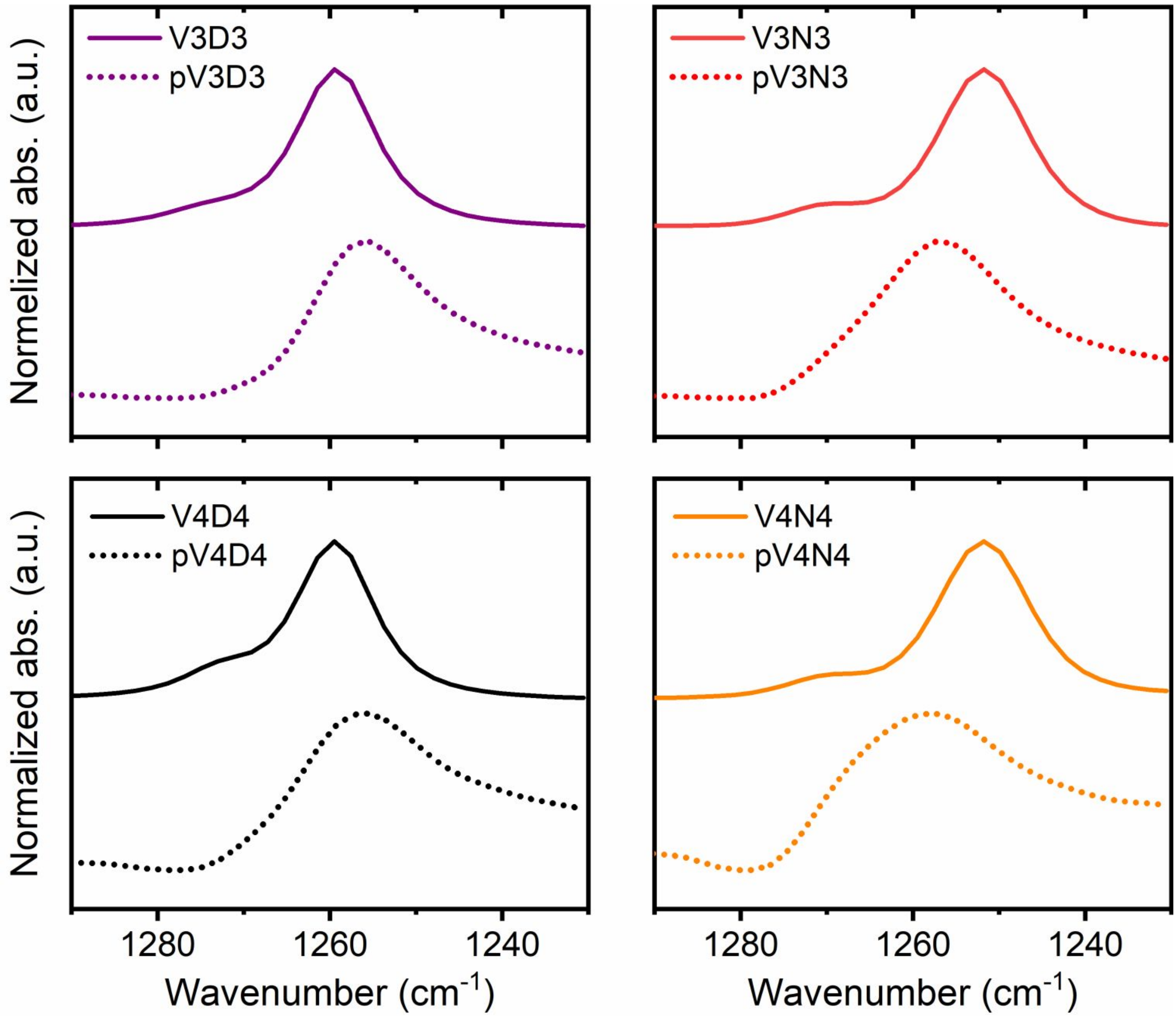

Figure S6. FTIR detail of the Si–CH_3 stretching region for the as-deposited polymer layers and their respective monomers. The pV3D3 and the pV4D4 polymer layers shows the D configuration of their silicon atom whereas the pV3N3 and the pV4N4 exhibits a shift of the Si-CH_3 peak toward higher wavenumber.

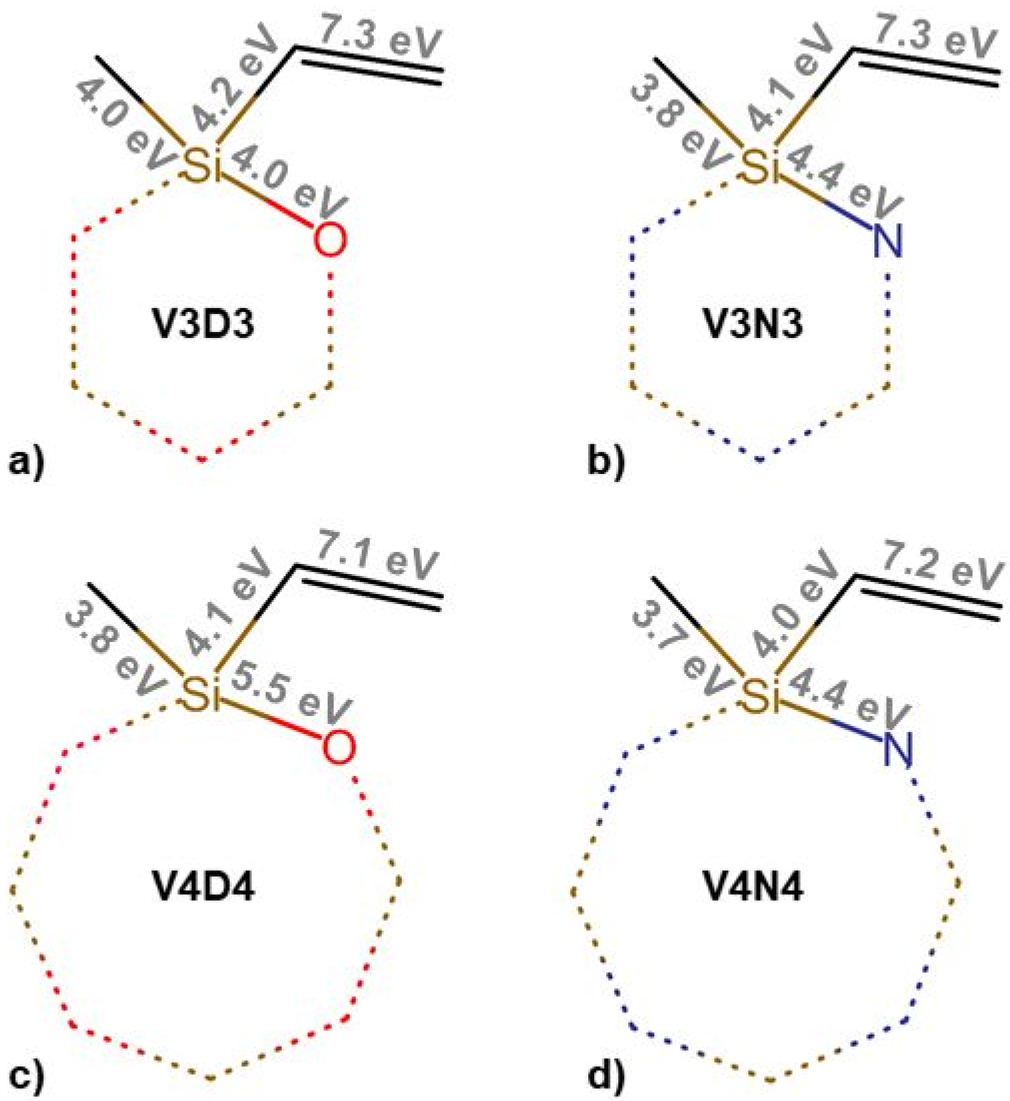

Figure S7. Bond dissociation energies (BDE) of (a) V3D3, (b) V3N3, (c) V4D4 and (d) V4N4 calculated with DFT geometrical and frequency optimization.

Table S7. Theoretical and experimental atomic composition of the different as-deposited AP-PiCVD layers, i.e. pV3D3, pV3N3, pV4D4 and pV4N4.

	Si (at.%)	**O (at.%)**	**C (at.%)**	**N (at.%)**
V3D3 & pV3D3 (theo.)	20.0	20.0	60.0	-
pV3D3(experimental)	23.5	19.5	57.0	-
V3N3 & pV3N3 (theo.)	20.0	-	60.0	20.0
pV3N3(experimental)	21.5	19.2	53.5	5.8
V4D4 & pV4D4 (theo.)	20.0	20.0	60.0	-
pV4D4(experimental)	21.5	21.8	56.5	0.2
V4N4 & pV4N4 (theo.)	20.0	-	60.0	20.0
pV4N4 (experimental)	21.8	19.6	48.6	10

References

(1) Aresta, G.; Palmans, J.; van de Sanden, M. C. M.; Creatore, M. Initiated-Chemical Vapor Deposition of Organosilicon Layers: Monomer Adsorption, Bulk Growth, and Process Window Definition. *J. Vac. Sci. Technol. A Vacuum, Surfaces, Film* **2012**, *30*, 041503.

(2) O' Shaughnessy, W. S. Gao, M.; Gleason, K. K. Initiated Chemical Vapor Deposition of Trivinyltrimethylcyclotrisiloxane for Biomaterial Coatings. *Langmuir* **2006**, *22*, 7021–7026.

(3) Lin-Vien, D.; Colthup, N. B.; Fateley, W. G.; Grasselli, J. G. *The Handbook of Infrared and Raman Characteristic Frequencies of Organic Molecules*; **1991**.

(4) Socrates, G. *Infrared and Raman Characteristic Group Frequencies*; **2004**.

(5) Tu, H.-E.; Chen, Y.-H.; Leu, J. Low-k SiCxNy Films Prepared by Plasma-Enhanced Chemical Vapor Deposition Using 1,3,5-Trimethyl-1,3,5-Trivinylcyclotrisilazane Precursor. *J. Electrochem. Soc.* **2012**, *159*, G56.

(6) Trujillo, N. J.; Wu, Q.; Gleason, K. K. Ultralow Dielectric Constant Tetravinyltetramethylcyclotetrasiloxane Films Deposited by Initiated Chemical Vapor Deposition (ICVD). *Adv. Funct. Mater.* **2010**, *20*, 607–616.

(7) Chen, N.; Reeja-Jayan, B.; Liu, A.; Lau, J.; Dunn, B.; Gleason, K. K. iCVD Cyclic Polysiloxane and Polysilazane as Nanoscale Thin-Film Electrolyte: Synthesis and Properties. *Macromol. Rapid Commun.* **2016**, *37*, 446–452.

(8) Lubguban, J.; Rajagopalan, T.; Mehta, N.; Lahlouh, B.; Simon, S. L.; Gangopadhyay, S. Low-k Organosilicate Films Prepared by Tetravinyltetramethylcyclotetrasiloxane. *J. Appl. Phys.* **2002**, *92*, 1033–1038.

List of Publications

Peer-reviewed international journals

2020	Abessolo Ondo, D.; Loyer, F.; Boscher, N. D.; *Significance of Double Bonds and Cyclic Structure on the AP-PECVD of Low-k Organosilicon Insulating Layers. Submitted in Plasma Processes and Polymers*, submitted to Plasma Process. and Polym.
2020	Abessolo Ondo, D.; Leturcq, R.; Boscher, N. D. *Plasma-initiated chemical vapour deposition of organosiloxane thin films: From the growth mechanisms to ultrathin low-k polymer insulating layers*. Plasma Process; and Polym. *17*, e2000032. https://doi.org/10.1002/ppap.202000032
2019	Abessolo Ondo, D.; Loyer F.; Werner, F.; Leturcq R.; Dale P. J.; Boscher N. D. *Atmospheric-Pressure Synthesis of Atomically Smooth, Conformal, and Ultrathin Low-k Polymer Insulating Layers by Plasma-Initiated Chemical Vapor Deposition.* ACS Appl. Polym. Mater. *1, 3304*. https://doi.org/10.1021/acsapm.9b00759
2018	Abessolo Ondo, D.; Loyer, F.; Chemin, J.-B.; Bulou, S.; Choquet, P.; Boscher, N. D. *Atmospheric Plasma Oxidative Polymerization of Ethylene Dioxythiophene (EDOT) for the Large-Scale Preparation of Highly Transparent Conducting Thin Films*. Plasma Process. and Polym. *15*, 1700172. https://doi.org/10.1002/ppap.201700172
2018	Knapp, C. E.; Chemin, J.-B.; Douglas, S. P.; Abessolo Ondo, D.; Guillot, J.; Choquet, P.; Boscher, N. D. Room-Temperature Plasma-Assisted Inkjet Printing of Highly Conductive Silver on Paper. Adv. Mater. Technol. 3, 1700326. https://doi.org/10.1002/admt.201700326

Acknowledgments

“Get ready for the most intensive years of your life.” This was a well thought sentence a wise Ph.D. told me before starting my Ph.D. At that time, the sentence did not catch my attention. But, being at the end of this journey made me realise how careful we should always be when reading wise people messages.

A thesis is not an achievement of only one person, but it is the result of a teamwork between the PhD candidate and his/her supervisor(s), collaborators, colleagues, friends, and family. For that reason, I would like to thank all the people who accompanied me on this journey.

I would like to thank Professor Mariadriana Creatore from Eindhoven University and Professor Phillip Dale from the University of Luxembourg for following my progress and their useful advices through all these years as members of my CET, and for accepting to be part of my jury members.

I thank Professor Phillip Dale for being the president of the jury, and the external jury members Professor Françoise Massines and Doctor David Muñoz-Rojas for accepting to review my doctoral thesis as well as for the discussions and interest shown in for my work.

I particularly thank my supervisor Doctor Nicolas Boscher from LIST for his supervision throughout this journey. An amazing patient and wise researcher who transformed me into a researcher. Our teamwork started five years ago with my master internship, after which I had never stop to grow scientifically, professionally and personally. I could never thank him enough for this incredible opportunity I experienced.

I am thankful to my colleagues and friends I met during my time at LIST, those that left and all those that arrived since. Thank you Ula, François, Peppe, Kamal, Florian, Lluís, Vene, Miguel, Olivier D.-C., Lauriane, Edyta and Paul G. for all our coffee breaks and laughs. This experience would not have been the same without you.

Thank you Hameeda, Olivier B., Greg, Alex, Marta, Charlotte, Acerina, Mike, Rathaiah and Riyad. It was nice to discuss with you every day.

Je remercie aussi ces amis de longue date; Désir, Mika et Tomo, qui malgré la distance ont su me motiver.

Je tiens à remercier tout particulièrement ma famille pour leur soutien indefectible. Nda mbo asse, ma ve mi n'akiba! Merci à Sabrina, mon fry, rencontrée en milieu de thèse, devenue une amie spéciale et un soutien psychologique incontournable.

Je remercie ma maman, ma Dési et tout spécialement les hommes de ma vie: mon fils Mathis, mon père, mon Martian et mon Papy, pour leurs encouragements continus et leur soutien. Merci à Irène et John, mes beaux-parents, pour toutes ces heures de babysitting, m'ayant permis de me replonger dans la rédaction de ma thèse.

I am deeply thankful to the one who handled my stress during this journey, mein herz Paul B. Thank you for your incredible support and your infinite love.

I thank the Luxembourg National Research Fund (FNR) for financial support through the MASSENA project (PRIDE15/10935404) which was the basis for my thesis research.